Static, Dynamic Mechanical and Fatigue Properties of Cement-Asphalt Mortars

A thesis submitted to

University College London

for

The degree of Doctor of Philosophy (PhD)

by

Yongliang LIU

Dept. of Civil, Environmental and Geomatic Engineering

University College London

February 2017

Static, Dynamic Mechanical and Fatigue Properties of Cement-Asphalt Mortars

A thesis submitted to

University College London

for

The degree of Doctor of Philosophy (PhD)

by

Yongliang LIU

Dept. of Civil, Environmental and Geomatic Engineering

University College London

February 2017

I, Yongliang LIU, confirm that the work presented in this thesis is my own. Where information has been derived from other sources, I confirm that this has been indicated in the thesis.

ACKNOWLEDGEMENTS

First of all, I would like to express deep gratitude to my supervisors, Dr Yun BAI, Dr Xiangming KONG and Dr Tingyu HAO, for their guidance and support during the research work. Thanks for Dr BAI's making me 'suffering' once and again, from which I had learned how to read critically and think critically, Dr KONG's open-mindedness, which allowed me to conduct research work freely, and Dr HAO's financial support at the hardest but critical time. In a word, without them, this thesis would have ever been completed in the end.

Secondly, I would like to extend a big 'Thank you' to Prof Peiyu YAN and Dr Jianguo HAN from Institute of Building Materials, School of Civil Engineering, Tsinghua University, Beijing, China. They helped me a lot when I made test samples in the concrete laboratory and performed mechanical tests with a loading machine. The same 'Thank you' is to Prof Fazhou WANG and Dr Yunpeng LIU from School of Materials Science and Engineering, Wuhan University of Technology, Wuhan, China, who liaised with a construction company to supply us with an asphalt emulsion needed in the experimental work and kindly tested the basic properties. And I would like to say 'Thank you' to Dr Yaodong JIA as a research associate at AIM Group, who provided me some advice. Because of his advice, I moved from London to Northampton for writing up, living there with his family in the last half a year.

Finally, I am greatly indebted to my wife, Wendy ZHANG, who accompanied me in the UK throughout those hard years, my baby girl, Elsa LIU, who gave me a lot of happiness during the process of writing up, and other family members in China, who encouraged me for whatever I did in the past years. I am also indebted to my friends and colleagues, Dr Yonghui ZHU, Dr Ningbo LI, Dr Yanrong ZHANG from Tsinghua University, and all members from AIM Group at UCL and KONG Group at Tsinghua University. My best friends in life since high school, such as Zhijun CHEN, Guilin CAO, Dr Fangdan JIANG and Fei Duan,

and best men in universities, such as Dapeng CUI, Dr Wei SUN, Dr Qianyi SONG and Zhibin REN, gave me so much support as well.

The financial support from UK-China Science Bridge (SB), China Scholarship Council (CSC) and UCL Faculty of Engineering Sciences Scholarship is appreciated. And the research work is partly sponsored by a Royal Society of the UK & National Nature Scientific Fund of China (NSFC) Exchange Project.

天将降大任于是人也，必先苦其心志，劳其筋骨，饿其体肤，空乏其身，行拂乱其所为，所以动心忍性，曾益其所不能。

——孟子

PUBLICATIONS

- Xiangming KONG, **Yongliang LIU**, Yanrong ZHANG, Zhenlin ZHANG, Peiyu YAN and Yun BAI, Influence of temperature on mechanical properties of cement asphalt mortars, *Materials and Structures*, 2014,47, pp: 285-292
- **Yongliang LIU**, Xiangming KONG, Yun BAI and Tingyu Hao, Fatigue testing and properties of two typical cement asphalt mortars, 37st Cement and Concrete Science Conference: Novel Developments and Innovation in Cementitious Materials, 11th-12th Semptember 2017, University College London, London, UK
- **Yongliang LIU**, Xiangming KONG, Yun BAI and Tingyu Hao, Fatigue properties of two typical cement asphalt mortars used in slab tracks of high speed railways, Young Researcher's Forum II: Construction Materials, 19th February 2014, University College London, London, UK
- **Yongliang LIU**, Xiangming KONG, Peiyu YAN, Yun BAI, Desmond Robinson and P. A. Muhammed Basheer, Comparison between two typical cement-asphalt mortars used in slab tracks of high speed railways, 31st Cement and Concrete Science Conference: Novel Developments and Innovation in Cementitious Materials, 12th-13th September 2011, Imperial College London, London, UK

ABSTRACT

High-speed railway or rail (HSR) is a hot topic all over the contemporary world. And there is a growing tendency towards the application of nonballasted or slab tracks in HSR. Cement-asphalt mortar (CAM), a composite of Portland cement and asphalt emulsion, is widely used as a cushion layer in the two prevailing prefabricated concrete slab tracks of HSR in China, namely CRTS I and CRTS II. After a few years' operation and service, however, premature cracking has been identified in the CAM layer along part of CRTS I and CRTS II. This is mainly caused by the fatigue of CAMs under repetitive traffic loading, that is, mechanical fatigue. In this research work, therefore, static, dynamic mechanical and most importantly, fatigue properties of the two typical CAMs, namely CAM-I and CAM-II, were investigated.

Using a 4-point bending (4PB) test method, static or quasi-static mechanical properties of these two CAMs were studied. Results indicated that the 4PB test method was suitable for characterising their static bending properties in the laboratory, and more reliable results could be obtained, especially on modulus of elasticity, compared to the compression test method which was usually used for formulation design and quality evaluation. However, irrespective of the test methods used, CAM-I and CAM-II were found to be distinctively different in their static mechanical properties and behaviour at room temperature, due to the changes in the microstructures of their binding materials, cement-asphalt binder (CABs), used in CAMs at different A/Cs.

The primary functions of CAMs as the cushion layer in CRTS I and II, especially damping, had been demonstrated to be in close relation to their viscoelasticity. Based on the DMA method, the temperature spectra of dynamical modulus and loss factors of CAMs or CABs were obtained to characterise their temperature susceptibility and viscoelasticity, respectively. On the temperature spectrum of CAM-I, the two characteristic temperatures of the asphalt binder, T_g implied to be around -20 °C and $T_{R\&B}$ measured to be 48 °C, could be determined, and

these two not only defined the viscoelastic zone for CAM-I and the immediate temperature range for the fatigue tests of CAM-I, but also the two boundaries of service temperatures for CAM-I and CAM-II under traffic loads. The higher A/C caused a decrease in dynamic modulus of CAMs but an increase in their loss factors and temperature susceptibility, and a balance should be considered between them in the future design of new CAMs.

For the first time, 4PB fatigue of CAM-I and CAM-II were investigated using two different fatigue test schemes, and the results indicated that, in terms of the fatigue behaviour, the CAM-I can be considered as a cement-modified asphalt mortar whilst CAM-II an asphalt-modified cement mortar. Therefore, it is preferable to use the asphalt mixture-based fatigue test configuration for CAM-I and this fatigue test scheme was an ideal one to be used. Additionally, it was found that low temperature was beneficial to the fatigue life of CAM-I whereas high temperature was detrimental to its fatigue life. On the other hand, the fatigue test configuration of cement-based materials including plain concretes is favourable to use for CAM-II but might not suitable for CAM-II, especially when the influence of the reversal stress, *R*, or the test temperature was separately considered. Different from plain concrete materials, the reversal stress or the test temperature had a significant impact on the fatigue life of CAM-II. Higher temperature would greatly reduce its fatigue life, and this temperature should not be higher than $T_{R\&B}$ of the asphalt binder used. Much longer fatigue life of CAM-II was observed under low temperatures if the same stress, instead of normalised stress level, was applied, and CAM-II was more like plain concretes when temperature fell to around T_g of the asphalt binder.

TABLE OF CONTENTS

LIST OF FIGURES

LIST OF TABLES

LIST OF ABBREVIATIONS

A list of abbreviations used in the thesis is presented alphabetically.

2PB, 3PB, or 4PB	2-point, 3-point or 4-point bending;
A	Asphalt binder;
A/C	Asphalt-cement ratio, m(A)/m(c);
AC	Asphalt concrete;
AE	Asphalt emulsion;
AFt	Ettringite;
C	Portland cement;
CAB	Cement-asphalt (emulsion) binder;
CAEC	Cement-asphalt emulsion composite;
CAM	Cement-asphalt (emulsion) mortar;
C_3A	Aluminate;
CA_4F	Ferrite;
C_2S	Alite;
C_3S	Belite;
C-S-H	Calcium silicate hydrate;
CS	Chemical shrinkage;
CW	Capillary water;

DB	Deutsche Bahn AG (Germany Railway);
DE	Dissipated energy;
DER	Dissipated energy ratio;
DF	De-foaming agent;
DMA	Dynamic mechanical analysis;
EPU	Expanded polyurethane;
ESEM	Environmental scanning electron microscopy;
fcp	fresh Portland cement paste;
FEL	Fatigue endurance limit;
FEM	Finite element method;
GP	Water-filled gel pores or space;
GW	Gel or absorbed water;
HC	Solid hydrate cement;
hcp	Hardened Portland cement paste;
HP	Hydration product;
HPC	High performance concrete;
HSL	High-speed line;
HSR	High-speed railway or rail;
ICE	Intercity Express;
IDE	Initial dissipated energy;
IDT	Indirect tension;

ITZ	Interfacial transition zone;
JNR	Japanese National Railway;
LCA	Life-cycle analysis;
LCC	Life-cycle cost;
LVDT	Linear variable differential transformer;
MDOF	Multi degree-of-freedom;
MTS	Material Test System;
M-E	Mechanistic-empirical;
OD	Outside diameter;
OPC	Ordinary Portland cement;
PCC	Portland cement concrete;
P/C	Polymer-cement ratio, m(P)/m(C);
PCA	Portland Cement Association;
PDL	Passenger dedicated line;
PDSE	Pseudo dissipated strain energy;
PMM or PMC	Polymer-modified mortars or concretes;
RC	Reinforced concrete;
RH	Relative Humidity;
S	Sands or fine aggregates;
S/B	Sand-binder ratio, m(S)/m(A+C);
S/C	Sand-cement ratio, m(S)/m(C);

SCB	Semi-circular bending;
SCC	Self-compacting concrete;
SD	Standard deviation;
SDOF	Single degree-of-freedom;
SEM	Scanning electron microscopy;
SP	Superplasticizer;
T/C	Tension/compression;
Tem.	Temperature;
UIC	International Union of Railways;
UT/C	Direct axial tension/compression;
VECD	Viscoelastic continuum damage;
W	Total water;
W/C	Water-cement ratio, m(W)/m(C);

LIST OF SYMBOLS

A list of symbols used in this thesis is given as follows.

a, b, c	Fitting coefficients of C_f
b	Wideness of the beam specimen;
C	Damping coefficient;
C_c	Critical damping coefficient;
C_f	Frequency influence efficient;
D	Dynamic magnification factor;
E	Elastic modulus or modulus of elasticity;
E^*	Complex modulus;
$\|E^*\|$ or E_d	Dynamic modulus
E'	Storage modulus;
E''	Loss modulus;
E/E_o	Stiffness ratio;
E_a	Activated energy;
E_c	Young's modulus in compression;
E_{di}	Dynamic modulus at the loading cycle of i;
E_o or S_o	Initial stiffness or dynamic modulus;
E_r	Relative modulus of elasticity;

ER	Energy ratio;
$E_r'(T, \omega)$	Relative dynamic storage modulus;
E'_{-100}	Dynamic storage modulus at -100 ˚C
E_t	Young's modulus in tension
F	Loads applied;
F_A	Amplitude of fatigue loads;
f	Loading frequency;
f'_c	Compressive strength;
G_f	Failure energy;
h	Height of the beam specimen;
k	Stiffness
k^*	Complex stiffness;
k_1, k_2 or k_3	Fitting coefficients to fatigue test data
L	Effective length of the beam specimen;
m	Degree of hydration;
MOR	Modulus of rupture, i.e. flexural strength;
n	Number of loading cycles;
N_1	The end of stage II during fatigue damage;
N_f	Number of cycles to failure;
$N_{f,\,50}$	Number of cycles to failure based on classical failure criterion (50% reduction in stiffness);

$N_{f,\ ER}$	Number of cycles to failure based on the modified ER-based failure criterion;
p(t)	Dynamic force;
R	Stress ratio;
R	Universal gas constant;
S	Normalised stress level;
S_6	Normalised stress level corresponding to 10^6 loading cycles;
S_a	Stress amplitude;
S_m	Mean stress;
S_{max}	Maximum stress;
S_{min}	Minimum Stress;
T	Period of repetitive loads
T_{eff}	Effective temperature;
T_g	Glass transition temperature;
TR	Transmissibility ratio;
$T_{R\&B}$	Softening point temperature;
v(t)	Dynamic displacement;
V_A	Volume of asphalt binder;
V_c	Volume of unreacted cement;
V_C	Initial volume of cement;
V_{CS}	Volume of chemical shrinkage;

V_{CW}	Volume of capillary water;
V_{GP}	Volume of gel pores;
V_{HC}	Volume of hydrated cement;
V_{HP}	Volume of hydrated product;
V_W	Initial volume of water;
w or w_i	Dissipated energy at the loading cycle of I;
W_d/c	Total retained water;
$W_d\ v_d\ /\ v_W\ c$	Retained water volume;
α, β	Fitting coefficients to fatigue test data;
δ and tan δ	Lag or phase angle, and loss factor;
Δ	Deflection at the centre of the beam specimen;
Δ_A	Amplitude of fatigue deflection;
ΔS	Stress range;
ε	Strain;
ε_a or ε_o	Strain amplitude;
ε-	Controlled-strain;
ε_6	A strain level corresponding to 10^6 loading cycles or fatigue strain;
ε_c	Compressive strain;
ε_f	Failure strain;
ε_{FEL}	Fatigue strain to infinite fatigue life;

ε_m	Mean strain;
ε_t	Tensile strain applied in fatigue tests;
ε_{cp}	Strain value corresponding to peak stress, σ_{cp};
η	Hysteretic damping factor;
v_W	Specific volume of water
ρ_A, ρ_C or ρ_W	Density of asphalt binder, cement and water;
ξ	Damping ratio;
σ	Stress;
σ_6	A stress level corresponding to 10^6 loading cycles or fatigue strength;
σ_a	Stress amplitude;
σ_b	Bending strength;
σ-	Controlled-stress;
σ_c	Compressive stress;
σ_{cp}	Peak stress;
σ_{max}	Maximum stress applied;
σ_{pr}	Relative peak stress;
Φ_T	Shift factor;
φ_A	Volume fraction of asphalt binder;
φ'_A	Volume fraction of asphalt binder in two main binding phases;

φ'_{HP}	Volume fraction of hydration product in two main binding phases ;
φ_{HP}	Volume fraction of hydration product after excluding chemical shrinkage;
$\varphi_{HP,m}$	Volume fraction of hydration product before excluding chemical shrinkage ;
φ_{c}	Volume fraction of unreacted cement after excluding chemical shrinkage;;
$\varphi_{c,m}$	Volume fraction of unreacted cement before excluding chemical shrinkage;
φ_{CW}	Volume fraction of capillary water after excluding chemical shrinkage;;
$\varphi_{CW,m}$	Volume fraction of capillary water before excluding chemical shrinkage;
$\varphi_{CS,m}$	Volume fraction of chemical shrinkage before excluding chemical shrinkage;
ω	Angle velocity or frequency;
ω_{n}	Nature free-vibration frequency;
ω_{D}	Free-vibration frequency of a damped system

CHAPTER 1 INTRODUCTION

1.1 Background

1.1.1 High-speed railway or rail

High-speed railway or rail (abbreviated HSR) is a hot topic all over the contemporary world. But what is HSR? Obviously, there is no single and absolute standard to define high speed and its definitions vary a lot, which depends not only on the history of technological growth in railway engineering but also on the criteria used by different institutions or nations. However, up to date, a well-accepted general definition is the one proposed by the International Union of Railways (UIC), which defines HSR as new railway lines designed for speeds above 250 km/h (160 mph) and upgraded lines for speeds up to 200 km/h (120 mph). Whatever the definition of HSR is, it is at all events a combination of all railway elements together, which constitutes the system of infrastructure, rolling stock and operating conditions.

Speaking of HSR, as a matter of fact, there are two technical systems involved, one using the traditional wheel-rail technique and the other using the cutting-edge magnetic levitation (maglev) train technique. The latter has very limited applications probably because of its technical complexity and much higher initial construction cost, even though higher operational speeds (over 400 km/h) could be achieved (Vuchic and Casello, 2002). The first and only commercial trans-rapid maglev trains in the world have been put into operation in Shanghai, China, since April 2004. So in this thesis, HSR refers exclusively to the former system, the wheel-rail one, which is the mainstream form of railways in the present world. Although controversial in some aspects, HSR has undoubtedly become a revolutionary milestone in the history of railway engineering in the second half of the 20th century (Lacote, 2001, Smith, 2001, Takagi, 2005). It not only means reduced journey time, high capacity and high accessibility, but also

means high safety, high reliability, high efficiency, and high level of ride comfort for passengers. In comparison with other modes of transport such as road, water and air, HSR has already been proven to be more energy-efficient and environmentally friendly (Okada, 1994, Janic, 2003), and more economical and competitive in the long term for medium-distance transportation services (Nash, 1991, Leinson et al., 1997, Campos and Rus, 2009). Furthermore, as a stimulus for the development of national economies in the 21st century (Amos et al., 2010), it always involves a huge amount of capital investment, home or abroad, and infrastructure construction on a large scale, which creates jobs, growth and prosperity as a result. For instance, China's HSR network, which has been built in less than one decade with great success, is reported to promote the development of local economies along the lines, and moreover, mitigate the pressure of congestion and pollution in big cities to some extent, particularly in megacities like Beijing and Shanghai (Zheng and Kahn, 2013).

The first HSR line, Taikado Shinkansen linking Tokyo and Osaka in Japan, was opened in October 1964 when Tokyo Olympic games were held (Takatsu, 2007). Since then, the innovative concept started to spread into west European countries such as France, Germany, Italy, Spain, Netherlands, the UK (Arduin, 1994, Vickerman, 1997, Arduin and Ni, 2005, Ebeling, 2005), and also into South Korean (Kim, 2005, Lee, 2007) and China (Okada, 2007, Wang et al., 2009a). Presently, the vast majority of HSR lines are globally distributed in West Europe and East Asia (**Fig 1.1**), and China has the longest HSR network in the world (**Fig 1.2**), over 19,000 km (> 6,200 mi) being built since the first test passenger dedicated line (PDL), Qin-Shen PDL connecting Qinhuangdao to Shenyang in the northeast region of China, started to be built in 1999 and brought into service in 2003 (Jin and Chen, 2004). In the next decade or further, more PDLs, intercity express (ICE) lines and HSR corridors in China (Takgi, 2011), 13 designated high-speed corridors in the United States involving at least 26 states and $ 8 billion (£ 5 billion) (Peterman et al., 2009), and High-Speed Two (HS2) in the UK following High-Speed One (HS1) (DfT, 2009) will be planned, constructed and finally in operation, with an ambition to upgrade their public transportation systems.

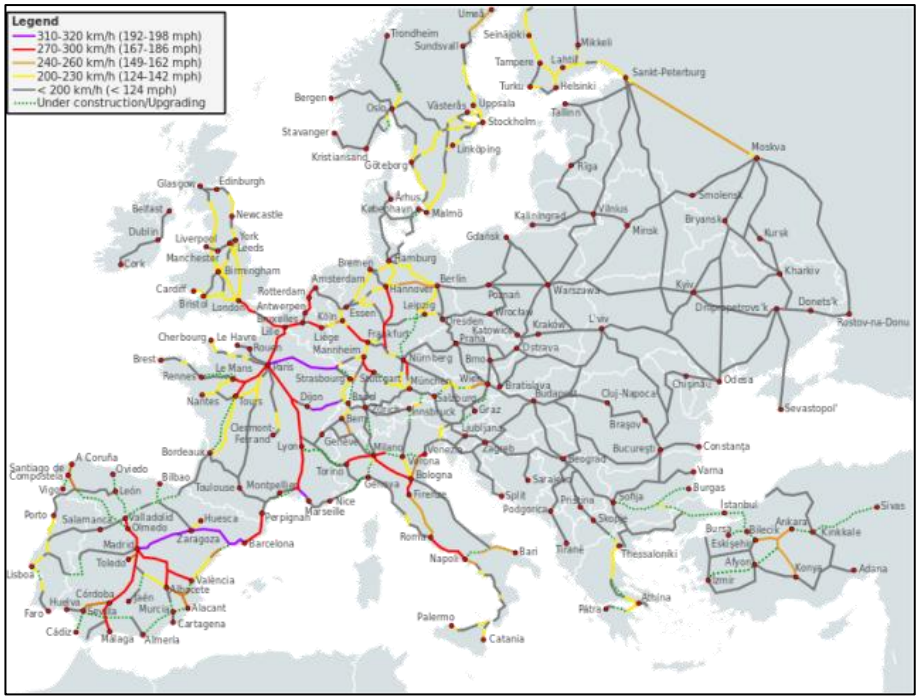

(a)

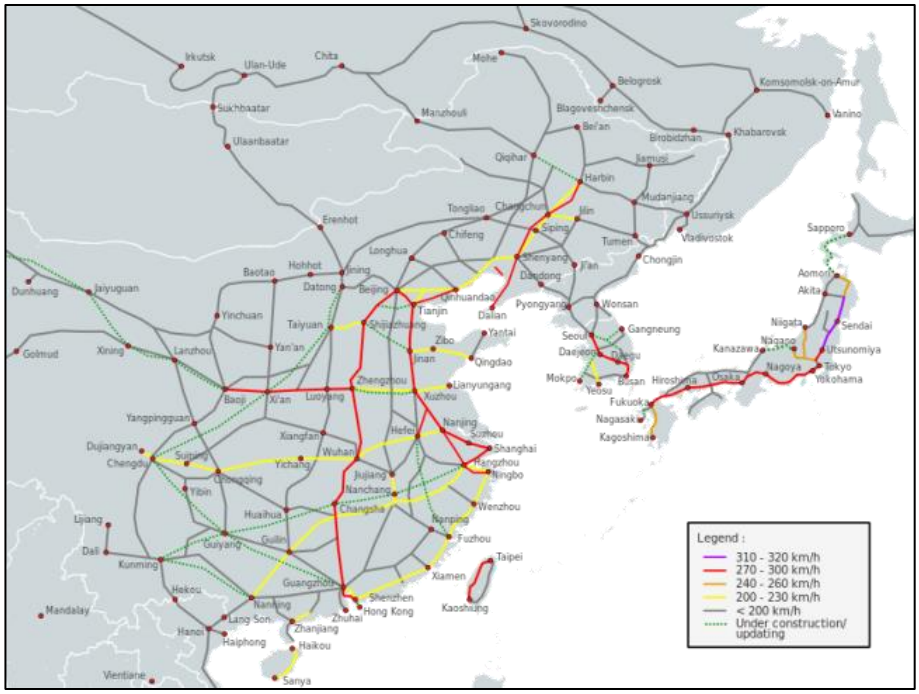

(b)

Fig 1.1 Operational HSR in (a) West Europe and (b) East Asia (wiki)

Fig 1.2 HSR network of China (wiki)

1.1.2 Nonballasted or slab track

With high speeds designed, there comes an increased requirement for high-quality railway systems which basically include high-speed trains, signalling and communications, railway tracks, and etc. Slab track, sometimes termed as nonballasted or ballastless track, is one of the most important technologies developed for modern HSR because of its great advantages, over conventional ballasted track, of reduced structural height and weight, lower requirement of maintenance work and hence higher availability, increased service life, higher lateral resistance and no churning up of ballast (Esveld, 2003b, Esveld, 2001, Esveld, 1997, Esveld, 1999, Mörscher, 1999, Esveld and Markine, 2006, Darroch et al., 2006).

Globally, there is a growing tendency towards the application of nonballasted or slab tracks, and various types of slab track systems have been successfully constructed in different HSR lines. Among them, the most famous ones are Shinkansen, Rheda2000, Züblin and Bögl (Bastin, 2006), and according to mileage, the two prefabricated concrete slab tracks, Shinkansen in Japan and Bögl in Germany, are the most widely-used, even if slab tracks built in China are not included (Michas, 2012). And in mainland China, CRTS (China Railway Track System) I and CRTS II as illustrated in **Fig 1.3**, which were further developed from Shinkansen and Bögl slab tracks, respectively, have been prevailingly used and constructed in PDLs in the past decade (Zhang and Zeng, 2013). These two slab track systems (seen from **Fig 1.3**) are very similar in the configuration of the structure and characterised by a prefabricated and precast reinforced concrete (RC) track slab, a cast-in-place concrete trackbed and an intermediate cushion layer. What's more, an installation technique of top-down and bottom-up combined is adopted for CRTS I and CRTS II, in order to shorten the overall construction time and best control the level and alignment for HSR operation. Due to this technique, a narrow gap (50 mm for CRTS I and 30 mm for CRTS II) between the top track slab and the bottom trackbed is allowed for and therefore, a grouting material is indispensably needed to fill up the gap and form the cushion layer after hardened. This cushion material is referred to as cement-asphalt mortar (CAM).

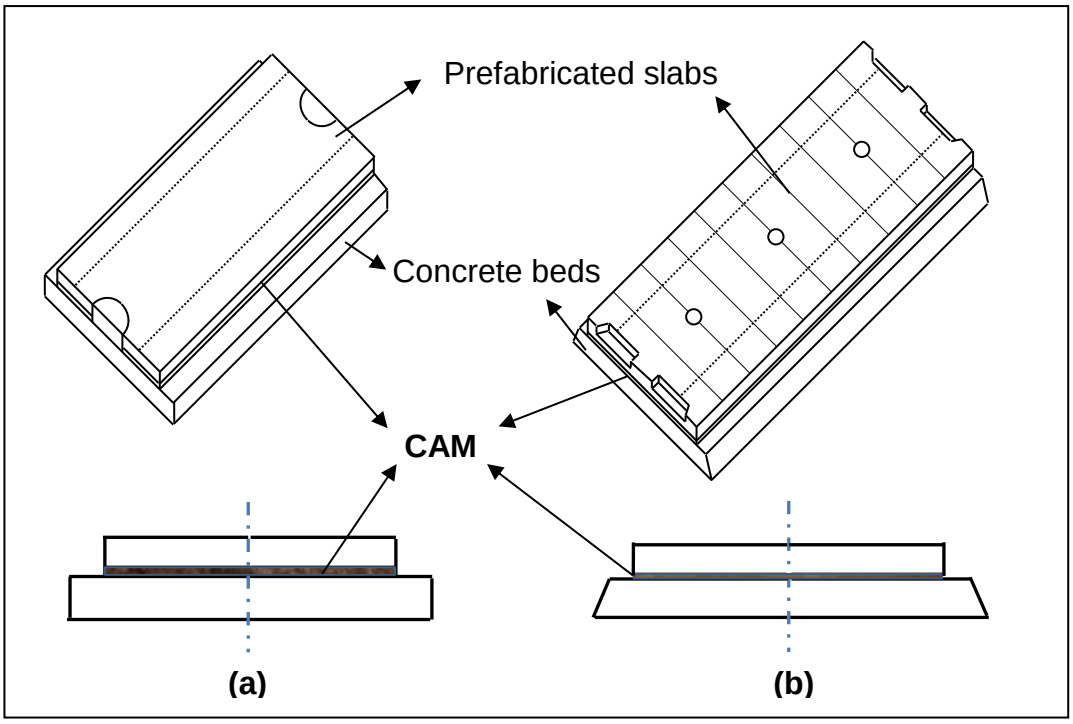

Fig 1.3 Schematic drawings of (a) CRTS I and (b) CRTS II

1.1.3 Cement-asphalt mortar

The cushion material CAM, also called cement and asphalt emulsion mortar or cement and emulsified asphalt mortar in some literature, is a novel inorganic-organic composite material, consisting primarily of Portland cement (C), asphalt emulsion(AE), water (W), fine aggregates (S) and chemical admixtures, and its properties are mostly determined by asphalt-cement ratio which can be defined as the ratio of asphalt binder (A) in the emulsion to Portland cement by weight (A/C, i.e. m(A)/m(C)) (Wang et al., 2008f, Liu et al., 2009).

Despite the fact that CRTS I and CRTS II have a similar configuration in the structural form, two totally different CAMs with different compositions (A/C) and properties are used as the cushion layer in the two slab tracks (Wang and Liu, 2012), one with higher A/Cs (0.6-1.2) and the other with lower A/Cs (0.2-0.6), respectively. Thanks to the extensive construction of slab tracks in the HSR network of China in the past decade, a majority of research work on CAMs has been carried out, but more attention is at first paid to CAMs with higher A/Cs, (termed as CAM-I in this thesis), mainly on their formulations (Zhao, 2003a), on-site construction technologies (Fu et al., 2002), and several fundamental properties such as fresh workability, volumetric stability during hardening and static mechanical properties (Wang, 2008, Wang et al., 2008d, Xu et al., 2009, Hu and Wang, 2009, Li et al., 2010a, Zeng et al., 2011)**,** and later on CAMs with lower A/Cs, (termed as CAM-II) (Wang et al., 2008e, A et al., 2009, Zeng et al., 2009, Li et al., 2011, Tan et al., 2011, Tan et al., 2012, Wang et al., 2013). These CAMs are reported to be typically viscoelastic solid materials at room temperature (Kong and Liu, 2009, Liu et al., 2011a, Liu et al., 2013), whose mechanical properties are dependent on temperature, strain rate or loading frequency, and pressure (Wang et al., 2008a, Xie et al., 2010, Kong et al., 2010a, Kong et al., 2010b, Liu et al., 2013, Kong et al., 2014, Hu et al., 2012). As cushion materials in CRTS I or CRTS II, it is well accepted that CAMs are mainly subjected to dynamic traffic loads from train-rail-slab track interactions (Zhai et al., 1999, Zhai et al., 2009). After just a few years' operation and service of HSR in mainland China, however, premature cracking has been identified in the CAM layer along part of CRTS I and CRTS II.

This issue just mentioned could be potentially serious because it would lead to quick weakening and deterioration of the cushion layer in the track structures, thus influencing ride comfort for passengers and even running safety of high speed trains (Xiang et al., 2009). There could be many different mechanisms behind this cracking phenomenon, but the major mechanism is most likely to be fatigue of CAMs under repetitive traffic loading, which is the basic assumption throughout this thesis. And as an important structural layer in those two slab tracks, the CAM layer is mainly subjected to bending (Zhao, 2003b, Liu et al., 2010). However, the fatigue behaviour of CAMs with varying A/Cs is scarcely concerned and understood (Wang and Liu, 2008, Li et al., 2010b), especially under bending. Therefore, it is of necessity and significance to investigate the flexural fatigue behaviour of different CAMs. For simplicity and comparison, the emphasis is better to be given to two typical CAMs, namely, CAM-I and CAM-II used in CRTS I and CRTS II, respectively. On the other hand, as we need to know, the operation of HSR lines is through complicated geological and weather conditions in different regions of mainland China. From one region to another, the environmental temperature to which these slab tracks are exposed during operation could be significantly different. And it has been reported that the mechanical properties of both types of CAMs are susceptible to temperature (Kong et al., 2010b, Wang et al., 2010b, Hu et al., 2012, Liu et al., 2013, Kong et al., 2014). Hence, it is important to take the temperature effects into account when studying the flexural fatigue of these two CAMs.

1.2 Aim and objectives

The overall aim of this research project is to investigate the flexural fatigue properties of two typical CAMs, namely CAM-I and CAM-II, which are commonly used in the two most widely-used slab track systems of HSR network in China, CRTS I and CRTS II, respectively. To achieve this aim, the following objectives have been considered.

(1) To study the static bending properties of CAM-I and CAM-II at room temperature, in order to evaluate the static bending behaviour of the two CAMs, so that the fundamental bending parameters could be obtained for fatigue tests;

(2) To study the dynamic mechanical properties of CAM-I and CAM-II under various temperatures, in order to evaluate the temperature susceptibility and the viscoelasticity of the two CAMs, so that the most suitable temperature range could be identified for fatigue tests;

(3) And above all, to study the flexural fatigue properties of the two typical CAMs and the influence of temperature on the fatigue behaviour, in order to understand the fundamental mechanisms of flexural fatigue of the two CAMs under different temperatures.

1.3 Organisation of the work

The structure of this thesis is organised into seven chapters followed by references at the end of thesis and then two appendices. Following up is a brief introduction to each chapter.

Chapter 1 Introduction

This chapter introduces the background of the research work, and the overall aim and objectives are outlined.

Chapter 2 Literature review

Chapter 2 is a general review chapter, which is composed of four parts. The first part overviews different slab tracks used in HSR and highlights the two most commonly used ones, CRTS-I and CRTS-II, in which CAMs are used as a cushion layer. The second and third parts generally review static and dynamic mechanical properties of CAMs and their binders, respectively. And in the final part, last but not least, the emphasis is placed on fatigue testing and properties of two extreme materials, namely, asphalt mixtures and cement-based materials used in pavements, because of rare literature on fatigue of CAMs available, in an attempt to establish fatigue test schemes for CAM-I and CAM-II.

Chapter 3 Experimental programme

Chapter 3 describes the experimental programme in this thesis and introduces each raw material used in these two CAMs, their mix proportions, the manufacturing process of the test specimens and all test schemes at great length used in the programme.

Chapter 4 Static mechanical properties of CAMs at room temperature

Chapter 4 deals with the static mechanical properties of CAM-I and CAM-II tested by two test methods at room temperature, one of which is a newly-developed 4-point bending (4PB) method, and the other is the traditional compression test method.

Chapter 5 Dynamic mechanical properties of CAMs and their binders

The topic of Chapter 5 is the dynamic mechanical properties of CAM-I and CAM-II under various temperatures tested by a DMA method, in comparison to those of their binders, CAB-I and CAB-II, respectively.

Chapter 6 4-point bending fatigue of CAM-I and CAM-II

The subject of Chapter 5 is the fatigue responses of CAM-I and CAM-II tested in the laboratory under 4-point bending (4PB), but in a different mode of loading, either controlled-strain or controlled-stress. The test temperature is considered as the main influencing factor.

Chapter 7 Conclusions and recommendations for future work

In the final chapter, conclusions will be drawn based on experimental results and discussion, and some recommendations will be given as a reference for further research work in the future.

CHAPTER 2 LITERATURE REVIEW

2.1 Introduction

This chapter reviews the literature related to the current research, which mainly consists of the following four parts. The first part overviews different slab tracks used for HSR worldwide, with an emphasis being given to the prefabricated concrete slab tracks which are most commonly constructed around the world. In particular, the two prevailing slab track systems widely used in China's HSR network, namely CRTS I and CRTS II, are introduced in detail. Additionally, the primary functions of the CAMs in these two slab tracks are also discussed and compared in the context of different track systems. In the second part of the review, the composite mechanism of each CAM at different A/Cs (m(A)/m(C)) is presented and the relationship between the static mechanical properties (under compression) and the composition and microstructure of the binder in each CAM system is discussed, together with their related test methods. Then, the third part mainly reviews the dynamic mechanical properties of the CAMs and the relationship to their binders in line with the test methods currently adopted for assessing the dynamic mechanical properties of each CAM system. In the final part, the test methods used to assess the fatigue of asphalt mixtures and cement-based materials are reviewed separately. Based on this, a research hypothesis on developing different test protocols or schemes for assessing the fatigue of different CAMs (i.e. CAM I and CAM II) is established.

2.2 Slab tracks for HSR: an overview

2.2.1 Introduction

Slab track, also called nonballasted or ballastless track, is a modern form of track structure where the ballast layer is replaced by Portland cement concrete (PCC) or asphalt concrete (AC).

Nowadays, slab tracks are being widely constructed in HSR networks in Japan, Germany and China (Ando et al., 2001, Bastin, 2006, Jin et al., 2006). As early as 1965, the former Japanese National Railway (JNR) started to develop 'new track structures' in order to address the high maintenance costs incurred in its first HSR in 1964, and this finally led to the invention of a Shinkansen slab track system. As of 2007, 57 % of the Shinkansen network in Japan has been constructed with this slab track system (Takai, 2007). On the other hand, German built the earliest test line for slab tracks in 1972 and since then has developed more than 20 different track forms (Eisenmann et al., 1994). From 1991 until now, Deutsche Bahn AG (German Railway, abbreviated as DB) has increasingly used different slab tracks on the high-speed lines (HSL) in Germany (Liu et al., 2010). In the past 20 years or so, the world has seen a revolutionary development in the application of slab track systems in China. During the period from 2008 to 2014, it has been estimated that over 90 % of the new PDLs in China have been built with slab track systems with a design speed of 350 km/h. Without any doubt, China now possesses the longest network of slab tracks in the world. In other countries like Netherlands, Austria, Italy, Spain, South Korea, and etc., this new track technology has also been used in part of their HSR lines.

Compared with the conventional ballasted track, it has been generally agreed that the slab tracks have the following advantages (Esveld, 2001, Fumey et al., 2002, Lichtberger, 2005, Bastin, 2006).

- Reduced height and weight of the track structure;
- Higher track precision, stability and lateral resistance;

- Higher availability, punctuality and much less traffic hindrance (thanks to practically little or no maintenance for the track);
- Increased service life and lower life-cycle costs (LCC);
- Flexibility and end-to-end effectiveness in applications;
- No problems with churning up of ballast at high speed.

Meanwhile, their disadvantages are also obvious (Esveld, 2001, Fumey et al., 2002, Lichtberger, 2005, fib, 2006), which include:

- Longer construction time;
- Higher initial construction costs;
- Higher level of vibration and noise emission during service;
- More time and efforts needed for the rehabilitation in the event of a derailment or any damage to the track.

Nonetheless, nonballasted or slab tracks still showcase apparent advantages over the traditional ballasted track throughout their whole design life based on the life-cycle analysis (LCA) from technical, economic and environmental aspects (Hanna, 1981, Zoeteman and Esveld, 1999, Koriath et al., 2003, Kiani et al., 2008). This is, in particular, the case when a new HSR line is to be constructed. In the future, with an increase in train speed or axle load or a combination of both, it is strongly believed that more and more countries across the world would realise the importance of slab tracks and make favourable decisions to build suitable railway track systems for their own HSR lines. Such a trend is unstoppable in a foreseeable future.

To better understand the concept of slab tracks, in the following sections, the origin of the railway track as well as the traditional ballasted track, which is the main track form in most railway lines around the world and even in some HSR lines of countries like France and the UK, are firstly reviewed. Then, among the different slab tracks, the prefabricated concrete slab tracks, which are the most widely-constructed systems in HSR, are introduced in detail. Finally, the two prevailing slab tracks used in China's HSR network, namely CRTS I and CRTS II, are presented, and primary functions played by the CAMs in these two track structures are discussed.

2.2.2 Ballasted track

Railway track has changed little in concept since the world's first commercial railway line was built in the northern England in the middle of 1820s (Iwnicki, 2009). Even in today's world, most of the railway track across the globe still takes the form of conventional ballasted track (as shown in **Fig 2.1**), where two longitudinal rails are mounted onto the transversely-arranged sleepers (mostly manufactured from wood or concrete). The sleepers sit on a bed of crushed rocks, namely ballast, which is laid above the subgrade (Dahlberg, 2006). Fastenings or railpads are basic components used to connect the rails to the sleepers, and a sub ballast layer, as a transition layer, is compacted between the ballast and the subgrade.

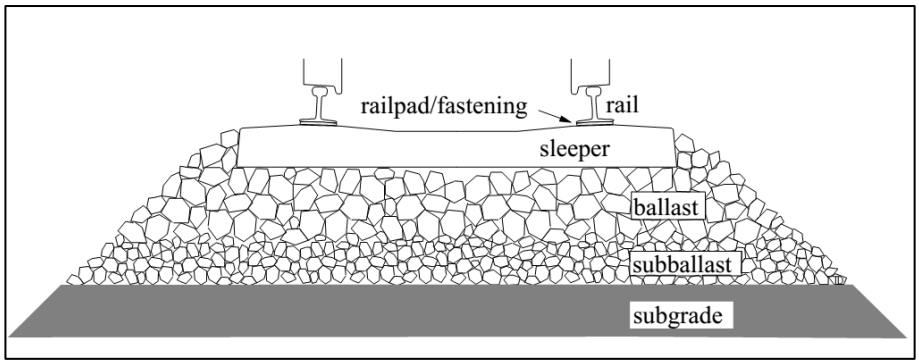

Fig 2.1 Cross section of conventional ballasted track (Dahlberg, 2003)

Because of this simple design, the traditional ballasted track is easy and quick to lay, maintain and renovate at a relatively low cost. In addition to two basic functions, i.e. guiding the train and carrying the load (Dahlberg, 2006), the ballasted track has also demonstrated high elasticity, strong noise-absorbing capacity (Esveld, 1997) and very good drainage properties. Nevertheless, the ballasted track has shown a poor lateral resistance (Esveld, 2001). If trains run directly on such a railway track at high speed, it tends to accelerate the ballast fouling and cause differential settlements. To ensure the operation safety of the trains, in this case, regular routine maintenance is required more frequently, leading to higher maintenance costs and reduced availability. Therefore, the ballasted track system is usually considered not suitable for HSR.

2.2.3 Slab tracks used in HSR

2.2.3.1 Introduction

Since the mid-1960s, increasingly, different types of slab tracks have been developed and constructed in HSR lines across the world, but there is no such a unified classification for them at present. Various classifications have been proposed and they could be categorised into either 4 groups (Tayabji and Bilow, 2001), 5 groups (britpave), 6 groups (Esveld, 2001, Lichtberger, 2005, Schilder and Diederich, 2007, Quante and Ogilvie, 2001) or even 7 groups (UIC). This has, unnecessarily, caused lots of confusion. To increase the clarity, a new classification system has been proposed in this thesis as shown in **Table 2.1**, which divides the slab tracks into 8 groups, according to the construction method and the top-down superstructure.

From this table, it can be immediately noticed that most of the slab tracks are manufactured from concrete, which means relatively high stiffness for the track structure. In terms of the construction method, monolithic construction is the most preferred, compared with the direct installation. In most circumstances, the two rails are discretely supported in the traditional way on sleepers, but there is a future trend to use concrete track slabs, either precast or cast-in-place, to replace the traditional sleepers, albeit sleepers are still used in some slab track systems, such as Rheda and Züblin. Amongst different slab tracks, Shinkansen in Japan and Bögl in Germany, as highlighted in red font in the table, are the two most widely-constructed slab track systems in the world (Michas, 2012), and both systems are under the category of prefabricated concrete slab tracks. Furthermore, in China, these two slab tracks, under the name of CRTS I and CRTS II, have been widely used to construct the world longest HSR network. Therefore, the following section mainly focuses on the review of prefabricated concrete slab tracks, including CRTS I and CRTS II used in China’s HSR network.

Ballast-less or Slab Tracks							
Direct Installation		**Monolithic Construction**					
Discrete Rail Support						**Continuous Rail Support**	
With Sleepers				**Without Sleepers**			
Sleepers on top of asphalt or concrete roadbeds		Sleepers in concrete		Prefabricated concrete slabs	Monolithic in-situ concrete slabs	Embedded rail	Clamped rail
AC	PCC	Embedded	Encased				
ATD	BTD	Rheda family	Sonneville	**Shinkansen**	PACT	ERC	Cocon
GETRAC	NFF	Heitkamp	Stedef	**Bögl**	Hochtief / FFC	Edilon	ERL
Walter	Corus	Züblin	Walo	ÖBB-OPRR	BES / BTE	BBEST	SFF
SATO			STR	IPA	NBU	Deck Track	SAARGUMMI
FFYS			IDBT	CRTS I, II, III	NBT		
IVES				PCAT	DFST		

Table 2.1 Classification of slab tracks

2.2.3.2 Prefabricated concrete slab tracks

Generally, there are three different types of prefabricated concrete slab track systems, Shinkansen, Bögl and ÖBB-OPRR. In this section, a brief introduction to these slab tracks and their applications is given below.

1. Shinkansen / IPA /CRTS I

Since 1972, prefabricated concrete slab tracks have been successfully built in Shinkansen. The Shinkansen slab track (shown in **Fig 2.2**) is characterised by precast top RC track slabs and an intermediate layer made of CAMs with high A/Cs (i.e., CAM-I). Along the railway line, slabs are separately arranged with free end-to-end restraints, and CAM-I was poured into perfusion bags tailor-made by non-woven fabrics. To resist the lateral and longitudinal forces, circular concrete stoppers or bollards are designed and cast in place as part of the concrete roadbed, and after final installation, the gap between stoppers and slabs is filled with an expanded polyurethane (EPU). After more than 40 years in service (Takai, 2007), although in different track forms as shown in **Fig 2.3**, The Shinkansen slab track has proved to be a safe, economical and effective alternative to the traditional ballasted track.

Following its success in Japan, this technique has been introduced to Italy and China, leading to the development of two similar slab track systems in each country, i.e. IPA in Italy and CRTS I in China, respectively. However, these two systems have some differences from the original Shinkansen slab track. The most significant difference between IPA and the Shinkansen lies in the stoppers or bollards which have been named as locating lugs in IPA, and these are precast along with the concrete slabs, instead of being cast in-place in the concrete roadbed (Round, 1993). In China, CRTS-I is mainly built on HSR in the north-eastern region where the weather is considered to be comparable to that in Japan, for example, Ha-Da PDL linking Harbin to Dalian (shown in **Fig 2.4**). However, in some applications, particularly in long tunnels, perfusion bags are said to be no longer used to hold the CAM-I, and fresh CAM-I is directly injected into the gap during construction.

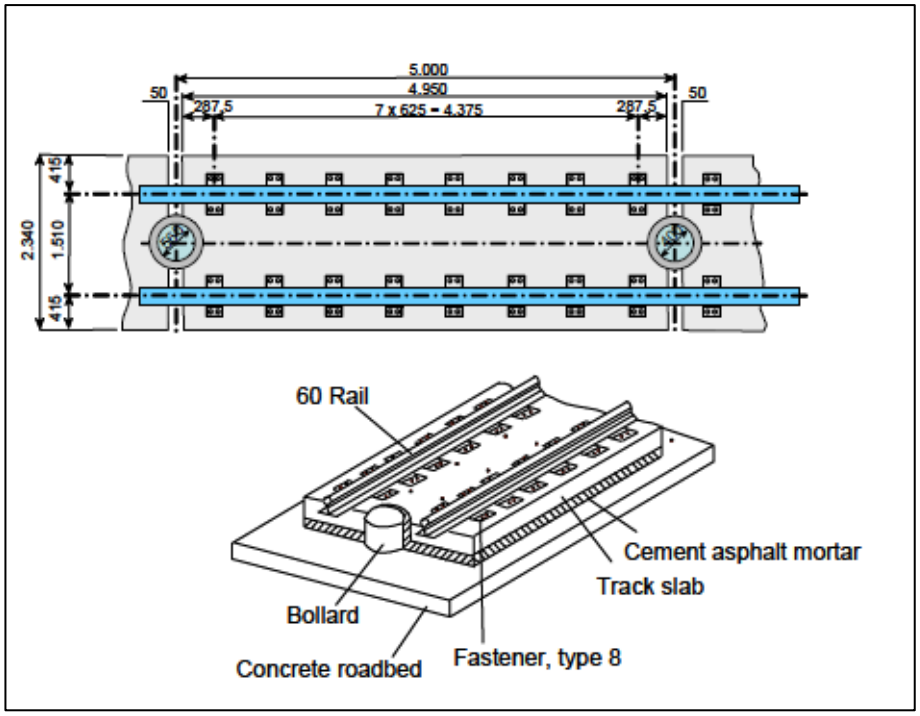

Fig 2.2 Shinkansen slab track (Esveld, 2003a)

(a)

(b)

Fig 2.3 Shinkansen slab tracks in Japan: (a) Type RA; (b) Type J (JRTT)

Fig 2.4 Shinkansen slab track on Ha-Da PDL of Northeast China

2. Bögl / CRTS II

Bögl is another famous prefabricated concrete slab track owned by Max Bögl Group. It is, at present, the most-commonly constructed slab track system worldwide (Michas, 2012) since the first test line built in Germany in 1977 (Schöll, 2008). Different from the Shinkansen slabs, Bögl slabs are prestressed in the transverse direction and connected continuously in the longitudinal direction by buckets and nuts (shown clearly in **Fig 2.5**). On the surface of the top slabs, there are designed transversal cracking joints, to allow cracking to some extent during service, and grouting holes, to inject a material called bitumen-cement gout, namely CAM-II, as the intermediate layer.

In addition to its application in the HSL in Germany, Bögl slab track was also used in Jing-Jin (Beijing-Tianjin) ICE, for the first time in China, in 2006 (MaxBögl) (seen from **Fig 2.6**). Later, it was then adopted into PDLs like Jing-Wu (Beijing-Wuhan) and Jing-Hu (Beijing-Shanghai), formally named as CRTS II under Chinese system.

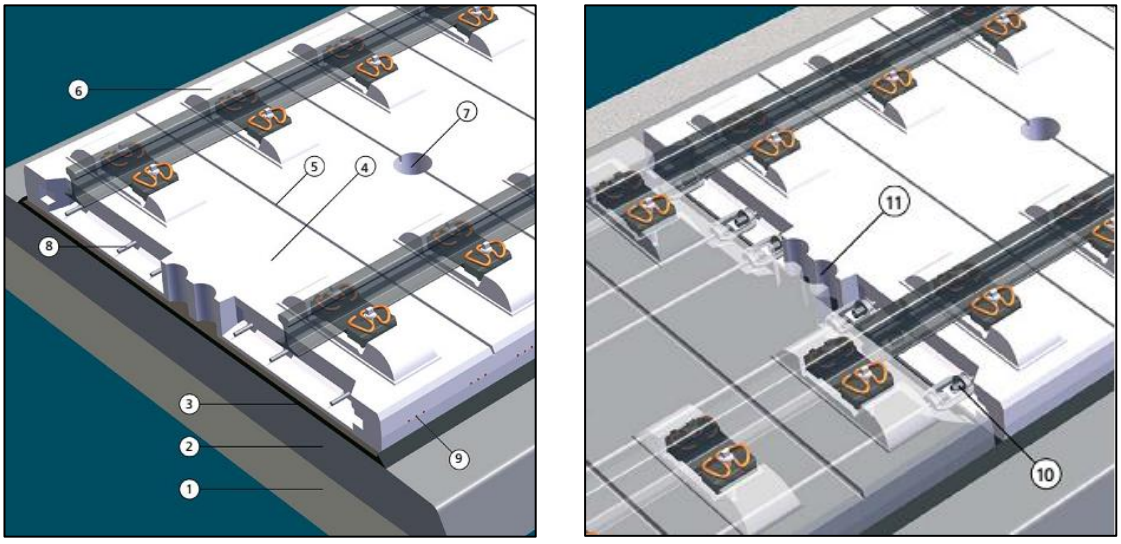

Fig 2.5 Structural components of Bögl (MaxBögl): 1 Frost protection layer (FPL); 2 Hydraulically bonded layer (HBL); 3 Bitumen-cement grout; 4 Precast slab; 5 Design cracking joint; 6 Rail support; 7 Grouting holes; 8 GEWI Steel; 9 Pre-stressed steel; 10 Turn-buckets and nuts; 11 Construction joint

(a)

(b)

Fig 2.6 Bögl slab tracks on (a) the NBS Nuremberg–Ingolstadt or (b) Jing-Jin ICE (MaxBögl)

3.ÖBB-PORR

ÖBB-PORR (shown in **Fig 2.7**) is a slab track system developed in Austria and for the first time constructed as a test track in 1989 (Fumey et al., 2002). Its unique characteristics include using track base plates as the upper layer with

large rectangular openings (the top view in **Fig 2.7**) and using a self-compacting concrete (SCC) to replace CAMs as the cushion layer. Similar to Shinkansen slabs, the track plates are placed along the railway line one by one with free ends. The main difference is that those openings, on the one hand, are used as grouting holes for the SCC and on the other hand, can be combined into a reinforcement network with the infilling SCC, functioning as shearing panels to provide longitudinal and lateral fixings for the track plates. Under these plates, moreover, a layer of an elastomer, as shown by the red line in **Fig 2.7**, is glued to resist vibrations.

This track system has mainly been constructed in Austria (seen from **Fig 2.8**) and Germany (Pichler and Fenske, 2013), not only on bridges and in tunnels, but also on open earthwork sections.

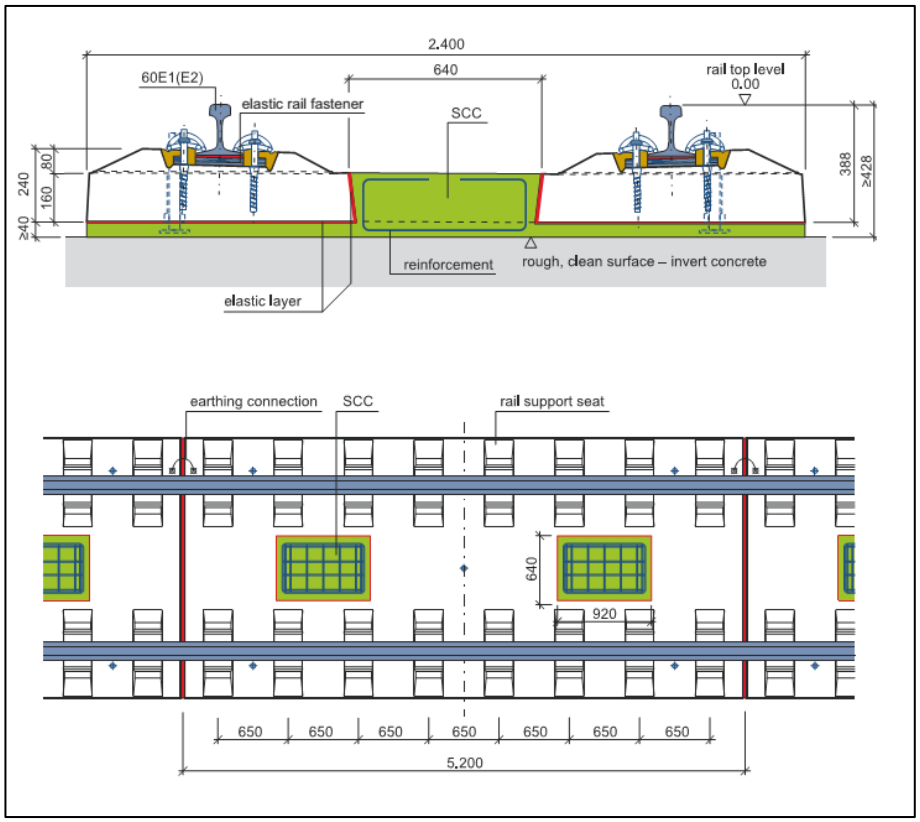

Fig 2.7 Cross section and top view of ÖBB–PORR (PORR)

Fig 2.8 ÖBB–PORR in Langenlebarn, Austria (Pichler and Fenske, 2013)

Other similar slab track systems (as shown in **Fig 2.9** and **Fig 2.10)** have been developed as well in different countries since then, but, evidently, primarily based on the fundamental principles of the above three slab track systems. Their characteristics in common are:

- Prefabricated concrete top slab or plate;
- Cast-in-place concrete roadbed on a treated foundation;
- An intermediate elastic layer cushioned between the above two.

It is found that, interestingly, the design of these prefabricated concrete slab tracks mentioned above is very similar to that of pavements, except that loads are applied to the two rails which are directly connected to the concrete slabs. Using an analogy between them, in this sense, structural performances of such a group of slab tracks could be reasonably simulated and understood. It is more than evident that, considering the difference in mechanical properties of the cushion layer, Shinkansen and Bögl slab tracks are analogical to semi-rigid pavements while ÖBB-OPRR is more like a concrete or rigid pavement.

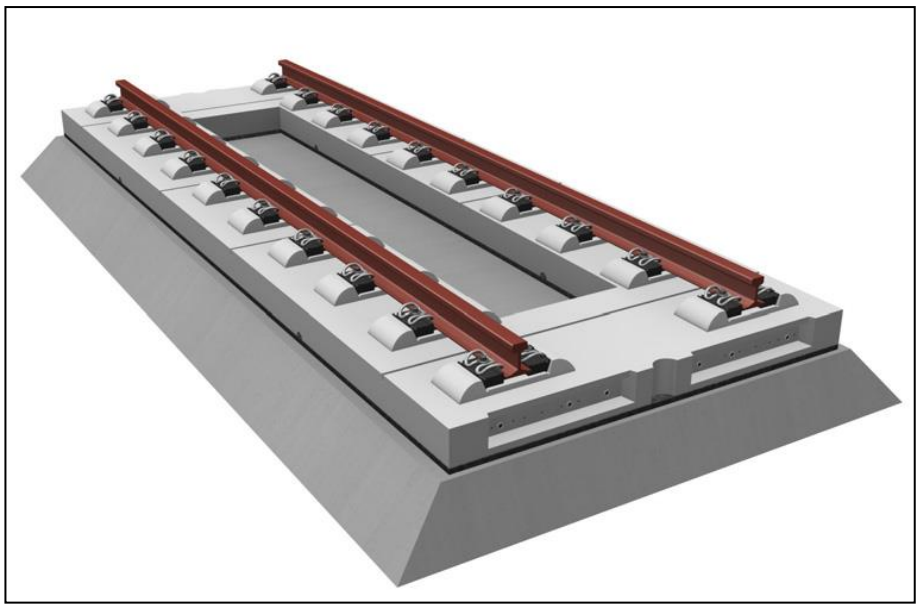

(a)

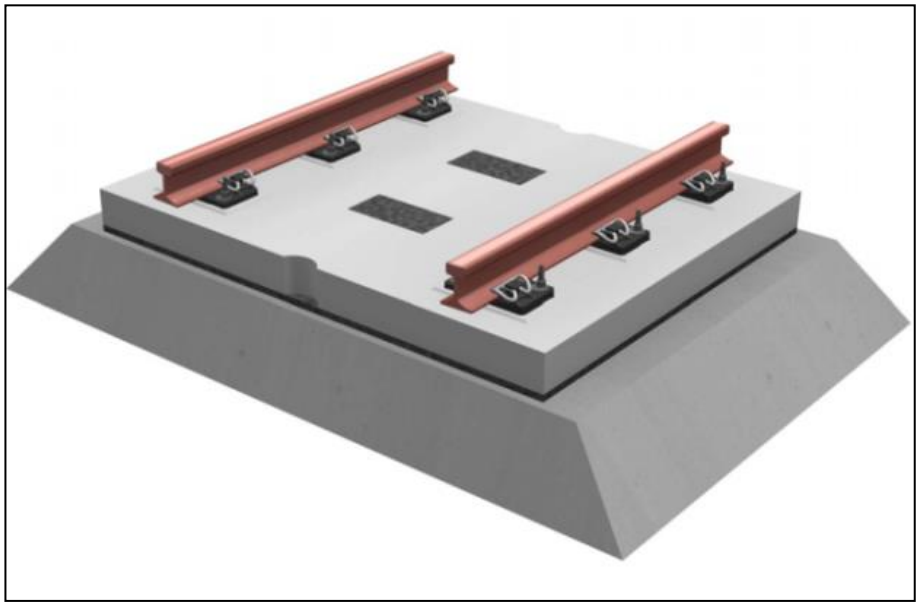

(b)

Fig 2.9 Prefabricated concrete slab tracks in South Korea: (a) Type A; (b) Type B (Jang et al., 2008)

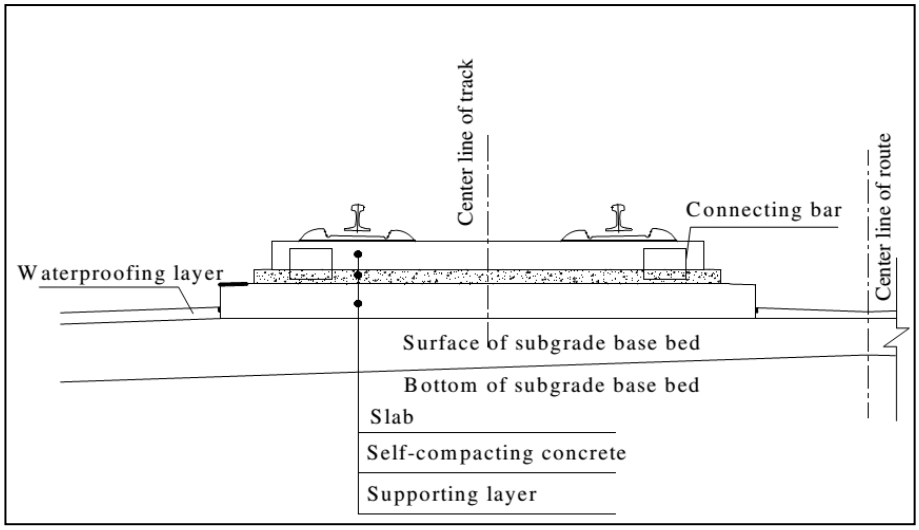

(a)

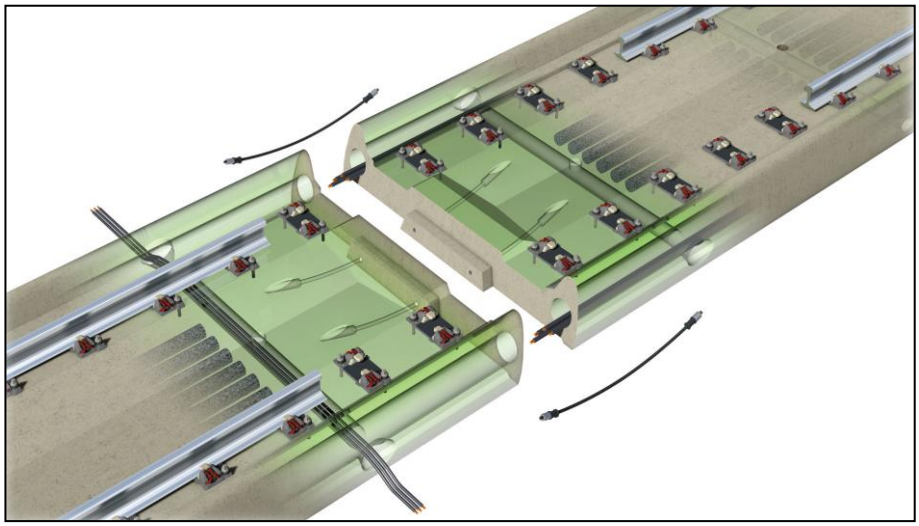

(b)

Fig 2.10 Structures of (a) CRTS III (Zhu, 2012) and (b) PCAT (PCAT)

2.2.3.3 CRTS I and II used in China's HSR network

During the period between 1999 to 2006, two test HSR lines, Qin-Shen PDL and Sui-Yu PDL (Ren et al., 2009), were purposefully constructed in China to test and compare different slab tracks. After a comprehensive consideration of the overall cost, construction technique and structural performance, Shinkansen and Bögl slab tracks became the preferences (later named as CRTS I and

CRTS II (seen from **Fig 2.11**), respectively, under Chinese system). At present, these two are the main slab track forms in China's huge HSR network. **Table 2.2** shows typical slab tracks built in China's main HSR lines, among which over half of them are built with CRTS I or CRTS II.

The popularity and the experience of these two slab tracks in China's HSR network have, once again, clearly demonstrated their advantages over other slab tracks. For example, prefabricated slabs can be manufactured in a factory with high quality and high precision; a combination of top-down and bottom-up construction can speed up the track construction, and, the adjustable CAM layers can facilitate possible rehabilitation during service. But there are some issues in practice, one of which rests with the CAM layer. Normally, slab tracks have a design life of 50-60 years. However, the design life of the CAM layer is about 20-30 years, only half of that of slab tracks, which indicates that, during the life cycle, at least one renewal or replacement of the whole layer is needed. Unfortunately, cases of the deterioration of this CAM layer have already been reported in China within just a few years' operation (as mentioned in **Section 1.1.3** of **Chapter 1)**, indicating the seriousness of this issue in reality.

(a)

(b)

Fig 2.11 Slab tracks used in China (a) CRTS I at Qin-Shen PDL (Freudenstein et al., 2010); (b) CRTS II at Jing-Jin ICE (MaxBögl)

Table 2.2 CRTS I and CRTS II used in China's HSR network

HSR	Designed Speed	Length (km)	CRTS	Length (km)	Open Date
Jing-Jin ICE	350 km/h	115	II	115	01/08/2008
Jing-Hu PDL	350 km/h	1433	II (I*)	1268	16/10/2012
Ha-Da PDL	350 km/h	904	I	847	01/12/2012
Jing-Wu PDL	350 km/h	1121	II (I*)	975	26/12/2012

* denotes that CRTS I was built as well in some tunnels along the HSR line but the total length is unknown.

2.2.4 Functions of CAMs in CRTS I and II

In the two prevailing slab tracks used in China's HSR network, namely CRTS I and CRTS II, the intermediate layer is an important component and for different track systems, different CAMs have been used. However, why such composite materials are chosen and what their functions remain unclear. To answer these basic questions, models on simulating the structural performances of CRTS I and II have been reviewed and presented below, in an attempt to illustrate the primary functions of CAMs in slab track structures.

As structural materials cushioned in CRTS I and II, CAMs play at least two important roles or functions, which can be indirectly verified by numerical modelling on dynamics of these two slab tracks. It is easy to understand that, in either CRTS I or CRTS II, the fundamental function of CAMs is to sustain static and dynamic traffic loads from wheel-rail interactions and transmit them to the foundation. In corresponding modelling work, the CAM layer can, thus, be simplified and treated as a series of elastic springs (**Fig 2.12**), providing basic elasticity for the track system (Yen and Lee, 2007, Ren et al., 2010). In addition to the elasticity quantified by the elastic modulus, E, or the stiffness, k, the other more important function provided by the CAM layer is structural damping, in other words, to resist or attenuate the vibrations generated by moving trains at high speed. To take such an effect into account in the dynamics of CRTS I or CRTS II, the CAM layer is always modelled as a spring-dashpot system (**Fig 2.13**) (Zhai et al., 1999, Zhai et al., 2009, Lei and Zhang, 2011, Lei and Wang, 2014). This viscous damping is well characterised by the damping coefficient, c, or the damping ratio, ξ. And here, it can be easily recognised that one of the main reasons for choosing CAMs as a cushion layer is to introduce elasticity and viscous damping into CRTS I or CRTS II. As we know, meanwhile, CAMs are typically viscoelastic materials, suggesting that there exists an intrinsic relationship between their viscoelasticity as engineering materials and structural functions in the track system, especially damping.

In a few cases, only the function of the elasticity of CAMs is considered in the analysis of the vibrations of CRTS I or CRTS II under dynamic traffic loads without considering the damping effect, which seems too ideal and far from the

practice. So, to simulate the vibrations more accurately, in most cases, both effects of the CAM layer in slab tracks, i.e. elasticity and damping, are considered as the input of material parameters, as listed in **Table 2.3**. From this table, we can see that the elasticity of the CAM layer is well represented by the stiffness, *k*, or the modulus of elasticity, *E*, but their values vary in different references and sometimes seems contradictory. As regard to the viscous damping, in the same way, the values of damping coefficient or damping ratio are found to be arbitrary. Therefore, it is necessary, from the viewpoint of a structural engineer, to clarify these fundamental coefficients, which will be detailed in **Section 5.5** of **Chapter 5**.

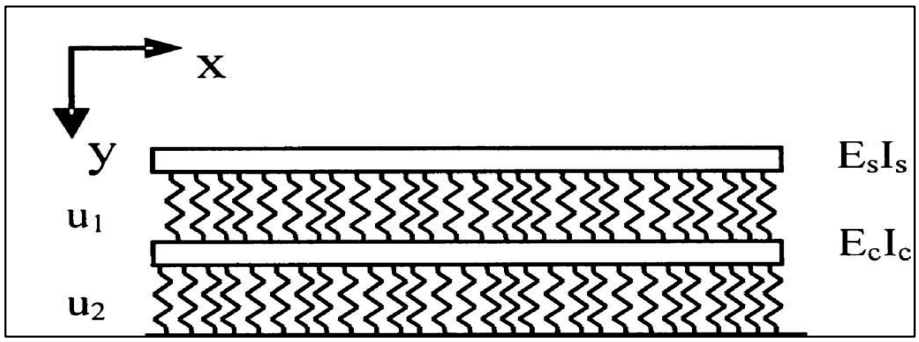

(a)

(b)

Fig 2.12 The CAM layer simplified as a series of springs in (a) CRTS I (Yen and Lee, 2007) or (b) CRTS II (Ren et al., 2010)

Table 2.3 Elasticity and damping coefficients for the CAM layer used in numerical modelling of CRTS I and II

CRTS	Coefficients		Reference
	Elasticity	Damping	
I	k =1.25×10^9 N/m^3 or E=300 MPa	c =8.3×10^4 N.s/m^2	(Zhai et al., 1999, Zhai et al., 2009, Zhai et al., 2010)
	k =1.25×10^9 N/m^3	c =3.458×10^4 N.s/m^3	(Zhao, 2011)
	E=100 MPa	ξ=0.20	(Bian et al., 2011)
	E=200 MPa or 400 MPa	ξ=0.035	(Fang et al., 2011, Fang and Cerdas, 2015)
	E=100 MPa	c =8.3×10^4 N.s/m	(Zhang et al., 2012a)
	k =2×1.5×10^9 N/m^2	c =2×8.3×10^4 N.s/m^2	(Zeng et al., 2014)
	E=100 MPa	ξ=0.10	(Poveda et al., 2015)
II	k =3.3×10^{10} N/m^3	c =3.458×10^4 N.s/m^3	(HE et al., 2007)
	k =7.0×10^8 N/m^2	c =8.0×10^5 N.s/m^2	(Hu and Wu, 2010)
	k =0.9×10^9 N/m	c =8.3×10^4 N.s/m	(Lei and Zhang, 2011, Lei and Wang, 2014)
	E=7,000-10,000MPa	N/A	(Sun et al., 2013)
	k =4.335×10^{11} N/m	c =1.0×10^6 N.s/m	(Zhang et al., 2014)

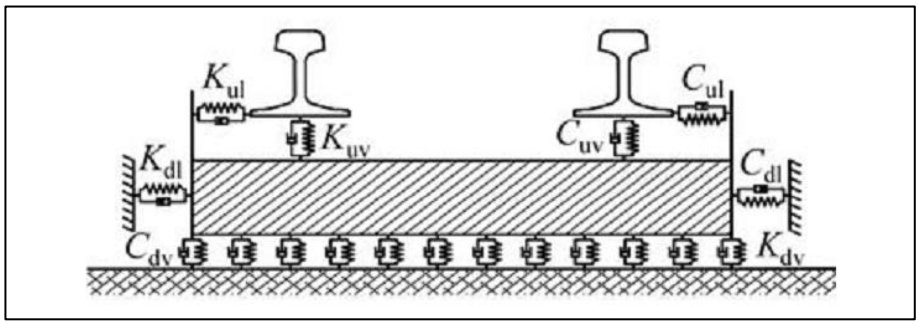

(a)

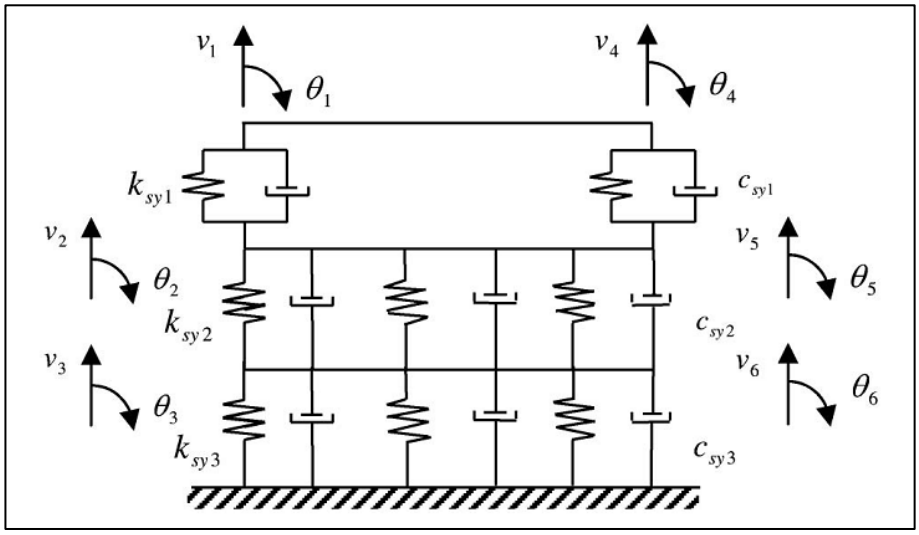

(b)

Fig 2.13 The CAM layer modelled as a spring-dashpot system in (a) CRTS I (Xiang et al., 2009) or (b) CRTS II (Lei and Zhang, 2011)

2.2.5 Summary

In the first part of this review chapter, an overview of the different slab tracks used in the HSR networks around the world is presented and the main attention has been paid to the two prefabricated concrete slab tracks most widely used in China, CRTS I and CRTS II, where CAMs have been frequently used as the cushion layer. Based on all the information presented, the following key points can be summarised.

1. The future trend to use different types of slab tracks in HSR lines around the world is unstoppable.
2. Prefabricated concrete slab tracks are the most popular systems used in the HSR network in the world, and they are similar to pavements in design. Shinkansen and Bögl slab tracks are analogical to semi-rigid pavements while ÖBB-PORR is more like a concrete or rigid pavement.
3. In China's HSR network, CRTS I and CRTS II are the most widely-used systems because of their advantages over other slab tracks, but in practice, there are some issues with the CAM layer.
4. The primary functions of the CAM layer, as a spring-dashpot system, are to provide both elasticity and damping for CRTS I and CRTS II.

2.3 Static mechanical properties of CAMs

2.3.1 Introduction

CAMs are composite materials primarily consisting of Portland cement, asphalt emulsion, fine aggregate, water and a small addition of chemical admixtures. Their properties are mainly influenced by the relative content of asphalt binder in the emulsion and Portland cement, i.e. A/C, which is reported to be ranging from around 0.2 to 1.2 (Wang et al., 2008f, Liu et al., 2009).

It is well known that PCC and AC are two most popular building materials used in a wide range of applications, particularly road pavements, and their binding materials are Portland cement and asphalt binder, respectively. As paving materials in pavements, both PCC and AC have their own advantages and disadvantages. Generally, for instance, PCC has a higher initial cost than AC, but lasts longer and requires lower maintenance costs during its service life (Delatte, 2008). On the other hand, AC is easier to construct, maintain and repair (Fwa, 2006), but highly susceptible to temperature and moisture, while for PCC, cracking remains to have been an unresolved issue for a long time (Huang, 2004). In this context, it seems as if composites of Portland cement and asphalt emulsion, combining some characteristics of PCC and AC, could not be a new concept. However, unlike PCC or AC, these composites have been not fully understood at present and related research work with regards to the composite mechanisms is relatively limited. Furthermore, the applications of these composites are found to be restricted to some specialised ones and in a small amount, such as surfacing, cold-in-place recycling (CIR) and rehabilitation in pavements, sealing, patching, building waterproofing, and etc. (Li et al., 1998a, Li et al., 1998b, Li et al., 1999, Hu et al., 2003, Pouliot et al., 2003, Song et al., 2006, Yan et al., 2007, Rose and Bryson, 2009, Brown and Needham, 2000a, Issa et al., 2001, Montepara and Guiliani, 2001, Hodgkinson and Visser, 2004, Oruc et al., 2006a, Oruc et al., 2007, Ashteyat and Ramadan, 2009, Jalili and Niazi, 2009), until only recently, CAMs as one of such composites are frequently used in the construction of slab tracks.

In the two prefabricated concrete slab tracks, i.e. CRTS I and CRTS II, CAMs as cushion materials perform at least three fundamental functions. Firstly, during the slab installation stage, the fresh CAMs are used to grout or fill the gap between the prefabricated track slabs and the cast-in-place concrete trackbeds in order to achieve the integrity of the track structure. After hardened, CAMs in service start to fulfil two other structural functions, namely, to transmit traffic loads from the train-rail-slab track interactions to the foundation and, to reduce the vibrations of the track slabs generated by the high-speed trains, which has been verified in **Section 2.2.4**. Owing to the specific functions of CAMs in those two slab tracks, their mechanical properties are of prime concerns and interests for both material scientists and structural engineers, as these properties can be used to guide the formulation design, quality evaluation and structural stress analysis. Therefore, in this section, the static mechanical properties of CAMs have been reviewed in detail. In particular, the composite mechanism of CAMs, including the interactions between Portland cement and asphalt emulsion, the resultant microstructures, and the related test methods and test results, are presented. An attempt is also made at the end of this section to compare the mechanical properties of CAM-I and CAM-II. Based on this, the suitability of the currently adopted test methods for assessing the static mechanical properties of different CAMs is discussed.

2.3.2 CAMs as composites

2.3.2.1 Interactions between Portland cement and asphalt emulsion

Portland cement is a hydraulic binder that starts to set and then hardens once in contact with water because of a series of chemical reactions (so called hydration) between different mineral phases and water (Neville, 1999).

Asphalt emulsion or emulsified asphalt is formed by dispersing small droplets of asphalt binder, or asphalt cement, or bitumen in water. It is solidified or broken down by flocculation and coalescence of asphalt droplets (shown in **Fig 2.14**) (Salomon, 2006). The terms here, asphalt binder, asphalt cement, or bitumen, have been used interchangeably in the literature (Krishnan and Rajagopal, 2003). However, to avoid confusion, the term, asphalt binder, will be used in place of asphalt cement or bitumen throughout this thesis.

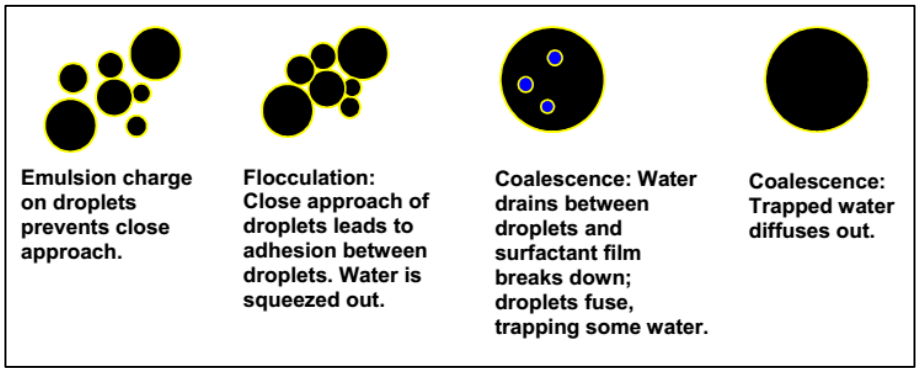

Fig 2.14 Breakdown of asphalt emulsion (Salomon, 2006)

As Portland cement and asphalt emulsion function under two different binding mechanisms, when they are mixed together, the interactions between them take place in such a way that the adsorption of asphalt droplets onto the cement grains retards the hydration whilst the consumption of water in the process of cement hydration accelerates the breakdown of asphalt emulsion as illustrated in **Fig 2.15** (Hu et al., 2009, Yang et al., 2010, Zhang et al., 2012b). Experimentally, they are mainly reflected in two aspects, namely the retarding effect on the hydration of Portland cement and the accelerating effect on the setting or breaking of asphalt emulsion.

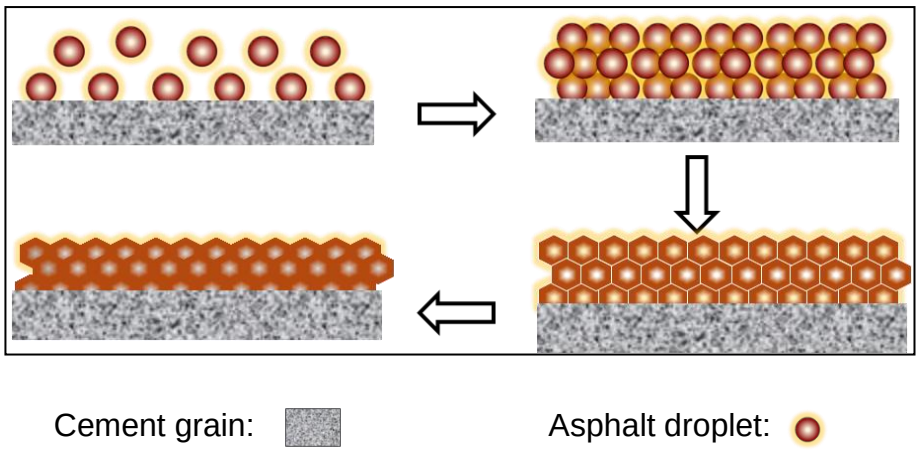

Fig 2.15 Schematics of the asphalt membrane formation on cement grains (Zhang et al., 2012b)

For the first time, Wang et al. (2008b) studied the setting time of Portland cement with different additions of asphalt emulsion and found that the delayed setting is due to the retarding effect of asphalt emulsion on the hydration of Portland cement and this was, in turn, influenced by the A/C and the type of Portland cement used (Wang et al., 2008c). By means of calorimetry during the hydration process, Zhang et al. (2010) and Yang et al. (2010) recorded the retarding effect on cement hydration in details and reconfirmed that a higher A/C leads to a greater retarding effect. Further research work (Zhang et al., 2012b) showed that the addition of anionic asphalt emulsion into Portland cement results in a more significant retarding effect than cationic asphalt emulsion, which is probably attributed to the difference in their saturation adsorption on cement grains. Regarding the accelerating effect on the setting, or breaking of asphalt emulsion, on the contrary, a little work could be found. The work of James et al. (1996) on asphalt emulsion mixtures demonstrated that a small addition of ordinary Portland cement, at best around 5% of the total by weight, accelerates the setting process and shortens the curing time needed. Later research work reaffirmed this conclusion (Brown and Needham, 2000a, Oruc et al., 2007).

Using the measurement of X-ray diffraction (XRD), Yang et al. (2010) firmly proved that, except for cement hydration, there is no other chemical reaction to

be detected, which indicates that, whatever the effect is, the interactions between Portland cement and asphalt emulsion are most probably physical.

2.3.2.2 The microstructures of cement-asphalt binders

As the hydration of Portland cement and the breakdown of asphalt emulsion proceed, a cobinder system is formed in the end, which is termed as a cement-asphalt binder (CAB). In this system, as it is called, the two binding phases are hardened Portland cement paste (hcp) and asphalt binder, resulting from cement hydration and emulsion breaking, respectively.

Portland cement consists of four main solid oxide phases, namely alite (C_3S), belite (C_2S), aluminate (C_3A) and ferrite (CA_4F), all of which can react with water chemically. When Portland cement is mixed with water, a series of chemical reactions take place. As a result, Portland cement and water are consumed and the hydration products are produced, such as calcium silicate hydrate (C-S-H), crystalline calcium hydroxide (CH) and ettringite (AFt). This process results in the formation of hcp as the binding phase of cement-based materials like mortars and concretes. Further knowledge on cement hydration and its hydration products can be obtained in other references (Tailor, 1997, Bensted and Barnes, 2002, Hewlett, 2004). In the hcp, the C-S-H gel is the main component, and responsible for the binding and strength development. As an amorphous colloidal gel, the C-S-H exists in a variety of forms in the hcp and contains pores in different size and shape. When cement hydration comes to an end, the porous C-S-H gel occupies most volume of the hcp and forms a highly complex microstructure that could be represented by one of the models for hcp proposed by Powers and Brownyard (1946), Feldman and Sereda (1970), Wittmann (1977), and Jennings and Tennis (1994) as depicted in **Fig 2.16**. The Powers-Brownyard model, among the four models, is the most classical one. To make it understood further, after more than half a century, Professor Brouwers recapitulated this classical model and refined it, enabling the quantification of the mass and volume distribution of various hydration products as a function of the composition of the clinker, water-cement ratio and degree of cement hydration (Brouwers, 2004, Brouwers, 2005, Brouwers, 2007, Brouwers, 2012).

Theoretically, therefore, the composition of any hcp and the volume fractions of every component in this hcp can be derived.

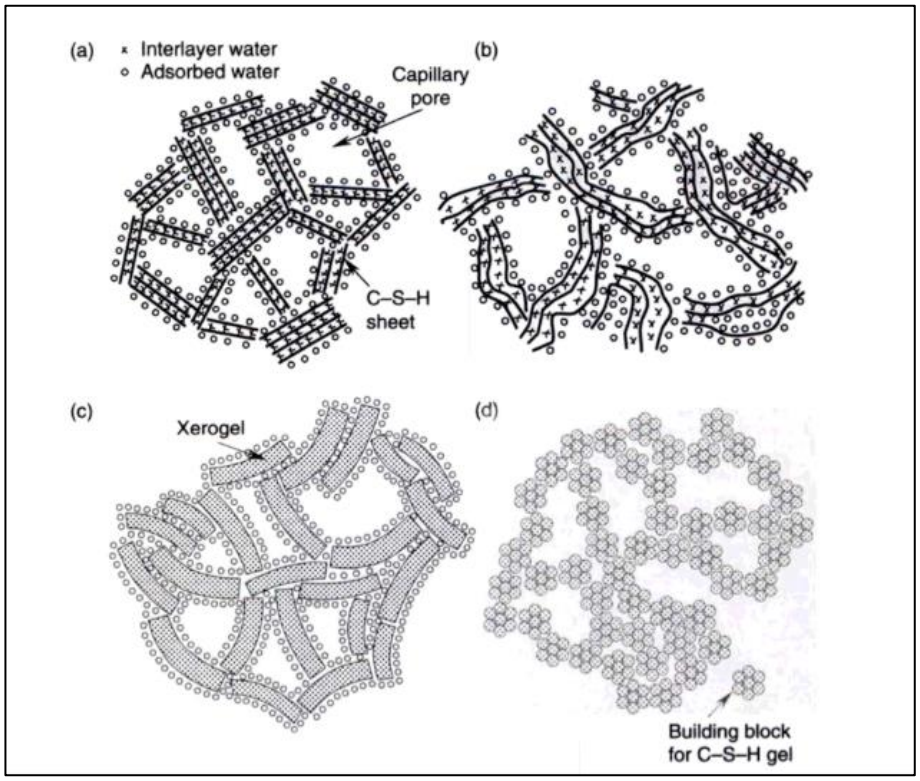

Fig 2.16 Schematic representation of the most commonly mentioned models for C-S-H gel. (a) the Powers-Brownyard model; (b) the Feldman-Sereda model; (c) the Munich model by F. Wittmann; and (d) the Colloid model by H. Jennings and P. Tennis (Aligizaki, 2005)

Asphalt binder, on the other hand, is traditionally regarded as a colloidal system and its internal microstructure, no matter whether it is a SOL type or GEL type as schematically shown in **Fig 2.17** (Read and Whiteoak, 2003), is largely decided by the four main chemical components, namely asphaltenes, resins, aromatics and saturates (Loeber et al., 1998, Lesueur, 2009). As an organic adhesive material, generally, asphalt binder itself has an extremely complicated microstructure. In a macroscale level, however, it can be reasonably considered into one continuous phase.

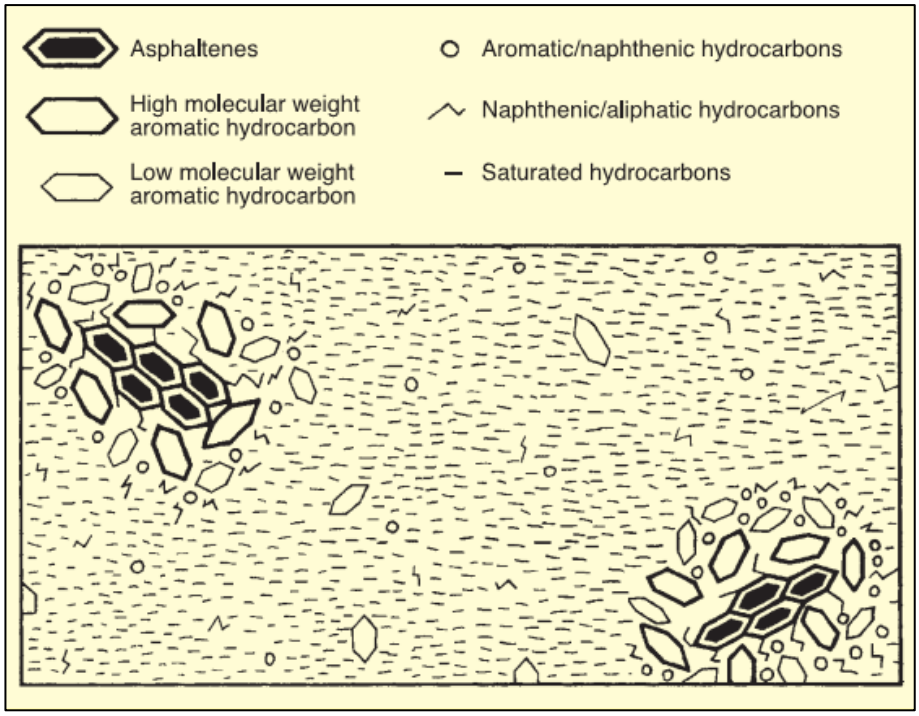

(a)

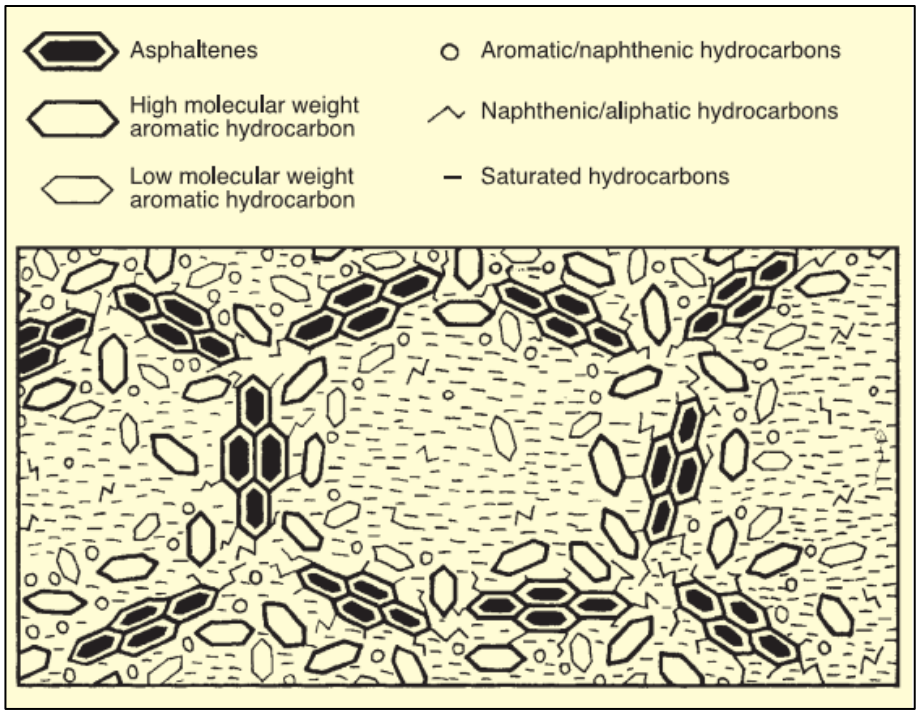

(b)

Fig 2.17 Schematic representation of a (a) SOL type or (b) GEL type asphalt binder (Read and Whiteoak, 2003)

As the cobinder, hcp and asphalt binder physically constitute a hardened CAB, the microstructure of which, obviously, is controlled by the content of hcp relative to asphalt binder, in other words, by the A/C. With the change of A/C, hcp or asphalt binder is competitive to be the principal binding material in CABs. Through studying the mechanical properties of CAMs at room temperature with different A/Cs ranging from 0.2 to 1.0, Liu et al. (2009) found that there was a threshold A/C relating to a transition zone in mechanical properties. Some microstructural models were, thus, proposed (Liu et al., 2009, Liu et al., 2013), as encased in **Fig 2.18**, to illustrate their findings. In their models, hcp is the principal binder if A/C is low, whilst asphalt binder replaces hcp as the main phase if A/C becomes very high. In the transition zone, it was presumed that the two binders have equal volume in CABs and form a special microstructure of bicontinuous phases. Based on this assumption, the A/C value was calculated to be around 0.6, which was consistent with the experimental results, though no direct evidence has been provided.

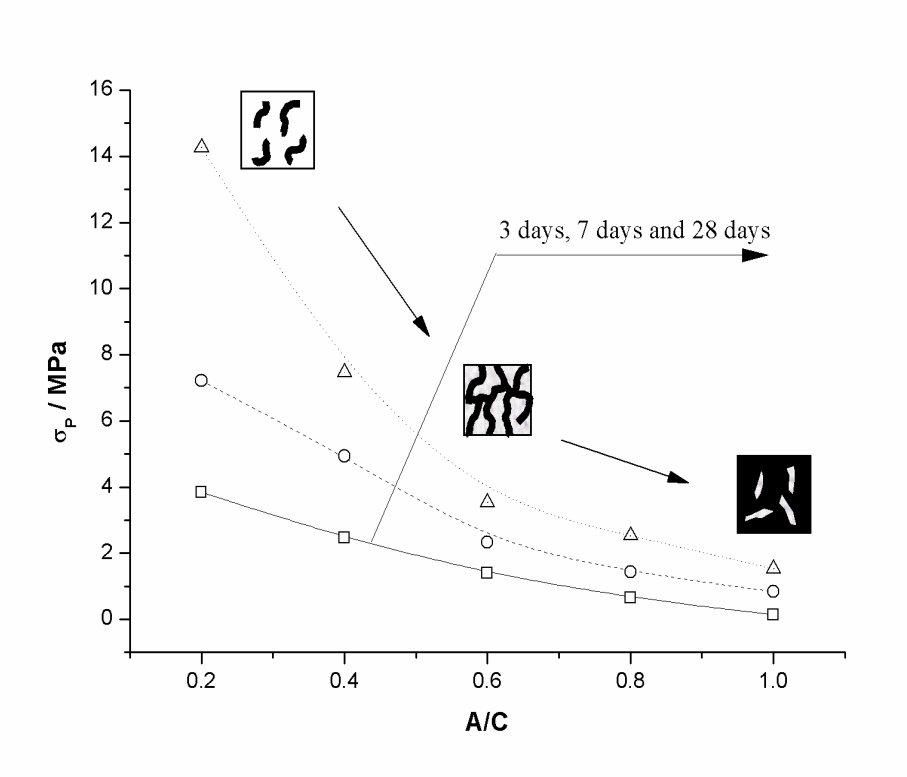

Fig 2.18 Compressive strengths of CAMs and the microstructural models for their binders with different A/Cs (Liu et al., 2013)

Direct observation of the microstructures of hardened CABs, however, is not so easy, which is mainly due to the nature of asphalt binder. Asphalt binder, unlike hcp, is a soft material or semi-solid at ambient temperature and highly sensitive to environmental conditions, such as temperature or pressure. This means that, in the process of sample preparation or during the operation of a microscope, the morphology of the CAB can be easily damaged, especially when the A/C is high. However, using an environmental scanning electron microscopy (ESEM), Yang et al. (2010) investigated the microstructure evolution of one CAB at a A/C of 0.35 within the first 24 hours of hydration, and claimed to observe a hardened skeleton consisting of an interpenetrating network of hydration products and continuous asphalt membrane randomly attached on the surface of the cement hydrates. Similar network microstructures were also observed by a scanning electron microscopy (SEM) at the age of 7 days with a wide range of A/Cs, from low to high (Wang and Li, 2009, Wang and Sha, 2009, Wang et al., 2009b, Wang and Sha, 2010). However, it should be highlighted that all these are just some pilot efforts in elaborating the rather complex microstructure of CABs. Further research work is still needed. It is considered that a good understanding of the microstructures of CABs is important, because just like hcp in cement-based materials (Ramachandran et al., 1981, Aligizaki, 2005), the properties and behaviour of CABs, which are significantly affected by their compositions and microstructures, control the properties and behaviour of their composites including CAMs. This will be discussed in detail in the next section.

2.3.2.3 Cement-asphalt emulsion composites

When aggregates are mixed into CABs, the composite formed is called cement-asphalt emulsion composites (CAEC), which could be generally regarded as a two-phase composite consisting of the matrix phase, i.e. the CAB, and the dispersion phase, i.e. the aggregate.

From the previous review, it can be deduced that the microstructure and the properties of the hardened CAB, which could be subdivided into two main binding phases, namely hcp and asphalt binder, should be the key factors affecting the microstructure and the properties of CAEC. In particular, the A/C could be a decisive parameter. Therefore, based on the A/C, the CAEC can be

categorised into three groups or families as listed in **Table 2.4**. From this classification, it can be noticed that, as A/C increases, the principal phase in CABs turns from hcp into asphalt binder.

Table 2.4 Classification of CAEC

CAEC	A/C	The main phase in CABs
Asphalt emulsion as modifier in the mortars or concretes	< 0.2	hcp
Cement-asphalt emulsion mortars (CAMs) or concretes	0.2 ~ 0.6	hcp
	~ 0.6	hcp and asphalt binder
	0.6 ~ 1.2	asphalt binder
Portland cement as filler in cold asphalt emulsion mixes	> 1.0	asphalt binder

When the A/C is lower than 0.2 (A/C<0.2), the resultant composites falls into the first family of latex-modified mortars or concretes, which is similar to polymer-modified mortars (PMM) or concretes (PMC) (Kardon, 1997, Ohama, 1997). In addition to the retarding effect on cement hydration (as concluded in **Section 2.3.2.1)**, it was found that at the fresh stage the asphalt emulsion has typical plasticizing or water-reducing effects, similar to a role played by superplasticizers in the water-cement system (Li and Liang, 2001). After the mixing, it has been proposed that the adsorption of asphalt droplets onto Portland cement grains prevents the flocculation of cement particles, leading to the improvement in the fresh properties, i.e. workability. However, an obvious improvement in the workability was not observed until the A/C approached 0.2 (Zhang et al., 2012b). In the hardened CAB composites, it should be noticed that when the A/C is lower than 0.2, hcp is the main binding phase and the

asphalt membrane formed by asphalt droplets is mainly incorporated or engulfed into hcp. Consequently, the mechanical properties and durability of the CAECs will be affected. In general, when A/C increases, the strength and the modulus of elasticity of these composites decreases (Pouliot et al., 2003), although flexural strength changed little (Song et al., 2006). But the deformation ability (Xian et al., 2006, Pouliot et al., 2003, Rose and Bryson, 2009) and the durability (Song et al., 2006) of these composites are usually enhanced with more asphalt emulsion incorporated. To conclude, like any other emulsions, asphalt emulsion functions as a cement modifier in these composite materials, mainly to improve their workability at the fresh stage, and to enhance their deformability and durability during the hardening stage.

In cold asphalt emulsion mixes, on the contrary, asphalt binder is the principal binding material and the A/C is relatively high (A/C >1.0). In this case, Portland cement works as an active filler and its product, hcp, is entrapped into the asphalt binder. Due to the consumption of water by cement hydration, which increases the viscosity of asphalt emulsion and raises the rate of coalescence (James et al., 1996, Brown and Needham, 2000b), even a small addition of Portland cement, at best around 5% of the total binder by weight, into cold asphalt emulsion mixes can accelerate the curing process (James et al., 1996). Most importantly, the addition of Portland cement can enhance their mechanical properties (Wang and Wang, 2011), for example, strength (James et al., 1996, Brown and Needham, 2000b, Wang et al., 2005b) and modulus of elasticity (Wang et al., 2005b, Oruc et al., 2006b, Oruc et al., 2007, Ozsahin and Oruc, 2008), improve their resistance to permanent deformation (Oruc et al., 2006b, Oruc et al., 2007) and water damage (James et al., 1996, Oruc et al., 2006b, Oruc et al., 2007), and reduce their temperature susceptibility (Oruc et al., 2006b, Oruc et al., 2007).

The third group of CAEC is the one with intermediate A/Cs, as obviously shown in **Table 2.4**. In this case, when CABs are combined with fine aggregates, it forms cement-asphalt emulsion mortars, i.e. CAMs, the main system to be investigated in this thesis. Moreover, it should be noted that when CABs are combined with both fine and coarse aggregates, this form cement-asphalt

emulsion concretes, which can be used in pavements as a base course (Li et al., 1998a, Li et al., 1998b, Li et al., 1999, Wang, 2004, Zhou et al., 2006). Based on the previous review, this CAEC family could be subdivided into three groups, depending on whether hcp, or asphalt binder, is the principle binding phase in the co-binder system. When the A/C is relatively low, hcp occupies the majority of the total volume in CABs and becomes the main binding material. In this case, the system formed is similar to PMMs or PMCs. However, as the A/C increases, it reaches the transition zone at around 0.6 where the hcp and the asphalt binder have equal volume fraction in the binding phase in hardened CABs. In this zone, some abrupt changes in the fresh properties (Zhang et al., 2011b), curing effects (Liu et al., 2011b), and susceptibility of mechanical properties to temperature (Liu et al., 2013, Kong et al., 2014) have been reported. This could probably be attributed to the bicontinuous phase, in which the interfacial zone between hcp and asphalt binder plays an important role (Kong et al., 2014). If A/C continues to increase, approximately up to the A/Cs used in cold asphalt emulsion mixes, asphalt binder starts to dominate and the hcp starts to act as the secondary part (i.e. as a hydraulic filler). In the light of the A/Cs from the above table and the microstructural aspects of the hardened CABs, it is evident that cement-based materials and asphalt mixture could be considered as the two extreme cases of CAEC. This analogy will be further elaborated in the future discussions in this thesis.

In summary, CAEC can be considered as a hybrid between cement-based materials and asphalt mixtures, in which the hcp is formed by the hydration of Portland cement and the asphalt binder is coalesced from asphalt emulsion. The mixture of hcp and asphalt binder in the hardened matrix, thus, functions together as cobinders or comatrix cementing the fine or coarse aggregates or both as a whole. A/C is the dominant parameter to determine the composition and microstructures of hardened CABs, which, in turn, controls the properties of the composites. CAMs, to a certain extent, can be considered as a special type of CAEC with intermediate A/Cs where the CABs acting as the cobinder and the fine aggregates or sands as the inertial filler or stiffener. It should be stressed that, throughout this thesis, the main emphasis will be given to the CAMs, namely, CAM-I and CAM-II.

2.3.3 Static mechanical properties

Static, quasi-static if strictly speaking, mechanical properties of CAMs refer to the responses to a static load, usually tested in the laboratory under standard conditions, including strength and modulus of elasticity.

To characterise static mechanical properties of different CAMs and, thus, to obtain relevant mechanical parameters, different test methods are used for CAM-I and CAM-II, which is summarised in **Table 2.5**. It can be concluded from this table that the most common mode of strength testing for CAM-I is to use compression tests on cylinder or cubic CAM specimens with different sizes. The loading process is controlled at a constant displacement or strain, ε-, whilst the loading rate may vary in order to achieve constant displacement or strain. The rate is usually controlled in the range from 0.5 to 1.0 mm/min. This test method was originally specified for CAM-I by Railway Technical Research Institute (RTRI) in Japan (Wang and Han, 2002). The underlying assumption for this test method is that the CAMs are mostly subjected to compression in the slab tracks. Indeed, structural analysis on dynamics of CRTS-I or CRTS-II indicated that the compressive stresses dominated the stress distribution in the CAM layer, rather than the tensile stresses (Liu et al., 2010). As a result, it was considered that the tensile stresses could be ignored. However, this assumption is questionable because, firstly, CAMs are mainly subjected to bending in the two slab tracks (Zhao, 2003b), even though tensile stresses are relatively low. Additionally, most of the modelling work on slab tracks is simplified by only taking into account the vibrations in the vertical direction, which, to a certain extent, underestimated the stress/strain. Possibly influenced by the test method for CAM-I, on the other hand, test methods for CAM-II also include the typical compression test configuration used for CAM-I, but frequently, a test method for cement mortars is used instead (shown in **Table 2.5)**, in accordance with a Chinese Standard, **GB/T 17671**, which is similar to a British standard, **BS EN 196-1**. In this method, a standard prism is loaded in the centre point under flexure in the first step. After broken into two, they are then compressed within a test rig until failure. Using this method, both the flexural and compressive strengths can be obtained. In contrast to the test method for CAM-I, in this test, the two loading processes are controlled by force or stress, σ-.

Table 2.5 Test methods used for CAM-I and CAM-II

CAM	Loading Mode	Size of Test Specimens	Control Mode & Loading Rate	Reference
I	Compression	Φ 50×50	*ε*-, 1.0 mm/min	(Liu et al., 2009, Kong et al., 2010a, Kong et al., 2010b, Liu et al., 2011b, Yin et al., 2013, Fu et al., 2013)
		Φ 70×140	*ε*-, 0.001/min	(Wang et al., 2015)
		40×40×40	*ε*-, 0.5 mm/min	(Wang et al., 2008a, Wang and Liu, 2008, Wang et al., 2010b)
		70.7×70.7×70.7	N/A	(Tian and YU, 2010)
	Flexure & Compression	40×40×160	*σ*-, **GB / T17671**	(Hu et al., 2011)
II	Compression	Φ 50×50	*ε*-, 1.0 mm/min	(Liu et al., 2009, Kong et al., 2010a, Kong et al., 2010b, Liu et al., 2011b)
		Φ 70×100	*ε*-, 1.0 mm/min	(Wan et al., 2014)
		Φ 50×50	*σ*-, 100 N/s	(Rutherford et al., 2014)

CAM	Loading Mode	Size of Test Specimens	Control Mode & Loading Rate	Reference
II	Flexure & Compression	40×40×160	σ-, **GB / T17671**	(Wang et al., 2008e, Adhikari et al., 2009, Wang et al., 2011a, Tan et al., 2011, Tan et al., 2012, Hu et al., 2012, Yao and Sun, 2012, Huang et al., 2013)
		70×70×280	σ-, **GB / T17671**	(Qiu et al., 2013a, Qiu et al., 2013b)

In addition to strength, modulus of elasticity is another most important material property for CAMs. From the compression tests, the stress-strain curves of the CAMs can be obtained, and on these curves, the maximum stress, i.e. strength, and the tangent modulus at the origin can be calculated based on the assumption of linear elasticity. In the flexure and compression test methods for CAM-II, however, only two mechanical strength values can be obtained, namely flexural and compressive strengths. To measure the modulus of elasticity, a test method for testing compressive modulus of PCC is used (Dept. of Sci & Tech, 2008b). However, the test procedure for this method is complicated and this method should be treated with caution.

Similar to cement-based materials, the compressive strength is much easier to be tested and obtained in laboratories for CAMs. A lot of experimental work on CAMs indicated that their compressive strengths and modulus of elasticity are mainly dependent on the A/C and environmental temperature. As discussed in the previous section, in hardened CAMs, A/C determines the composition and microstructure of CABs formed by hcp and asphalt binder, thus influencing the

mechanical properties of their composites. In general, higher A/C leads to lower strength and modulus (Wang et al., 2008f, Wang et al., 2008e, Liu et al., 2009, Adhikari et al., 2009, Li et al., 2010b, Tan et al., 2011, Li et al., 2011, Tan et al., 2012, Liu et al., 2013). Other factors, like sand-cement ratio (S/C) or water-cement ratio (W/C) (Wang et al., 2008f, Wang et al., 2008e, Adhikari et al., 2009, Tan et al., 2011, Tan et al., 2012), also bring about some changes in the mechanical properties of CAMs, but play a less important role. Due to the inclusion of asphalt binder, the properties of CAMs are highly temperature-dependent. In particular, the mechanical properties are very much susceptible to the environmental temperature. When the test temperature decreases, especially when it is lower than room temperature (20 ˚C), the two typical mechanical parameters, i.e. compressive strength and modulus of elasticity, are enhanced. However, when the temperature rises above room temperature, the compressive strength and the modulus of elasticity tends to decrease with the increase of temperature, even though less remarkable (Wang et al., 2010b, Kong et al., 2010b, Liu et al., 2013). Moreover, the temperature susceptibility is increased with the increase of the asphalt (or the A/C). This implies that CAM-I should have a higher temperature dependence than CAM-II. To characterise this temperature dependence quantitatively, Wang et al. (2010b) introduced a temperature stability coefficient (TSC), whilst Kong et al. (2010b) proposed a temperature sensitivity factor instead. It is now gradually recognised that the primary source of the strength of CAMs is the hcp (Wang et al., 2011b, Tan et al., 2011) while the susceptibility to temperature is mainly attributed to the asphalt binder (Kong et al., 2014).

Since strength is much easier to be obtained than modulus of elasticity in most cases, attempts have been made to calculate the elastic modulus from the strength. Through testing the compressive strengths and the moduli of elasticity of a group of CAM-I, Zhao et al. (2008) regressed a linear relationship between elastic modulus, E_c, and compressive strength, f'_c, or peak stress on a stress-strain curve, σ_{cp}, as shown in **Equation (2-1)** below.

$$E_c = 410.55 f'_c \left(\text{or } \sigma_{cp}\right) - 441.74 \qquad (2\text{-}1)$$

Using an Arrhenius-like equation to describe the change of elastic modulus or peak stress of CAMs at different temperature, and defining the relative elastic modulus, E_r, and the relative peak stress, σ_{pr}, by dividing the modulus and the peak stress at any temperature by those at room temperature, respectively, Kong et al. (2014) revealed an interesting and simple relationship between the modulus and the peak stress or compressive strength (**Fig 2.19**). For various CAMs within a temperature range from -40 ˚C to 80 ˚C, it was found that the relative elastic modulus is in direct proportion to the square root of the relative peak stress or strength, as clearly expressed in **Equation (2-2)** below.

$$E_r \propto \sqrt{\sigma_{pr}} \tag{2-2}$$

Using the above equation, the elastic modulus of CAMs at any temperature can be estimated from the compressive strength and the elastic modulus measured at a given temperature, such as room temperature. This makes it possible for the engineers to predict the mechanical properties of CAMs under any practical service conditions.

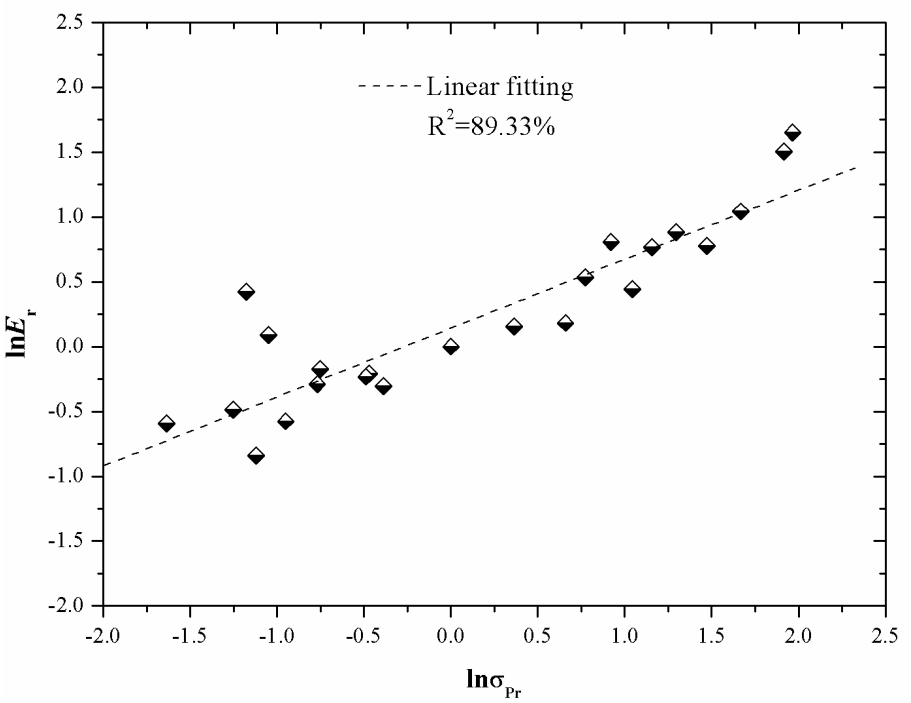

Fig 2.19 Correlation between E_r and σ_{pr} of all CAMs (Kong et al., 2014)

On the basis of above review, it can be concluded that much of the previous research on the mechanical properties and the behaviour of CAMs has mainly focused on compression and this is, in particular, the case for CAM-I. Although for CAM-II, the flexural strength has also been measured, it is just used as a secondary criterion in a tentative specification.

2.3.4 Comparison between CAM-I and CAM-II

As discussed in **Section 2.3.2**, the properties of CAMs are controlled by the composition and microstructure of their composite binders, CABs. Within the CAB, the two main binding materials, hcp and asphalt binder, contribute totally different mechanical properties to the resulting CAB and, hence, CAM.

With its highly heterogeneous microstructure, hcp has a large volume of pores, often filled with water, which ranges in diameter from 0.5 nm to 10,000 nm (Mindess et al., 2003). Due to these pre-existing pores, or flaws as stated in the fracture mechanics, hcp is much more like a brittle glass in fracture or failure (Radjy and Hansen, 1973, Struble et al., 1989). On the contrary, it is well-established that asphalt binder is a typically viscoelastic material (Lethersich, 1942, Poel and Der, 1954, Cheung and Cebon, 1997a, Cheung and Cebon, 1997b) and its mechanical properties are strongly affected by the environmental temperature. At room temperature, asphalt binder is a rubber-like soft material with super deformation ability; when it is hot, asphalt binder behaves like a viscous fluid, whilst when it is cold, it behaves like an elastic solid. Because of these huge differences existing between these two binders, CAMs can be separated into two main types, namely CAM-I and CAM-II, in order to satisfy the requirements of CRTS I and CRTS II, respectively. In CAM-I, the soft asphalt binder is the main binding phase whereas the brittle hcp dominates CAM-II. Therefore, in two Chinese tentative specifications (Dept. of Sci & Tech, 2008a, Dept. of Sci & Tech, 2008b), the requirements of the mechanical properties of these two CAMs are distinctively different (as listed in **Table 2.6** below) (Wang and Yan, 2009). For example, the minimum values of compressive strengths for CAM-I at the age of 1 day, 7 days and 28 days as required in the specifications are about one twentieth to one tenth (1/20 ~ 1/10) of those of CAM-II. The compressive modulus of CAM-II is about 20 ~ 100 times of that of CAM-I. Nevertheless, it should be pointed out that two totally different test methods are specified and used in these specifications for testing the compressive strength and the modulus of elasticity of CAM-I and CAM-II. The details of these differences are denoted in **Table 2.6**.

Table 2.6 Requirements of mechanical properties for CAM-I and CAM-II in two tentative specifications (Dept. of Sci & Tech, 2008a, Dept. of Sci & Tech, 2008b)

Test Items		CAM-I	CAM-II
Flexure Strength	1 d	N/A	≥1 MPa
	7 d		≥2 MPa
	28 d		≥3 MPa
Compressive Strength[#]	1 d	≥0.1 MPa	≥2 MPa
	7 d	≥0.7 MPa	≥10 MPa
	28 d	≥1.8 MPa	≥15 MPa
Modulus of Elasticity*		100~400 MPa	7,000~10,000 MPa
Fatigue		N/A	No failure at 10^4 cycles

Note: Two superscripts, [#] and *, denote that different samples and loading schemes are used in the mechanical tests for CAM-I and CAM-II.

[#] For testing compressive strength, cylinder samples (Φ 50 mm×50 mm) of CAM-I are loaded using displacement-controlled mode at the loading rate of 0.5-1.0 mm/min, in order to get their full stress-strain curves; in comparison, standard prisms (40 mm×40 mm×160 mm) of CAM-II are compressed using force-controlled mode until complete failure and the loading rate is 2,400 N/s (**GB /T 17671**);

* Compressive modulus of CAM-I can be obtained via calculating the tangent modulus at the original point of stress-strain curves; for testing modulus of elasticity of CAM-II, another group of prims with the size of 100 mm×100 mm×300 mm are loaded in the vertical direction in accordance with a Chinese standard for PCC, **GB /T 5081**.

For the purpose of comparison, the compression test method specified for CAM-I was used by Kong et al. (Kong et al., 2010b, Kong et al., 2014) to test different CAMs including CAM-I and CAM-II under various temperatures between -40 ˚C and 80 ˚C. Their results showed that, at room temperature, the compressive strengths or the modulus of elasticity of CAM-II is around six times of those of CAM-I. Although the values of elastic modulus for CAM-I are within the range as required in the specification, surprisingly, for CAM-II, they are lowered by almost one order of magnitude than those specified in the tentative specification. These comparative results are obviously inconsistent with those summarised in **Table 2.6**. This could become even more complicated if the change of temperature is considered because the CAMs are typical viscoelastic materials and their mechanical properties are susceptible to the temperature change. As can be seen from **Fig 2.20**, the compressive strengths or Young's modulus of different CAMs are getting closer with the decrease of temperature, implying that their difference is becoming narrowed, even close to zero at very low temperature. In contrast, high temperature would enlarge the difference. But at the temperature above 40 ˚C, it was found that CAMs with higher A/Cs start to be destabilised.

The above contradictory results indicate that there is some problem with the compression test method used for CAM-I and CAM-II, which will be further discussed in **Chapter 4**. Moreover, it is further realised that the environmental temperature is an indispensable and significant factor to be considered in testing and evaluation of mechanical properties of different CAMs.

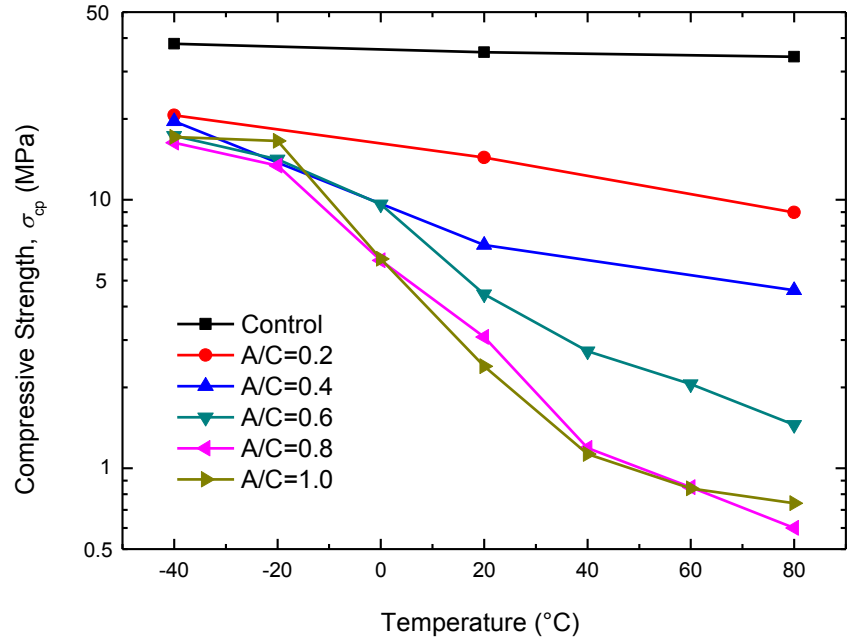

(a)

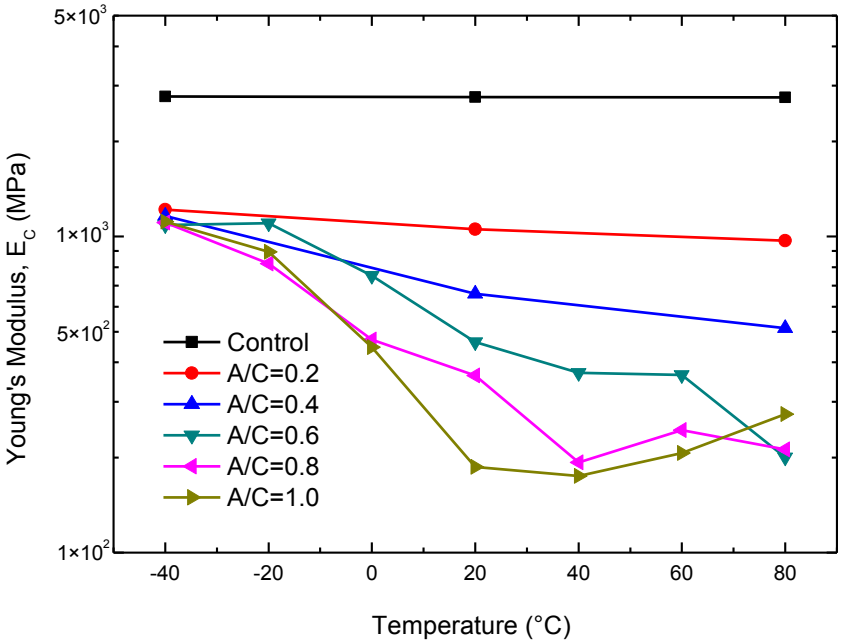

(b)

Fig 2.20 (a) Compressive strength and (b) Young's modulus of CAMs under different temperatures (revised after Kong et al. (2014))

2.3.5 Summary

In this review part, the composite mechanism of CAMs with a range of A/Cs and their static mechanical properties are discussed together with the test methods. The key points can be summarised as follows.

1. The interactions between Portland cement and asphalt emulsion result in the formation of CABs, and their composition and microstructures are mainly controlled by the A/C. The properties and behaviour of CABs, in turn, would affect the properties and behaviour of their composites including CAMs.
2. A CAM could be regarded as a two-phase composite, in which CAB functions as the co-binder and fine aggregates as the inertial filler. The two typical CAMs used in CRTS I and II, namely CAM-I and CAM-II, are closely related to asphalt mixtures and cement-based materials, respectively.
3. Much of the previous research work on static mechanical properties and behaviour of CAMs has focused on compression because of a possibly questionable assumption.
4. Strength and modulus of elasticity of CAMs are mainly influenced by the A/C and environmental temperature. Higher A/C or temperature leads to lower strength and modulus.
5. Environmental temperature is an indispensable and significant factor to be considered in testing and evaluating the mechanical properties of different CAMs.

2.4 Dynamic mechanical properties of CAMs and CABs

Generally, dynamic mechanical properties refer to the response of a material when it is subjected to a cyclic or periodic load or displacement. But for viscoelastic materials like polymers, it has been well accepted that this term refers to their viscoelastic properties exclusively according to **ASTM D4092−07** and that the load or the displacement is restricted within the linear region during the measurements.

Theoretically, when a viscoelastic solid material is subjected to a periodical strain as **Equation (2-3)**, its stress response shows a phase lag with respect to the strain, as shown in **Equation (2-4)**.

$$\varepsilon = \varepsilon_a \sin \omega t \tag{2-3}$$

$$\sigma = \sigma_a \sin(\omega t + \delta) \tag{2-4}$$

Where, ε is the strain applied, σ is the stress, ω is the angular velocity and δ is the phase angle. ε_a and σ_a are the two amplitudes.

The complex modulus, E^*, is defined as shown in **Equation (2-5**). Here, E' is the dynamic storage modulus and E'' is the dynamic loss modulus, which can be calculated according to **Equation (2-6)** and **(2-7).**

$$E^* = \frac{\sigma}{\varepsilon} = E' + iE'' \tag{2-5}$$

$$E' = \frac{\sigma_a}{\varepsilon_a} \cos \delta \tag{2-6}$$

$$E'' = \frac{\sigma_a}{\varepsilon_a} \sin \delta \tag{2-7}$$

The phase angle δ is an important parameter to characterise the viscoelasticity of the material but its tangent value, tanδ, is always used, as the loss factor (shown in **Equation (2-8)**).

$$\tan\delta = \frac{E''}{E'} \tag{2-8}$$

The norm of the complex modulus, l*E**l, is defined as dynamic modulus (shown in **Equation (2-9)**). In most cases, loss factors are small values far less than 1 (tanδ<<1), and thus dynamic modulus approximates to dynamic storage modulus as illustrated in **Equation (2-10)**.

$$\left|E^*\right| = \sqrt{E'^2 + E''^2} = \frac{\sigma_a}{\varepsilon_a} \tag{2-9}$$

$$\left|E^*\right| = \sqrt{E'^2(1+E''^2/E'^2)} = E'\sqrt{1+\tan^2\delta} \approx E' \tag{2-10}$$

To measure the viscoelasticity of the material in the laboratory, there are two controlling methods (Menard, 2008). One controlling method is, at a constant temperature, to measure the dynamic mechanic properties of the material within a range of frequencies, and the other is to measure its dynamic mechanical properties over a range of temperatures but at a given frequency. As a result, frequency spectrum and temperature spectrum can be produced, respectively, providing some basic information on the viscoelasticity of the material.

Due to the incorporation of asphalt binder which is a typically viscoelastic material over a wide range of temperatures and loading frequencies or strain rates (Lethersich, 1942, Poel and Der, 1954, Cheung and Cebon, 1997a, Cheung and Cebon, 1997b), CAMs are typically viscoelastic materials. But for some unknown reasons, the dynamic mechanical properties of CAMs have not received the same degree of attention as the static mechanical properties. Zhu et al. (2008) tested the frequency spectrum of dynamic modulus for a CAM-II using direct axial tension/compression (UT/C) and indicated that its dynamic modulus slightly increased with frequency. Rutherford et al. (2014) used the same method to measure the frequency spectra of three CAMs with different

A/Cs and found that the increasing trend of dynamic modulus with the loading frequency is more remarkable if A/C is higher. Dynamic mechanical analysis (DMA), a test method for viscoelastic polymer solids, was firstly used by Kong and Liu (2009) to test temperature spectra and frequency spectra of three typical CABs. Their temperature spectra of dynamic modulus and loss factor, for example, are shown in **Fig 2.21**. Results showed that higher temperature or A/C leads to the lower dynamical modulus of CABs. The peak value of the loss factor, which is used to characterise the viscoelasticity, is higher when more asphalt binder is included. This method was found to be easy and quick, but had a strict requirement on the size of the test specimen (40 mm×10 mm×4 mm). The reason for testing CABs instead of CAMs was simply because test specimens of CABs are more convenient to make.

To sum up here, this part has introduced the theoretical basis for dynamic mechanical properties of viscoelastic materials and reviewed a limited research work and related test methods on dynamic mechanical properties of CAMs, i.e. viscoelasticity, and their binders. The DMA test method has been trialled on different CABs and viscoelastic spectra can be obtained. And this method is probably a feasible one to obtain dynamic mechanical properties of CAMs over a range of temperatures, which will be used to explore the proper temperature range considered for their fatigue tests as demonstrated in **Chapter 5**.

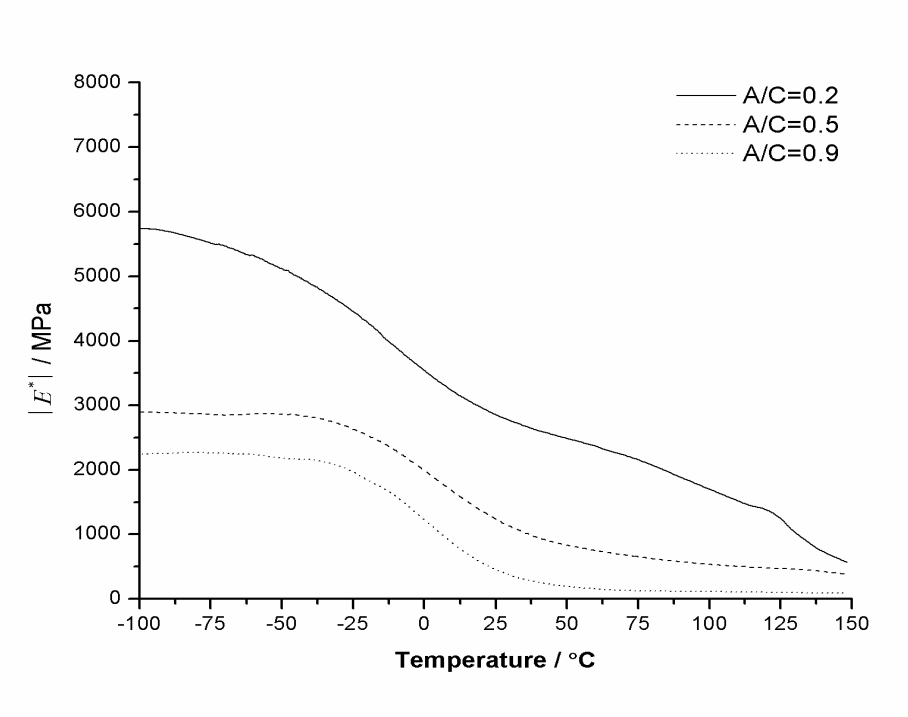

(a)

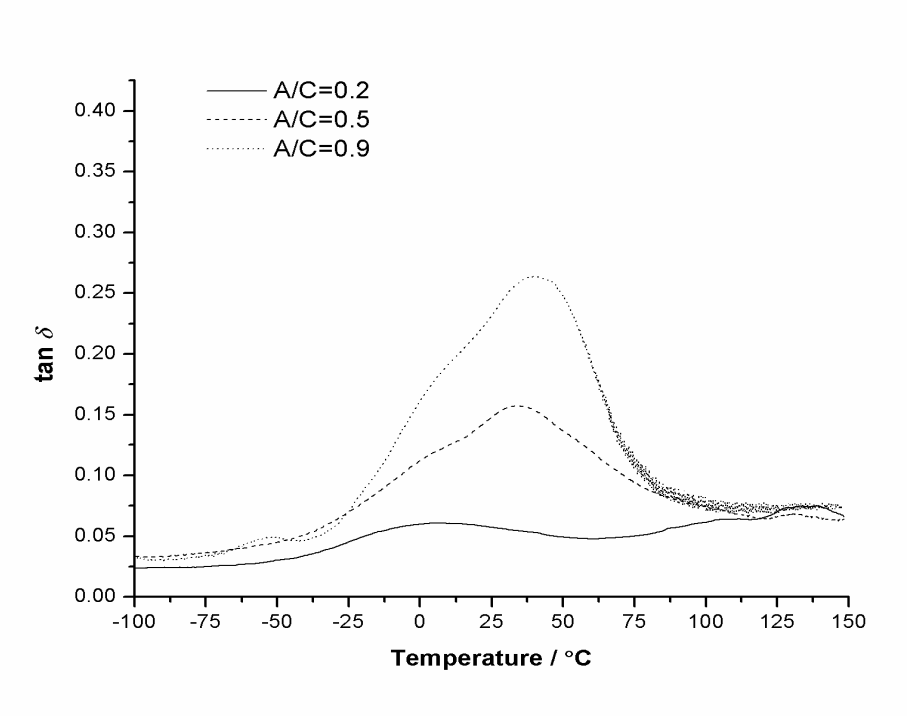

(b)

Fig 2.21 (a) Dynamic modulus and (b) loss factor of three typical CABs at the frequency of 1 Hz (Liu et al., 2013)

2.5 Fatigue testing and properties of CAMs, asphalt mixtures and cement-based materials

2.5.1 Introduction

As stated in **ASTM standard E1150**, fatigue is defined as ”*the process of progressive localized permanent structural change occurring in a material subjected to conditions that produce fluctuating stresses and strains at some point or points and that may culminate in cracks or complete fracture after a sufficient number of fluctuations*”. By definition, fatigue of the material is actually one of its dynamic mechanical properties under a cyclic stress or strain lower than its ultimate stress or strain which it can withstand in a monotonous loading. Unlike the viscoelastic properties as just mentioned in the preceding part, nevertheless, damage accumulates during fatigue in the long term until failure occurs after a certain number of cycles, which means that the stress or the strain applied is far over the linear region.

As a phenomenon occurring in materials, fatigue has been recognised as one of the main failure modes in solids and structures since research work on fatigue was inaugurated by pioneers like Albert and Wöhler in the early and middle nineteenth century (Schütz, 1996). It is estimated that over 80% of the failure of structures could be attributed to fatigue of materials or components (Schijve, 2003). In the two prevailing prefabricated concrete slab tracks used in China’s HSR network, CRTS I and CRTS II, without exception, the main issue as described in **Section 1.1.3** of **Chapter 1** and **Section 2.2.3** in this chapter has been known to be premature cracking of the CAM layer, primarily as a result of repeated traffic loadings from train-slab track interactions (Zhai et al., 1999, Zhai et al., 2009). In other words, premature cracking that has occurred in the CAM layer of CRTS I and II is mainly caused by the fatigue of CAMs under traffic-induced dynamic loads, that is to say, mechanical fatigue. Temperature-induced fatigue, called thermal fatigue, is also possible to be one of the causes or mechanisms, but beyond the scope of this thesis. In literature, however, the fatigue properties and behaviour of different CAMs is scarcely concerned and understood (Wang and Liu, 2008, Li et al., 2010b).

Considering the fact that only very limited research work on the fatigue of CAM-I and CAM-II is available in the literature, whilst, on the other hand, CAM-I and CAM-II are close to the two extreme materials, namely, asphalt mixtures and cement-based materials, as summarised in previous **Section 2.3**, the main focus of the following review has been given to the fatigue testing and properties of asphalt mixtures and cement-based materials, respectively. Based on this, a possible solution on how to test the fatigue properties of CAM-I and CAM-II has been proposed towards the end of this section.

2.5.2 Fatigue of CAMs

In CRTS I and CRTS II of HSR, CAM-I and CAM-II are mainly subjected to dynamic bending (Zhao, 2003b, Liu et al., 2010) from the train-rail-slab track interactions (Zhai et al., 1999, Zhai et al., 2009) over its service life. Therefore, the main type of fatigue which needs to be concerned is the flexural fatigue. It should be noted that only very limited research has been reported in the literature on the fatigue of CAM-I and CAM-II, which are reviewed below.

Wang and Liu (2008) investigated the fatigue properties of a CAM-I under different stress levels and temperatures, using the compression test method, and concluded that a higher stress level and a lower temperature (-20 °C) compared to room temperature resulted in a shorter fatigue life. Under uniaxial compression, Li et al. (2010b) studied the influence of the number of loading cycles, loading amplitude, steady state value and frequencies on the residual strength of a CAM-II. Most recently, Qiu et al. (2013b) used a three-point bending (3PB) configuration, which is similar to that used in concrete, to test the fatigue of a CAM-II at different temperatures. It was found that the fatigue life was shortened with the increase of the stress level and temperature. The contradictory results regarding the temperature effect on fatigue of CAM-I and CAM-II obtained from Wang and Liu (2008) and Qiu et al. (2013b) are possibly attributed to the difference in the test methods used in the fatigue tests, the compression test method in Wang and Liu (2008)'s study and the 3PB test method in Qiu et al. (2013b)'s work.

As discussed in **Section 2.3.2**, CAM-I is different from CAM-II in properties due to the difference in the A/C, but whether it is reasonable to use different fatigue test methods for different CAMs remains an unanswered question, and the suitability of different test methods and the reliability of the test results could be found nowhere. At the same time, it has been recognised that the two typical CAMs are close to asphalt mixtures and cement-based materials, respectively, the fatigue of which has been well defined. Therefore, it is necessary to get a basic understanding of the fatigue testing and properties of asphalt mixtures and cement-based materials, separately, and seek to potential solutions for those typical two CAMs, CAM-I and CAM-II.

2.5.3 Fatigue of asphalt mixtures

2.5.3.1 Introduction

Asphalt mixture is an engineering material consisting of asphalt binder and aggregate, sometimes termed as an asphalt-aggregate mix, and most frequently used in asphalt or flexible pavements.

For asphalt or flexible pavements, fatigue induced cracking at intermediate temperatures, which is associated with repetitive loadings from moving traffic, is generally accepted to be one of the three primary distresses, namely rutting or permanent deformation, fatigue cracking, and low temperature or thermal cracking (Huang, 2004). And it has been long believed (Kingham, 1973, Brown et al., 1985, Brown, 1997) that such cracks initiate usually from the bottom of the asphalt layer, where the mixture is in a state of tension, and then propagate upwards to the surface (as shown in **Fig 2.22**). The maximum principal tensile stress or strain is considered to be critical to initiating fatigue cracking. Therefore, in laboratories, fatigue tests are designed and conducted, in order to replicate such a phenomenon and to define the fatigue of asphalt mixtures via different test variables. Those variables, for convenience, can be divided into the following three categories, namely, mixture variables, loading conditions, and environmental conditions (Epps and Monismith, 1972):

- Mixture variables: mixture composition, characterization and content, manufacturing method, modulus, and etc.;
- Loading conditions: test method, mode of loading, load magnitude, loading frequency, rest period, wave form, type of specimen, and etc.;
- And environmental conditions: temperature, moisture, and etc.;

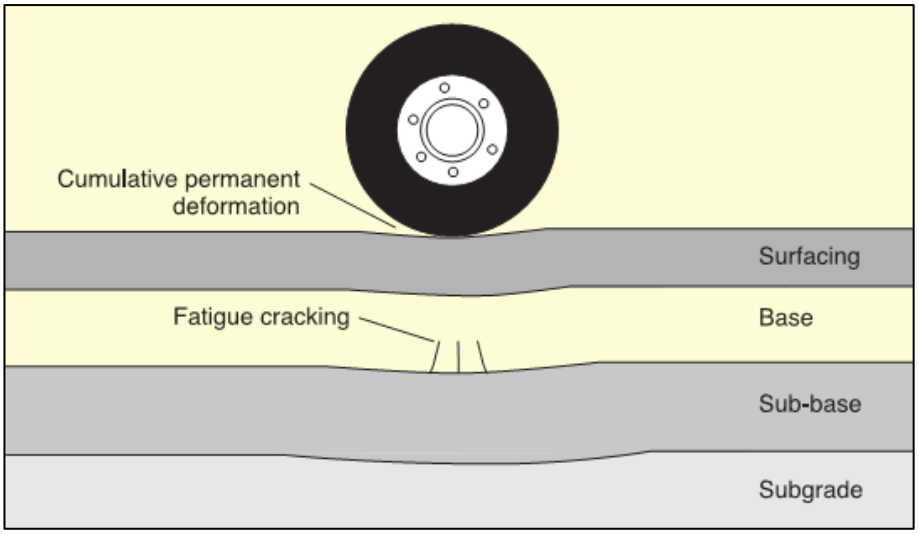

Fig 2.22 Fatigue cracking in asphalt or flexible pavements (Read and Whiteoak, 2003)

Based on the classical phenomenological approach (Wen, 2001, Maggiore, 2014), this section will review fatigue test schemes used for lean asphalt mixtures in the laboratory, including test variables and results considered in this thesis such as test method, mode of loading, fatigue failure criteria, the ε-N curve obtained and the influence of temperature.

2.5.3.2 Test methods in laboratories

Various test methods as shown in **Fig 2.23** below are usually used in the experimental work for characterising the fatigue of asphalt mixtures in asphalt or flexible pavements, and the commonly-used fatigue test methods in laboratories include simple flexure (Rowe, 1993, Deacon et al., 1995, Khalid, 2000a, Khalid, 2000b, Cocurullo et al., 2008, Pettinari et al., 2012, Li et al., 2013), supported flexure (Barksdale and Miller, 1977), direct axial tension/compression(UT/C) (Shatnawi, 1997, WEN, 2003, Li et al., 2013, Tapsoba et al., 2015, Tapsoba et al., 2012), indirect tension (IDT) or diametral (Brown, 1995, Khalid, 2000a, Khalid, 2000b, WEN, 2003, Cocurullo et al., 2008), shearing (Boudabbous et al., 2013b), triaxial tests(Porter and Kennedy, 1975), wheel-track testing (Rowe, 1996, Hartman et al., 2001) and other types of fatigue test methods.

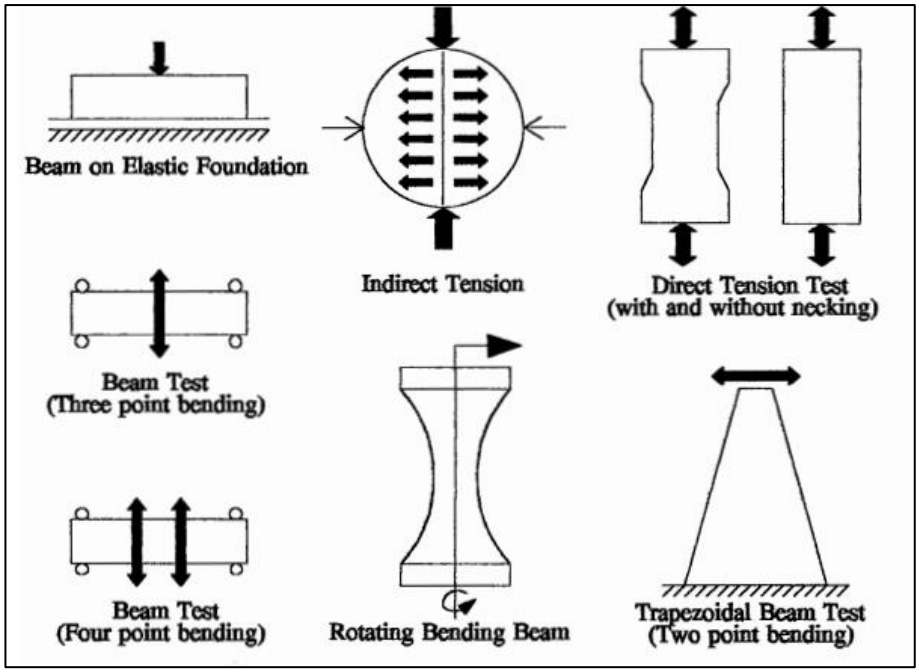

Fig 2.23 Some of the commonly-used fatigue test methods (Rowe, 1996)

The test method used in the laboratory definitely affects fatigue responses of asphalt mixtures. Hence, the selection of an effective and suitable fatigue test method from the above mentioned ones is of primary importance. Rao-Tangella et al. (1990) had reviewed different fatigue test methods and recommended the repeated simple flexure test as the most suitable method for assessing the fatigue properties of asphalt mixtures. A similar conclusion has also been reached by a similar evaluation of different test procedures for measuring fatigue properties of bituminous mixtures (Matthews et al., 1993). The simple flexure fatigue test could be designed in several different modes, such as semi-circular bending (SCB), 2-point bending (2PB), 3-point bending (3PB) and 4-point bending (4PB). Amongst these, the 4PB fatigue test is perhaps the most accepted one and it has become a standard test method for determining fatigue behaviour of different asphalt paving mixtures in different countries around the world, including **ASTM Designation: D7460-10**, **AASHTO T321-03**, **SHRP Designation: M-009** (in the US), **EN 12697-24: 2012** (in European Union and the UK), **AG: PT/T233** (Australia) and **JTJ 052-2000** (in China).

2.5.3.3 Mode of loading

Fatigue tests of asphalt mixtures can be performed in laboratories either under a controlled stress (i.e. controlled-stress test, σ-) or under a controlled strain (i.e. controlled-strain test, ε-). Under the controlled-stress mode, a constant stress is applied and the resultant strain increases with the loading cycles, whilst under the controlled-strain mode, the strain is maintained constant and the stress varies with the loading cycles. In both cases, the stress divided by the strain, referred to as stiffness or dynamic modulus, decreases with the loading cycles, as demonstrated in **Fig 2.24** below, where stiffness ratio is defined as the stiffness at the loading cycle of n relative to initial stiffness.

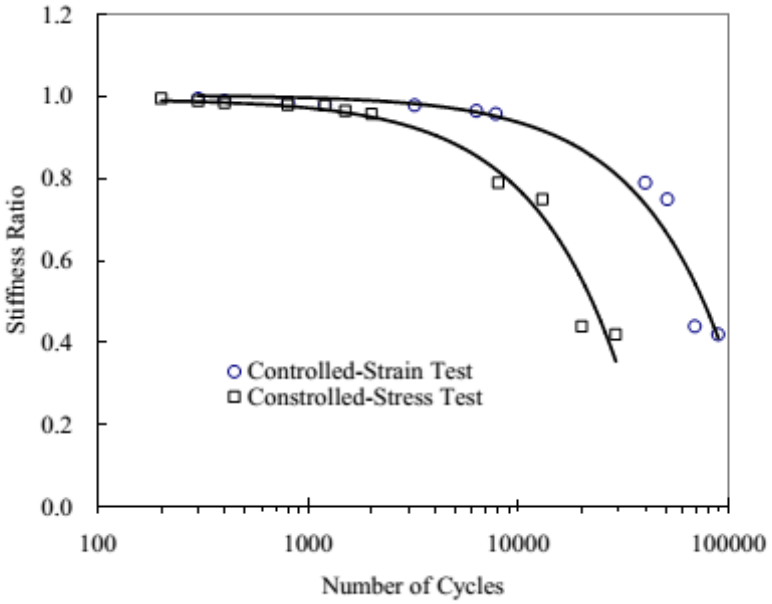

Fig 2.24 Different modes of loading in a 4PB fatigue test (Xiao, 2006)

Mode of loading is one of the primary factors affecting the fatigue response of asphalt mixtures. Generally, as can be seen from **Fig 2.24** above, longer fatigue lives are obtained in controlled-strain tests than controlled-stress tests (Sousa et al., 2003, Xiao, 2006). From the cracking mechanistic viewpoint, this can be attributed to the fact that controlled-stress tests essentially measure the loading cycles necessary for crack initiation whereas in controlled-strain tests, apart from crack initiation, the crack propagation is also considered (Rao-Tangella et

al., 1990, SHRP, 1994). The selection of the mode of loading for fatigue tests in laboratories is, therefore, important, and its basic principle is to reflect the critical loading mode causing fatigue cracking in the field as closely as possible. In asphalt pavements, for instance, a thick layer with high stiffness is best tested using a controlled-stress mode, whereas a controlled-strain mode of fatigue tests is more applicable to a thin flexible pavement layer (Pell, 1973). It can be concluded, hereupon, that what mode of loading is chosen for an asphalt mixture depends on not only the material properties but also the state of loads or deformation of the mixture in asphalt or flexible pavements.

2.5.3.4 Failure criteria

Under controlled-stress test conditions, fatigue failure is generally defined as the breaking or complete fracture of the test sample and it is evident at the end of fatigue tests. On the other hand, in controlled-strain tests, the definition of fatigue life, i.e. the number of loading cycles to failure (N_f) is much complex and sometimes could be even controversial.

There are basically two categories of failure criteria in controlled-strain tests, one based on stiffness or dynamic modulus, the other based on dissipated energy (DE) (Shen and Carpenter, 2007b, Maggiore, 2014). In the first case, stiffness ratio, E/E_o, is plotted with loading cycles (shown in **Fig 2.25)**. Obviously, the change of the stiffness versus loading cycles with four distinct regions can be closely associated with cracking initiation and propagation (Rowe and Bouldin, 2000). This is the basis for stiffness-based failure criteria (Lundström and Isacsson, 2004, Artamendi and Khalid, 2005, Tarefder and Bateman, 2013) and the most commonly used is the phenomenological approach of 50% reduction in initial stiffness, $N_{f,\ 50}$. In the case of DE-based criteria, on the other hand, dissipated energy is regarded as a good indicator of the damage as fatigue proceeds (Pronk and Hopman, 1991). To accurately define the failure point, several DE-based methods are reported in literature, such as initial dissipated energy (IDE) (Rowe, 1993), cumulative dissipated energy (CDE) (Pronk and Hopman, 1991, Bhasin et al., 2009), dissipated energy ratio(DER) or energy ratio (ER) (Pronk and Hopman, 1991, Rowe and Bouldin, 2000, Shen and Lu, 2010, Abojaradeh, 2013) and ratio of dissipated

energy change (RDEC) (Ghuzlan and Carpenter, 2000, Ghuzlan and Carpenter, 2006, Shen et al., 2006, Shen and Carpenter, 2007a, Bhasin et al., 2009, Shen and Lu, 2010, Boudabbous et al., 2013a). In an early work by Prof. Schapery and Prof. Kim (Schapery, 1984, Schapery, 1990, Kim et al., 1995, Lee and Kim, 1997), a viscoelastic continuum damage (VECD) model is used in fatigue data analysis to separate the viscoelastic dissipated energy from the total dissipated energy. By so doing, dissipated energy is converted into pseudo dissipated strain energy (PDSE), which is directly related to the damage incurred during a fatigue test. Based on PDSE, several similar failure criteria for the DE-based criteria could be used in fatigue data analysis (Lee et al., 2000, Kim et al., 2003, Soltani and Anderson, 2005, Bhasin et al., 2009, Luo et al., 2012a, Luo et al., 2012b, Zhang et al., 2013, Sabouri and Kim, 2014). Other failure criteria, for instance, load-deformation hysteresis loop failure criterion (Al-Khateeb and Shenoy, 2004, Al-Khateeb and Shenoy, 2011), strain-based failure criterion used for wheel-tracking tests (Hartman et al., 2001, Liao et al., 2011), crack length criterion (Bhasin et al., 2009) and strain ratio criterion (Wen et al., 2013) for IDT tests, are rarely used for analysis.

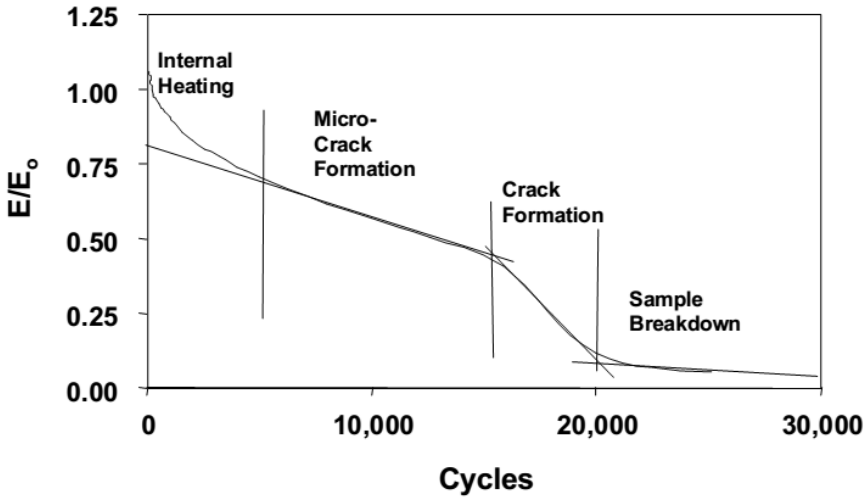

Fig 2.25 Four distinct regions of fatigue behaviour of asphalt mixtures (Rowe and Bouldin, 2000)

Of all those fatigue failure criteria mentioned above, DE-based failure criteria are thought to be better than stiffness-based ones, but complex procedures of

processing huge amount of fatigue test data are needed. Although it is conservative, empirical and not based on a verified principle, however, the traditional failure criterion, $N_{f,50}$, is claimed to be simple but rational to use in fatigue test data analysis with a strong correlation with DE-based failure criteria (Shen and Lu, 2010).

2.5.3.5 ε-N curve

It is believed that the dominant factor affecting the fatigue life of asphalt mixtures is the maximum tensile strain rather than the stress, irrespective of the mode of loading (Saal and Pell, 1960, Pell et al., 1961, Pell, 1973, Matthews et al., 1993). The fatigue test results in laboratories clearly show that there is a relationship between the tensile strain applied, ε_t, and the number of cycles to fatigue, N_f. This observed relationship can be expressed in the following form as shown in **Equation (2-11)**, where k_1 and k_2 are two material constants.

$$N_f = k_1 \left(\frac{1}{\varepsilon_t} \right)^{k_2} \tag{2-11}$$

A typical ε-N curve is shown in **Fig 2.26** if such a relationship is drawn in double logarithmic scales. Obviously, this log-log relationship is linear between the tensile strain applied and the fatigue life in the primary fatigue zone. But, when the tensile strain falls to a level below which fatigue life goes to infinity, such a strain level is referred to as fatigue endurance limit (FEL), ε_{FEL}, postulated by C. L. Monismith et al. (1970). Its existence has been confirmed by subsequent research work, and its value, though difficult to test through the routine fatigue test methods, could be obtained via different methodologies using the concept of DE (Carpenter et al., 2003, Shen and Carpenter, 2005, Carpenter and Shen, 2006), the Weibull statistic function (Prowell and Brown, 2006), mechanistic empirical (M-E) design principles (Thompson and Carpenter, 2006) or the elastic-viscoelastic correspondence principle (Bhattacharjee et al., 2009). This value mainly depends on the type of the mixture and test temperature, ranging from 70 μm/m to 350 μm/m (Shen and Carpenter, 2007b). Instead of ε_{FEL}, in practice, a strain level corresponding to 1 million (10^6) loading cycles, ε_6, is

extrapolated from the ε-N curve and used for comparison and evaluation, as schematically shown in **Fig 2.26**.

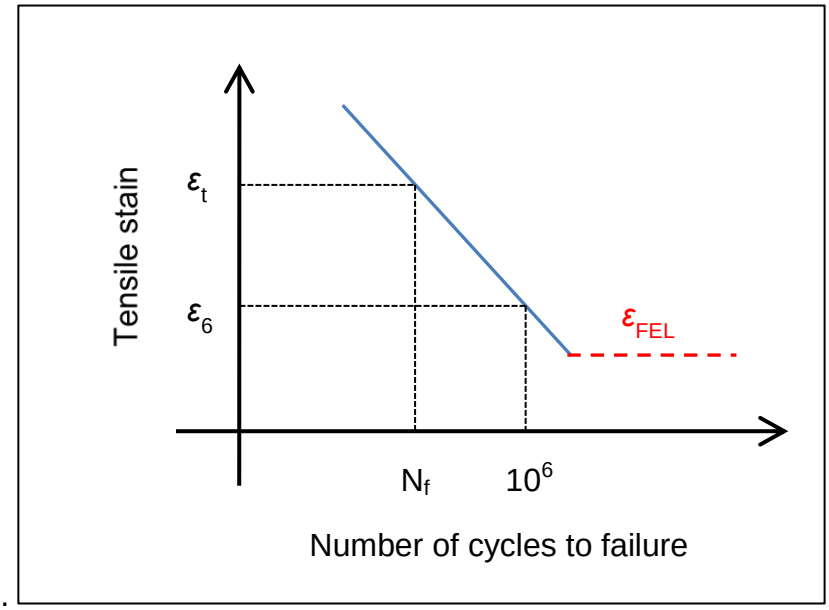

Fig 2.26 Schematics of a typical ε-N curve

2.5.3.6 Influence of temperature

Asphalt mixtures are well known to be typical viscoelastic materials (Shen, 2001) and their mechanical properties and behaviour, either static or dynamic, are strongly influenced by the test temperature. Therefore, it is without any doubt that temperature to which asphalt mixtures are exposed has a great influence on their fatigue properties.

Fatigue strength or life of asphalt mixtures is highly dependent on atmosphere temperature (Saal and Pell, 1960, Pell et al., 1961, Kim et al., 1991, Deacon et al., 1994, Hsu and Tseng, 1996, Adhikari and You, 2010, Nejad et al., 2010, Dondi et al., 2013). Generally, lower temperature produces longer fatigue life, but this law only works for asphalt mixtures at intermediate temperatures. If the test temperature falls below an extremely low value, asphalt mixtures show typical brittleness like elastic solids; if the temperature goes too high, they could be destabilised, due to the high susceptibility of asphalt binder to temperature. However, the definition of 'intermediate' in literature is not so clear. Usually, the

temperature range around room temperature (20 °C) from 5 °C to 30 °C is accepted as intermediate (Tsai, 2001). But meanwhile, the test temperature could be set as low as -10 °C or as high as 40 °C. In brief, the influence of temperature on the fatigue of asphalt mixtures is as significant as those on their static and dynamic mechanical properties.

To incorporate the influence of test temperature into a fatigue life model, one methodology is to consider its effect on the stiffness or dynamic modulus (Saal and Pell, 1960, Pell et al., 1961). Thus, an equation based on **Equation (2-11)** was proposed (Pell, 1987), as shown in **Equation (2-12)**, and used as the Asphalt Institute model (AI, 1989).

$$N_f = k_1 \left(\frac{1}{\varepsilon_t}\right)^{k_2} \left(\frac{1}{S_o}\right)^{k_3} \tag{2-12}$$

Where, S_o is the initial stiffness or dynamic modulus; factors like k_1, k_2 and k_3 are material constants fitted from the fatigue test data.

Other methodologies include the use of temperature conversion factor from the time-temperature equivalence concept (Deacon et al., 1994) and effective temperature, T_{eff} (El-Basyouny and Jeong, 2009).

2.5.4 Fatigue of cement-based materials

2.5.4.1 Introduction

Cement-based materials, including concrete, are purportedly the most widely used construction and building materials in the world. Their application could not only be in such civil infrastructures subjected to static loads as buildings and hydraulic dams (Neville, 1995), but also in those structures subjected to repetitive dynamic loads like offshore structures, bridges, pavements (Oh, 1986) and in recent years slab tracks in HSR.

In concrete structures, no matter what kind of loads they are (either static or cyclic), cracking is a common phenomenon and governed by the tensile properties (Cornelissen, 1984). In rigid or concrete pavements, for instance, the principal mode of structural failure is the fatigue cracking that is caused by repeated bending loads applied at stress levels less than the ultimate static strength of the concrete, i.e. flexural strength (Smith et al., 2002) and very similar to the fatigue cracking in asphalt or flexible pavements as mentioned in the previous **Section 2.5.3**. Owing to the quasi-brittle feature of cement-based materials, on the other hand, the compressive strength is a very important mechanical parameter, much easier to be tested and obtained in laboratories when compared with others. The main target of testing fatigue of cement-based materials under compression is, therefore, to relate their fatigue properties to the compressive strength, as in the case of the testing of modulus of elasticity, flexural strength and tensile strength. Regarding fatigue failure mechanisms under fatigue loading in the form of compression or tension as shown in **Fig 2.27**, the failure of plain concretes is closely associated with local micro-cracking, initiating within the matrix hcp, or along the interfacial transition zone (ITZ) between the hcp and the aggregate, or, in a few cases, from the aggregate, or their combination (Susmel, 2014). When micro-cracks propagate to form one critical crack, failure takes place suddenly without any warning. This is almost the same failure mechanism with that of concretes under a static load. Research work on fatigue of cement-based materials has sustained for nearly 120 years since Consedére and De Joly conducted the first fatigue tests on mortars in 1898 (Nordby, 1958, Murdock, 1965, Antrim, 1965, John et al.,

1968). For this reason, their fatigue test schemes including fatigue test method, mode of loading and failure criterion have been well defined and known.

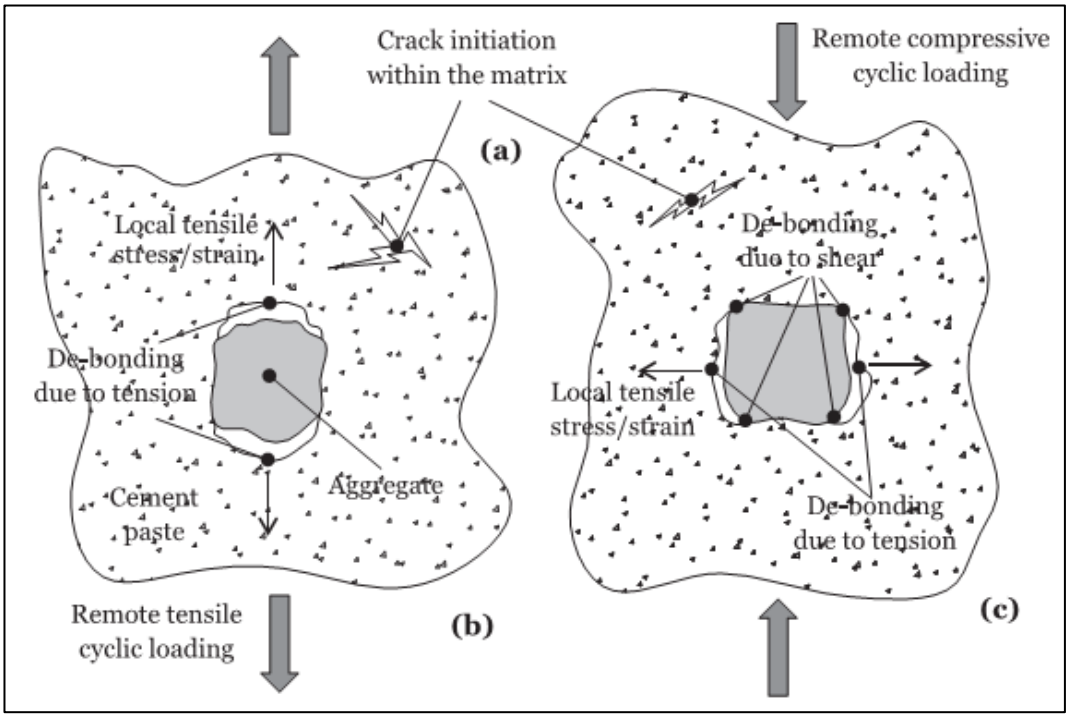

Fig 2.27 Crack initiation in plain concretes subjected to fatigue loading (Susmel, 2014)

On the basis of the phenomenological approach, likewise, this section will review test schemes used for fatigue testing of cement-based materials, basic analysis methods of test results and two main control variables considered. Since CRTS I and CRTS II are analogical to composite or semi-rigid pavements as discussed in the first review part, the main focus will be on plain concretes used in rigid pavements.

2.5.4.2 Test schemes

Fatigue test methods of cement-based materials in laboratories are relatively mature, and there are primarily three modes, namely in compression (Antrim and McLaughlin, 1959, Gray et al., 1961, Bennett and Muir, 1967, Hop, 1968, Raju, 1970, Sparks and Menzies, 1973, Tepfers and Kutti, 1979, Sparks, 1982, Holmen, 1982, Furtak, 1984, Alliche and Francois, 1986, Petkovic et al., 1990,

Do et al., 1993, Dyduch et al., 1994, Gao and Hsu, 1998, Pindado et al., 1999, Mu et al., 2004, Bun et al., 2011, Ruiz et al., 2011, Pang et al., 2012), in flexure or bending (Murdock and Kesler, 1958, Hilsdorf and Kesler, 1966, Galloway and Raithby, 1973, Raithby and Galloway, 1974, Raithby, 1979, Klaiber and Lee, 1982, Oh, 1986, Oh, 1991, Shi et al., 1993, Redjel, 1995, Zhang et al., 1996, Zhang and Wu, 1997, Roesler et al., 2005) and in a few cases in tension or tension/compression (T/C) (Tepfers, 1979, Tepfers, 1982, Cornelissen, 1984, Cornelissen and Reinhardt, 1984, Reinhardt et al., 1986, Yun et al., 2003). The former two modes as shown in **Fig 2.28**, obviously, account for the majority, and in concrete or rigid pavements, the commonly used one is in 4 PB. A summary of fatigue test methods for plain concretes can be referred to in Susmel (2014)‘s recent work.

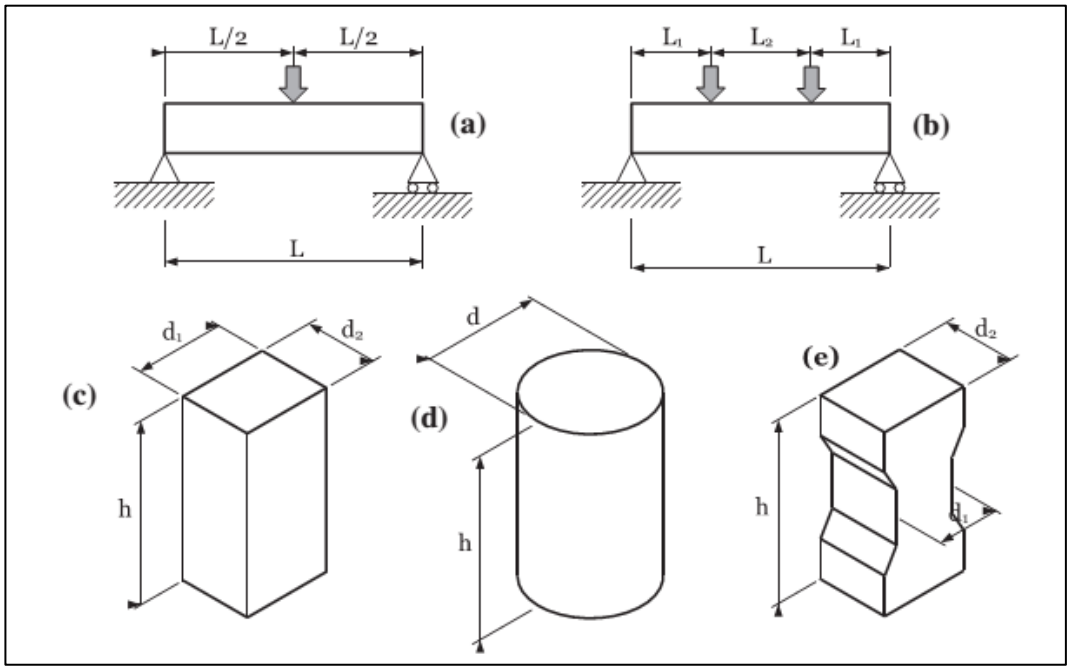

Fig 2.28 Fatigue test methods used for plain concrete: (a) 3PB or (b) 4PB, flexure or bending, (c) or (d) compression, and (e) tension or tension/compression (Susmel, 2014)

There is little, if any, controversy in the mode of loading and failure criterion used in fatigue tests of cement-based materials. Controlled-stress mode is used for almost all fatigue tests because it is generally agreed that critical tensile

stresses in concrete structures control the fatigue behaviour. In the design of concrete pavements, for example, the maximum bending stress created at the bottom of the slab is considered to be critical for fatigue (Klaiber and Lee, 1982, Oh, 1986, Smith et al., 2002). With regard to fatigue failure, it is firmly related to the damage during the process of fatigue. Fatigue damage in plain concretes is accepted to be a nonlinear process and exhibits three distinct stages, a deceleration stage (**Stage I**), a steady-rate stage (**Stage II**) and an acceleration stage (**Stage III**) as shown schematically in **Fig 2.29**. The final stage of crack propagation, **Stage III**, usually happens in a few loading cycles in concretes and could be ignored. Cracking initiation at the end of **Stage II**, N_1, is, therefore, reasonable to approximate to complete failure, that is to say, $N_1 \approx N_f$. This failure criterion is the classical one under stress-controlled mode. Of course, there are some other fatigue failure criteria for concretes, based on strain (Tepfers, 1979, Saito, 1983, Cornelissen, 1984, Do et al., 1993), or strain rate (Sparks and Menzies, 1973, Do et al., 1993), or probabilistic models (Oh, 1986, Shi et al., 1993), but they are rarely used.

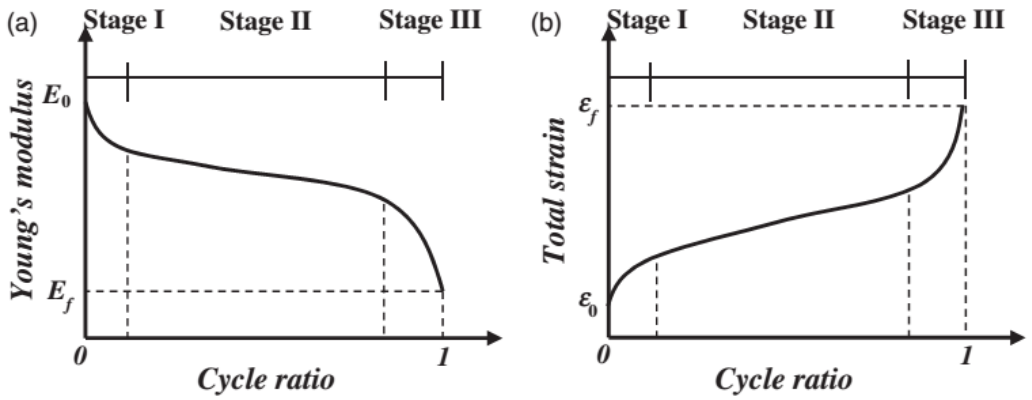

Fig 2.29 Typical fatigue damage process of concrete: (a) degradation of Young's modulus and (b) evolution of total strain (Liang et al., 2016)

2.5.4.3 The Wöhler curve

Traditionally, the classical Wöhler curve for a metallic material represents the relationship between the stress amplitude applied in fatigue tests, S_a, and the fatigue life, N_f (Schijve, 2009). But for quasi-brittle cement-based materials, it is

usually expressed in terms of the stress-to-strength ratio, S, as shown in **Equation(2-13)**, versus the logarithm of the number of cycles to failure, log N_f (Antrim and McLaughlin, 1959, Gray et al., 1961, Bennett and Muir, 1967, Raithby, 1979, Tepfers, 1979, Cornelissen and Reinhardt, 1984, Oh, 1986, Shi et al., 1993). Such a semi-logarithmic relationship is graphically plotted as the S-N curve, whose mathematic formula is shown in **Equation (2-14).**

$$S = \frac{S_{\max}}{f_c^{'}(\text{or MOR})} \tag{2-13}$$

$$S = \alpha - \beta \log N_f \tag{2-14}$$

Where, S_{max} is the maximum stress applied, f'_c is the compressive strength of the concrete and MOR is the modulus of rupture or the flexural strength; α and β are two fitting coefficients to the fatigue test data.

In the case of bending fatigue, a PCA (Portland Cement Association) model is plotted in **Fig 2.30**, as the typical S-N curve used in the design of concrete in rigid pavements. From the curve, there is a linear zone when the normalised stress level is above 0.55 (S > 0.55). The ordinate to the horizontal asymptote of this curve is the stress level at which the specimen will withstand an infinite number of loading cycles and is called the fatigue limit as the red line shows. For plain concretes, there is no indication of a definite fatigue limit (Murdock and Kesler, 1958, Antrim and McLaughlin, 1959), but in the design, the PCA model has a fatigue limit of 45 % strength (S = 0.45). It is customary, for convenience, to specify a so-called fatigue strength for a given number of cycles to failure, S_6 for instance, a normalised stress level corresponding to 2 million (10^6) loading cycles, to compare and evaluate the fatigue resistance of different concretes.

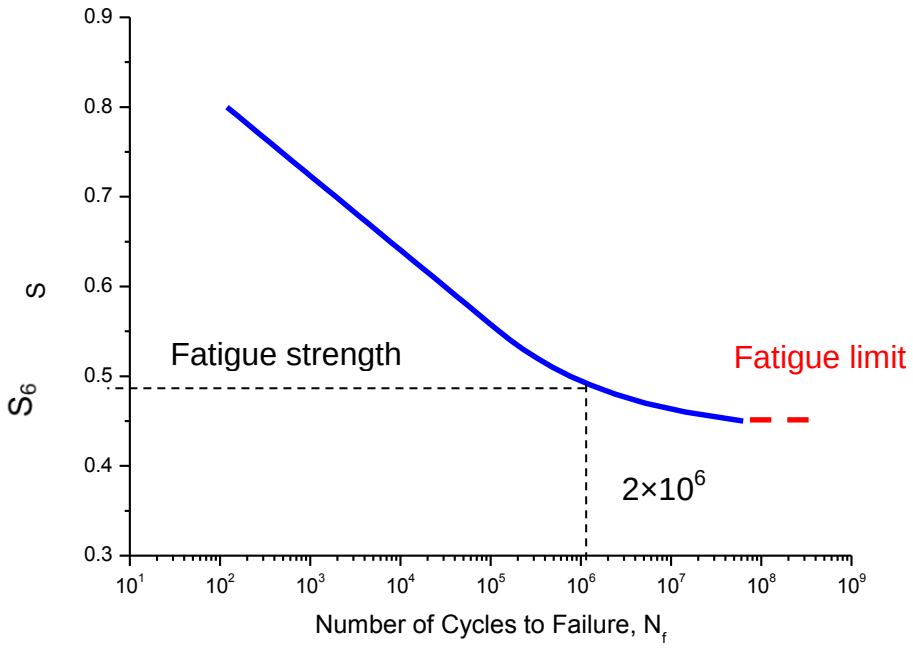

Fig 2.30 A typical S-N curve for designing PCC used in rigid pavements (after Titus-Glover et al. (2005))

2.5.4.4 Influence of stress ratio, *R*

The S-N curve is always drawn for a constant stress ratio, *R*, the ratio of minimum stress, S_{min}, to maximum stress, S_{max}, in fatigue loading. When the *R* value changes, it is the stress range, ΔS, that changes accordingly as can be seen in **Equation (2-15)**. If *R* increases, at constant stress level, the range of stress decreases. Therefore, the influence of stress ratio can be deduced from the effect of stress range on fatigue of concretes.

$$\Delta S = S_{max} - S_{min} = S_{max}(1-R) \qquad (2\text{-}15)$$

Research work has shown that the stress range has an influence on fatigue resistance of plain concretes (Murdock and Kesler, 1958, Aas-Jakobsen, 1970, Tepfers, 1979, Tepfers and Kutti, 1979). And the fatigue strength is dependent on the stress range and increases as the stress range is reduced (Murdock and Kesler, 1958). A modified Goodman diagram is shown **Fig 2.31** to describe the

fatigue strength at different stress ranges. This is the case of $R \geq 0$. When $R < 0$, stress reversals will be applied. Early research work on compressive fatigue of concrete materials indicated that stress reversals would not reduce the fatigue resistance (Murdock and Kesler, 1958, Galloway and Raithby, 1973). Later in the 1980s, under tension/compression (T/C), Tepfers (1982) found that stress reversals slightly reduced the fatigue life, and therefore were detrimental to the fatigue resistance of concrete, which was confirmed by Dr Cornelissen's work (Cornelissen, 1984, Cornelissen and Reinhardt, 1984). Zhang et al. (1996) reconfirmed this finding through 4PB fatigue tests of concretes. To conclude, R will affect fatigue of plain concretes when $R \geq 0$ and higher R will produce longer fatigue life; stress reversals ($R < 0$) will never influence their fatigue resistance in compression but slightly lower their fatigue life if in tension or flexure.

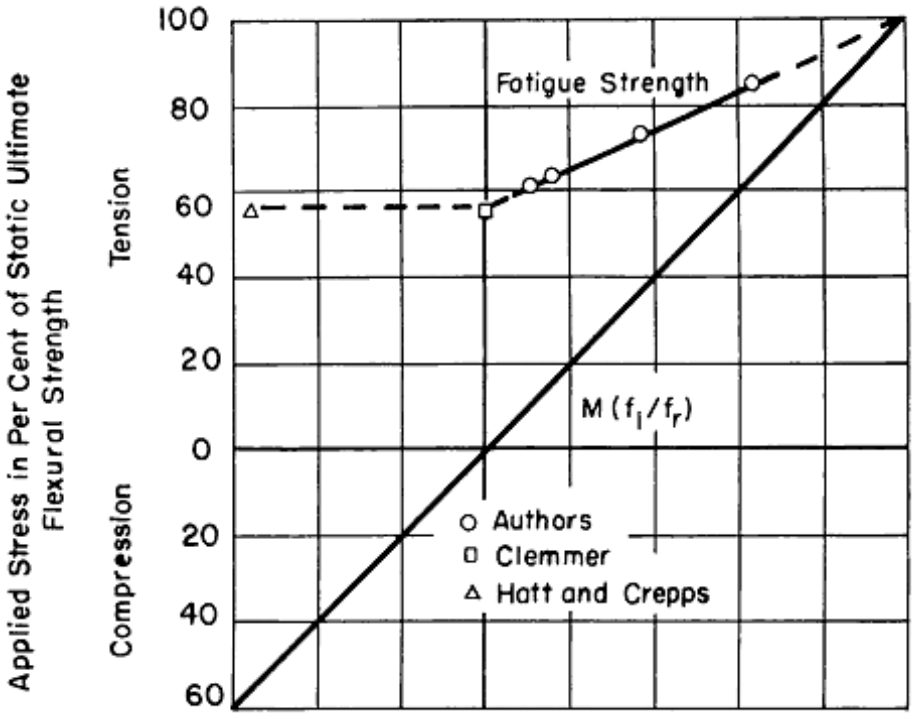

Fig 2.31 Modified Goodman diagram showing the effect of the stress range on fatigue strength (10^7 cycles) (after (Murdock and Kesler, 1958))

2.5.4.5 Refined S-N curves

To take *R* values into consideration, Aas-Jakobsen (1970) proposed a fatigue equation for plain concretes in compression as shown in **Equation (2-16)** and the fitting coefficient, *β*, was calculated to be 0.0640. Tepfers and Kutti (1979) revised it to 0.0685 and found that it was also applicable to tensile fatigue (Tepfers, 1979). Oh (1986) obtained a slightly different value, 0.0690, from flexural fatigue tests. It is noted that no stress reversal is considered and only when $R \geq 0$ for this equation as shown in **Fig 2.32**.

$$S = 1 - \beta(1 - R)\log N_f \tag{2-16}$$

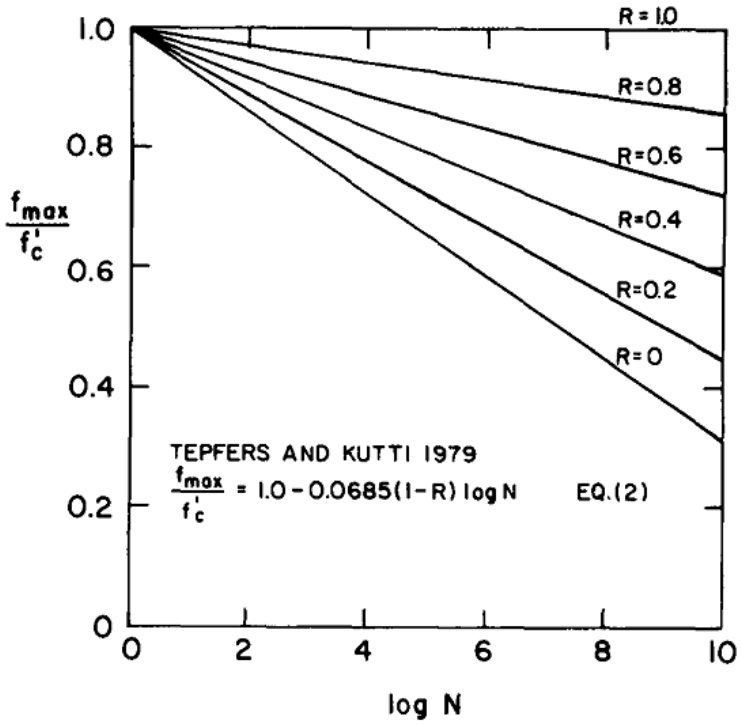

Fig 2.32 Refined S-N curves for different R values, R≥0 (Hsu, 1981)

Based on the fatigue equation mentioned above, Hsu (1981) made some improvements by considering the rate of loading and subsequently derived two equations, **Equation (2-17)** or **Equation (2-18)** as shown below, for low cycle or high cycle fatigue, respectively, where T is the period of repetitive loads. Again, no stress reversal is yet considered ($R \geq 0$).

$$S = 1 - 0.0662(1 - 0.556R)\log N_f - 0.0294\log T \tag{2-17}$$

$$S = 1.20 - 0.20R - 0.133(1 - 0.779R)\log N_f - 0.0530(1 - 0.445R)\log T \tag{2-18}$$

To take into consideration the reversal stress, Zhang et al. (1996) developed another fatigue equation, which is similar to the original one, as shown in **Equation (2-19)**. Where, C_f is a frequency influence coefficient as shown in **Equation (2-20)** and a, b, c are three fitting coefficients; R' = R if $R \geq 0$ and R' = $R * f_{tc}$ for $R < 0$. Here, f_{tc} is the ratio of tension strength to compression strength. Irrespective of loading frequency, the further refined S-N curves can be seen in **Fig 2.33**. From this diagram, it is clearly indicated that stress reversals ($R < 0$) definitely has a negative influence on fatigue life but not significant.

$$S = C_f\left[1 - \beta(1 - R')\log N_f\right] \tag{2-19}$$

$$C_f = ab^{-\log f} + c \tag{2-20}$$

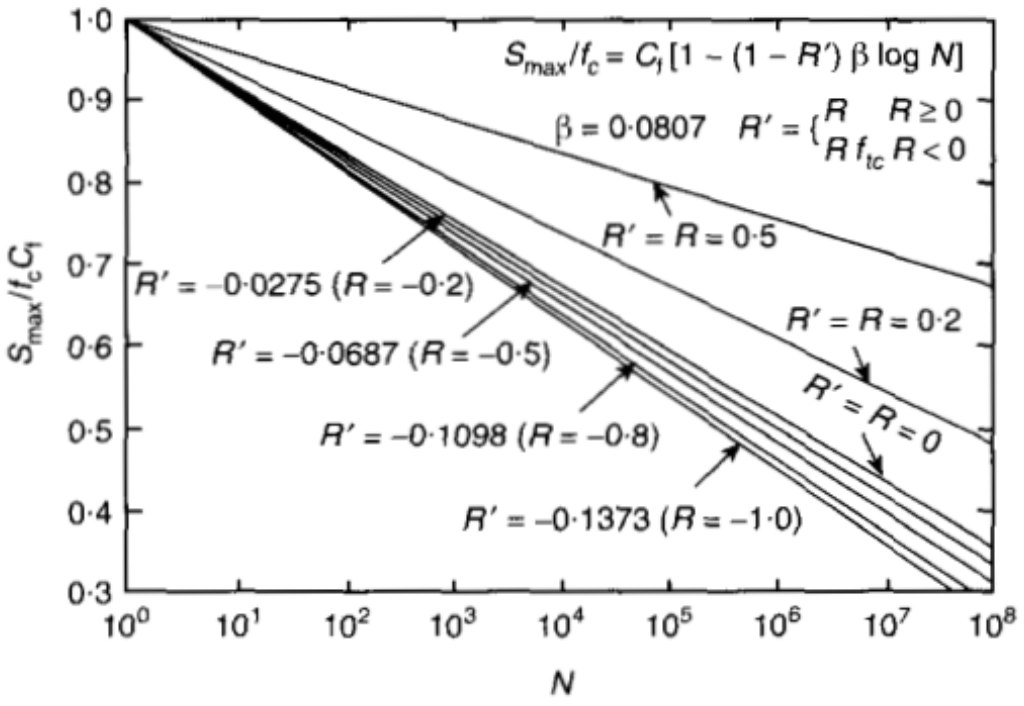

Fig 2.33 Further refined S-N curves for different R values (-1≤R≤0.75) (Zhang et al., 1996)

2.5.4.6 Influence of temperature

The temperature of the mortar or concrete specimens at the time of testing, i.e. the test temperature, affects their mechanical properties in compression or tension, including strength and modulus of elasticity (Saemann and Washa, 1957, McNeeley and Lash, 1963). Generally, lower test temperature results in higher strength and modulus of elasticity, except for extreme temperatures, extremely low or high (Rostásy et al., 1979, Neville, 1995, Neville, 1999). Under normal in-service temperatures (0 °C ~ 80 °C), nevertheless, the change of the compressive strength of plain concrete is thought to be not much (CEB-FIP, 1993), as clearly shown in **Fig 2.34** below.

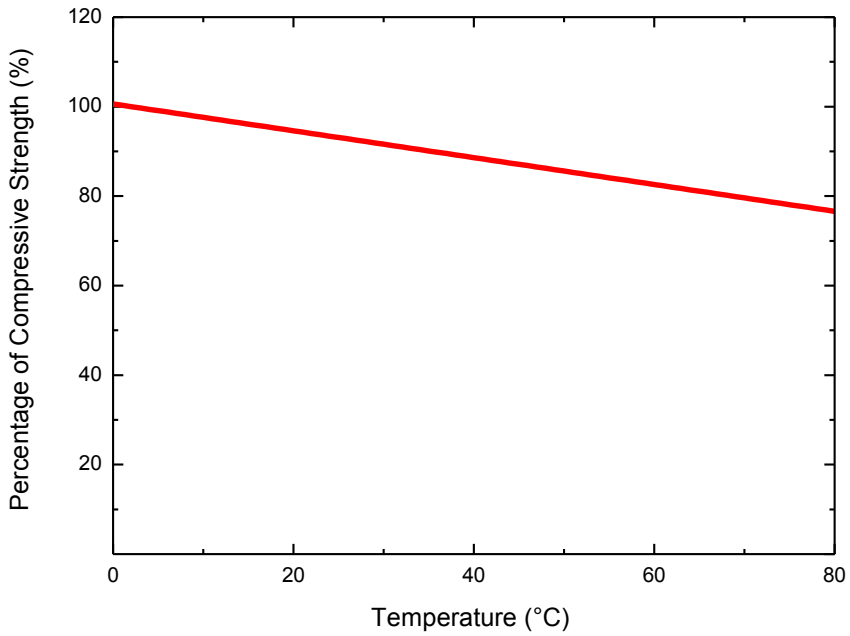

Fig 2.34 Change of compressive strength of plain concrete within a temperature range from 0 °C to 80 °C (After (CEB-FIP, 1993))

There is no literature, however, concerning the influences of test temperature on fatigue of cement-based materials including plain concretes. This is possibly

because, under normal in-service conditions, such influences are insignificant and not considered, unless thermal fatigue caused by temperature gradients occurs. But this is another topic beyond the scope of this thesis. Thus, to conclude, the influence of the test temperature on the fatigue properties of concrete materials could be negligible, if a normal temperature range around room temperature is considered as used in this thesis.

2.5.5 Current issues and a potential solution

One of the main purposes of the literature review presented in this part is to identify the most suitable fatigue test schemes for the two typical CAMs, namely CAM-I and CAM-II, so that both the fatigue behaviour and the mechanisms could be further explored appropriately.

Based on the information reviewed in this part, it becomes evident that there is a need to design a suitable fatigue test apparatus in the laboratory to assess the fatigue of CAM-I and CAM-II before the fatigue properties of each cushion material can be properly evaluated. This is because, at the material level, CAM-I could be considered as a cement-modified asphalt mortar whereas CAM-II an asphalt-modified cement mortar. From the review presented, on the other hand, it has been clearly shown that different fatigue test configurations have been used for two different paving materials, asphalt mixtures and plain concretes, respectively. Hence, it is reasonable to ask whether CAM-I and CAM-II should be tested differently according to their dominant material properties and performance. Consequently, the validity and reliability of the very limited fatigue test methods reported in the literature for CAM-I and CAM-II used in CRTS I and CRTS II also need to be challenged.

Since CRTS I and CRTS II are analogical to semi-rigid pavements as discussed in **Section 2.2.4**, in a similar way, critical bending stresses or strains in the CAM layer could be considered as the dominating factor for fatigue properties of different CAMs. Therefore, a potential solution could be to design two different accelerated performance-based fatigue test schemes for the two CAMs based on a 4PB configuration because the 4PB configuration is the most accepted one for both asphalt mixtures and cement-based materials like plain concrete used in pavements. In particular, the controlled-strain 4PB fatigue tests could be a suitable method for assessing the fatigue of CAM-I whereas the controlled-stress 4PB could be a suitable method for CAM-II, because CAM-I and CAM-II used in those two slab tracks, in terms of material compositions and properties, are close to asphalt mixtures and cement-based materials, respectively. Further details on the test configuration to be used during the fatigue tests will be introduced in **Chapter 3** of this thesis.

2.5.6 Summary

Based on the information reviewed in the last section, the following key points could be summarised.

1. Fatigue properties of CAM-I and CAM-II have been scarcely concerned and understood, especially under bending.
2. Fatigue cracking of asphalt mixtures in flexible pavements is primarily related to critical bending strains and their fatigue test results could be expressed by ε-N curves. The main test variables need to be considered include strain amplitude or level applied and temperature.
3. Fatigue cracking of concretes, one of cement-based materials, in rigid pavements is controlled by critical bending stresses and their fatigue test results could be plotted in S-N curves. The main controlling variables include stress level applied, stress ratio *R* and temperature.
4. Influence of temperature is significant on fatigue of asphalt mixtures but insignificant on fatigue of plain concretes.
5. The controlled-strain 4PB fatigue tests could be a suitable test method for assessing the fatigue of CAM-I, whereas the controlled-stress 4PB fatigue test a suitable method for CAM-II.

2.6 Concluding remarks

A critical literature review has been presented in this chapter for different slab tracks including CRTS I and CRTS II used in China's HSR network, static and dynamic mechanical properties of different CAMs, and above all, fatigue testing and properties of different CAMs, asphalt mixtures and cement-based materials. In combination with the problem statement and the overall aim in **Chapter 1**, it is well recognised that, to assess the bending fatigue properties of the two typical CAMs, namely, CAM-I and CAM-II, different test protocols or schemes should be developed on the basis of fatigue testing of asphalt mixtures and cement-based materials, respectively. And as a result, the potential solution is proposed to use the controlled-strain 4PB fatigue tests for CAM-I whilst the controlled-stress 4PB fatigue tests for CAM-II. This is the research hypothesis throughout this thesis.

CHAPTER 3 EXPERIMENTAL PROGRAMME

3.1 Introduction

To achieve the overall aim and objectives of the research work established in **Section 1.2** in **Chapter 1**, a detailed experimental programme was developed in this chapter after a critical literature review in **Chapter 2** to assess the static, dynamic mechanical and most importantly, fatigue properties of the two typical CAMs, and the results will be fully reported in **Chapters 4-6**, respectively.

Because of the availability of some raw materials used specifically in the CAM layer of CRTS I or CRTS II in China's HSR network such as asphalt emulsion and manufactured fine sands, and fatigue loading facilities, the manufacturing of CAB and CAM test samples and all compression and bending tests including fatigue ones were performed in the concrete laboratory of Institute of Building Materials, School of Civil Engineering, Tsinghua University, Beijing, China. And DMA tests were performed in School of Materials Science and Engineering, Tsinghua University, Beijing, China.

3.2 Experimental programme

To test the bending fatigue properties of the two typical and different CAMs, namely, CAM-I and CAM-II, it has been proposed to use the controlled-strain 4PB fatigue tests for CAM-I whilst the controlled-stress 4PB fatigue tests for CAM-II. Therefore, in the laboratory, a specified 4PB test configuration is required to be designed for testing their quasi-static bending properties firstly and then 4PB fatigue of both CAMs. Furthermore, to study the influence of temperature on their fatigue behaviour, it is necessary to explore the reasonable temperature range before fatigue tests and the feasible test method is probably to use the DMA as mentioned in the review chapter.

In this thesis, the overall experimental work was carried out in three phases as demonstrated in the flow chart below (**Fig 3.1**). Further details on each phase would be given in the first sections of **Chapters 4**, **5**, and **6**.

Phase I Static mechanical tests of CAMs at room temperature

In the first phase, quasi-static bending properties and behaviour of CAM-I and CAM-II were tested at room temperature on a newly-developed 4PB apparatus, with a Portland cement mortar as the control. In comparison, their compressive properties were also tested according to the traditional test method as specified in a tentative specification. In this way, fundamental bending parameters could be obtained for fatigue tests.

Phase II DMA of CAMs and their composite binders, i.e. CABs, under different temperatures

Almost at the same time, in the second phase, the temperature spectra of different CAMs would be measured by the DMA test method at a given loading frequency, compared with the temperature spectra of their corresponding CABs to be tested under the same test conditions. Based on these temperature spectra, a further understanding on the temperature susceptibility and the viscoelasticity of CAMs could be obtained, and the most suitable temperature range used for fatigue tests would be determined.

Phase III. 4-point bending (4PB) fatigue tests of CAM-I and CAM-II

Following **Phase I** and **Phase II**, the third phase was to verify the research hypothesis and could be subdivided into two as shown in **Fig 3.1**.

a. 4PB fatigue tests of CAM-I

Controlled-strain 4PB fatigue tests of CAM-I would be performed at room temperature at first, to obtain its ε-N curve. And then the influence of temperature would be considered.

b. 4PB fatigue testing of CAM-II

Controlled-stress 4PB fatigue tests of CAM-II would be performed at room temperature, and its Wöhler curve could be obtained. Then Influence of stress ratio and temperature would be taken into account.

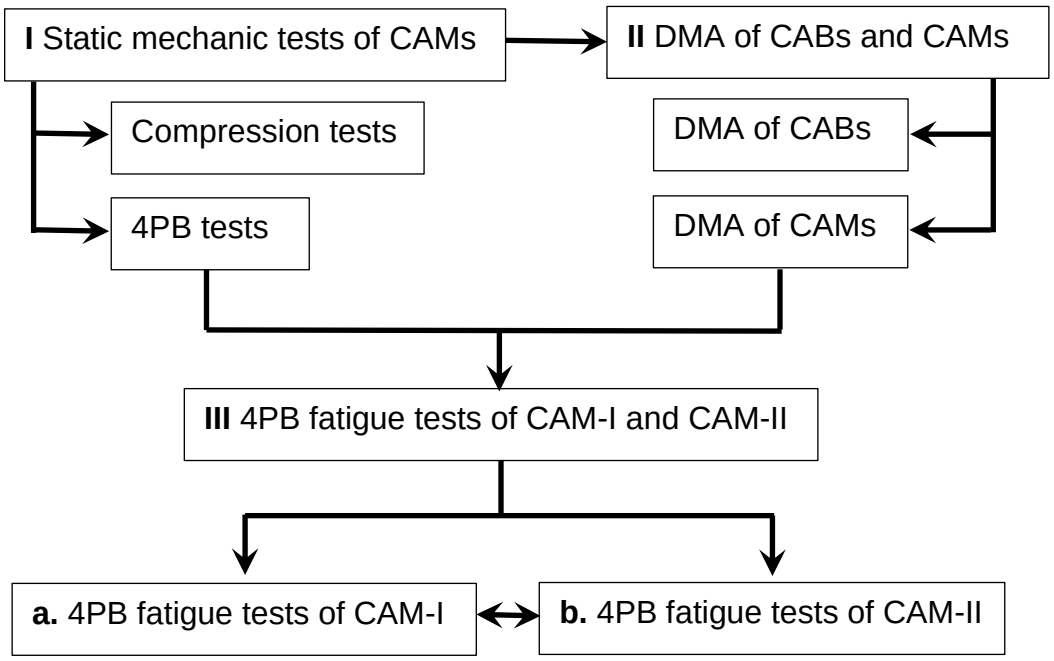

Fig 3.1 Flowchart of overall experimental programme

3.3 Raw materials

CAMs were manufactured in the laboratory primarily out of Portland cement (C), asphalt emulsion (AE), fine aggregates or sands (S), water (W) and a small addition of certain chemical admixtures. The properties of each raw material are given below.

3.3.1 Portland cement

Portland cement is an essential and important component in CABs and CAMs. In this research, ordinary Portland cement (OPC), P·O 42.5 conforming to a Chinese standard (**GB 175-2007**) and manufactured by Beijing Jinyu Cement Corporation, was used as the inorganic binder in the mixes. Its chemical and mineral composition is listed in **Table 3.1** below. The physical properties of this cement used including the setting times and the strengths (**Table 3.2**) were determined according to two Chinese standards, **GB/T 17671-1999** and **GB/T 1346-2001**.

Table 3.1 The composition of ordinary Portland cement (*wt* %)

Chemical composition								
SiO_2	**Fe_2O_3**	**Al_2O_3**	**SO_3**	**MgO**	**CaO**	**Na_2O**	**K_2O**	**L.O.I**
23.47	2.97	7.41	2.39	1.97	60.28	0.14	0.62	2.80
Mineral composition								
C_3S		**C_2S**		**C_4AF**		**C_3A**		
49.58		28.04		8.57		7.28		

Table 3.2 Properties of ordinary Portland cement

Water content for standard consistence	Initial setting time (min)	Final setting time (min)	Soundness	Flexural strength (MPa)			Compressive strength (MPa)		
				3d	7d	28d	3d	7d	28d
27.5 %	172	262	Satisfied	5.5	7.0	8.7	27.9	40.9	51.7

3.3.2 Asphalt emulsion

Asphalt emulsion is another essential component in the mixes. An anionic emulsified asphalt used in the Hu-Yong PDL which links Shanghai to Nanning was used for manufacturing the CAM samples. Prior to the manufacture of CAM samples, basic tests for asphalt emulsion were performed in accordance with **JTJ 2002** in the laboratory in the School of Materials Science and Engineering, Wuhan University of Technology, Wuhan, China. Its basic physical properties are listed in **Table 3.3**.

Table 3.3 Properties of anionic asphalt emulsion

Tests on emulsion		**Tests on residue from distillation**	
Engler viscosity (25℃, Pa.s)	11.0	Solid content (%)	60.9
Mean particle diameter (μm)	4.2	Penetration (25℃, 100g, 5s, 0.1mm)	71.0
Modulus of particle size (μm)	3.4		
Sieve test (1.18mm, %)	0.0	Softening point (R&B, ℃)	48.0
Storage stability (1d, 25℃, %)	0.5	Ductility(15℃, cm)	>100.0
Storage stability (7d, 25℃, %)	3.0	Solubility in trichloroethylene	99.6%

3.3.3 Fine aggregate

Manufactured fine sand, as fine aggregates, was fully dried and packaged in bags for use. The fine sand in bags was provided by Research Institute of High-Performance Concrete (HPC), Central Research Institute of Building and Construction, Beijing, China (RIHPC, CRIBC). The grading curve can be seen in **Fig 3.2**, which was tested by using a Chinese standard for sands, **GB/T 14684-2011**. The curve below showed that the particle diameter of 98.1 % of the sands was less than 1.18 mm and about 80 % had a diameter more than 0.3 mm.

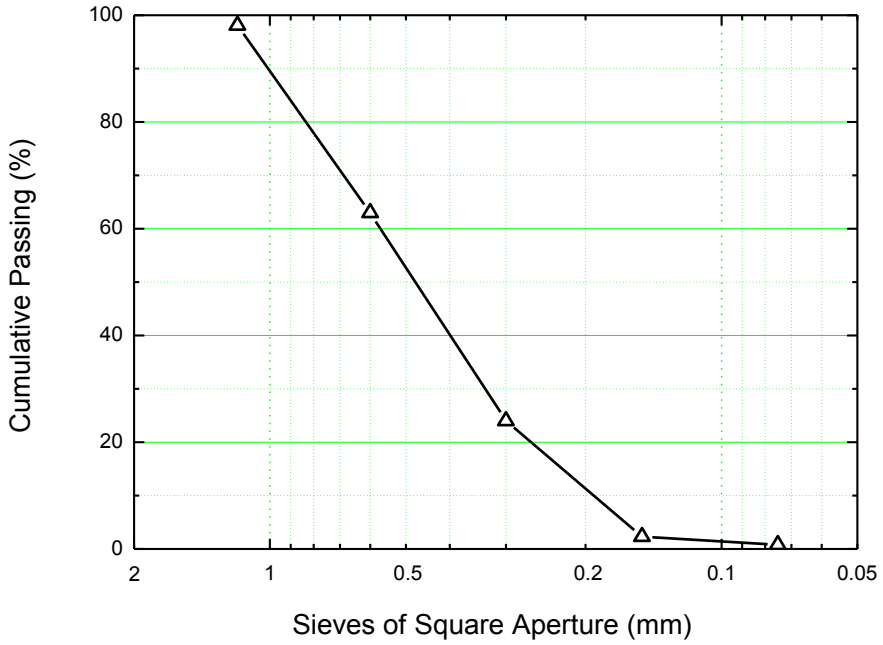

Fig 3.2 The grading curve of fine sands

3.3.4 Water

Tap water was used for all mixes.

3.3.5 Chemical admixtures

Two chemical admixtures were used in CAMs. To reduce or dissipate the foam formed in the process of mixing, a silane-type defoaming agent, DF642, was employed. The dosage was 0.2 % relative to the solid asphalt binder by weight in the CAMs. A polycarboxylate-type super-plasticizer (SP) was used to ensure the fresh properties can meet the requirements as specified in the specification if necessary. Thus, 0.075 % of superplasticizer was added into the control mortar by the weight of Portland cement. However, for the two CAMs studied in this research, no SP was added because of their good fluidity when mixed in the laboratory.

3.4 Mix proportions

Because the focus was on CAMs in the research work, it was necessary to determine the mix proportions of two typical CAMs first, CAM-I and CAM-II. Then the mix proportions of their corresponding binders, namely CAB-I and CAB-II, could be determined immediately. At the same time, a Portland cement mortar and an hcp were formulated as the control.

3.4.1 Mix proportions for CAMs

Since A/C was known to be the decisive factor (Wang and Liu, 2012, Kong et al., 2014), the first and important step was to decide the A/C in a CAM system. For comparison, it was chosen to be 1.0 for CAM-I and 0.2 for CAM-II.

According to the formulations of CAM-I in the early literature (Zuo et al., 2005, Wang et al., 2008f, Zhao et al., 2008), the ratio of sand to Portland cement by mass (S/C) was between 1.2 and 2.0, and the ratio of the total water to Portland cement by mass (W/C) was between 0.7 and 0.9. To study the influencing factors on the compressive strength of CAM-II, on the other hand, a wide range of S/Cs and W/Cs had been used in the later literature (Wang et al., 2008e, A et al., 2009, Tan et al., 2011, Tan et al., 2012), but to reach a balance between the fluidity and the strength, it was better to make S/C less than 1.6 and W/C less than 0.6. Integrated with the formulations of CAMs with different A/Cs (0.2 ~ 1.0) used in Dr. Kong's work (Liu et al., 2009, Kong et al., 2010a, Kong et al., 2010b), in the end, the sand-binder ratio (S/(A+C)) was designed to be a constant value, 1.5 for both CAM-I and CAM-II, while the W/C was set to be different, 0.8 for CAM-I and 0.5 for CAM-II. The addition amount of the deforming agent was 0.2 % by mass relative to asphalt binder, and mini-slump tests would be performed to determine the amount of superplasticizer to be added. As mentioned in the previous section, no superplasticizer was used for two CAMs and 0.075 % of superplasticizer to Portland cement by mass was added to the control. The final mix proportions of CAM-I, CAM-II and the control were determined, as listed in **Table 3.4**.

In practical use, aluminium powder and expansive agent (Hu et al., 2008, Wang et al., 2010a) were also used in CAMs, to control the volumetric stability of CAMs during the curing process. But their amount in CAMs was small, and the influences on the final mechanical properties of CAMs were not clear. For simplicity, therefore, none of them was used in the mix proportions.

Table 3.4 Mix proportions of CAM-I and CAM-II (by mass)

Type	A/C	C	AE		A+C	S	Tap water	DF	SP	W/C
			A	Water						
CAM-I	1.0	1260	1260	809	2520	3780	199	2.5	0.0	0.8
CAM-II	0.2	2100	420	270	2520	3780	780	0.8	0.0	0.5
Control	0	2520	0	0	2520	3780	1260	0.0	4.4	0.5

Note: A, AE, C, S, W, SP and DF represents asphalt binder, asphalt emulsion, Portland cement, sands, total water, superplasticizer and de-foaming agent.

3.4.2 Mix proportions for CABs

Mix proportions for CAB-I and CAB-II were determined based on those of CAM-I and CAM-II, respectively. In this case, they had the same A/C and W/C as could be seen from **Table 3.4** above. Likewise, the control hcp could use the basic formulation of the Portland cement mortar, but it was found to bleed badly during mixing with some superplasticizer. In this case, no superplasticizer was chosen to be used in the hcp. The final mix proportions of CAB-I, CAB-II and the hcp were determined as well, as shown in **Table 3.5**.

Table 3.5 Mix proportions of CAB-I and CAB-II (by mass)

Type	A/C	C	AE	Tap water	DF	W/C
CAB-I	1.0	100.0	164.2	15.8	0.20	0.8
CAB-II	0.2	100.0	32.8	37.2	0.04	0.5
hcp	0.0	100.0	0.0	50.0	0.0	0.5

Note: The abbreviations used herein are consistent with those in **Table 3.4**

3.5 Manufacturing of test specimens

After mix proportions for CABs and CAMs were fully determined, it was time to manufacture their test specimens for different mechanical tests. The whole process included the preparation of the raw materials and the moulds, mixing, casting, curing and cutting.

3.5.1 Preparation of the materials

Raw materials such as asphalt emulsion, manufactured fine sands and Portland cement were ordered before mixing, and stored in the laboratory properly.

The asphalt emulsion was sealed off in two buckets and stored in a room with constant temperature below 25 ˚C, to make sure its storage stability before use. Manufactured fine sands in bags were piled in the corner of the concrete laboratory hall with waterproofing plastic films covered. And ordinary Portland cement from the same batch was ordered at once for use one week before the mixing work was planned to be started. All chemical admixtures were held in bottles and stored in a cool place for use.

3.5.2 Preparation of the moulds

In the experimental, different CAM samples were designed for static, dynamic mechanical and fatigue tests under different conditions. Thus, different moulds were prepared for manufacturing different test specimens.

For the compression tests of CAMs, PVC moulds (**Fig 3.3 (a)**) with the outside diameter (OD) of 53 mm and the height of 120 mm were cut by a saw from a commercial PVC tube. A cut-through notch along the height was made to facilitate the demoulding process of CAM samples. For their bending tests or fatigue tests, standard steel moulds (**Fig 3.3 (b)**), which were usually used for making standard beam samples (size, 40 mm × 40 mm × 160 mm) to test both flexural and compressive strengths of mortars (**GB/T 17671**), were prepared. For the dynamic mechanical tests of CAMs and CABs, a self-made steel mould, consisting of two outside thick plates and one intermediate thin plate as shown in **Fig 3.4**, was used to produce small beam samples (Thickness = 4 ~ 6mm). All moulds were brushed with a thin layer of a demoulding agent used for concrete before the mixing process started.

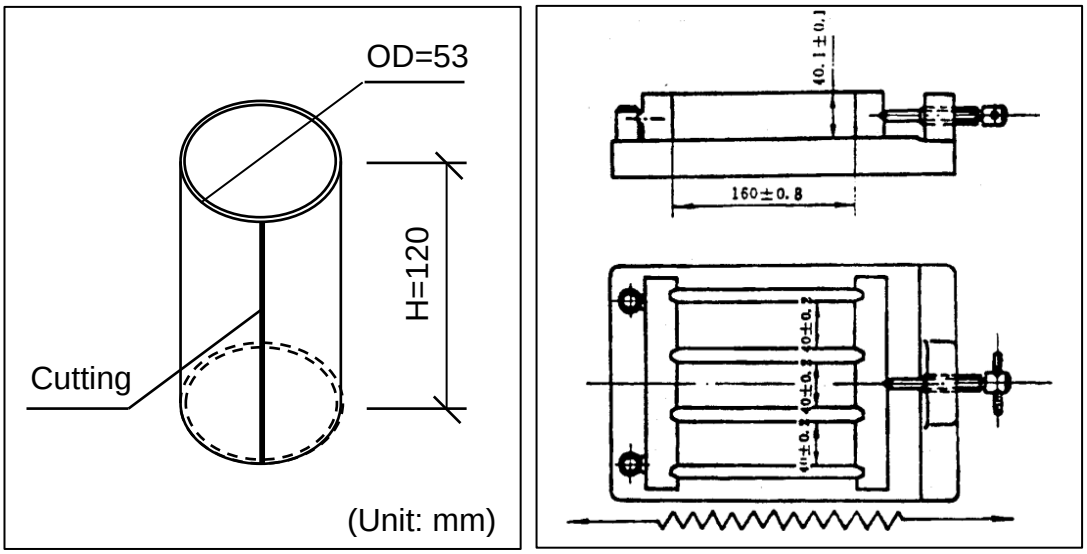

(a) **(b)**

Fig 3.3 Moulds for making CAM samples used in (a) compression and (b) bending (GB/T 17671)

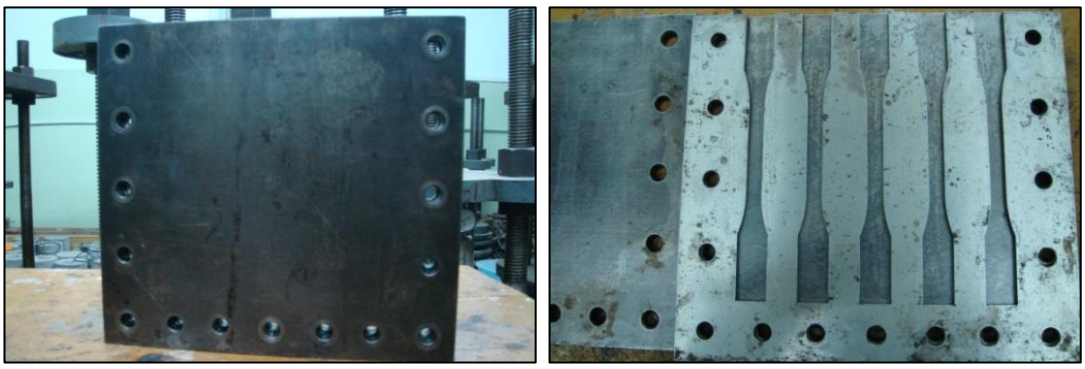

(a) **(b)**

Fig 3.4 A self-made steel mould with (a) two outside thick plates (b) one insider thin plate

3.5.3 Mixing method

It was reported that the sequence of adding raw materials during mixing, the mixing speed used or the mixing time, had an influence on the mechanical properties of CAMs (Wang et al., 2007, Xie et al., 2011, Zhang et al., 2011a, Zeng et al., 2013). To obtain well-mixed fresh CAMs, a 5-min mixing method was used and the basic principle was to add solid materials into the liquids.

At a low stirring speed of 25 rpm, firstly, a stirring mixer (**Fig 3.5**) was poured in with asphalt emulsion, and then water plus a small amount of superplasticizer. This took about half a minute. Next step, Portland cement was added into the liquid mixture and the stirring speed was increased to 50 rpm, for one minute. Immediately, fine sands were added into the fresh CABs and stirred for two and a half minutes. The final step was to mix the deforming agent into the CAM mixture and the stirring speed went back to 25 rpm, lasting for one minute. After this process, the freshly-mixed CAM mixture was ready for casting.

For fresh CABs, the same mixing method was used but in a smaller mixer which was usually for use in making cement pastes.

Fig 3.5 The CAM mixing in a 2.5-Litre stirring mixer

3.5.4 Casting

After the 5-min mixing process was finished, the fresh CAMs were slowly cast into different moulds without vibration. The whole process was usually finished within half an hour. To avoid the water evaporation quickly and guarantee a high humidity of the curing environment, plastic membranes were used to cover the casting surfaces of the fresh CAMs.

The casting of fresh CABs was a little more difficult in practice because of the wideness of openings (4 ~ 6 mm) as shown in **Fig 3.6**. In this case, a small vibration was needed to guarantee the fresh CABs totally into the openings.

Fig 3.6 The casting of CAMs in the concrete laboratory

3.5.5 Curing regime

Research work by Liu et al. (2011b) had suggested that the curing of CAMs at an early age was crucial for CAM-II and dry curing was beneficial to the strength development of CAM-I. Therefore, a unified curing regime was conducted for the two CAMs as follows.

After casting, CAM samples with the moulds together were cured for 1 ~ 3 days in a standard curing room, at 20 °C (room temperature), and relative humidity (RH) > 95 %, and then they were removed from the moulds and stayed in that room until the age of 7 days. At that age of curing, they were transferred to another standard room with constant temperature (23±2) °C and RH ((65±5) %) and cured for at least 6 months for different mechanical loading tests.

The same curing regime, to be consistent, was used for CAB samples.

3.5.6 Cutting procedure

Due to the hydration of Portland cement, the shrinkage happened during the process of curing. Generally, a small amount of aluminium powder and expansive agent (Hu et al., 2008, Wang et al., 2010a) were mixed into the fresh CAMs to control the early-age and the later-age shrinkage. But in this research work, as stated in **Section 3.4.1**, none of these two raw materials would be used and shrinkage of CAMs would be allowed. So after hardening, the CAM samples were finally obtained with rough and uneven surfaces because of the free shrinkage.

To make sure that test specimens had almost a standard size for compression or bending tests, cutting was conducted on a machine as shown in **Fig 3.7**. Cylinder specimens with the height of 50 mm, which would be used for compression tests, were cut from longer cylinder CAM samples. For bending tests, beam specimens with the size of 30 mm×40 mm×160 mm were made by cutting the free shrinkage surfaces away from the original CAM samples. The cutting machine was designed for this purpose. The procedure was divided into two as shown in **Fig 3.8**. Firstly, place a CAM prism onto the platform of the cutting machine with its free surface faced to the sawing blade, make sure the moulding surface in line with the edge and fixate the sample using two movable screws at the two ends. Secondly, start the machine and move the platform forward manually at a very low rate. Due to the difference in mechanical properties of CAM-I and CAM-II, by the way, different sawing blades for soft or hard materials were used in the process of cutting.

Fig 3.7 A cutting machine for mortar and concrete

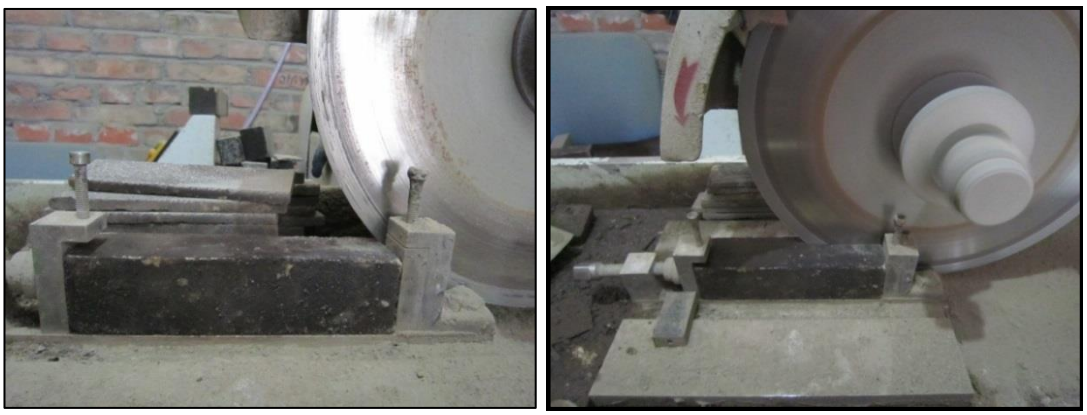

(a) **(b)**

Fig 3.8 The cutting process of CAMs: (a) fixation and (b) cutting

3.6 Test facilities and methodologies

This section mainly introduced the basic test methods or protocols used to measure the workability, the static and dynamic mechanical properties, and most importantly, the 4PB fatigue of CAMs.

3.6.1 Mini-slump test

Mini-slump tests in accordance with a tentative specification for CAM-II (Dept. of Sci & Tech, 2008b) were performed before CAM sample making, to make sure all CAMs manufactured with adequate self-compacting properties.

The test procedure was as follows. After fully mixing, fresh CAM was poured into a hollow cylinder with the diameter of 50 mm and the height of 190 mm, which was pre-moistened and put in the centre of a glass plate (400 mm×400 mm) as shown in **Fig 3.9**. As fast as possible, next, the hollow cylinder was moved upwards vertically and the mortar spread onto the glass plate until a stable circle was gradually formed. Using a ruler, in the last step, the diameter of the circle, i.e. spread diameter, was measured. The same procedure was repeated for the same mortar after it was stored for 30 min. In this way, spread diameters of this CAM at the time of 5 min and 30 min were obtained. In the specification, the spread diameter of fresh CAMs at 30 min should not be less than 280 mm. From the results as depicted in **Fig 3.10**, obviously, spread diameters of CAM-I, CAM-II and the control Portland cement mortar met that requirement, although there was a decrease to an extent for any mortar as time went from 5 min to 30 min.

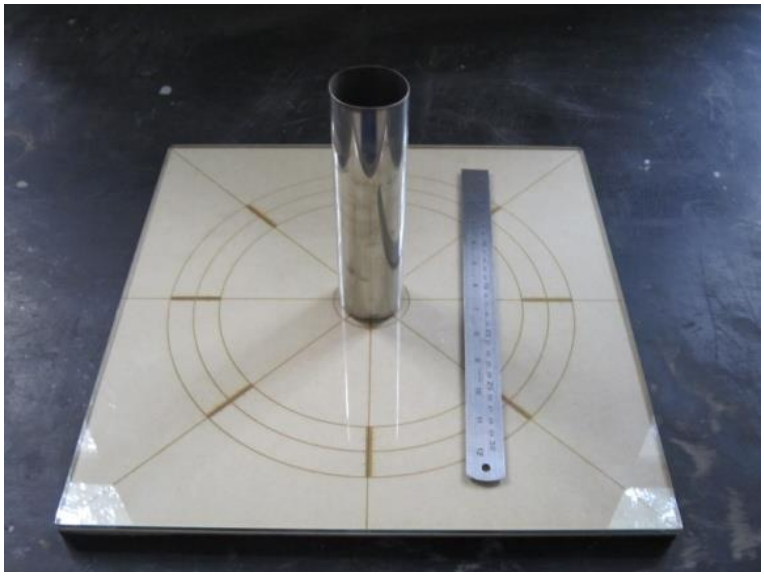

Fig 3.9 A mini-slump test setup for CAMs

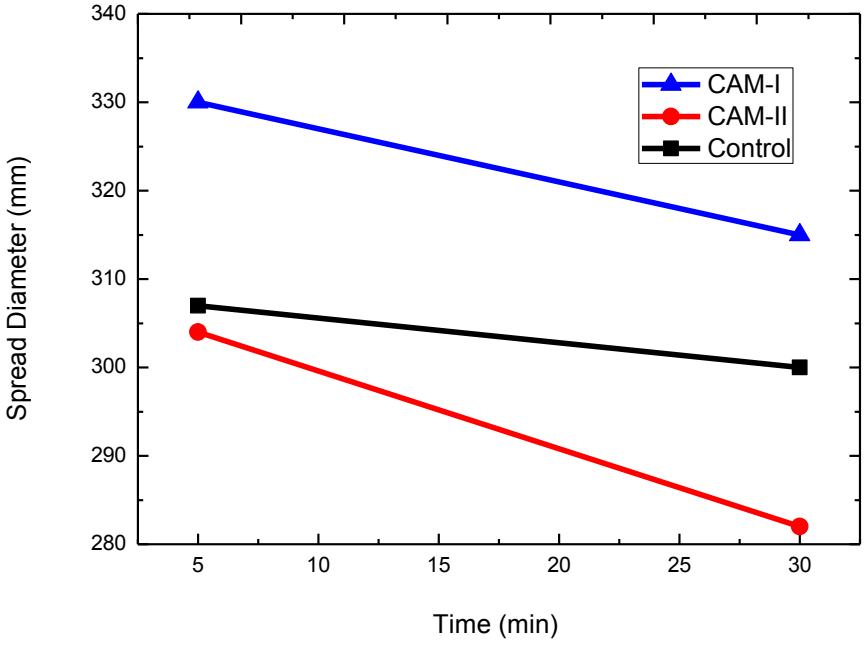

Fig 3.10 Spread diameters of CAM-I, CAM-II and the control

3.6.2 Compression test

Uni-axial and monotonous compression tests of CAMs were performed at room temperature on an electro-hydraulic servo-control Material Test System (i.e., MTS 810) as seen in **Fig 3.11**. The loading mode was controlled by vertical displacement of two grips and the rate was1.0 mm/min (Dept. of Sci & Tech, 2008a). At least 3 samples were used for each test and the mean values were used as mechanical parameters. Prior to loading, two loading surfaces of the samples were coated with French chalk to reduce the surface restraint effect and stress concentration.

By loadings on different CAM samples, force-displacement curves of CAMs could be directly obtained. And it was pre-assumed that strains on axially loaded samples were uniform along the height and the area of the section was unchangeable through the whole process. Hence, engineering strains and stresses, ε_c and σ_c, could be calculated by dividing the displacement by the original height (ε_c = Displacement / Height), and the force by the area of section (σ_c = Force / Area), respectively. On a compressive stress-strain curve, the maximum stress value was defined as peak stress, σ_{cp}, i.e. compressive strength, and the corresponding strain value, ε_{cp}, as peak strain. Such a curve was at all times composed of two portions, the ascending portion till the peak value and the descending portion after the peak. The tangent modulus at the original point, E_c, was used as Young's modulus, to characterise the elastic deformability of the CAMs. This test method was generally used for measuring the compressive strength and the elastic modulus of CAM-I, but for comparison, it was used for both CAMs in this thesis.

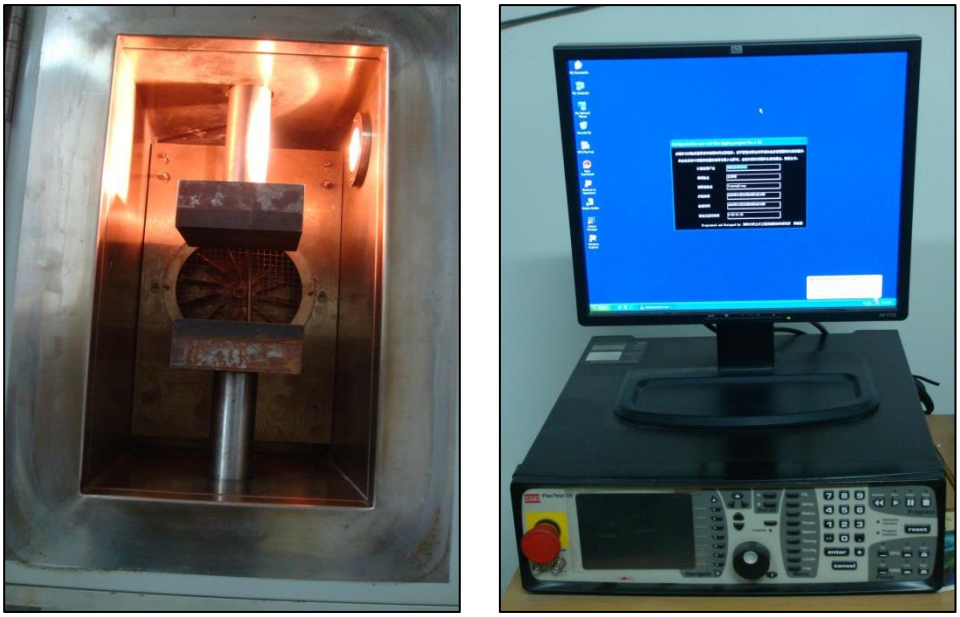

(a) **(b)**

Fig 3.11 A material test system (MTS 810) (a) loading frame (b) controller

3.6.3 Dynamic mechanical analysis

To obtain temperature spectra of CABs or CAMs at a given frequency, small samples were tested on a Du Pont instrument DMA 2980 equipment (**Fig 3.12**) operating in a single cantilever bending mode, from -100 ˚C to 100 ˚C at the constant frequency of 10 Hz. The theoretical basis can be referred to in **Section 2.4** of the previous chapter.

The operation process was in this way. Firstly, a CAB or CAM specimen was clamped by one end on the equipment in an environmental chamber. Next, the temperature in the chamber was lowered to -100 ˚C (liquid N_2 used), and equilibrated isothermally for at least 5 minutes. Finally, small and controllable dynamic vibrations were continuously exerted to the other end of the specimen by the DMA equipment, with a temperature ramp of 5 ˚C per min to 100 ˚C. The whole test process took nearly one hour for one specimen. For polymers, as usual, one specimen is enough to obtain a temperature spectrum (Yang et al., 2004). For one CAB, it was indicated that the temperature-sensitive range measured on different specimens remains unchangeable, although the absolute values of their dynamic modulus are sometimes hugely differently (Liu, 2009) because they are assumed to be homogeneous but heterogeneous in fact. However, the main objective of DMA tests is to explore the most suitable temperature range used for fatigue tests. In this case, just one CAB or CAM specimen was used for a temperature spectrum.

(a)

(b)

Fig 3.12 (a) Du Bond instrument DMA 2980 and (b) test specimens

3.6.4 A 4PB apparatus developed for CAMs

To perform bending tests for two typical CAMs in the laboratory, especially fatigue in bending, an apparatus should be designed and the 4PB was a good option. This section would introduce the concept of design for a newly-developed 4PB apparatus, operation procedures with this apparatus on the MTS and the analysis method of fatigue test data obtained.

3.6.4.1 Apparatus design

In the design of a 4PB apparatus, there were two considerations. One of them was how to choose the loading surface and the loading zone on a CAM specimen in bending tests, the size of which was 30 mm×40 mm×160 mm. As illustrated in **Fig 3.13** above, the two moulding surfaces of the CAM beam were chosen as the loading and supporting surfaces, and the loading zone was set up in the middle, with a length of 120 mm, i.e. L=120. One-third of the length was the pure bending zone.

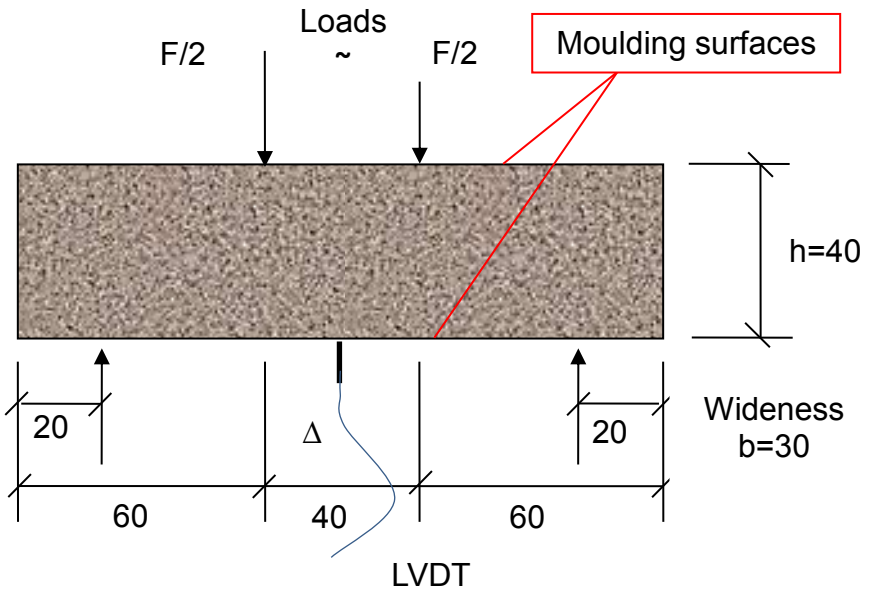

Fig 3.13 Schematics of 4PB testing on a CAM specimen

The other consideration was how to make the apparatus compatible with the MTS machine. To this end, connecting bars were used to exert loads, F, static

or dynamic ones, and a special LVDT (Linear variable differential transformer) compatible with the controller of the MTS was placed in the centre, to measure the deflection during loading first, Δ, and secondly to turn the control mode from load-controlled into deflection-controlled. In this way, the maximum tensile stress, σ_t, and the maximum tensile strain, ε_t, at the outer fibre of the beam specimen could be calculated based on the classical beam theory, as shown in **Equation (3-1)** and **Equation (3-2)**.

$$\sigma_t = \frac{FL}{bh^2} \tag{3-1}$$

$$\varepsilon_t = \frac{108\Delta h}{23L^2} \tag{3-2}$$

On the basis of the design concept above, a newly-developed 4PB apparatus, as can be seen from **Fig 3.15 (a)**, was manufactured by a company in Beijing and outfitted with an LVDT (**Fig 3.15 (b)**). This apparatus was mainly comprised of two parts. The upper part was movable with two load points while the lower part was the supporting base with two reaction points. Four quadrate hollow frames, to fit the CAM specimen in, were held in position using four cross rollers, in order to provide some translation and rotation on all load and reaction points, and four screws were used to lock/unlock the beam specimen. The LVDT was fixated through a hole on a small bridge in the upper part. Its measuring range was ±1.000 mm with a high precision of 0.001 mm. This apparatus was very similar to the IPC Global 4PB device used in the US and Australia for fatigue testing of different asphalt mixtures but on a smaller scale. Therefore, it could be called mini-4PB apparatus or device for CAMs.

By using two steel connectors and connecting bars, the mini 4PB apparatus would be installed on the MTS machine before any bending test. The whole loading process was controlled via the controller of the MTS machine, for example, control mode, loading rate or frequency, and data acquisition. To condition the temperature of the tests, in addition, an environmental chamber, as shown in **Fig 3.16**, was tailor-made and placed into the loading frame of the

MTS, to accommodate the mini-4PB apparatus. The air temperature in the chamber could be adjusted from -70 °C to 100 °C.

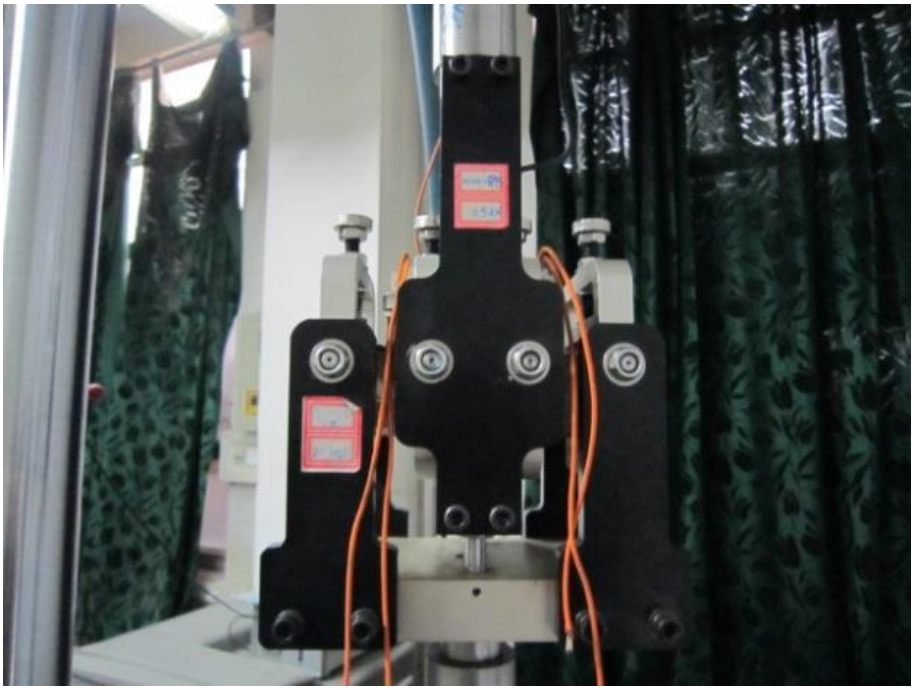

(a)

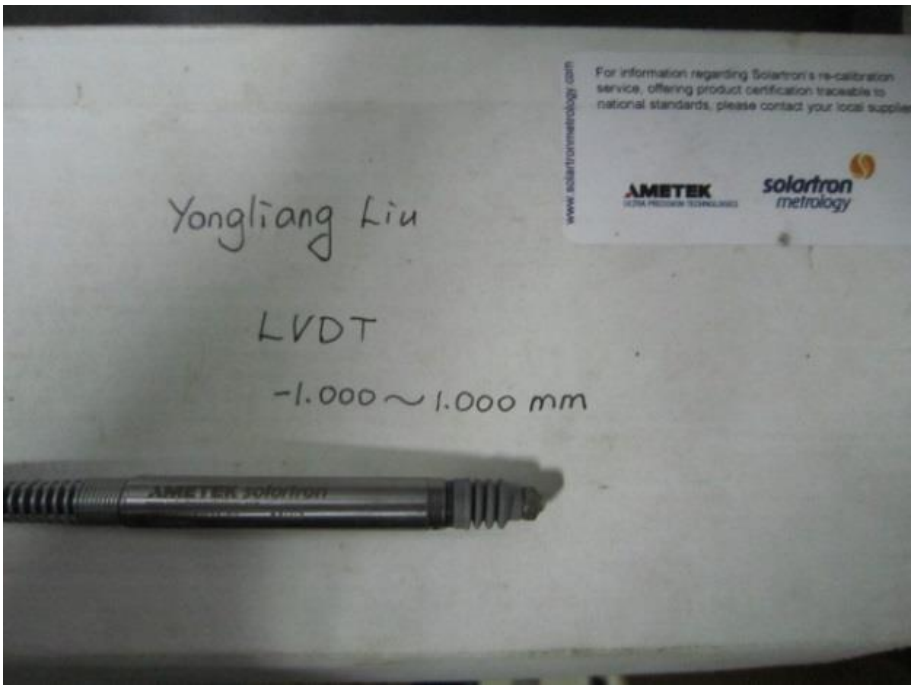

(b)

Fig 3.14 (a) The 4PB apparatus on the MTS with (b) an LVDT

Fig 3.15 The 4PB apparatus in an environmental chamber on the MTS

3.6.4.2 Operation procedures

In a bending test, there was a strict sequence of procedures operated to follow as detailed in **Appendix I**. These procedures were tried and concluded from the operation of the MTS with the mini-4PB apparatus.

In the interface of the MTS, the whole loading process could be programmed in advance. For monotonous bending tests of CAMs, it was easy to programme and exert a linear deflection on the two typical CAMs at a loading rate of 0.001 mm/s and at least 3 beams were used for one test. In contrast, for 4 PB fatigue, the programming of the dynamic cyclic loads was more complex. As mentioned in **Section 2.5** of **Chapter 2**, the fatigue of CAMs was significantly influenced by such loading conditions as mode of loading, load magnitude, the shape of wave form, loading frequency and rest period. But at the initial stage of apparatus development, for simplicity, a continuous sinusoidal waveform with a loading frequency of 10 Hz and no rest period was chosen. As a result, only two factors, mode of loading and load magnitude, were considered. In the fatigue test of

CAM-I, for example, the controlled-strain mode was used, the main variable was the amplitude of the sinusoidal strain wave, ε_a, and the mean strain was set to zero, i.e. ε_m=0, as the dashed line shows in **Fig 3.16**. Because the controlled-stress mode was used for fatigue testing of CAM-II, in a similar way, a stress cycle of fatigue loadings could be characterised by the stress amplitude (S_a) and the mean stress (S_m), or by the maximum stress (S_{max}) and the minimum stress (S_{min}), or even by the stress range (ΔS) and stress ratio (R) (Schijve, 2009). These parameters were interrelated as described in **Equation (3-3)** ~ **(3-6)**. In the case of CAM-II, S_{max} and *R* were preferred.

$$S_a = \frac{S_{max} - S_{min}}{2} \tag{3-3}$$

$$S_m = \frac{S_{max} + S_{min}}{2} \tag{3-4}$$

$$\Delta S = S_{max} - S_{min} \tag{3-5}$$

$$R = \frac{S_{min}}{S_{max}} \tag{3-6}$$

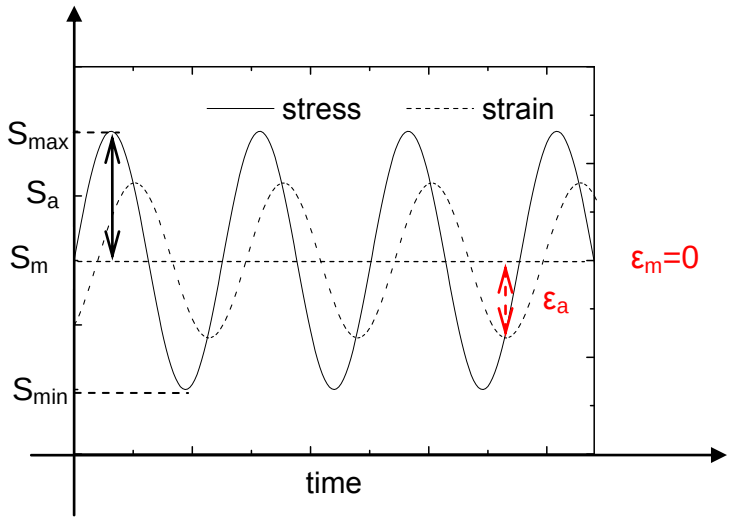

Fig 3.16 Characteristics of fatigue loadings for CAMs in the controlled-strain or controlled-stress mode

3.6.4.3 Fatigue data analysis method

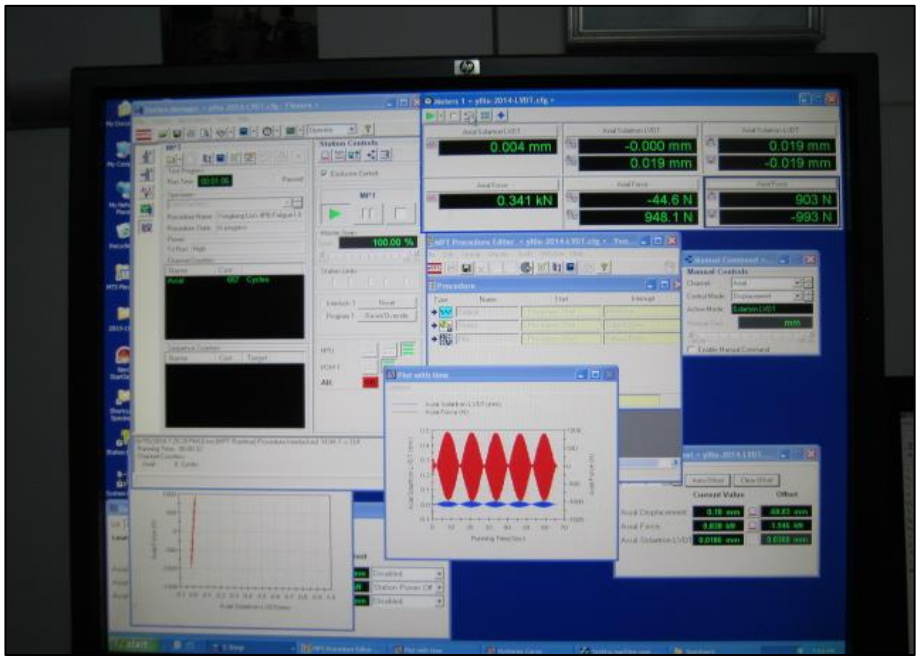

Fig 3.17 The interface for fatigue tests on the MTS

During the 4PB fatigue test, the typical interface could be seen in **Fig 3.18**. To obtain enough fatigue data, 50 points were recorded in every cycle. After a few hundreds or thousands of cycles, the data size was huge. A programming of MATLAB (Zhang, 2006) to process the fatigue test data, therefore, was compiled and shown in **Appendix II**. The basic principle was to fit the data of F and Δ in a cycle using two assumptive equations, **Equation (3-7)** and **(3-8)**, and get the amplitudes of force and deflection, F_A and Δ_A.

$$F(t) = F_0 + F_A \sin(\omega t + \delta_F) \tag{3-7}$$

$$\Delta(t) = \Delta_0 + \Delta_A \sin(\omega t + \delta_\Delta) \tag{3-8}$$

Where, ω was the angular frequency and ω=2πf; F_0, δ_F, Δ_0 and δ_Δ were other four variables fitted from the fatigue data, but not concerned.

Those fitted variables, F, F_0, F_A and Δ, Δ_0, Δ_A, could be converted into stresses and strains as shown in **Equation (3-9)** and **Equation (3-10),** and thus stiffness

or dynamic modulus, E_d, and dissipated energy, w, as defined in **Equation (3-11)** and **Equation (3-12)**, could be calculated from one cycle to another. It was necessary to point out here that, if compared with dynamic mechanical parameters from DMA in the preceding **Section 3.6.3**, the dynamic modulus, *E*, and the lag angle related to dissipated energy, δ, were different in physical meanings due to damage incurred and accumulated during fatigue loading, though they were defined and calculated in the same way.

$$\sigma(t) = \sigma_0 + \sigma_a \sin(\omega t + \delta_F) \tag{3-9}$$

$$\varepsilon(t) = \varepsilon_0 + \varepsilon_a \sin(\omega t + \delta_\Delta) \tag{3-10}$$

$$E_d = \frac{\sigma_a}{\varepsilon_a} \tag{3-11}$$

$$w = \pi \sigma_a \varepsilon_a \sin\delta \tag{3-12}$$

Fatigue test data is known to be scattered statistically. To obtain a typical ε-N curve for an asphalt mixture, there requires at least 6 specimens (**ASTM Designation: D7460-10**). On an S-N curve of concrete, on the other hand, it is believed that, under tightly controlled conditions, 5 specimens per data point are sufficient to produce meaningful results (Paskova and Meyer, 1994). In order to obtain reliable fatigue test data and fatigue curves in a limited duration, 3 data points for one fatigue curve and at least 3 beams for each data point were used in this thesis.

CHAPTER 4 STATIC MECHANICAL PROPERTIES OF CEMENT-ASPHALT MORTARS AT ROOM TEMPERATURE

4.1 Introduction

In CRTS I or CRTS II, the intermediate layer is made out of CAM-I or CAM-II, respectively, and sandwiched between the precast RC track slabs and the cast-in-place concrete trackbed (as shown **Fig 1.3** in **Chapter 1**). One of the cushion layer's primary functions is to sustain traffic loads from the top and transmit them to the foundation, which is highlighted in **Section 2.2.4**.

Owing to the specific role of the CAM layer in those two slab tracks, mechanical properties and behaviour of CAMs, as engineering structural materials, are of prime concern for both researchers on materials and structural engineers. It is well established that static mechanical properties of CAMs, usually tested in the laboratory under standard conditions, are important and indispensable in the process of their formulation design and quality evaluation. On the other hand, mechanical parameters obtained by mechanical loading tests on CAMs are fundamental for numerical modelling of the two prefabricated concrete slab tracks with the CAM layer, to evaluate the structural performances of these two slab tracks, which in turn helps to guide the redesign of such cushion materials. It was pre-assumed that the compressive stresses dominated in the CAM layer while the tensile ones could be negligible. Because of this, much of previous research work focused on compressive properties of CAMs (Wang et al., 2008f, Liu et al., 2009, Liu et al., 2013, Kong et al., 2014). However, as mentioned in **Section 2.3.3** of the review chapter, such an assumption is questionable. And based on the modelling work, CAMs are known to be mainly subjected to bending in slab tracks (Zhao, 2003b, Liu et al., 2010). In this case, the validity of the traditional compression test method used for CAMs is challenged.

In this chapter, therefore, on a newly-developed mini-4PB test apparatus, static bending properties of two typical CAMs at room temperature, CAM-I and CAM-II, were for the first time tested and discussed, with a Portland cement mortar as the control. In comparison, their compressive properties and behaviour at room temperature were measured using the traditional compression test method as well. Then a comparison between the two CAMs was conducted to demonstrate their differences in static mechanical properties and behaviour. As discussed in **Section 2.3** of **Chapter 2**, the properties and behaviour of CAMs are controlled by the properties and behaviour of their composite binders, CABs. To elucidate the differences, furthermore, microstructural models of the two corresponding CABs could be established by a theoretical calculation on volume fractions of each phase in these CABs based on the classical Powers-Brownyard model (Powers and Brownyard, 1946). At the end of this chapter, the two test methods were compared to evaluate the newly-developed 4PB test method.

The objectives of this chapter are:

- To study the static compressive properties of CAM-I and CAM-II at room temperature in accordance with the compression test method;
- To study the static bending properties of CAM-I and CAM-II at room temperature using the newly-developed 4PB test method, in order to obtain fundamental bending parameters as a reference for fatigue tests in **Chapter 6**;
- To evaluate the suitability of the 4PB test method and the reliability of the test results, through comparing mechanical properties and behaviour of the two typical CAMs from the two test methods.

4.2 Experimental programme

To achieve the objectives in this chapter, an experimental programme of static mechanical loadings on CAMs was developed as shown in the flow chart of **Fig 4.1**, and conducted in three stages as follows.

Stage 1: Uniaxial compressive properties of CAM-I, CAM-II and the control Portland cement mortar were tested at room temperature, in accordance to one of the two tentative specifications;

Stage 2: Bending properties of CAM-I, CAM-II and the control Portland cement mortar were tested at room temperature by using a newly-developed 4PB test method;

Stage 3: Static mechanical properties of CAM-I and CAM-II obtained from the two different test methods were compared.

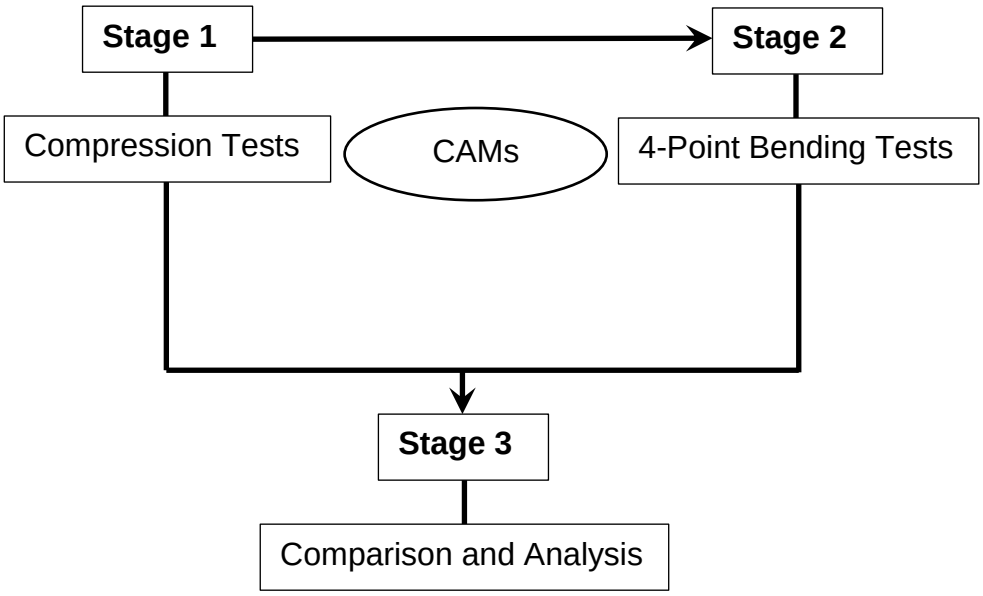

Fig 4.1 Flow chart of the experimental programme in Chapter 4

4.3 Compressive properties of CAM-I and CAM-II at room temperature

To understand the differences in mechanical properties of CAM-I and CAM-II, traditional uni-axial compression tests according to one of the two tentative specifications were used to obtain their compressive stress-strain curves and mechanical parameters under compression such as compressive strength and Young's Modulus. Meanwhile, deformation and failure mode during loading was recorded and analysed.

4.3.1 Compressive stress-strain curves

It is well accepted that, as the control, the Portland cement mortar is typically a quasi-brittle solid. From its stress-strain curve (the green line in **Fig 4.2**), the cement mortar deformed linearly elastic to over 80% of compressive strength before a small amount of plastic deformation till the peak value and a sudden fall in stress after the peak occurred.

When 20% of asphalt binder/cement (CAM-II, A/C=0.2) was incorporated into Portland cement mortar, a significant reduction in compressive strength and Young's modulus at room temperature happened but it deformed (the red line in **Fig 4.2**) more like the control cement mortar in a quasi-brittle manner. The after peak softening portion showed that its deformability had been improved.

When A/C went high to 1.0, in contrast, CAM-I were capable of undergoing a large amount of deformation under compression at room temperature (the black line in **Fig 4.2**) in spite of the lowest compressive strength and modulus of elasticity among CAMs.

The change in compressive stress-strain curves clearly indicated that, at room temperature, CAM-I was more like a ductile material which had relatively high deformation ability while CAM-II deformed in a typically quasi-brittle manner, the same with the control Portland cement mortar.

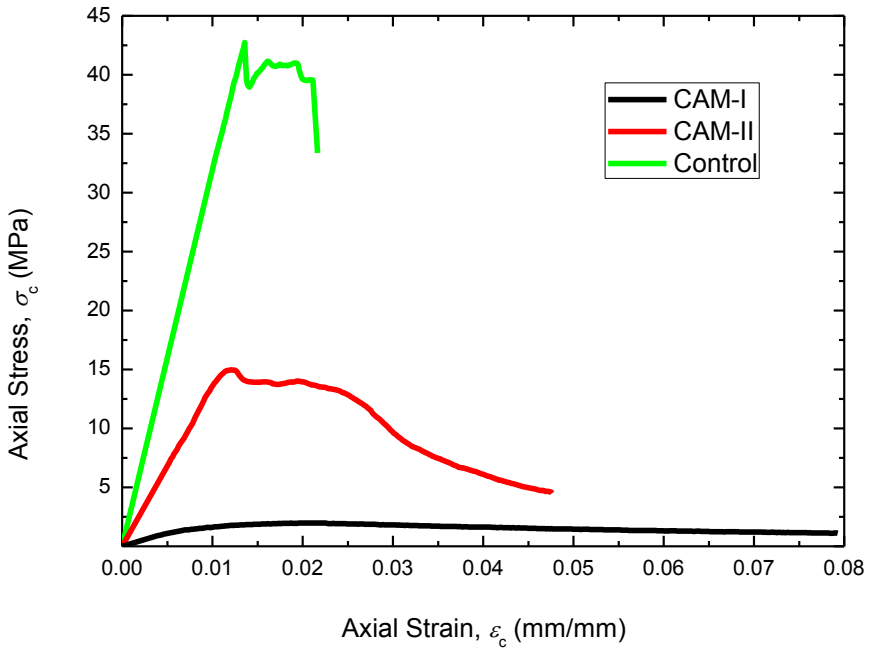

Fig 4.2 Compressive stress-strain curves of CAMs

4.3.2 Compressive strength and modulus

Due to the addition of asphalt emulsion into Portland cement mortar, seen from **Fig 4.3 (a)** and **(b)**, both compressive strength and Young's modulus of two typical CAMs, CAM-I and CAM-II, were significantly reduced.

Quantitatively, from **Table 4.1**, the strength of CAM-II at room temperature was nearly one-third of that of Portland cement mortar, and for CAM-I, its strength was only 2.04 MPa, less than one twentieth. Meanwhile, the elastic modulus was reduced at a rate lower than the strength, which had been reported as well in a previous research work (Kong et al., 2014). The Young's modulus of CAM-II was more than 1.2 GPa while CAM-I had an elastic modulus of close to 0.3 GPa. But the peak strain value of CAM-I was larger than that of CAM-II, as shown in **Table 4.1**, because of more asphalt binder included or higher A/C. It was also noted that the values of elastic modulus were almost 3~5 times lower than those for ordinary Portland cement mortars under compression (Neville, 1999), mainly because of the rough way to calculate the strain values in **Section 3.6.2**, in which the real strain was replaced by the mean strain.

Table 4.1 Mechanical parameters of CAMs under compression

	σ_{cp} / MPa	E_c / MPa
CAM-I	2.04 (±0.13)	286.60 (±23.47)
CAM-II	14.58 (±0.43)	1293.71 (±64.05)
Control	41.24 (±2.52)	3179.45 (±137.83)

Note: Standard deviations (SDs) were shown in the brackets.

It could be concluded that the incorporation of asphalt binder into Portland cement mortar reduced the compressive strength and the Young's modulus significantly. Therefore, CAM-I with a higher A/C (1.0) has much lower strength and modulus compared to CAM-II with the A/C of 0.2.

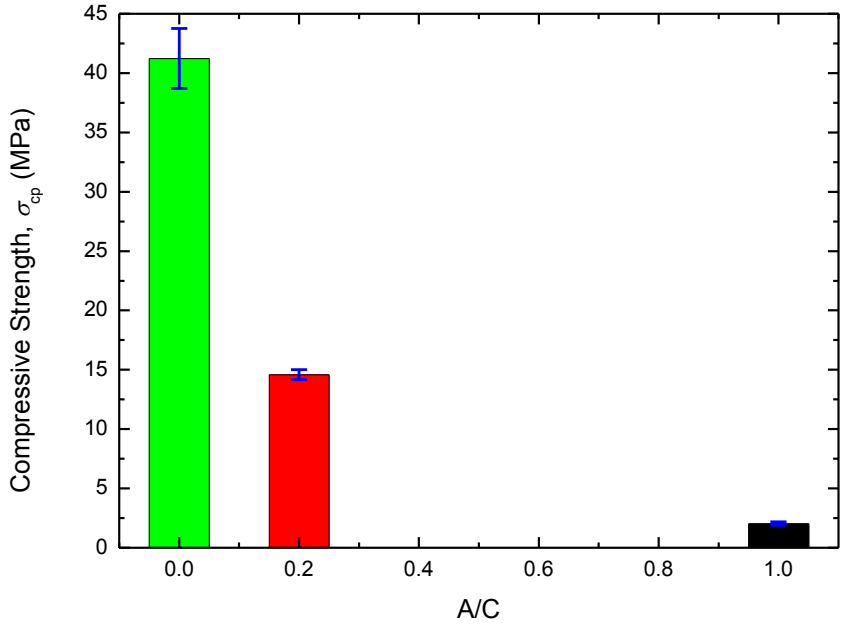

(a)

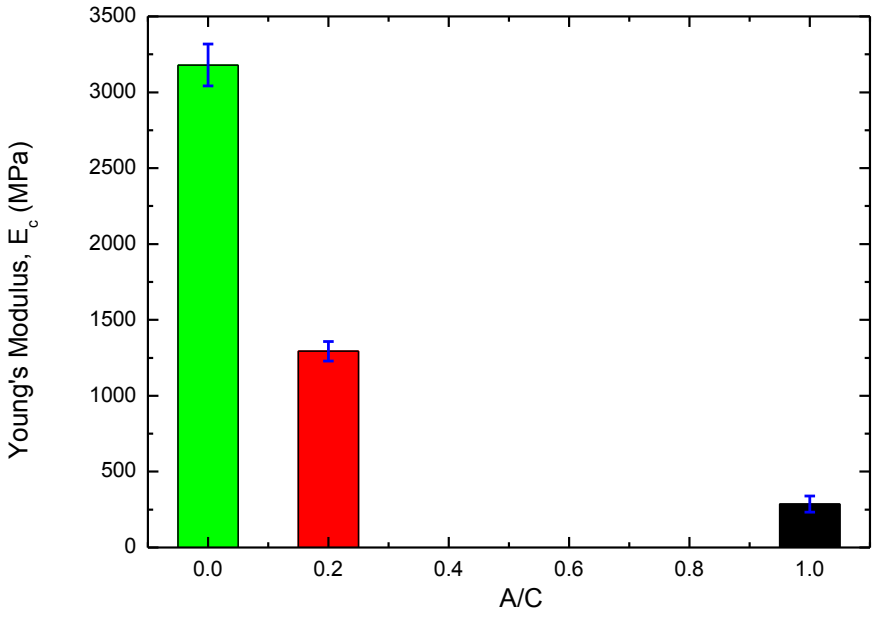

(b)

Fig 4.3 (a) Compressive strength and (b) Young's modulus of CAMs

4.3.3 Deformation and failure mode

In addition to the difference in mechanical parameters like compressive strength and modulus of elasticity, CAM-I and CAM-II deformed and failed during loading in their different manners as recorded.

At room temperature, the control Portland cement mortar exhibited splitting failure mode as shown in **Fig 4.4**, which features quasi-brittle fracture of concrete-like materials under compression. During the process of compression, sharp and short noises could be heard when cracking started.

More like the Portland cement mortar, CAM-II deformed and fractured in a quasi-brittle manner and cut-through cracks (**Fig 4.5 (b)**) along the height could be observed on the surface after failure. But a weaker brittleness was observed experimentally.

As compressive stresses were applied to CAM-I, however, no visible cracks could be found on the surface even if they reached the peak ones. After the peak stresses, there existed a gradual, slow and almost linear decline in stresses (**Fig 4.2**), i.e. strain softening, and it showcased a drum-like failure mode (**Fig 4.6**) at a high strain value until small and short random cracks could be seen in the central zone of the surface.

Based on deformation and failure mode recorded in the process of loading, the failure of CAM-I was associated with finite plastic deformation whereas CAM-II failed in relation to macro-cracking, initiation and propagation.

(a) **(b)**

Fig 4.4 (a) Before failure and (b) after failure of Portland cement mortar

(a) **(b)**

Fig 4.5 (a) Before failure and (b) after failure of CAM-II

(a) **(b)**

Fig 4.6 (a) Before failure and (b) after failure of CAM-I

4.3.4 Summary

Uniaxial compressive properties of CAMs were tested at room temperature using the traditional compression test method, and the results could be summarised as follows.

1. The change in stress-strain curves indicated that, at room temperature, CAM-I were more like ductile materials which had high deformability while CAM-II deformed in a typically quasi-brittle manner like Portland cement mortar;
2. The incorporation of asphalt binder into Portland cement mortar reduced both compressive strength and modulus significantly and this decreasing trend increased with the A/C. Therefore, CAM-I had much lower strength and modulus compared to CAM-II;
3. On the basis of compressive deformation and failure mode observed in the process of loading in the laboratory, the failure of CAM-I was associated with finite plastic deformation whereas CAM-II failed in relation to macro-cracking.

4.4 Bending properties of CAM-I and CAM-II at room temperature

A mini-4PB test apparatus was developed for use in fatigue tests of CAMs. Here, using this apparatus, bending properties of CAM-I and CAM-II were firstly tested, to obtain stress-strain curves, bending parameters and failure mode. These parameters will provide some reference for fatigue tests.

4.4.1 Stress-strain curves

Seen from **Fig 4.7**, it was more than evident that CAM-II failed in a brittle manner like the control, Portland cement mortar, whereas CAM-I showed typical ductile behaviour under bending.

But it should be noted that the bending strength of CAM-II was not reduced, on the contrary, slightly improved (**Fig 4.8 (a)**), which was probably due to the modification of asphalt emulsion in Portland cement mortar. In polymer modified mortars (PMMs), due to water-reducing effects at fresh state and the filling and sealing effects of the impermeable polymer films after hardened (Afridi et al., 1995, Saija, 1995, Strawhecker and Manias, 2000, Aggarwal et al., 2007, Kong and Li, 2009), the addition of emulsion into Portland cement mortar greatly densified the pore structure and the interfacial transition zone (ITZ), resulting in an improvement in mechanical properties, especially adhesion and tension. In this case, their flexural strength could be improved with the polymer-cement ratio (P/C). It was reported that flexural strength started to increase with the P/C of 10% and reach a peak one when P/C is 15% (Pascal et al., 2004). Of course, such P/C values depended on the type of the emulsion used and different emulsions had different ones (Bureau et al., 2001, Wang et al., 2005a).

For asphalt emulsion-modified cement mortars, it was reported that the flexural strength changed slightly with the P/C or A/C range from 0 to 0.3 (Song et al., 2006). This CAM with low A/C to 0.2 fell into such PMMs.

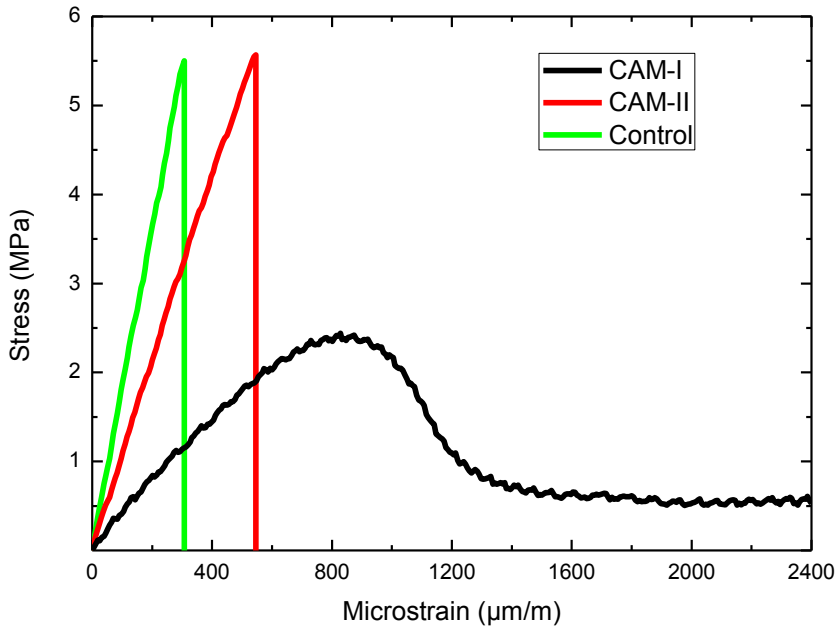

Fig 4.7 Bending stress-strain curves of CAMs

4.4.2 Bending parameters

From **Table 4.2**, it was found that four mechanical parameters could be obtained from the 4PB testing method, namely bending strength (σ_b), Young' Modulus (E_b) in bending, failure strain (ε_f) and failure energy (G_f). Two additional useful parameters, failure strain and failure energy, could be obtained in the newly developed method to characterise the deformation behaviour and fracture capacity of CAM-I and CAM-II. Failure strain could be defined as the peak strain when the stress reached the peak, i.e. σ_b, on stress-strain curves and failure energy, could be defined as the strain energy density to the failure strain, i.e. the integral area before the peak.

With the increase of A/C, Young's modulus of CAMs was reduced but the values were 8~14 times larger than those of compressive ones. Compared to Portland cement mortar, the failure strain and the failure energy of CAM-I and CAM-II were higher (**Fig 4.8 (b)**), which clearly showed the important function of asphalt binder in CAMs in enhancing the deformability.

Table 4.2 Bending parameters of CAMs at room temperature

	σ_b (MPa)	E_b (MPa)	ε_f (μm/m)	G_f (J/m^3)
CAM-I	2.32	3,802.70	881	1,223.04
CAM-II	5.66	10,592.88	539	1,489.36
Control	5.22	16,438.35	319	909.54

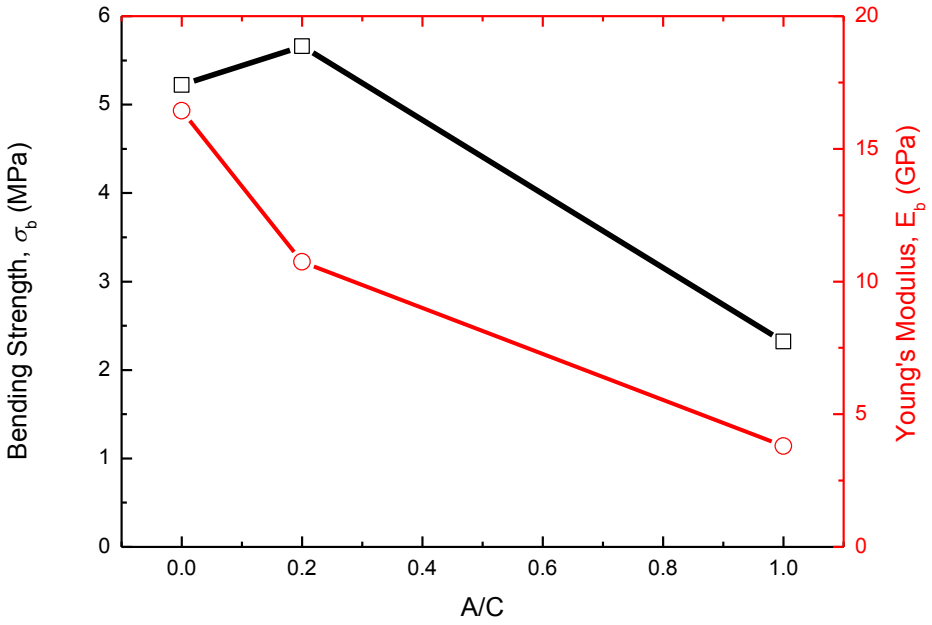

(a)

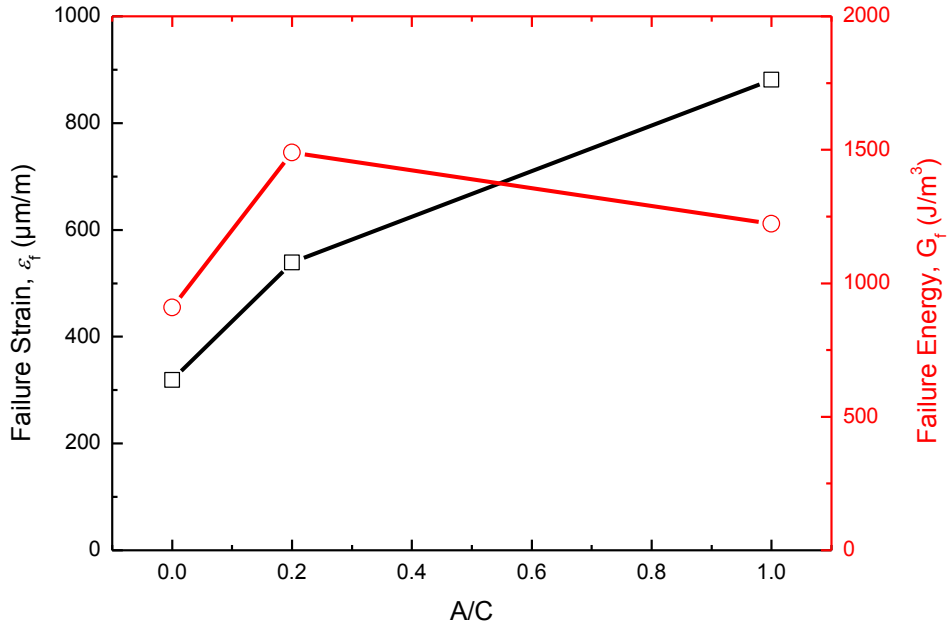

(b)

Fig 4.8 Bending properties of CAMs: (a) strength and modulus; (b) failure strain and failure energy

4.4.3 Failure mode

The failure modes of CAM-I and CAM-II as shown in **Fig 4.9** reconfirmed the two distinct deformation mechanisms in CAM-I and CAM-II as concluded in **Section 4.3.3**.

Cracking (**Fig 4.9 (a)** and **(b)**) could be seen in the uniform bending zone of the samples for CAM-II, like the control. However, as a ductile material at room temperature, CAM-I (**Fig.4.7**) could undergo large plastic deformation. Even after failure (**Fig 4.9 (c)**), it was hard to perceive the cracks on the surface of the samples by naked eyes.

With stress-strain curves of CAM-I and CAM-II considered in combination with their failure modes, obviously, two distinct bending deformation mechanisms existed as in the case of CAMs under compression: the failure of CAM-I was associated with finite plastic deformation whereas CAM-II failed in relation to quasi-brittle cracking.

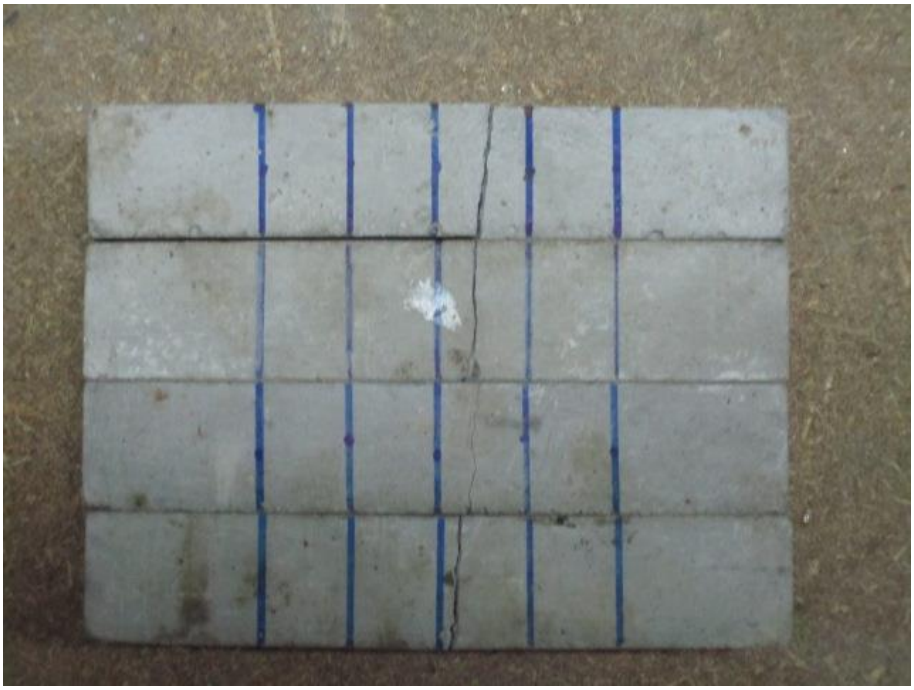

(a)

(b)

(c)

Fig 4.9 Failure modes of (a) Portland cement mortar, (b) CAM-II and (c) CAM-I under bending

4.4.4 Summary

Using the newly-developed 4PB test method, bending properties of CAM-I and CAM-II at room temperature were tested and the results reconfirmed some conclusions summarised in the preceding **Section 4.3.4**, which were listed as follows.

1. CAM-I was a typical ductile material at room temperature while CAM-II was a brittle material like Portland cement mortar;
2. The Young's modulus of CAMs decreased with the content of asphalt binder as well based on the 4PB method. When A/C=0.2, the bending strength was not reduced but slightly improved probably due to the modification of asphalt emulsion in Portland cement mortar;
3. Two additional mechanical parameters, failure strain and failure energy, could be obtained in the newly developed 4PB method to characterise the deformation and fracture behaviour of CAM-I and CAM-II;
4. Two distinct deformation mechanisms existed as in the case of CAMs under bending: the failure of CAM-I was associated with finite plastic deformation whereas CAM-II failed in relation to macro-cracking.

4.5 Discussion on two CAMs and two test methods

Based on those results from the two test methods above, this section would compare the mechanical properties of CAM-I and CAM-II at first and then propose microstructural models for their composite binders, CABs, in an attempt to elucidate the differences in their mechanical properties. Secondly, a simple evaluation of the newly-developed 4PB test method was conducted, compared to the traditional compression test method.

4.5.1 Comparison between CAM-I and CAM-II

4.5.1.1 Differences in mechanical properties of CAM-I and CAM-II

A comparison of mechanical properties at room temperature between two typical CAMs, CAM-I and CAM-II, could be seen in **Table 4.3**. It was easy to find that CAM-I had much lower compressive and bending strengths or elastic modulus than CAM-II. But because of more asphalt binder contained or higher A/C in CAM-I, the deformability was greatly improved. As far as the failure mode from observation was concerned, there were two totally different mechanisms, ductile and quasi-brittle, for CAM-I and CAM-II, respectively, which was in relation to plastic deformation, ε-, and cracking controlled by stress, σ-. It was also noted that the bending strength of CAM-II was nearly one fourth of the compressive strength compared to around one eighth for the control Portland cement mortar, whereas CAM-I had a slightly higher bending strength compared with the compressive one. Another big difference was between the modulus of the two CAMs under compression and bending, which would be discussed in the next section.

Generally, because of the difference in A/C, CAM-I and CAM-II exhibited totally different mechanical properties and behaviour at room temperature. CAM-I was a ductile material with low strength and modulus but high deformability while CAM-II was a quasi-brittle material with high strength and modulus. Therefore, it should be cautious to choose appropriate test methods to characterise their mechanical properties and behaviour, especially fatigue.

Table 4.3 Comparison between CAM-I and CAM-II at room temperature

Items		CAM-I	CAM-II
A/C		1.0	0.2
Compressive Parameters	σ_{cp} (MPa)	2.04	14.58
	E_c (MPa)	286.60	1293.71
Bending Parameters	σ_b (MPa)	2.32	5.66
	E_t (GPa)	3.80	10.59
	ε_f (μm/m)	881	539
	G_f (J/m^3)	1,223.04	1,489.36
Failure Mode		Ductile ε-	Quasi-brittle σ-

4.5.1.2 Volume fractions of each phase in hardened CABs

The differences in mechanical properties and behaviour of CAMs were most possibly attributed to their binders (Liu et al., 2013), namely, hardened CABs, and they could be regarded as two-phase composites as discussed in the review chapter: One was hcp and the other was asphalt binder. It was reported that no chemical reaction other than cement hydration occurred during the hardening process of CABs (Yang et al., 2010). Therefore, asphalt binder could be visualised as an inertial phase and the major volume change is due to the hydration of Portland cement in those CABs. Based on the classical Powers-Brownyard model (Powers and Brownyard, 1946), therefore, the hcp in CABs could be subdivided into three phases as well and a calculation of volume fractions of each phase in the hcp was to be conducted as follows.

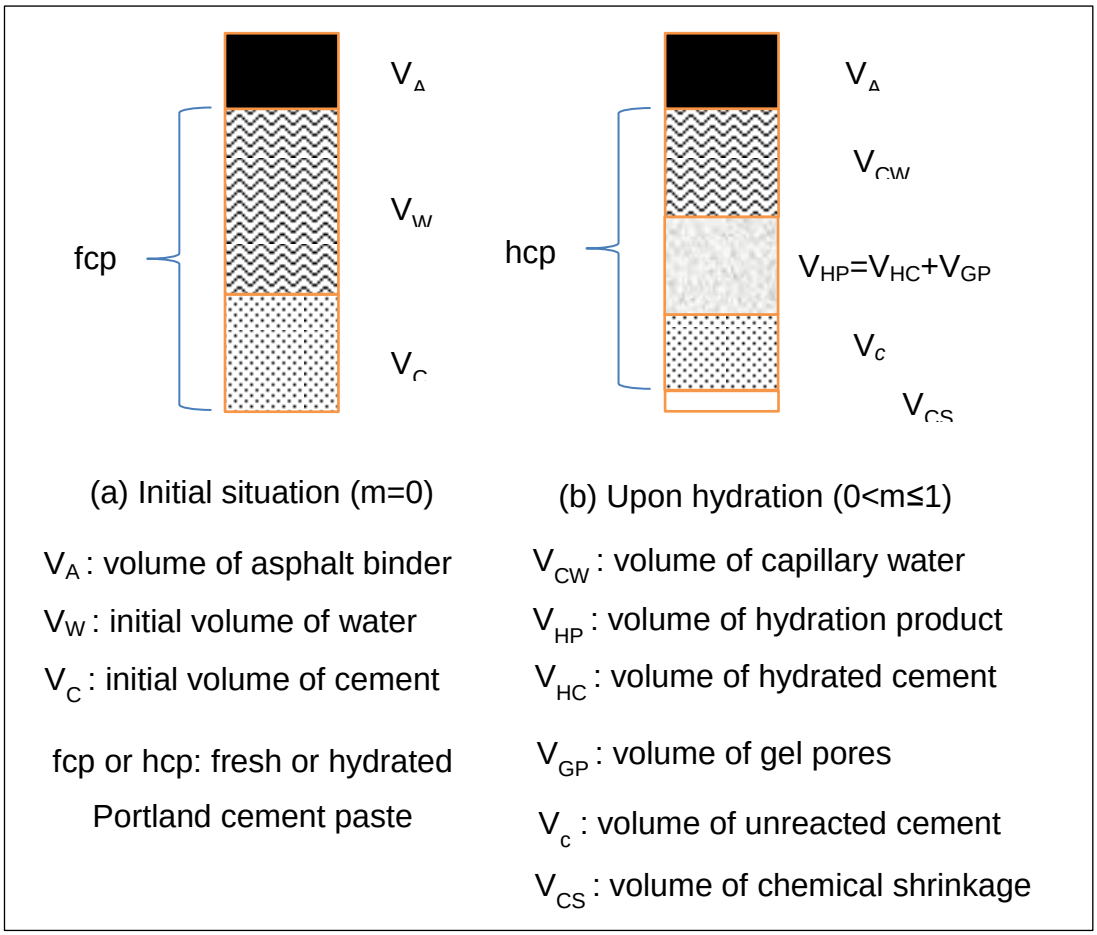

Fig 4.10 Breakdown of cement paste and hydration product in CABs

In the Powers-Brownyard model (Brouwers, 2004, Brouwers, 2005), three phases in the hcp are distinguished, namely capillary water or unreacted water (CW), unreacted cement (c) and cement gel or hydration product (HP) (**Fig 4.10 (b)**). The capillary water is considered as free water. It is assumed that during the process of cement hydration, there is no loss of free water into the air. The unreacted cement can be defined by the degree of hydration, m=(C-c)/C (0≤m≤1). The most important phase is the hydration product (HP), which is made up of solid hydrated cement (HC) and water-filled gel pores or space (GP). This part of the water in gel pores or space is referred to as gel or absorbed water (GW). The gel water is an integral part of gel pores or space within the influence of absorbing forces. Hence, the hydration product, as one phase, consists of hydrated cement and gel pores or space. From fresh CABs to hardened CABs (**Fig 4.10**), the volume of asphalt binder (A) remains

constant whereas chemical shrinkage (CS) which is firmly related to cement hydration happens in the phase of hcp. Whatever, the total volume of asphalt binder, hcp and chemical shrinkage is equal to the original volume of the fresh CAB, which could be regarded as a two-phase paste, asphalt binder and fresh Portland cement paste (fcp) (**Fig 4.10 (a)**). Therefore, the total volume subtracting the chemical shrinkage due to cement hydration is the volume of the hardened CAB. To further calculate the volume fractions of each phase in hardened CABs, two steps are needed. The first step to calculate the volume fractions of the two main phases in hcp, chemical shrinkage (Brouwers, 2007) and asphalt binder in the total volume. And in the second step, chemical shrinkage will be excluded from the total volume.

With chemical shrinkage and the inertial phase, asphalt binder, taken into account as a whole, in the first step, the volume fractions of each phase (**Fig 4.10 (a)**) can be calculated using **Equations (4-1)** ~ **(4-5)** (Brouwers, 2007).

$$\varphi_{A,m} = \frac{A/C \times \rho_W / \rho_A}{W/C + \rho_W/\rho_C + A/C \times \rho_W/\rho_A} \tag{4-1}$$

$$\varphi_{HP,m} = \frac{m(\rho_W/\rho_C + W_d \upsilon_d / \upsilon_W c)}{W/C + \rho_W/\rho_C + A/C \times \rho_W/\rho_A} \tag{4-2}$$

$$\varphi_{c,m} = (1-m)\frac{\rho_W/\rho_C}{W/C + \rho_W/\rho_C + A/C \times \rho_W/\rho_A} \tag{4-3}$$

$$\varphi_{CW,m} = \frac{m(W/C - m \times W_d/c)}{W/C + \rho_W/\rho_C + A/C \times \rho_W/\rho_A} \tag{4-4}$$

$$\varphi_{CS,m} = \frac{m(W_d/c - W_d \upsilon_d/\upsilon_W c)}{W/C + \rho_W/\rho_C + A/C \times \rho_W/\rho_A} \tag{4-5}$$

Where, $\varphi_{HP,m}$, $\varphi_{c,m}$, $\varphi_{CW,m}$ and $\varphi_{CS,m}$denote volume fractions of the three phases in hcp, i.e. hydration product, the unreacted cement and the capillary water, and chemical shrinkage due to the hydration of Portland cement at the degree of hydration of m.

ρ_A, ρ_C or ρ_W denotes the density of asphalt binder (A), Portland cement (C) or water (W). υ_W is the specific volume of water, $\upsilon_W = 1/\rho_W$.

W_d/c and $W_d\upsilon_d/\upsilon_W c$ are the total retained water and the retained water volume, respectively, which depend on the composition of Portland cement and can be obtained by **Equations (4-6)** and **(4-7)** (Brouwers, 2007).

$$\frac{W_d}{c} = 0.355x_{C_3S} + 0.366x_{C_2S} + 1.401x_{C_3A} + 0.482x_{C_4AF} - 0.091x_{C\bar{S}} \tag{4-6}$$

$$\frac{W_d\upsilon_d}{\upsilon_W c} = 0.281x_{C_3S} + 0.306x_{C_2S} + 1.103x_{C_3A} + 0.396x_{C_4AF} - 0.095x_{C\bar{S}} \tag{4-7}$$

Where, x_{C_3S}, x_{C_2S}, x_{C_3A}, x_{C_4AF} and $x_{C\bar{S}}$ denote mineral compositions of C_3S, C_2S, C_3A, C_4AF and $C\bar{S}$ in Portland cement, which can be found in **Table 3.1** from **Chapter 3**.

The second step is to exclude the chemical shrinkage and to calculate the volume fractions of each phase in hardened CABs as shown in **Equations (4-8) ~ (4-11)**.

$$\varphi_A = \frac{\varphi_{A,m}}{1-\varphi_{CS,m}} \tag{4-8}$$

$$\varphi_{HP} = \frac{\varphi_{HP,m}}{1-\varphi_{CS,m}} \tag{4-9}$$

$$\varphi_c = \frac{\varphi_{c,m}}{1-\varphi_{CS,m}} \tag{4-10}$$

$$\varphi_{CW} = \frac{\varphi_{CW,m}}{1-\varphi_{CS,m}} \tag{4-11}$$

In most cases, it is not possible that cement hydration is 100% completed, even in the pure hcp. Herein, If It is assumed that the degree of cement hydration is 90%, i.e. m=0.9, the volume fractions of asphalt binder, hydrated product and capillary water can be obtained as shown in **Table 4.4**. It is clear to see that when the A/C increases from 0.2 to 1.0, the main binding phase change from hydrated product to asphalt binder. To make it clearer, the volume fractions of two main binding phases in solid CABs can be further calculated and listed in the last two columns of **Table 4.4**.

$$\varphi'_A = \frac{\varphi_A}{\varphi_A + \varphi_{HP}} \tag{4-12}$$

$$\varphi'_{HP} = 1 - \varphi'_A \tag{4-13}$$

Table 4.4 Calculated volume fractions of phases in hardened CABs

	A/C	W/C	Hardened CABs (m=0.9)			Binding Phases	
			φ_A (%)	φ_{HP} (%)	φ_{CW} (%)	φ'_A (%)	φ'_{HP} (%)
CAB-I	1.0	0.80	48.23	29.81	20.43	61.80	38.20
CAB-II	0.2	0.50	20.54	63.50	12.7	24.44	75.56
Control	0	0.50	0.00	79.91	15.98	0.00	100.00

4.5.1.3 Microstructural models for hardened CABs

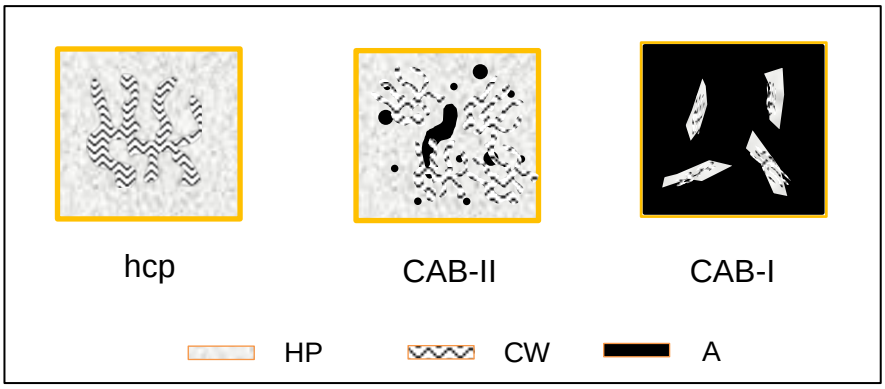

Fig 4.11 Microstructural models for hcp, CAB-II and CAB-I

Based on the calculation of volume fractions of the main binding phases in the preceding section, from CAB-II to CAB-I, it was indicated that an increase of the A/C from 0.2 to 1.0 in CABs brought about a change in the microstructure, thus leading to differences in mechanical properties and behaviour macroscopically of their composites, CAMs.

Therefore, microstructural models for CAB-I and CAB-II compared to hcp as shown in **Fig 4.11** were proposed. When A/C was 0.2, the volume fraction of asphalt binder was as low as 20.54 % and the hydrated product in hcp was the main binding phase. In this case, the asphalt binder functioned like soft filler into the hcp. That was why CAM-II is more like the control Portland cement mortar but modulus was lower compared with the control. In contrast, when A/C was 1.0, the main binding phase turned from the hydrated product to asphalt binder, and Portland cement worked as an active filler in CAM-I. Thus, the mechanical behaviour of CAM-I was more close to asphalt mixtures, a typical viscoelastic material. Here, it was confirmed that the differences in mechanical properties and behaviour of CAMs were mainly attributed to the microstructures of their binders, CABs. It was also implied that there definitely existed a transition zone between these two CAMs, which might be instructive to the design of new CAMs in the future.

4.5.2 Comparison of the two test methods

The two test methods were compared in three aspects, i.e. samples making, facility design and test results, although either of them could be used to test static mechanical properties of CAMs under compression or bending.

4.5.2.1 Sample making

For the traditional compression tests, the dimension of the CAM sample was ø50×50 mm (Dept. of Sci & Tech, 2008a), which was not in common use in the laboratory. So new moulds made of PVC or other materials were needed to be prepared in advance, to produce cylinder CAM samples.

If the new 4PB method was used, the CAM sample's dimension, 40×40×160 mm, was for standard mechanical tests of cement mortars and their mould could be found everywhere in the concrete laboratory. Possibly, for this reason, the determination of flexural and compressive strengths of CAM-II, as a material more close to Portland cement mortar, followed **GB/T 17671** (Dept. of Sci & Tech, 2008b), which was generally used for cement mortars. The only problem of this specification was that limited information on material properties, except for compressive and flexural strengths, could be obtained. Therefore, the new 4PB method was aimed at getting a full picture of static mechanical properties of CAMs under bending. Moreover, as in the case in **GB/T 17671**, the broken samples under bending could be used for further compression tests if necessary.

4.5.2.2 Facility design

It was obvious that compression tests were easier to perform, and the facility was simple and generally available in the laboratory. In contrast, to produce pure bending stresses or strains in CAM samples, the 4PB method had to use a complex configuration, a mini-4PB facility that followed the principle of some typical devices for testing fatigue of asphalt mixtures. Moreover, its operation procedure with the MTS machine was more complicated. From this viewpoint, it seemed easier or more convenient to use the traditional compression tests to characterise static mechanical properties of CAMs, with the purpose of quality evaluation. But this test method was possibly more suitable for quasi-brittle

materials like cement-based materials, which were characterised by much higher compressive strength than tensile or bending one. And the CAMs were known to be new composite materials between cement-based materials and asphalt mixtures, as discussed in **Section 2.3.2** of **Chapter 2**, from quasi-brittle to ductile at room temperature as A/C increased from 0.2 to 1.0. More than evident, it could be inappropriate to use the traditional compression test method when A/C was higher.

4.5.2.3 Test results

Test results from the two test methods were shown in **Table 4.3**. Because of different test methods used, it was not easy to say which test method generated more reliable results. But let start with the Young's modulus. Apparently, the modulus in bending was about 10 times higher than the compressive modulus for a certain CAM. And it was interesting to find that the bending modulus of CAM-II obtained by the newly-developed 4PB test method had the same order of magnitude with those in a tentative specification (Dept. of Sci & Tech, 2008b). Meanwhile, the elastic modulus of CAM-I obtained by traditional compression test method was consistent with its specification (100-300MPa), too (Dept. of Sci & Tech, 2008b). However, according to the general values of modulus of elasticity for Portland cement mortars (Neville, 1999) or asphalt mixtures (Huang, 2004), it was easy to conclude that the results of modulus from the 4PB test method were more reliable. Here, on contrary, it was found that the modulus of elasticity obtained from those traditional compression tests was more than ten times underestimated, which might be one of the reasons for underestimated stresses or strains in the CAM layer of CRTS I or CRTS II from the modelling work. Obviously, this underestimation was attributed to the rough way to calculate the strain value in the traditional compression test method as mentioned in **Section 3.6.2**. In addition, the 4PB test method could produce two more mechanical parameters on deformation and fracture capacity, which would be useful for further research.

In general, the newly-developed 4PB test method used here was suitable for characterising the mechanical properties of those two totally different CAMs in the laboratory and more reliable results could be obtained.

4.6 Chapter summary

In this chapter, a newly-developed 4PB test method was used to study the static bending properties of the two CAMs at room temperature, in comparison to the traditional compression test method, which was already used in mix design and quality evaluation of different CAMs. Results indicated that:

1. Because of the difference in A/C, CAM-I and CAM-II were distinct in compressive and bending properties and behaviour at room temperature. CAM-I was a ductile material with a low modulus of elasticity but high deformability whilst CAM-II deformed and failed more like quasi-brittle Portland cement mortar with a very high modulus of elasticity. The failure of CAM-I was associated with finite plastic deformation whereas CAM-II failed in relation to macro-cracking;
2. The differences in mechanical properties and behaviour of CAMs were mainly attributed to the microstructures of their binders, CABs. Based on the calculation, the main binding phase in hardened CABs was turned from hcp in CAB-II to asphalt binder in CAB-I, which was the main reason why the mechanical behaviour of CAM-I was more close to that of the asphalt mixture.
3. The newly-developed 4PB test method was proved to be suitable for characterising static mechanical properties and behaviour of the two totally different CAMs in the laboratory and more reliable results could be obtained.

CHAPTER 5 DYNAMIC MECHANICAL PROPERTIES OF CAMS AND THEIR BINDERS

5.1 Introduction

Due to the incorporation of asphalt binder, which is a typically viscoelastic material over a wide range of temperatures and loading frequencies or strain rates (Lethersich, 1942, Poel and Der, 1954, Cheung and Cebon, 1997a, Cheung and Cebon, 1997b), CAMs exhibited their viscoelasticity as well, a combination of elastic and viscous mechanical behaviour.

To characterise the viscoelasticity of CAMs, one test method has been used to test their creep or stress relaxation behaviour (Xie et al., 2014, Fu et al., 2015), but under compression. And there is another easy and quick way, DMA as discussed in **Section 2.4** of **Chapter 2**, which is well known to be one of the commonly-used tools to measure dynamic mechanical properties of materials, especially for viscoelastic ones like polymers (Shaw and MacKnight, 2005). This method has been successfully used to study the dynamic mechanical properties of CABs with different A/Cs under bending (Liu et al., 2009, Liu et al., 2011a, Liu et al., 2013), which has brought some insights into their viscoelasticity. Usually, two different spectra, temperature spectra and frequency spectra, are results from two controlling methods in a DMA (Menard, 2008). The former one is to measure dynamic mechanical properties of viscoelastic solids over a temperature range at a given frequency while the latter one is obtained using frequency sweep at a fixed temperature. Theoretically, results from those two methods are equivalent, but temperature effect is a more important factor to be considered in the design and evaluation of CAMs because of the wide application of the two prevailing slab tracks, CRTS I and CRTS II, in different regions of China with complicated and changeable climate and weather conditions. Therefore, the former one, the temperature spectrum, is of our interest most. If necessary, frequency effect to be considered, the frequency

spectrum at one temperature could be obtained through measuring different temperature spectra at a few frequencies and translating or shifting the resulting curves into a master curve based on the principle of frequency-temperature correspondence.

In this chapter, the test method of DMA in a single cantilever bending mode was used to investigate the dynamic mechanical properties of CAMs under different temperatures ranging from -100 ˚C to 100 ˚C at the frequency of 10 Hz, i.e. temperature spectrum, with the aim to explore their viscoelasticity and then define the temperature range used in following fatigue tests in **Chapter 6**. In comparison, the dynamic mechanical properties of their matrixes, CABs, were measured by the same method under the same conditions. Furthermore, the influence of loading frequency on their temperature spectra was studied and analysed, in order to get a full picture of dynamic modulus of CABs over a wide range of temperatures and loading frequencies.

The main objectives in this chapter are:

- To study the dynamic mechanical properties of CAB-I and CAB-II over a temperature range of -100 ˚C to 100 ˚C at the frequency of 10 Hz using the DMA method, as a reference for CAM-I and CAM-II;
- To study the dynamic mechanical properties of CAM-I and CAM-II under the same conditions as mentioned above, via the DMA method as well, in order to evaluate the temperature susceptibility and the viscoelasticity of the two typical CAMs, and determine the most suitable temperature range used in fatigue tests for both CAMs.
- To bridge the viscoelasticity of CAMs and the primary function of damping in slab tracks, in order to understand the implications of the viscoelasticity on damping.

5.2 Experimental programme

To achieve the above objectives, dynamic mechanical loadings of CABs and CAMs and analysis of CAMs' damping function in slab tracks were arranged in three stages as shown in the flow chart (**Fig 5.1**).

Stage 1: dynamic mechanical properties of CAB-I and CAB-II over a wide temperature range of -100 ˚C to 100 ˚C at the frequency of 10 Hz were tested, and the influence of frequency was studied;

Stage 2: dynamic mechanical properties of CAM-I and CAM-II over the same temperature range at the frequency of 10 Hz were tested and compared with those of CABs.

Stage 3: two common damping mechanisms in structures were discussed to explore the damping function of CAMs as structural materials in slab tracks.

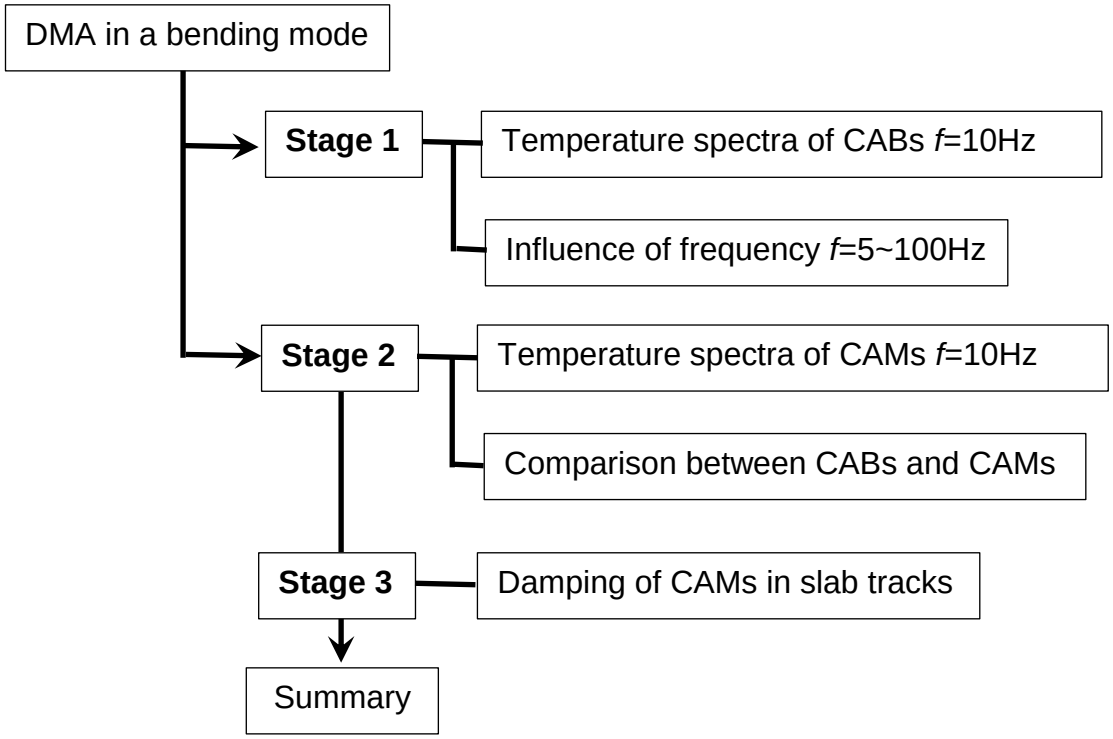

Fig 5.1 Flow chart of the experimental programme in Chapter 5

5.3 Dynamic mechanical thermo-analysis of CABs

DAM tests were performed on CABs to get their temperature spectra. As introduced in the previous **Section 2.4** of **Chapter 2**, two parameters, dynamic storage modulus and loss factors, were the focus of the research work, to characterise their dynamic mechanical properties, i.e., viscoelasticity. Then, the influence of loading frequency on their temperature spectra was studied.

5.3.1 Temperature spectrum

5.3.1.1 Storage modulus

Fig 5.2 showed the temperature dependency of dynamic storage modulus over a temperature range of -100 °C to 100 °C at the loading frequency of 10 Hz for CAB-I, CAB-II and hcp. It was clearly indicated that higher temperature or A/C resulted in lower storage modulus.

But it should be noted that, for CAB-II, its storage modulus presented an almost linear reduction with the temperature, more like the hcp. However, the dynamic modulus of CAB-I was strongly dependent on temperature, especially when the temperature was higher than -20 ˚C. From its temperature spectrum, it had two apparent shoulder zones, where there was a sharp change in storage modulus. One is around -20 ˚C and the other is around 50 ˚C. This phenomenon could be related to the glass transition temperature (T_g) and the softening temperature of asphalt binder (Lee et al., 1991) ($T_{R\&B}$=48 °C for the asphalt binder used in this work), respectively. It was well established that the asphalt binder or bitumen itself was a complex mixture with a typical colloid structure (Loeber et al., 1998, Lesueur, 2009), and transitions of its mechanical characteristics from the elastic glassy solid, the viscoelastic state, to the Newtonian fluid, could be generated with increasing temperature. The three transition zones of CAB-I, which could be seen in **Fig 5.2**, were characterised by the two characteristic temperatures, T_g and $T_{R\&B}$, of asphalt binder, between which was the viscoelastic state.

When the temperature was below -20 ˚C, a slight change in the modulus of both CABs could be seen because the asphalt binder was in a glassy state with high

modulus and their dynamic modulus are close to each other. Above this temperature, a sharp decrease in the storage modulus of CAB-I happened whereas CAB-II remained almost the same decreasing rate. The decrease of modulus in CAB-II with temperature is possibly associated with the water absorbed near the solid surface (Morlat et al., 1999). Such a huge difference could be explained by their different microstructures as discussed in the previous chapter, indicating that the main binding phase of CAB-I was asphalt binder while hcp was the main phase of CAB-II. When temperature approached $T_{R\&B}$=48 °C, the reducing rate of modulus in CAB-I started to slow down, an indication of the transition of the asphalt binder into another zone, the Newtonian fluid. It was implied that, as solid materials, CAB-I started to be destabilised. At this temperature, the dynamic modulus of CAB-I was as low as between 100~200 MPa while CAM-II still had a high modulus of more than 2,000 MPa. As the A/C increased from 0.2 to 1.0 (from CAB-II to CAB-I), to be obvious, the susceptibility of dynamic modulus to the test temperature was significantly increased, which was in connection with the huge differences in their microstructures.

From the analysis of temperature spectra of CABs, it was concluded that the incorporation of asphalt binder into Portland cement mortar lead to a reduction in dynamic modulus. But CAB-II was more like hcp in dynamic modulus while CAB-I was typically viscoelastic between two characteristic temperatures, T_g and $T_{R\&B,}$ which were possibly two important indicators for low temperature and high temperature properties of CABs or CAMs with high A/Cs. It was also found from **Fig 5.2** that the dynamic modulus of CAB-I was much more susceptible to the environmental temperature than that of CAB-II, especially when the temperature is higher than T_g, i.e. the glass transition temperature, of asphalt binder. According to the temperature spectrum of the dynamic modulus of CAB-I, T_g was implied to be around -20 °C, which is a reasonable value for asphalt binder (Lee et al., 1991).

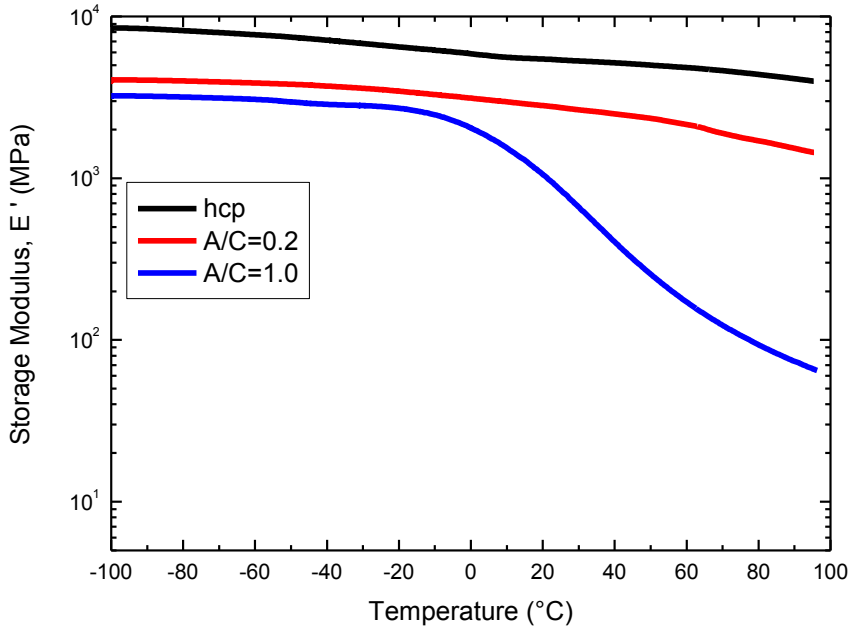

Fig 5.2 Storage modulus of CAB-I, CAB-II and hcp

5.3.1.2 Loss factor

For a typical viscoelastic material, the stress responded to an oscillating strain with a certain phase lag δ as described **Section 3.6.3**. Its tangent value tanδ, the loss factor, represented the mechanical dissipation per cycle of strain, whose magnitude revealed the prominence of viscoelasticity and whose position suggested the thermo-transition temperature of viscoelastic materials.

It was clearly indicated that, as seen from **Fig 5.3**, higher A/C generally resulted in larger tanδ at a given frequency of 10 Hz, implying that CABs with more asphalt binder could possess more evident viscoelastic feature. The loss factor of hcp (the black line in **Fig 5.3**) was very low, nearly 0.05, and seemed unchangeable over the temperature range. The viscoelastic feature of CAB-II was not so evident, too, but slightly pronounced when the temperature was over -20 °C. However, the most noticeable viscoelastic characteristics can be observed in CAB-I. Its loss factor kept a low value as that of CAB-II at very low temperatures, started to increase upon around -20 °C, the glass transition temperature, T_g, and peaked at around 50 °C, very close to the softening

temperature, $T_{R\&B}$=48 °C, which was consistent with the two characteristic temperatures as observed in the preceding section.

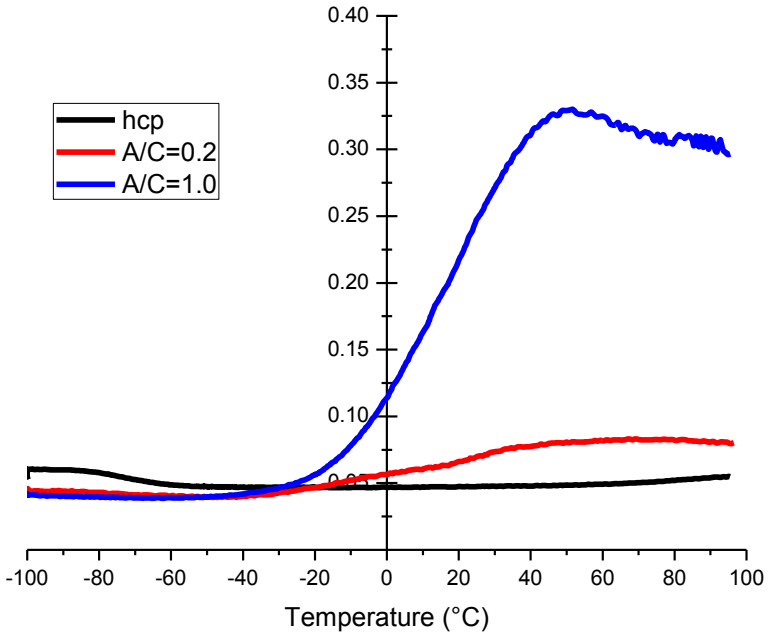

Fig 5.3 Loss factors of CAB-I, CAB-II and hcp

5.3.2 Influence of frequency on temperature spectrum

Temperature spectra were obtained at a fixed loading frequency, for instance, 10 Hz in the previous **Section 5.3.1**. But it was well accepted that dynamic modulus was loading frequency dependent as well (Liu et al., 2011a). Such a dependence on the frequency of vibrations exerted was more frequently used in dynamics of structures. In prefabricated concrete slab tracks, through numerical calculation, it was indicated that track slabs vibrated in the frequency range between 0 ~ 80 Hz (Zhai et al., 2010). Therefore, a frequency range from 5 Hz to 100 Hz was considered for use in the DMA tests to study the influence on the temperature spectrum of CABs.

5.3.2.1 Influence of frequency

Temperature spectra of storage modulus for CAB-II or CAB-I under different frequencies of 5 Hz, 10 Hz, 20 Hz, 50 Hz and 100 Hz were plotted in **Fig 5.4**.

It was not easy, at first sight, to find out the tendency of dynamic modulus of CAB-II and CAB-I under the influence of loading frequencies because of the scatter-ness of experimental results. But it might be simply concluded that, seen from **Fig 5.4**, the storage modulus of CAB-II and CAB-I under different frequencies remained the same trend over the temperature range. And the scatter-ness of storage modulus of CAB-II was greater than that of CAB-I. To further understand the influence of loading frequency on temperature spectra, obviously, a certain method might be considered to deal with the result, which would be presented in the following section and discussed to details.

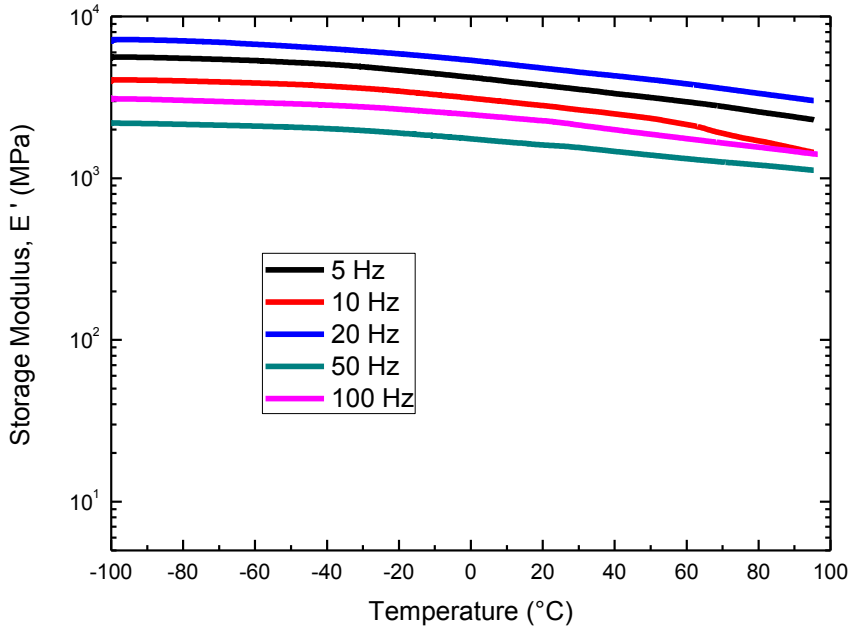

(a)

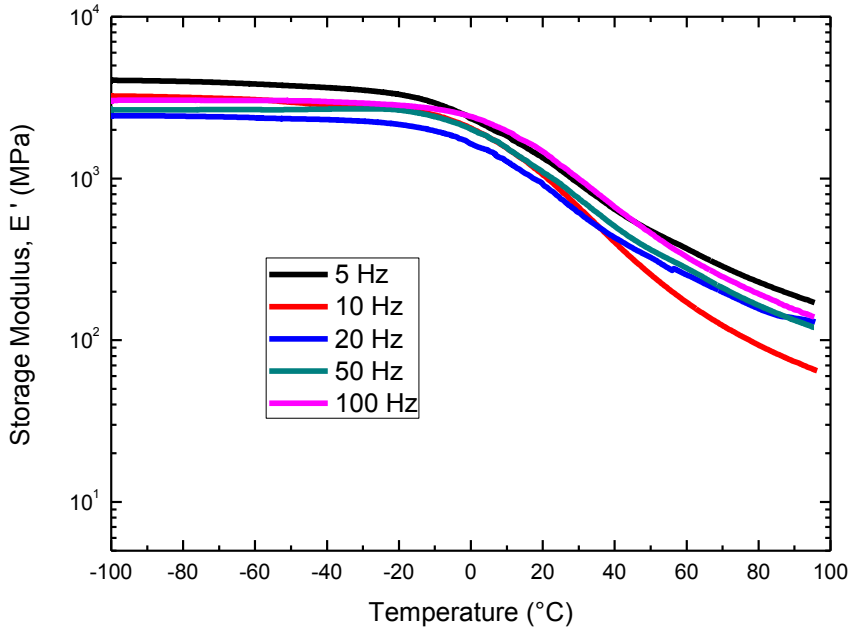

(b)

Fig 5.4 Influence of loading frequency on storage modulus of (a) CAB-II and (b) CAB-I

5.3.2.2 Normalised temperature spectrum

To eliminate the scatter-ness of test results as far as possible, a normalisation method was proposed for analysis in this section.

It was found that composite materials' being called as 'viscoelastic solids' was restricted to a temperature range, or correspondingly a frequency range based on the principle of time- or frequency-temperature correspondence (Ferry, 1980, Shaw and MacKnight, 2005), which indicated that the solid materials were never viscoelastic when temperature was low enough or loading frequency high enough. In **Section 5.3.1**, it was also verified that at very low temperatures, the dynamic modulus of CAB-I or CAB-II were highest but almost unchangeable with temperature, where could be called a plateau zone at low temperatures. Thus, the dynamic storage modulus value of CAB-I or CAB-II at the lowest temperature, -100 °C, E'_{-100}, was chosen as a reference value. And relative dynamic storage modulus was defined as the ratio of storage modulus at any temperatures to the storage modulus at -100 °C, E'_{-100}, as shown in the equation below.

$$E'_r(T,\omega) = \frac{E'(T,\omega)}{E'_{-100}} \tag{5-1}$$

Where, ω was the angular frequency, $\omega = 2\pi f$ and f was the loading frequency. For a given CAB, E'_{-100} was assumed to be a material constant. If the frequency was fixed at ω_o, the equation for the normalized temperature spectra of storage modulus was presented as follows (**Equation (5-2)**); if the temperature was kept invariable as T_o, on the other side, the normalized frequency spectra could be obtained as in **Equation (5-3)**.

$$E'_r(T,\omega)\Big|_{\omega=\omega_o} = E'_r(T,\omega_o) \tag{5-2}$$

$$E'_r(T,\omega)\Big|_{T=T_o} = E'_r(T_o,\omega) \tag{5-3}$$

After normalisation, normalised temperature spectra of the storage modulus of CAB-II or CAB-I under different frequencies were plotted in **Fig 5.5**.

For CAB-II, seen from **Fig 5.5(a)**, there existed a trend of its relative storage modulus to increase under higher loading frequency but it depended on the range of temperatures. When the temperature was lower than -20 °C, the influence of frequency on the normalised modulus of CAB-II was very limited, in other words, negligible. But above this temperature, the frequency effect started to manifest itself with the temperature. In contrast, such an effect was more pronounced on normalised storage modulus of CAB-I as shown in **Fig 5.5(b)**, especially over the temperature range from -10 °C to 30 °C. As the loading frequency increased logarithmically, the whole curves of normalised storage modulus of CAB-I trended to be moved to the right. This phenomenon as observed was typical for viscoelastic solids (Yang et al., 2004).

From the normalised temperature spectra of storage modulus of CABs, in addition, it was found that the storage modulus of both CABs decreased by 20 % when the temperature went from -100 °C to -20 °C. When temperature gradually rose to 60 °C, however, the storage modulus of CAB-II declined to 50 % ~ 60 % of the reference modulus, E'_{-100}, whereas those of CAB-I fall down sharply to less than 10%. Again, it was proved that CAB-I had a pretty higher temperature susceptibility to dynamic modulus than CAM-II.

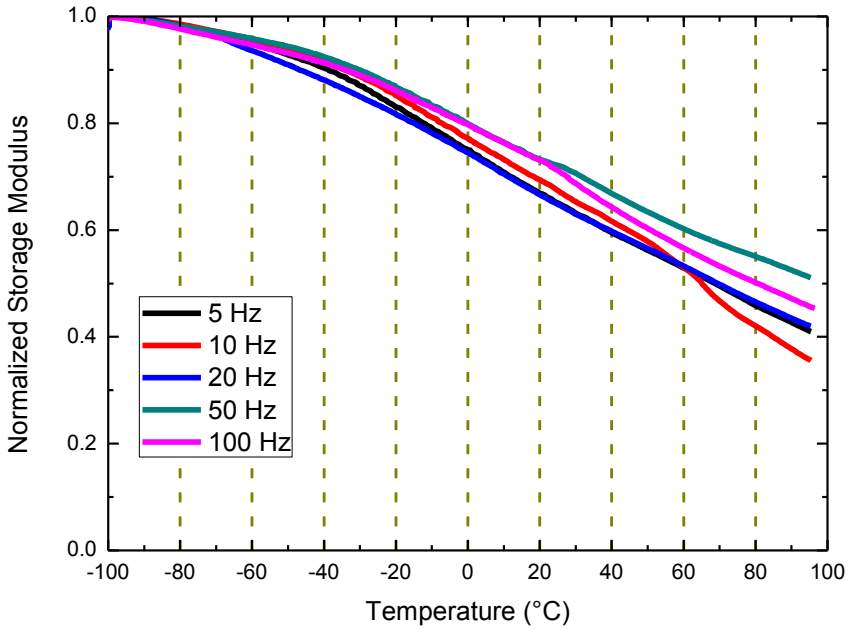

(a)

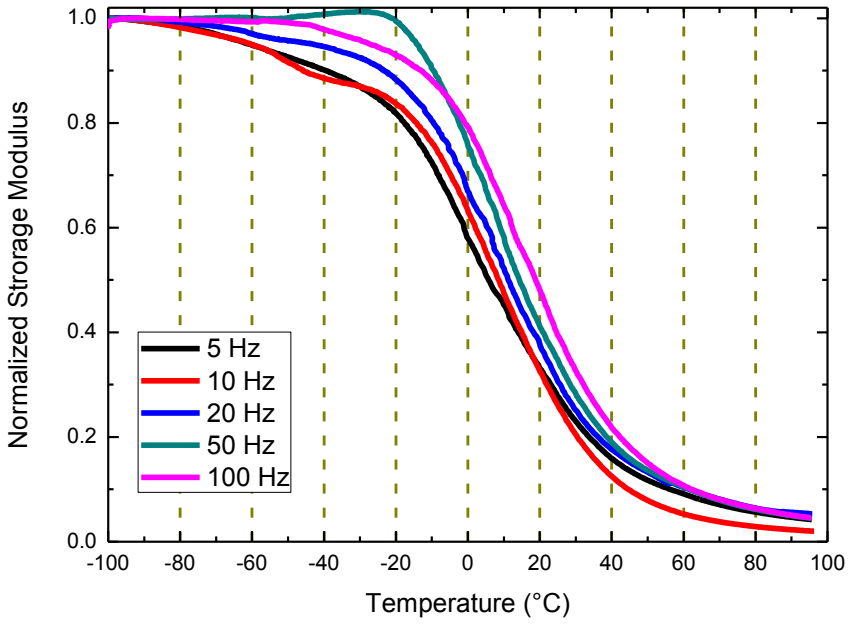

(b)

Fig 5.5 Influence of frequency on normalised temperature spectra of storage modulus of (a) CAB-II and (b) CAB-I

5.3.2.3 A method to obtain frequency spectrum

Following **Section 5.3.2.2**, it was found that the two types of spectra were interconvertible, via a simple calculation.

To obtain the normalised frequency spectrum of storage modulus of CABs at T_o (**Equation (5-3)**), a procedure of the calculation was conducted.

1. To calculate the shift factor firstly, ϕ_T, according to normalized temperature spectra under different frequencies;

$$\phi_T = \frac{\omega_o}{\omega} = \frac{f_o}{f} \tag{5-4}$$

This factor could be evaluated through two empirical equations, the WLF equation (Ferry, 1980) or the Arrhenius-like equation (Liu et al., 2011a) as follows.

$$\log \phi_T = \frac{C_1(T - T_o)}{C_2 + (T - T_o)} \tag{5-5}$$

Where, C_1 and C_2 were material constants.

or,

$$\phi_T = \exp[\frac{E_a}{R}(\frac{1}{T} - \frac{1}{T_o})] \tag{5-6}$$

Where, E_a was the activation energy and R was the universal gas constant.

2. To draw all points on E_r-ω curves over the same frequency range but under different temperatures, which were chosen around T_o;
3. To translate those curves, based on the principle of frequency-temperature correspondence (**Equation (5-7)**) (Yang et al., 2004).

$$E_r'(T, \omega) = E_r'(T_o, \phi_T \omega) \tag{5-7}$$

As a result, the normalised frequency spectrum of storage modulus at the temperature of T_o could be completed.

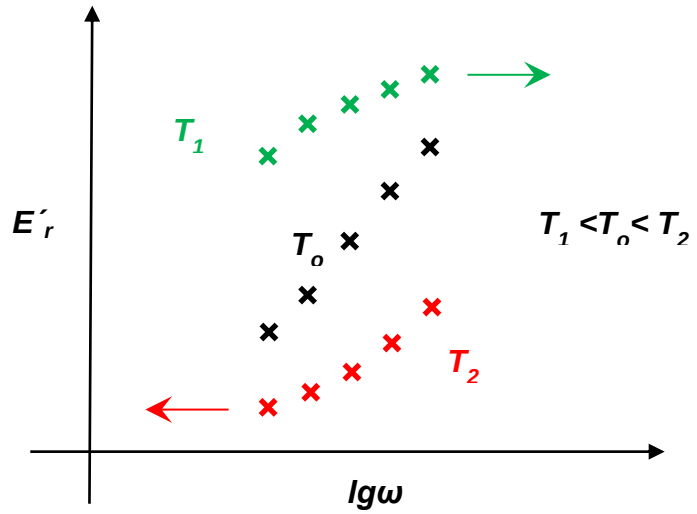

Fig 5.6 Schematic of the method to obtain normalised frequency spectra of storage modulus

Using the same method (**Fig 5.6**), normalised frequency spectra of storage modulus of CABs under different temperatures could be obtained. Thus, a full picture of dynamic storage modulus of a given viscoelastic CAB over a wide range of temperatures and loading frequencies could be available.

5.3.3 Summary

Temperature spectra of CAB-I and CAB-II at the fixed frequency of 10 Hz were measured by the DMA method in a bending mode and the influence of loading frequency was studied. Conclusions could be listed as follows.

1. Higher A/C resulted in lower dynamic modulus of CABs but higher loss factor which was firmly related to the viscoelasticity. CAB-II was more close to hcp in dynamic mechanical properties;
2. Two characteristic temperatures of asphalt binder, T_g and $T_{R\&B}$, defined the viscoelastic zone for CABs, especially for those with higher A/Cs and were found to be two important indicators, which would be probably used for characterising their low temperature and high-temperature properties, respectively; and at the same time, those two temperatures could provide some basis for the temperature range taken into account in fatigue tests in following **Chapter 6**;
3. Like temperature, loading frequency had an evident effect on the storage modulus of CABs. As the loading frequency increased logarithmically, the whole curves of normalised storage modulus of CAB-I trended to be moved to the right;
4. Normalised frequency spectra of CABs could be obtained through normalised temperature spectra based on the frequency-temperature correspondence. Thus, a full picture of dynamic storage modulus of any given CAB over a wide range of temperatures and loading frequencies could be available.

5.4 Dynamic mechanical properties of CAMs

DMA tests in a single cantilever bending mode were used to measure the dynamic mechanical properties of the two CAMs over a wide temperature range of -100 ˚C to 100 ˚C at the frequency of 10 Hz. Then the results were compared to those of CABs, to reveal the relationship between CABs and CAMs.

5.4.1 Temperature spectrum

Fig 5.7 showed temperature spectra of dynamic storage modulus and loss factors for CAM-I, CAM-II and the control, over a temperature range of -100 °C to 100 °C at the loading frequency of 10 Hz.

It was realised that, seen from **Fig 5.7 (a)** here and **Fig 5.2** in **Section 5.3.1.1**, the storage modulus of the two CAMs had the same tendency with those of their CABs as temperature changed from -100 °C to 100 °C, although much higher in value possible because of fine aggregates or sands incorporated. But the loss factors were greatly reduced (**Fig 5.7 (b)** and **Fig 5.3** in **Section 5.3.1.2**), almost by half. The introduction of fine aggregates or sands into CABs, obviously, changed CABs into CAMs with higher storage modulus but lower loss factor. And CAM-II had lower storage modulus and slightly higher loss factors in the viscoelastic zone than the control, Portland cement mortar, but the trend with temperature was very similar. It was reconfirmed that, like static mechanical properties in **Chapter 4**, dynamic mechanical properties of CAM-II was more close to those of Portland cement mortar as well.

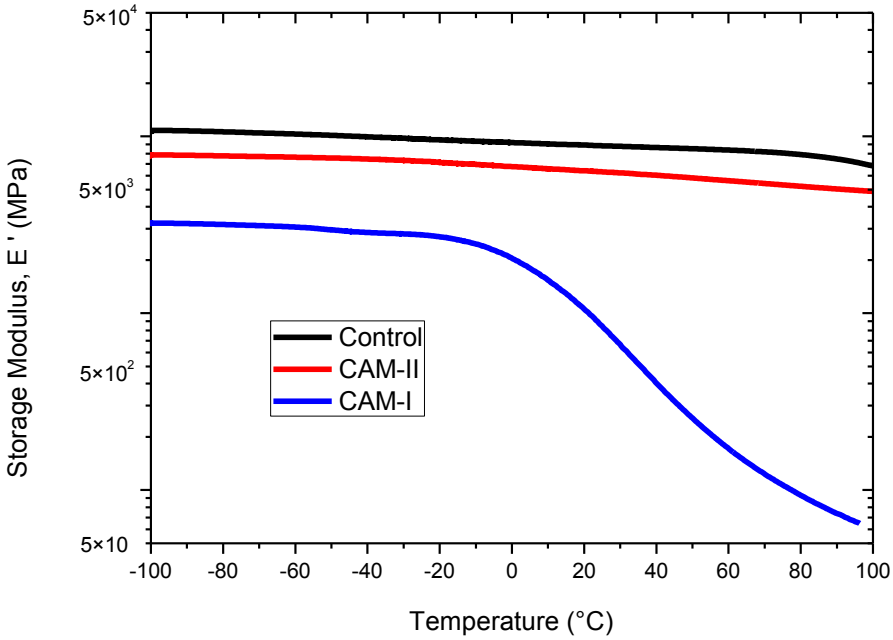

(a)

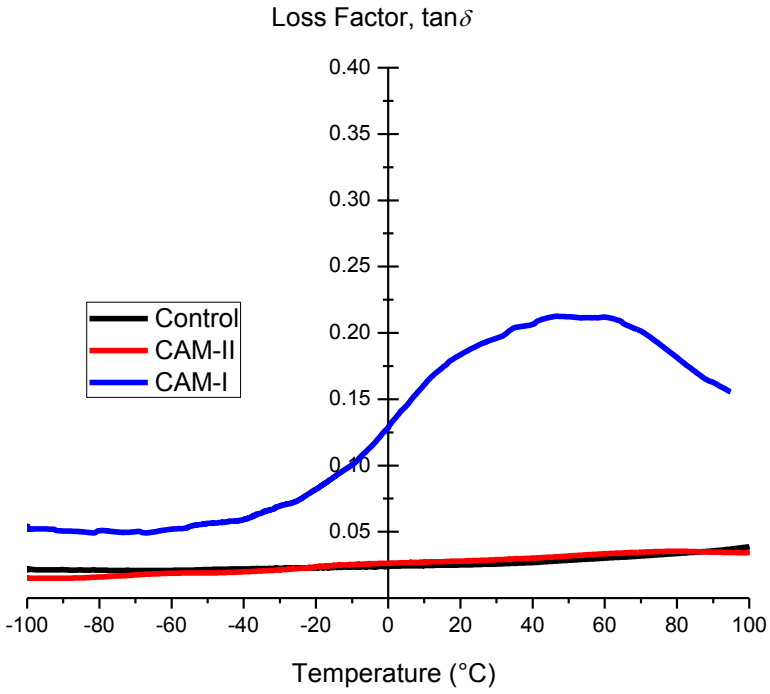

(b)

Fig 5.7 (a) Storage modulus and (b) loss factors of CAMs

5.4.2 Comparison between CABs and CAMs

It had been discussed in the previous chapter that CAMs could be regarded as two-phase composites in **Section 2.3.2**, CABs as the binder and fine aggregates as the filler, and mechanical properties of CAMs were mainly decided by those of CABs. It was also found that, in **Section 5.4.1**, storage modulus and loss factors of CAMs had a similar variation trend with temperature compared to those of CABs, except different in values. So in this section, storage modulus and loss factors of CAB-I or CAB-II and corresponding CAM-I or CAM-II were plotted together (**Fig 5.8** and **Fig 5.9**) for comparison.

It was obvious that from CABs to CAMs, generally, the storage modulus was increased but the loss factor was decreased, especially over the viscoelastic zone. When the temperature went from very low (-100 °C) to T_g, the storage modulus of both CABs and CAMs was almost linearly decreased at the same rate with temperature, while the loss factor was kept constant at a low value. Above that temperature, the storage modulus started to fall sharply and the loss factor started to increase. The higher the A/C in CABs or CAMs, the more remarked the change in dynamic mechanical properties. It was interesting to find that, from CAB-I or CAB-II to CAM-I or CAM-II, the change in storage modulus with temperature followed the same trend (**Fig 5.8 (a)** and **(b)**), which indicated that they maintained the same temperature susceptibility. Herein, it was possible that the inclusion of sands into CABs increased the dynamic modulus and decreased the loss factor, but never changed their susceptibility to environmental temperature, which meant that CAM-I or CAM-II had the same relative dynamic storage modulus with their corresponding CABs, CAB-I or CAB-II, as discussed in **Section 5.3.2**. It was indicated that, through measuring the dynamic mechanical properties of their matrixes, CABs, we could obtain the normalised spectra of dynamic storage modulus of CAMs over a range of temperatures or loading frequencies. For CAB-I and CAM-I, it was also found that their peak positions of loss factors with temperature remained around $T_{R\&B}$ (**Fig 5.9 (b)**), which indicated that this temperature was an important indicator for CAMs with high A/Cs as well. Above this temperature, those CAMs would be possibly destabilised as solid materials.

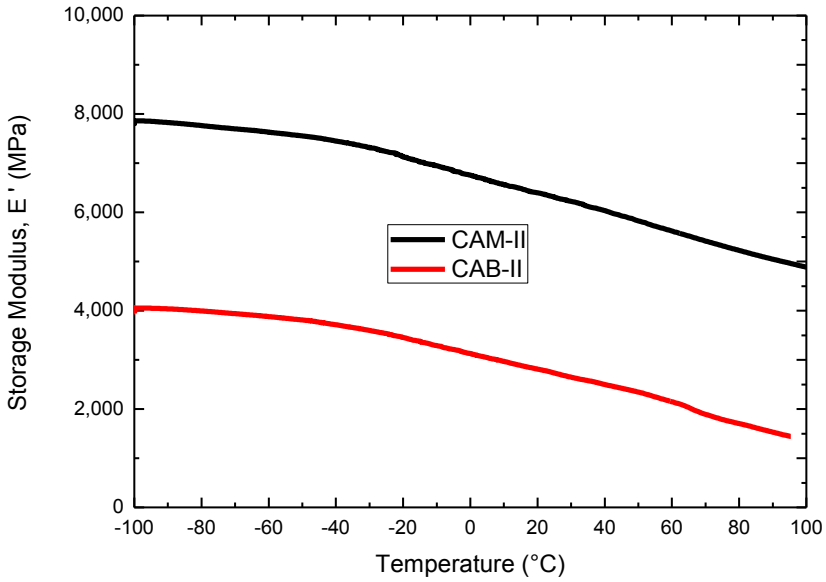

(a)

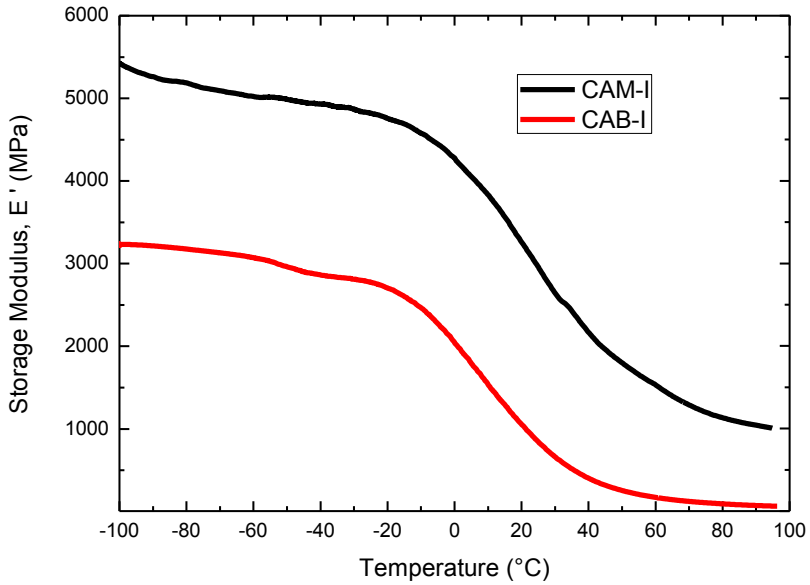

(b)

Fig 5.8 Storage modulus of CABs and CAMs

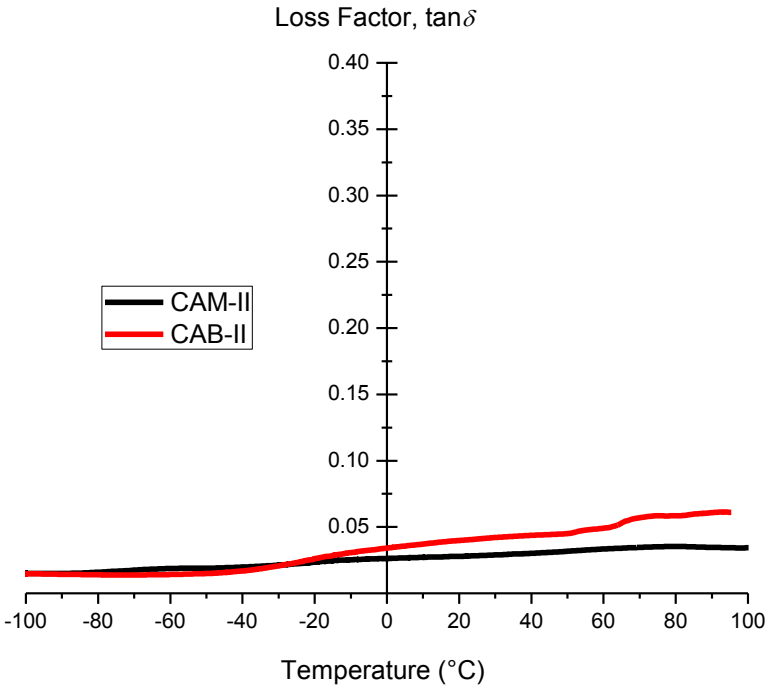

(a)

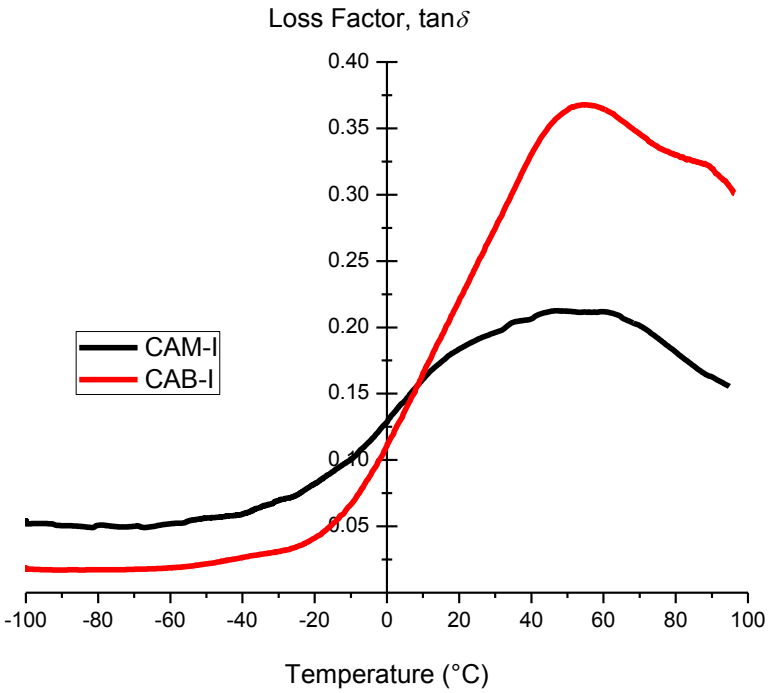

(b)

Fig 5.9 Loss factors of CABs and CAMs

5.4.3 Summary

Temperature spectra of the storage modulus and the loss factors of CAMs were measured by the DMA method in a bending mode over a wide temperature range of -100 ˚C to 100 ˚C at the fixed loading frequency of 10 Hz and the test results were compared with those of CABs in **Section 5.3.1**. Some conclusions could be drawn as follows.

1. Generally, the inclusion of fine aggregates or sands into CABs (from CABs to CAMs) increased the dynamic modulus and decreased the loss factor, but seemed never to change their susceptibility to environmental temperature;
2. The normalised spectra of the dynamic storage modulus of CAMs over a range of temperatures or loading frequencies could be obtained through measuring the dynamic mechanical properties of their matrixes, CABs, because they were found to be the same one;
3. The rough positions of the two characteristic temperatures of the asphalt binder, T_g and $T_{R\&B}$, remained almost unchanged for CAM-I and its matrix, CAB-I. It was indicated that, on the one hand, the main binding phase in CAMs with high A/Cs was asphalt binder; on the other hand, the inclusion of fillers, hcp or fine aggregates, into the asphalt binder would possibly not influence the two characteristic temperatures too much.

5.5 Damping of CAMs in slab tracks

To understand the importance of the viscoelasticity of CAMs, it is necessary to know their primary functions as structural materials in slab tracks, especially damping. In fact, in China, the use of CAMs as cushion materials in CRTS I and II is being argued among researchers and challenged by other construction materials like SCC. In this section, from the angle of a structural engineer, the author would like to discuss two common damping mechanisms in structures and attempt to bridge the viscoelasticity of the two CAMs and their damping in those two slab tracks.

5.5.1 Two damping mechanisms in structures

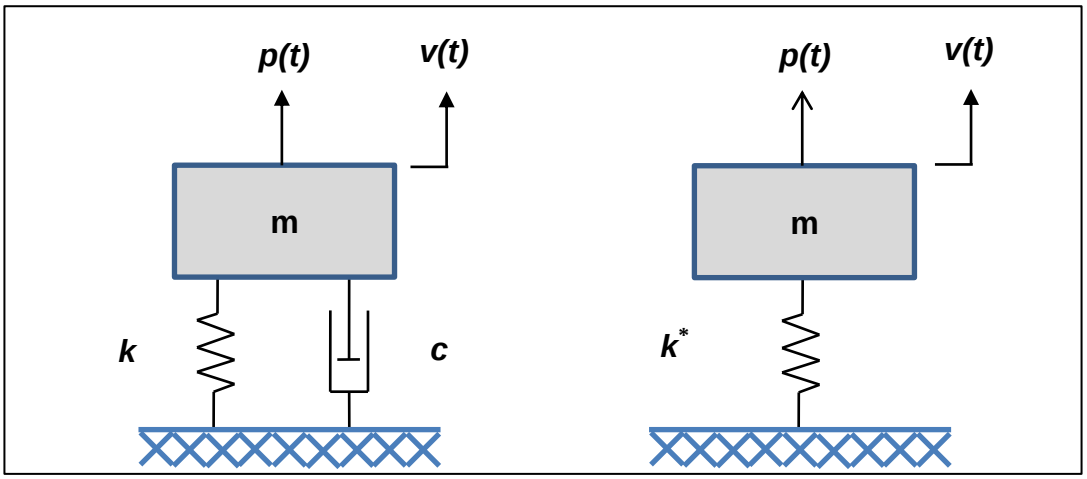

Fig 5.10 Schematics of two common damping mechanisms: (a) linear viscous and (b) linear hysteretic damping models

Here, for simplicity, a single degree-of-freedom (SDOF) structure is considered. There are two common damping mechanisms as shown in **Fig 5.10**, one is the linear viscous damping and the other is linear hysteretic damping. The former one is frequently used to simulate the dynamics of structures, whose basic equation can be written as in Equation (5-1).

$$m\frac{d^2\upsilon(t)}{dt^2}+c\frac{d\upsilon(t)}{dt}+k\upsilon(t)=p(t) \tag{5-1}$$

Where, m is the mass of the structure; *k* and *c* are stiffness and damping coefficient in the spring-dashpot system; *p(t)* and *v(t)* are the dynamic force exerted on the structure and the dynamic displacement as a response. It is assumed that the force is a harmonically varying load.

$$p(t)=p_o\sin(\omega t) \tag{5-2}$$

For the system starting from rest, i.e. *v(0)=v´(0)*=0, the general solution is shown as in the following equation.

$$\begin{aligned}\upsilon(t)&=\left[A\cos\omega_D+B\sin\omega_D\right]\exp(\xi\omega_n t)\\&+\frac{p_o}{k}\left[\frac{1}{(1-\beta^2)^2+(2\xi\beta)^2}\right]\left[(1-\beta^2)\sin\omega t-2\xi\beta\cos\omega t\right]\end{aligned} \tag{5-3}$$

Where, ω_n is the nature free-vibration frequency and ω_D is the free-vibration frequency of the damped system. β is the frequency ratio, defined as the ratio of the applied loading frequency to the natural frequency. ξ is the damping ratio, which equals to the damping coefficient divided by the critical damping coefficient, c_c.

$$\omega_n=\sqrt{\frac{k}{m}} \tag{5-4}$$

$$\beta=\omega/\omega_n \tag{5-5}$$

$$\omega_D=\omega_n\sqrt{1-\xi^2} \tag{5-6}$$

$$c_c=2m\omega_n \tag{5-7}$$

$$\xi=\frac{c}{c_c} \tag{5-8}$$

The first term in **Equation (5-3)** represents the transient response, which damps out immediately, while the second term represents the steady-state harmonic response, which will continue indefinitely. The constants A and B can be evaluated from the given initial conditions, *v(0)=v´(0)*=0. However, since the transient response damps out quickly, it is usually of little interest; therefore, the steady harmonic response, as shown in **Equation (5-9),** is the principal part as the structure vibrates.

$$\upsilon_p(t) = \frac{p_o}{k}\left[\frac{1}{(1-\beta^2)^2 + (2\xi\beta)^2}\right]\left[(1-\beta^2)\sin\omega t - 2\xi\beta\cos\omega t\right] \quad (5\text{-}9)$$

Based on this equation, two important structural factors for dynamics of the structure as follows are introduced.

Dynamic magnification factor, *D*, is defined as the ratio of the resultant harmonic response amplitude to the static displacement produced by the amplitude of the force. This factor is a reflection of vibration intensity, whereby a reduction in vibration of the structure can be evaluated.

$$D = \frac{p_o}{k}\frac{1}{\sqrt{(1-\beta^2)^2 + (2\xi\beta)^2}} / \left(\frac{p_o}{k}\right) = \frac{1}{\sqrt{(1-\beta^2)^2 + (2\xi\beta)^2}} \quad (5\text{-}10)$$

Transmissibility ratio, TR, of the support system is defined as the ratio of the maximum base force to the amplitude of the applied force, which is known as an important indicator of vibration isolation, to understand the level of vibration of the structure transmitted to the ground.

$$\mathrm{TR} = D\sqrt{1+(2\xi\beta)^2} \quad (5\text{-}11)$$

Those two factors abovementioned are demonstrated in **Fig 5.11** with the increasing frequency ratio under different damping systems.

When the loading frequency is close to the natural frequency of the structure, $\omega=\omega_n$, i.e. β=1, the structure is in the state of resonance, which is very

dangerous because it would produce the highest amplitude of vibrations and in the meantime the largest force transmitted to the ground (**Fig 5.10**). Therefore, in most cases, this situation should be avoided in the practical design. During the process when the structure started to vibrate, or came to a halt, i.e. β<1, increasing the damping ratio in the structure is an effective way to lower the values of *D* and TR, as a consequence, reducing the vibration intensity and isolating the vibration to the ground. In real structures like slab tracks which are subjected to random vibrations at all times, the primary frequency of vibration is usually larger than the natural frequency, i.e. β>1. In this case, a higher value of β or damping ratio, ξ, would generate better effects of vibration reduction and vibration isolation in slab tracks, or the nature frequency of the structures should be as low as possible.

In accordance to **Equation (5-4)** ~ **(5-8)**, therefore, it is easy to deduce that, to make sure the structure having good damping properties, the stiffness in the spring-dashpot system should be as low as possible and the damping ratio, rather than the damping coefficient, should be as high as possible.

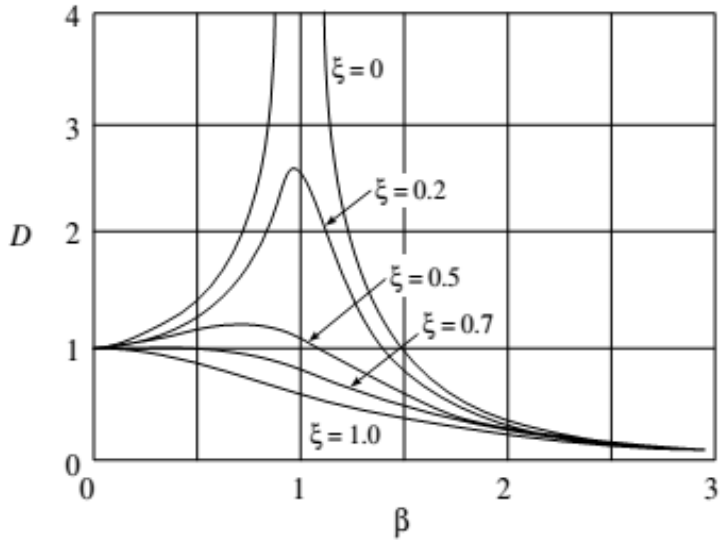

(a)

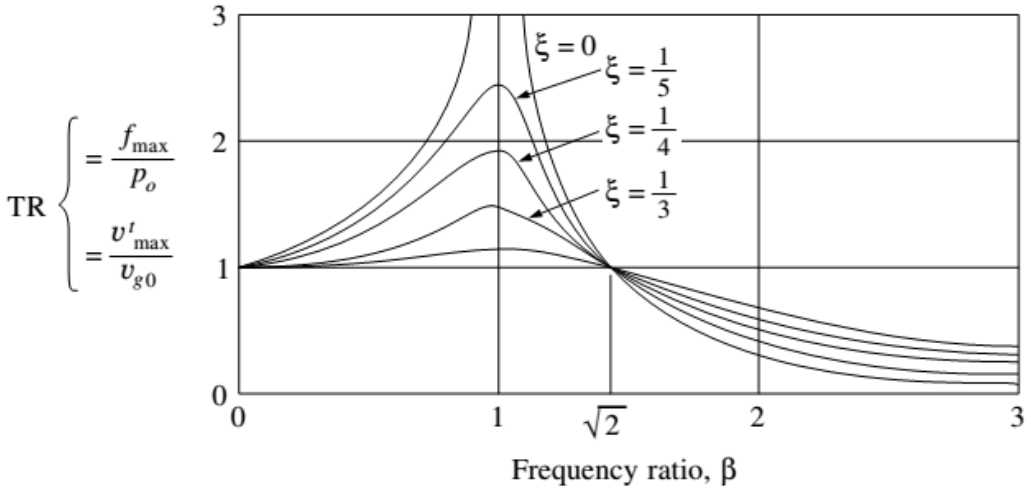

(b)

Fig 5.11 Variation of (a) dynamic magnification factor, D, and (b) transmissibility ratio, TR, with damping and frequency (Clough and Penzien, 2003)

For machines or structures with a high requirement on vibration reducing, it is not uncommon to use viscoelastic materials like rubbers or high damping metals and alloys as damping sources (Beards, 1996). Such a damping mechanism in structures is referred to as hysteretic and its dynamic and linear constitutive equation is shown as follows.

$$m\frac{d^2\upsilon(t)}{dt^2} + k^*\upsilon(t) = p(t) \tag{5-12}$$

$$k^* = k(1+\eta i) \tag{5-13}$$

Where, k^* is the complex stiffness and η is the hysteretic damping factor.

By analogy to equations of the steady state response in a structure with linear viscous damping, it is recommended to use **Equation (5-14)** to inter-correlate the two damping mechanisms (Clough and Penzien, 2003)

$$\eta = 2\xi \tag{5-14}$$

5.5.2 From viscoelasticity to damping

As discussed in **Section 2.2.4**, the CAM layer functions as a spring-dashpot system in slab tracks. And it has been known that CAMs are viscoelastic materials, whose complex modulus can be calculated from **Equation (2-3)** in **Chapter 2**. Compared with the complex stiffness in **Equation (5-13)**, it is easy to deduce such two new equations**, Equation (5-16)** and **Equation (5-17)**.

$$k \propto E' \approx \left|E^*\right| = E_d \tag{5-16}$$

$$\eta = \tan\varphi \tag{5-17}$$

According to those two equations above, it is evident to find that the two structural factors in structures like slab tracks, the stiffness and the damping coefficient, are firmly correlated to the dynamic modulus and the loss factors of CAMs, respectively. Provided that the viscoelasticity of CAMs is already known, the two dynamic factors in slab tracks can be obtained via **Equation (5-18)** and **Equation (5-19)**.

$$k = f(b,h)E_d \approx f(b,h)E' \tag{5-18}$$

$$c = 2m\omega_n\xi = \tan\varphi\sqrt{km} \tag{5-19}$$

Where, *f* is the shape function of the CAM layer*,* which is only dependent on the dimension, like the width, *b*, and the depth*, h*.

Here, in the final section of this chapter, the relationship between viscoelasticity of CAMs and their damping in slab tracks is successfully established. What should be kept in mind is that both of those two factors in structures, *k* and *c*, are not constant with temperature or frequency because, in **Section 5.4**, it was clearly revealed that both the storage modulus (*E´*) and the loss factors ($\tan\delta$) of CAMs are highly dependent on test temperature or loading frequency within a proper range. For an unknown reason, however, this fact is being always ignored in the modelling work of the two prefabricated concrete slab tracks with the CAM layer.

And it is concluded that, from the viewpoint of a structural engineer, lower storage modulus and higher loss factor of CAMs are reasonably required in these slab tracks because of their better damping effects in vibration reduction and vibration isolation, which means that it is better to choose CAMs with high A/Cs. But, from the viewpoint of a researcher in developing composite materials like CAMs, higher A/C leads to higher temperature susceptibility, which is not a good aspect in terms of the stability of solid materials. Therefore, to be concluded in a word, there is a balance between storage modulus, loss factor and temperature susceptibility when the design of new CAMs for slab tracks is considered in the future.

It is necessary to point out at the end that the two damping mechanisms are demonstrated by an SDOF structure which is subjected to steady state vibrations. Slab tracks, of course, are multiple degree-of-freedom (MDOF) systems, rather than an SDOF system, to undergo random transient vibrations, rather than steady state vibration, during the passage of high-speed trains in operation. Nevertheless, the basic principle is the same and it is convenient to assemble dynamic factors by using matrix, [*k*] or [*c*], as shown in **Equation (5-20)**, which are frequently used in the finite element method (FEM).

$$[m][\upsilon'']+[c][\upsilon']+[k][\upsilon]=[p] \tag{5-20}$$

5.5.3 Summary

Together with their constitutive equations in dynamics and solutions, two common damping mechanisms in structures, linear viscous and linear hysteretic damping, were introduced in this section. To characterise the damping in structures, two dynamic factors, *D* and TR, were analysed. Those two were found to be firmly related to dynamic mechanical parameters of viscoelastic materials. With the aim to explore the relationship between the viscoelasticity of CAMs and their primary function of damping in slab tracks, conclusions could be drawn as follows in this section.

1. Damping of CAMs in slab tracks manifests itself in two ways, vibration reduction and vibration isolation, which can be characterised by two structural factors, **D**ynamic magnification factor, *D*, and **T**ransmissibility **R**atio, TR;
2. Those two structural factors are found to be in close relation to two dynamic mechanical parameters of viscoelastic CAMs from the DMA tests , the storage modulus and the loss factor;
3. A balance should be considered between viscoelasticity and temperature susceptibility in the future design of cushion materials like CAMs and the proper A/C should be chosen.

5.6 Chapter summary

In **Chapter 5**, temperature spectra of dynamic modulus and loss factors of CAMs were measured by the DMA test method in a single cantilever bending mode and compared with those of their binders, CABs. Main conclusions as follows could be drawn from the experimental results.

1. The higher A/C caused a decrease in the dynamic modulus of CABs and CAMs but an increase in their loss factors and temperature susceptibility.
2. The rough positions of the two characteristic temperatures of the asphalt binder, T_g and $T_{R\&B}$ (48 °C), could be determined from the temperature spectrum of CABs or CAMs with high A/Cs, and those two temperatures defined the viscoelastic zone and would provide some reference for the proper temperature range considered in fatigue tests. T_g of the asphalt binder used in this work was implied to be around -20 °C.
3. The inclusion of fine aggregates or sands into CABs increased the dynamic modulus, decreased the loss factor, but never affected their susceptibility to environmental temperatures which indicated that CAMs had the same normalised temperature spectrum of dynamic modulus with their matrixes, CABs.
4. The primary function of CAMs in slab tracks, especially damping, is in close relation to the viscoelasticity of CAMs characterised by dynamic modulus and loss factor from the DMA tests, as clearly shown in two equations, **Equation (5-18)** and **(5-19)**.
5. Dynamic mechanical parameters are key to design and evaluation of CAMs used as the cushion layer in slab tracks.
6. A balance or compromise should be considered between viscoelasticity and temperature susceptibility in the future design of cushion materials like CAMs and a proper A/C should be chosen.

CHAPTER 6 4-POINT BENDING FATIGUE OF CAM-I AND CAM-II

6.1 Introduction

As the cushion layer, CAM-I and CAM-II are frequently used in CRTS I and CRTS II of China's huge HSR network, respectively, to sustain traffic loads from train-rail-slab track interactions (Zhai et al., 1999, Zhai et al., 2009), transmit them to the foundation, and most significantly resist or attenuate the vibrations generated by moving trains at high speed in two aspects, namely, vibration reduction and vibration isolation as discussed in **Section 5.5** of **Chapter 5**. After a few years' operation and service of HSR, however, premature cracking has been identified in the CAM layer along part of CRTS I and CRTS II.

Behind this cracking phenomenon in the cushion layer of CRTS I and II, the primary mechanism is most possibly to be fatigue of CAMs under repetitive traffic loading, that is, mechanical fatigue. This is the basic assumption in this thesis. To address such an important issue, the first but crucial step is to choose appropriate, rational and reliable fatigue test schemes for CAMs in the laboratory, with the aim at simulating the fatigue induced cracking in the field of CRTS I and CRTS II and defining the fatigue properties of CAMs, and the ultimate aim is to find a solution to cracking in the future years to come. In literature, however, fatigue of CAM-I (Wang and Liu, 2008), or CAM-II (Li et al., 2010b, Qiu et al., 2013b) was scarcely concerned and understood. Possibly because of different fatigue test methods used, furthermore, contradicting views could be found. Through a literature review on CAMs and experimental work as reported in **Chapter 4**, CAM-I and CAM-II were confirmed to be two totally different composite materials in mechanical properties due to the difference in A/C, although they had almost the same components. But interestingly, they were found to be close to two extreme and most commonly used materials, asphalt mixtures and cement-based materials, respectively, as discussed in **Section 2.3.2.3** of **Chapter 2**. Therefore, in the fourth part of the review

chapter, related fatigue test schemes of asphalt mixtures and cement-based materials were separately reviewed including fatigue test method, mode of loading, the analysis method of test results and main controlling variables to be considered, with the purpose of establishing different fatigue test schemes for CAM-I and CAM-II. And a potential and probably best option was proposed to directly use similar fatigue test schemes to asphalt mixtures and cement-based materials for CAM-I and CAM-II, respectively.

This chapter was the experimental work to validate this idea. For convenience, the same test method, 4PB, but with a different mode of loading, either controlled-strain or controlled-stress, would be used for fatigue tests of CAM-I and CAM-II, and a continuous sinusoidal loading wave would be applied under a given frequency of 10 Hz. Due to the viscoelastic nature of asphalt binder, environmental temperature is a significant factor to be considered for CAMs. For asphalt mixtures, as discussed in **Section 2.5.3.6** of **Chapter 2**, fatigue should be tested under 'intermediate' temperatures. Usually, the temperature range from 5 °C to 30 °C could be accepted as intermediate (Tsai, 2001). But meanwhile, the test temperature might be set as low as -10 °C or as high as 40 °C. In Dr Kong's previous research work (Kong et al., 2010b, Kong et al., 2014), the temperature range was chosen over -40 °C to 80 °C. Those temperatures were selected to cover the range that is normally encountered during the operation of HSR across mainland China. In **Chapter 5**, what's more, two characteristic temperatures, T_g and $T_{R\&B}$, of the asphalt binder used in this thesis, could be observed on the temperature spectra of CAM-I and its binder, CAB-I. As a result, T_g was implied to be around -20 °C, and $T_{R\&B}$ was tested and already known to be 48 °C. Those two temperatures defined the viscoelastic zone of CAM-I. Based on the viscoelastic zone as defined by T_g and $T_{R\&B}$, in this case, the intermediate temperature range would be set from 0 °C to 40 °C for fatigue testing of CAM-I. For CAM-II which is close to cement-based materials including plain concretes, on the other hand, the temperature range from -20 °C to 60 °C would be used in its 4PB fatigue, considering the two characteristic temperatures of the asphalt binder. In addition to temperature, stress ratio, *R*, would be taken into consideration for fatigue testing of CAM-II. In routine fatigue tests of plain concretes, the *R* value is set to

be a constant value, R = 0.1. Based on this value, for comparison, two typical R values, 0.2 and -1 were selected. In the case of R = -1, for example, a complete stress reversal would be applied on CAM-II, in order to study the influence of the reversal effect on its 4PB fatigue.

The main objectives of the final experimental chapter were:

- To study 4PB fatigue properties of CAM-I in the controlled-strain mode, with reference to asphalt mixtures, and study the influence of test temperature on its fatigue;
- To study 4PB fatigue properties of CAM-II in the controlled-stress mode, with reference to plain concretes, and study the influences of stress ratio, R, and test temperature on its fatigue.
- To evaluate the reasonability of applying these two different fatigue test schemes in testing the 4PB fatigue properties of CAM-I and CAM-II, respectively.

6.2 Experimental programme

To achieve the two objectives above mentioned, an experimental programme of 4PB fatigue tests on CAM-I and CAM-II was developed as shown in the flow chart of **Fig 6.1**, and would be conducted in two stages as follows.

Stage 1: 4PB fatigue of CAM-I would be tested in the controlled-strain mode (*ε*-) following the fatigue test scheme for asphalt mixtures, and the influence of temperature would be considered.

Stage 2: 4PB fatigue of CAM-II would be tested in the controlled-stress mode (σ-) using the same fatigue test scheme with plain concretes, and the influences of stress ratio, S, and temperature would be considered and compared with plain concretes.

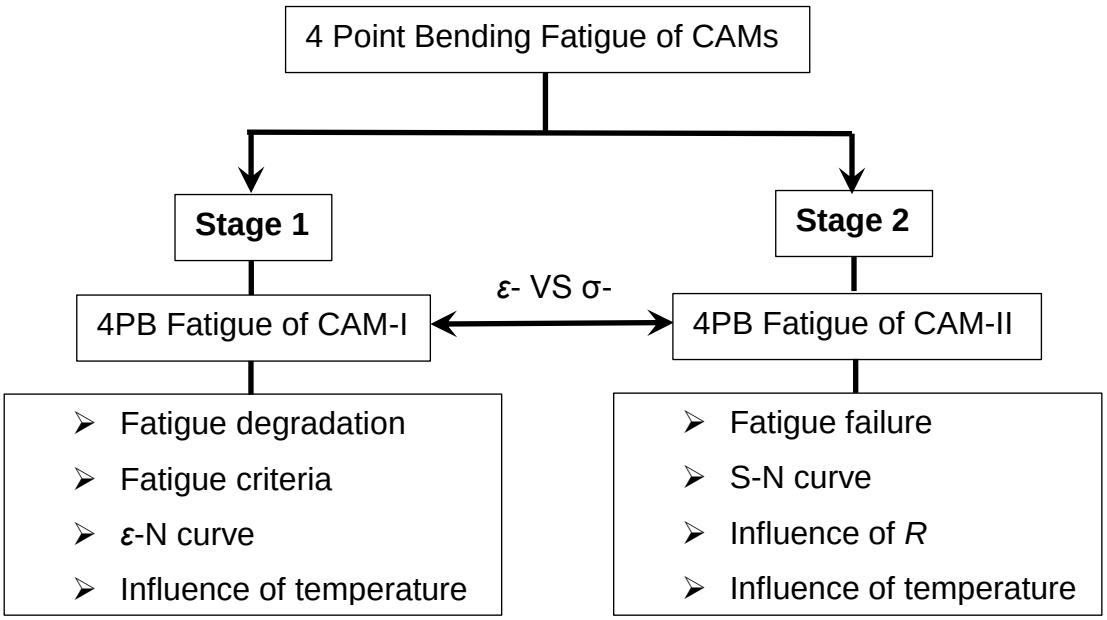

Fig 6.1 Flow chart of the experimental programme in Chapter 6

6.3 Controlled-strain 4PB fatigue of CAM-I

Fatigue properties and behaviour of CAM-I was measured in controlled-strain 4PB tests in the laboratory. To use the newly-developed 4PB apparatus effectively for fatigue testing, a trial fatigue test was conducted on a CAM-I beam with two purposes. The first one was to check the stability and validity of fatigue test data, and the second was to choose an appropriate failure criterion for data analysis. Following up was fatigue testing of several CAM-I beams with different strain levels and the classical ε-N curve could be obtained. Finally, the influences of temperature on bending properties and fatigue were analysed.

6.3.1 Fatigue degradation

Usually, it is uneasy to perform a fatigue test with a large strain level. In the trial fatigue test, therefore, a large strain level, ε_a = 650 μm/m based on its fracture strain (881 μm/m) from static bending tests in **Chapter 4** was applied on CAM-I by controlling the reversal of deflection during fatigue.

As fatigue testing proceeded, deflections and forces in the centre of the beam in every loading cycle were recorded with time. **Fig 6.2 (a)** showed the first 10 loading cycles in the trial fatigue test. Obviously, a sinusoidal deflection wave could be seen and the amplitude was maintained the same level from one cycle to another. And the amplitude of force tended to decrease in the tension zone, which could be confirmed by the hysteresis loop (**Fig 6.2 (b)**). Such a fact indicated that fatigue damage by tension, rather than compression, could be the major mechanism. Through a number of simple and iterative calculations in a **MATLAB 7.8.0**, the amplitudes of deflections and forces were converted into those of strains and stresses, ε_a and σ_a, respectively. The dynamic modulus and the hysteresis energy at the loading cycle of i, E_{di} and w_i, could be calculated according to **Equation (6-1)** and **Equation (6-2)**, as deduced from **Equation (3-11)** and **Equation (3-12)** in **Chapter 3**.

$$E_{di} = \frac{\sigma_a(i)}{\varepsilon_a(i)} \tag{6-1}$$

$$w_i = \pi \sigma_a(i) \varepsilon_a(i) \sin \delta(i) \quad (6\text{-}2)$$

Fatigue degradation of CAM-I was demonstrated in **Fig 6.3** and **Fig 6.4**. At the initial stage of fatigue, seen from **Fig 6.3**, the strain amplitude was higher to 700 μm/m compared to the design value and decreased to a stable value after almost 100 cycles of loading. This value could be obtained and was 646 μm/m, demonstrating that real value was slightly lower than the designed one. After a certain number of loading cycles, close to the fatigue failure zone, the strain level started to be unstably increased. As expected, on the other hand, the amplitude of stress decreased continuously within the loading cycles. As the stress amplitude or more evidently, dynamic modulus (**Fig 6.4**), evolved with loading cycles, four distinct zones of fatigue behaviour related to damage, like asphalt mixtures, could be seen (Rowe and Bouldin, 2000). This was a direct proof that, on fatigue, CAM-I is close to asphalt mixtures. The evolution of lag angle with loading cycles during fatigue testing was also plotted in **Fig 6.4**, which showed a reversed trend to increase during fatigue compared with dynamic modulus, but reached a peak value around the fatigue failure zone. The position of the peak value was thought to be possibly the point relevant to fatigue failure in asphalt mixtures (Tapsoba et al., 2012), but how to define the failure in a controlled-strain fatigue test is so different and controversial as discussed in **Section 2.5.3.4** of the review chapter. Next, fatigue failure criteria of CAM-I would be discussed.

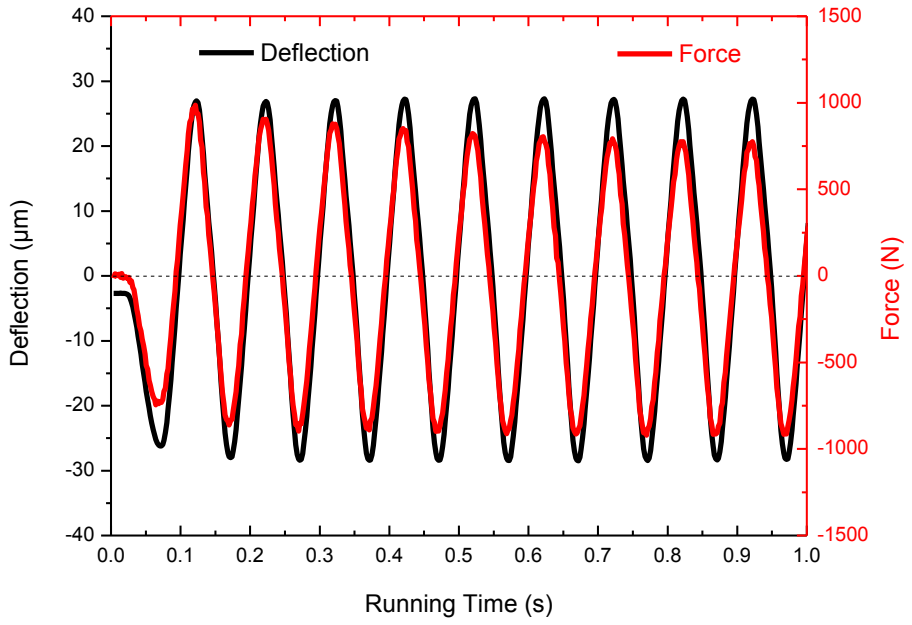

(a)

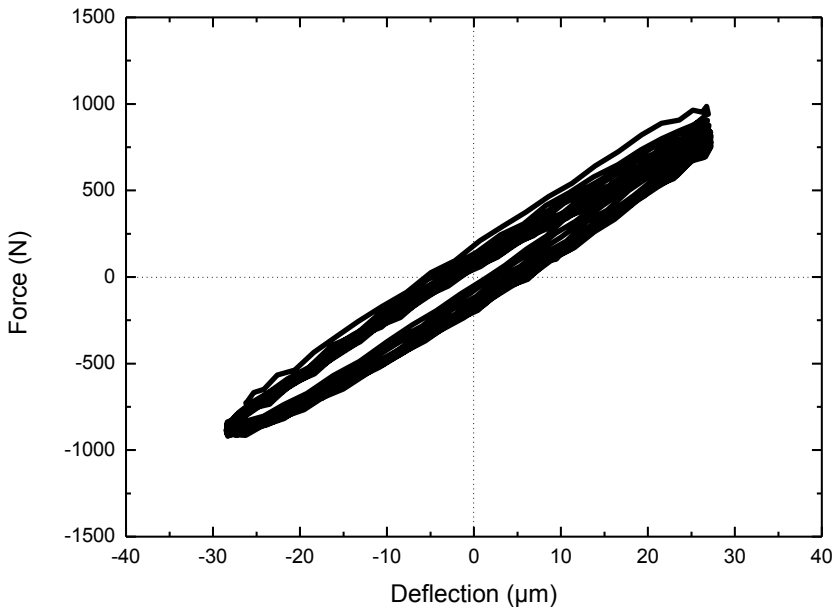

(b)

Fig 6.2 The first 10 cycles of a trial fatigue test of CAM-I: (a) deflection or force with time; (b) hysteresis loop

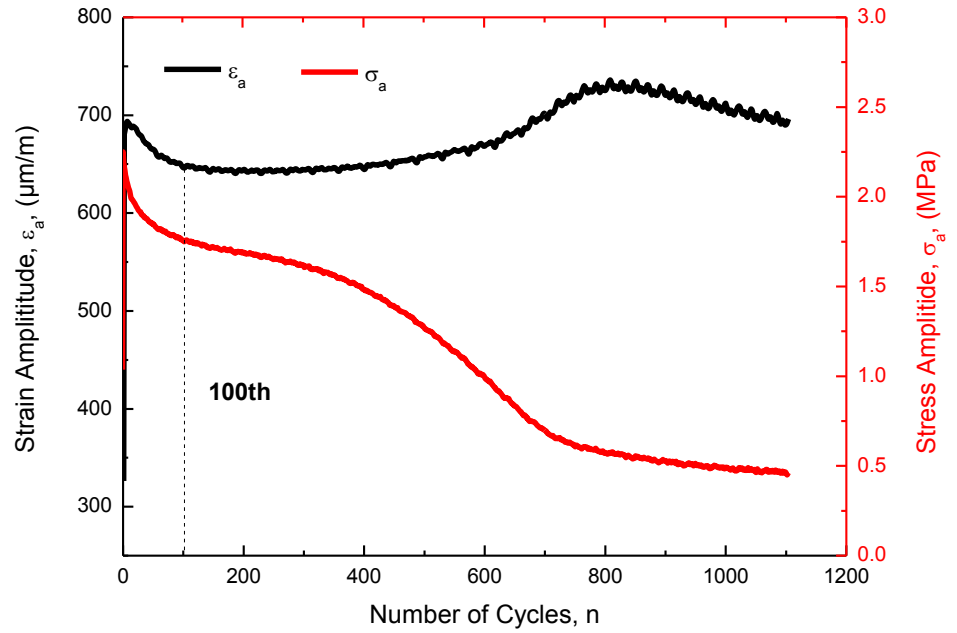

Fig 6.3 Evolution of strain amplitude and stress amplitude with loading cycles during fatigue testing of CAM-I

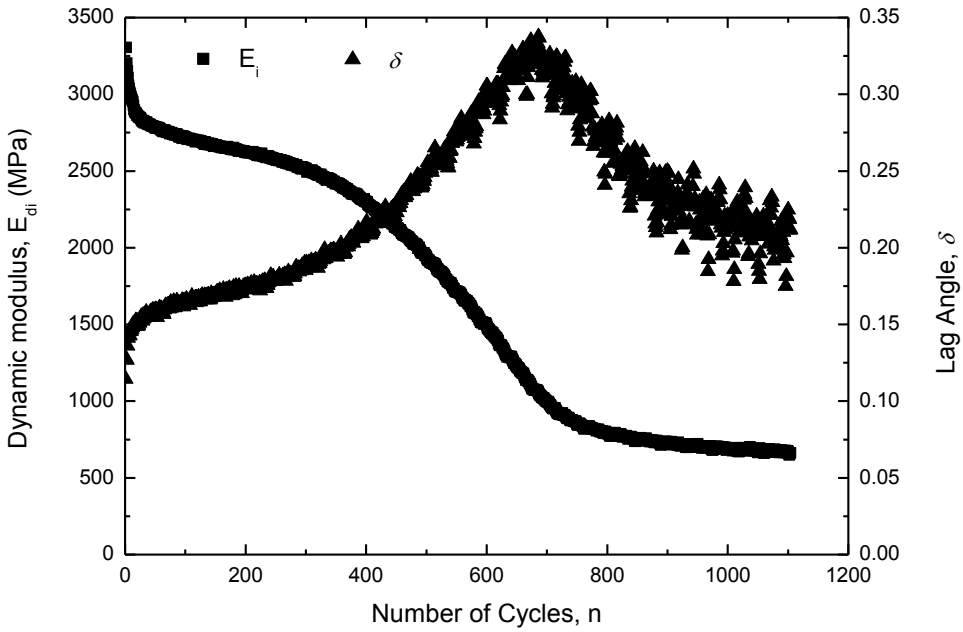

Fig 6.4 Evolution of dynamic modulus and lag angle with loading cycles during fatigue testing of CAM-I

6.3.2 Failure criteria

In controlled-strain fatigue tests, there exist mainly two basic categories of fatigue failure criteria (Maggiore, 2014), one based on stiffness or dynamic modulus, E_{di}, and the other based on DE, w_i, as well discussed in **Section 2.5.3.4** of the review **Chapter 2**. The traditional fatigue failure criterion, $N_{f,\ 50}$, which defines 50 % reduction in initial dynamic modulus as the failure point, is the most frequently used for data analysis because it is simple but rational (Abojaradeh, 2013). Amongst all DE-base failure criteria, a modified failure criterion based on energy ratio (ER) (Pronk and Hopman, 1991), $N_{f,\ ER}$, is believed to accurately define the beginning of the first transition point, N_1, where the merging of micro-cracks starts to develop a sharp one (Rowe and Bouldin, 2000, Shen and Lu, 2010, Abojaradeh, 2013). This criterion is now used in **ASTM Designation: D7460-10**, and the ER's calculation formula is clearly stated in **Equation (6-3)**. Then the number of cycles to failure can be decided by the peak location of an ER's curve versus loading cycles, n, and this method is better than other ones used in some fatigue failure criteria through defining a significant change in the slope of the curve or the intersection of two tangent lines as the transition point.

$$ER = \frac{nw_i}{w_o} \approx \frac{nE_i}{E_o} \tag{6-3}$$

Those two typical failure criteria for asphalt mixtures were used for fatigue data analysis of CAM-I for comparison. Using raw fatigue data, the number of cycles to failure determined by the traditional failure criterion, $N_{f,\ 50}$, or by the ER-based failure criterion, $N_{f,\ ER}$, was 566 or 642, respectively, which could be seen from **Fig 6.5**. Obviously, $N_{f,\ 50}$ was smaller than $N_{f,\ ER}$, confirming that the traditional failure criterion is conservative. In different standards, a revision of the raw fatigue data is so required that, for example, the first 50 cycles in **ASTM Designation: D7460-10** or the first 100 cycles in **EN12697-24: 2012**, should be excluded from analysis. Considering the initial stage of fatigue in **Fig 6.3** of the preceding **Section 6.3.1**, the first 100 cycles were excluded for CAM-I. After such revision, the same two fatigue failure criteria were applied again, giving two different numbers of cycles to failure, $N_{f,\ 50}$ = 525 and $N_{f,\ ER}$ = 542, as

shown in **Fig 6.6**. For better comparison, initial strain amplitudes, ε_a, initial dynamic modulus, E_o, and numbers of cycles to failure, N_f, from two classical fatigue failure criteria were listed in **Table 6.1**. More than evident, after fatigue data revision, the calculated initial strain amplitude was more close to the design strain level (650 μm/m), the initial dynamic modulus was reduced and the gap between numbers of cycles to failure based on two different failure criteria was narrowed. Despite all that, it was still arguable whether to exclude the first few cycles during fatigue data analysis because the number, 50 or 100, was pure empirical and its magnitude might be dependent on strain level applied. Another interesting fact, as shown in **Table 6.1**, **Fig 6.5(b)** and **Fig 6.6(b)**, was that the difference in numbers of cycles to failure before and after the first 100 cycles excluded from the raw data was precisely 100, which strongly indicated that the modified ER-based fatigue failure criterion is independent of the data revision and a better one used in CAM-I.

And take a look back at the end of **Section 6.3.1** that mentioned the location of the peak value of lag angle with the loading cycles possibly as the failure point. This number of cycles to failure was 686 for the raw fatigue data, and obviously larger than $N_{f,\ ER}$ (654). It was implied that such a method could be another failure criterion as well, although rarely concerned. In addition to crack initiation, nonetheless, this failure criterion included part of crack propagation. That was why its number of cycles to failure was relatively larger.

Table 6.1 Fatigue test results before and after data revision

	Initial strain amplitude ε_a	**Initial dynamic modulus E_o**	**Number of Cycles to failure**	
			$N_{f,\ 50}$	**$N_{f,\ ER}$**
Before	690 μm/m	3305 MPa	566	642
After	646 μm/m	2719 MPa	525	542

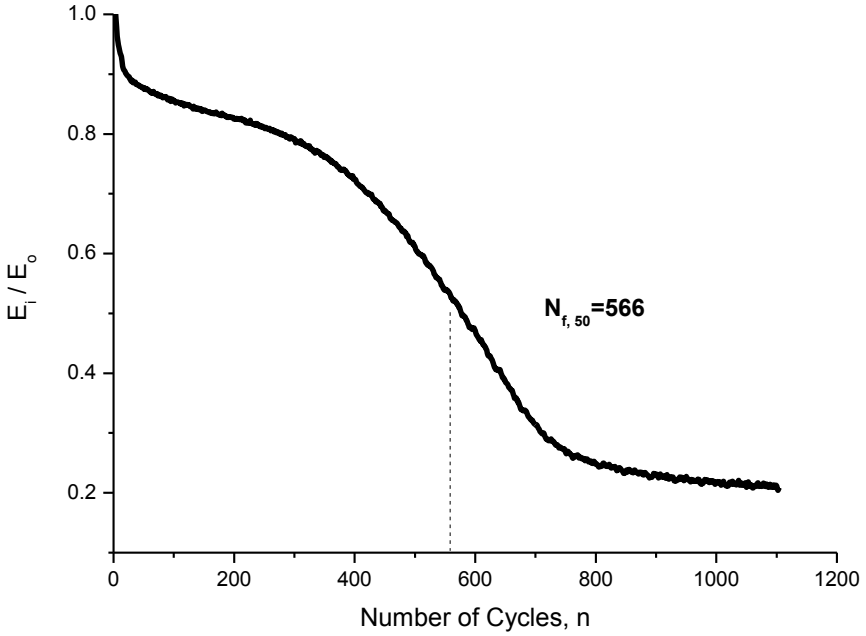

(a)

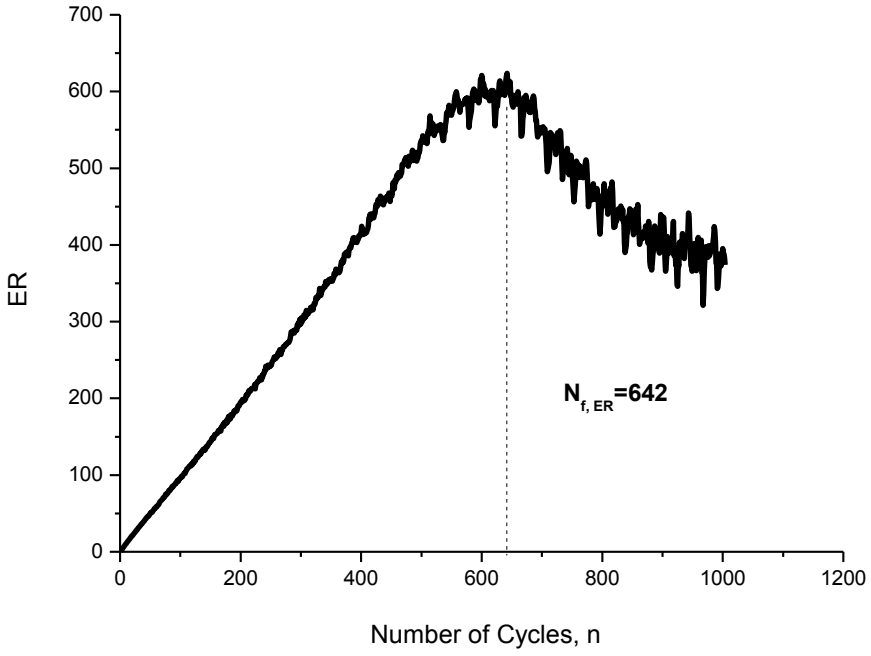

(b)

Fig 6.5 (a) $N_{f, 50}$ and (b) $N_{f, ER}$ using raw fatigue data

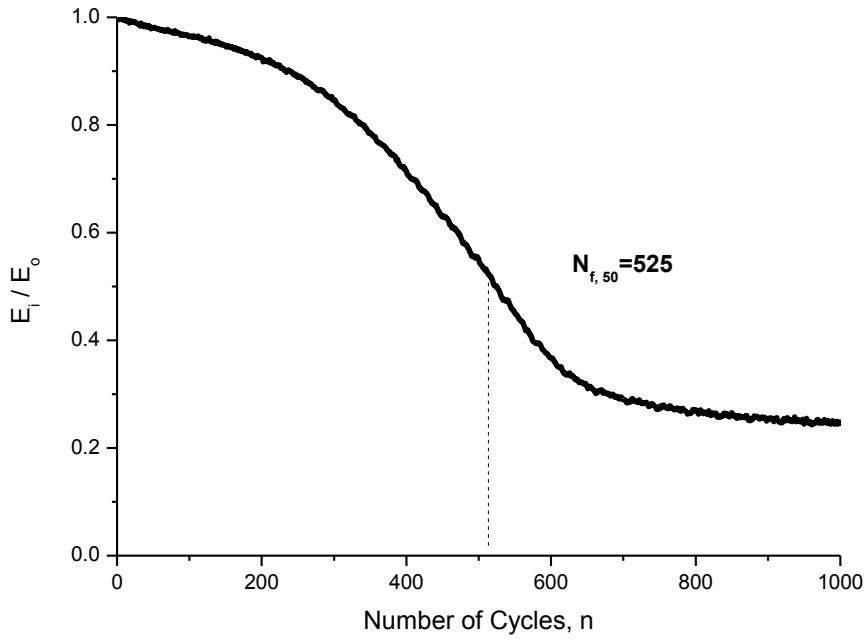

(a)

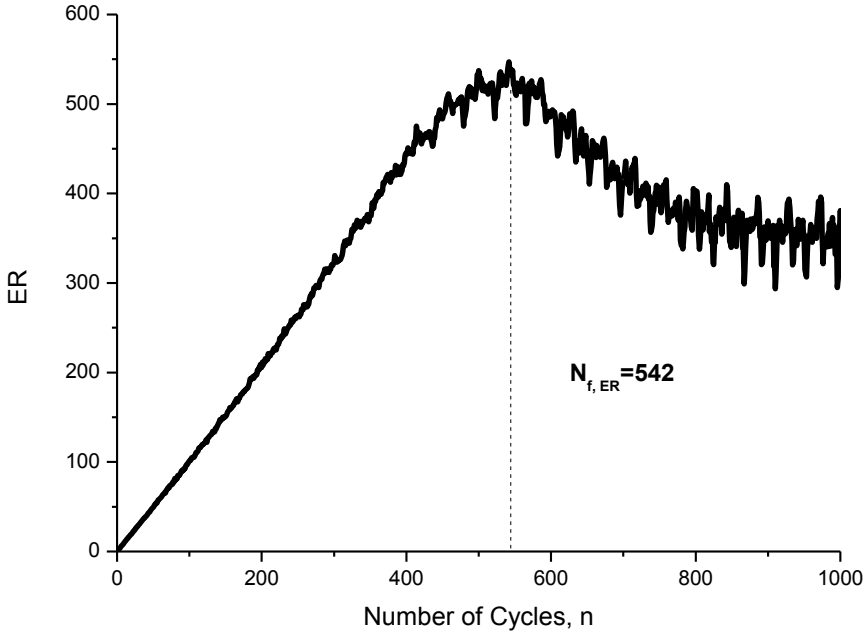

(b)

Fig 6.6 (a) $N_{f, 50}$ and (b) $N_{f, ER}$ using revised fatigue data

6.3.3 ε-N curve

A typical ε-N curve represents the relationship between the critical tensile strain, ε_t, and the number of cycles to failure, N_f. Three tensile strain levels, 300 μm/m, 400 μm/m and 500 μm/m, were designed for 4PB fatigue tests of CAM-I and environmental temperature was strictly controlled at 20 ± 1 °C, to avoid the possible temperature effect.

$$\varepsilon_t = \varepsilon_a \tag{6-4}$$

For 4PB fatigue of CAM-I, the amplitude of strain applied, ε_t, was taken as the critical tensile strain (**Equation (6-4)** above). However, as mentioned in the previous section, the strain amplitudes during the initial stage of fatigue were not stable values and that is why a raw fatigue data revision was required in the fatigue analysis. But in the concept of controlled-strain fatigue tests, these values should be maintained constant. Therefore, the real strain amplitude when fully stable fatigue testing was achieved, instead of the initial strain amplitude, was used and that was slightly different than the designed one. Regarding the fatigue failure criterion, the modified ER-based one was used on the raw fatigue data for analysis because it was better as proved in the previous section. As a result, the ε-N curve of CAM-I at room temperature was shown in **Fig 6.7**. Obviously, higher tensile strain level produced a lower number of cycles to failure, i.e. fatigue life. It seemed that the scatteredness of the fatigue test data increased as fatigue life increased, although a relatively small number of fatigue tests were conducted herein, and a fairly good linear relationship could be plotted in double logarithmical scales. Following up was to calculate main coefficients from the ε-N curve. Based on **Equation (2-11)** in **Section 2.5.3.5** of **Chapter 2**, k_1 and k_2 could be obtained using a nonlinear curve fit in the **OriginPro 8**. Next step was to calculate ε_6, via the two material constants. It was assumed that 1 million (10^6) cycles was still on the line far away and its law could be described in **Equation (6-5)**. This equation is divided by **Equation (2-11)** and the resulting equation is shown in **Equation (6-6)**, and immediately, ε_6 could be calculated by **Equation (6-7)**. From this equation, it was revealed that ε_6 was a material constant as well because both k_1 and k_2 are material

constants. The main coefficients, k_1, k_2 and ε_6 were listed in **Table 6.2**. The ε_6 value of CAM-I at room temperature was 188 μm/m.

$$10^6 = k_1 \left(\frac{1}{\varepsilon_6} \right)^{k_2} \tag{6-5}$$

$$\frac{N_f}{10^6} = \left(\frac{\varepsilon_6}{\varepsilon_t} \right)^{k_2} \tag{6-6}$$

$$\varepsilon_6 = 10^{\frac{\log(k_1)-6}{k_2}} \tag{6-7}$$

To further understand the meaning of the ε_6 value, a comparison was made as shown in **Fig 6.8**. The ε_6 values of asphalt mixtures used in European countries were from 11 different test methods via an inter-laboratory test campaign (Di Benedetto et al., 2004). **Fig 6.8** showed that the ε_6 value was influenced by fatigue test method and the 4PB test method got the relatively higher ε_6 values than others. Most importantly, the ε_6 value of CAM-I using the 4PB test method was comparable to those of asphalt mixtures (150 ~ 200 μm/m) with the same test method. This proved that CAM-I behaved more like asphalt mixtures and the controlled-strain 4PB test method used in this work was a rational and reliable choice for CAM-I.

Table 6.2 Main coefficients from the ε-N curve of CAM-I

Tem.	k_1	k_2	R^2	ε_6
20 °C	1.96×10^{23}	7.60	95.43 %	188 μm/m

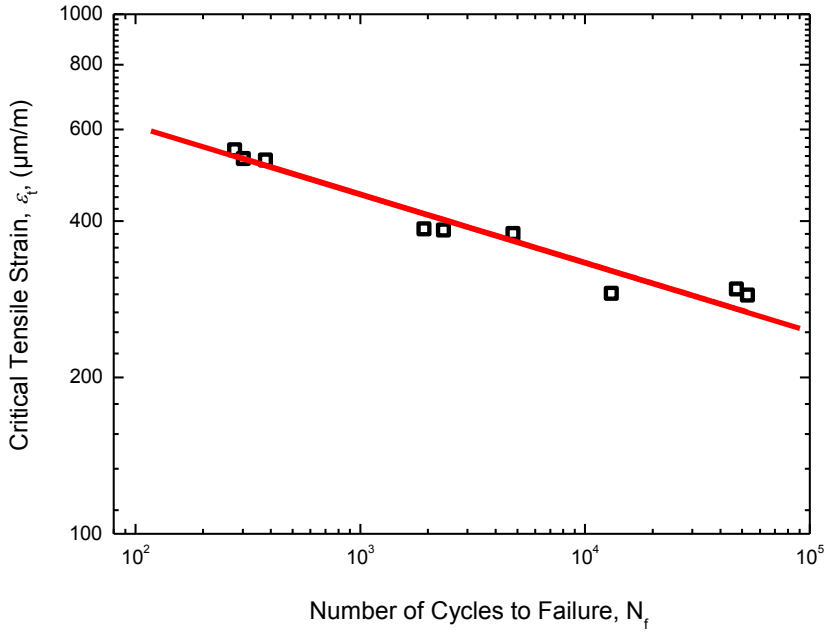

Fig 6.7 The *ε*-N curve of CAM-I at room temperature

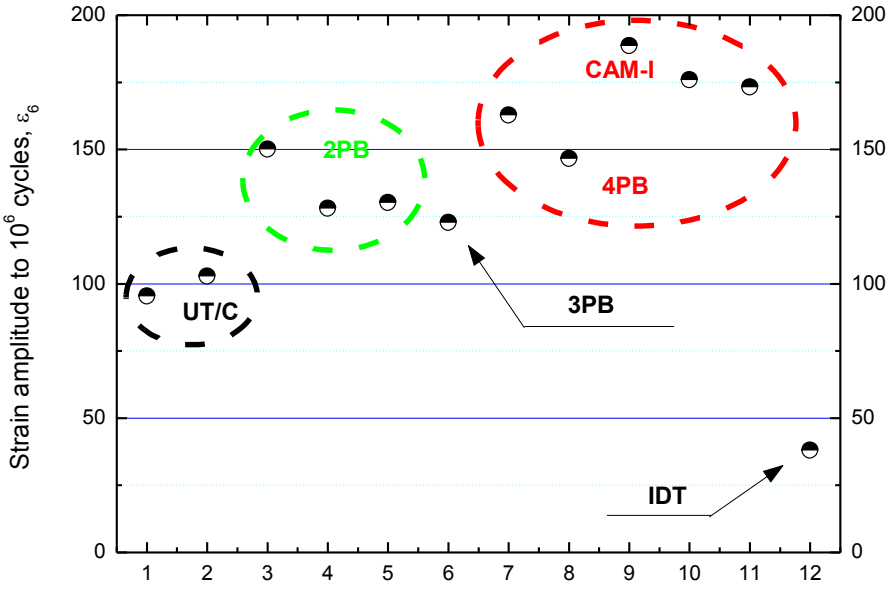

Fig 6.8 Comparison of the ε_6 value of CAM-I with those of asphalt mixtures used in European countries from different test methods

6.3.4 Influence of temperature

To study the influence of temperature on fatigue, static bending properties of CAM-I were tested under intermediate temperatures firstly, and basic bending parameters could be obtained. In the second place, controlled-strain fatigue tests were performed to obtain their ε-N curves for comparison and evaluation under different temperatures.

6.3.4.1 Bending properties at intermediate temperatures

Fig 6.9 presented stress-strain curves of CAM-I under 0 °C, 20 °C and 40°C. Within intermediate temperatures, those curves were similar, indicating that CAM-I remained a ductile material in the viscoelastic zone. And with the rise of temperature, bending strength (σ_b) and modulus (E_t) was enhanced, as shown in **Table 6.3** and Fig **6.10 (a)**. Fracture strain, ε_f , was slightly improved at 0 °C but reduced by about 200 μm/m at 40 °C. Fracture energy, as defined in **Section 4.2.2** of **Chapter 4,** followed the same trend with the bending strength and modulus. It was found that the influence of higher temperature (40 °C) on bending properties of CAM-I was more pronounced than that of lower temperature (0 °C), and that was contrary to the temperature effects on its compressive properties (Kong et al., 2014).

Stress-strain curves of CAM-I were tested in the laboratory as well under two boundary temperatures, -20 °C and 60 °C. Under the temperature of -20 °C, CAM-I was transformed into a brittle material (**Fig 6.11(a)**), whereas this composite almost could not sustain loads when the temperature reached 60 °C. These two phenomena could be explained by two important temperatures of asphalt binder, T_g and $T_{R\&B}$, as mentioned and discussed in **Chapter 5**. Obviously, T_g and $T_{R\&B}$ was possible to be the two lower and upper limits for service temperature, which is important in the future design of new CAMs with high A/Cs. When the test temperature was higher than $T_{R\&B}$, the CAM-I started to be destabilised due to the softening behaviour of asphalt binder; such composites would transition from viscoelastic solids to glassy ones if the test temperate fell to as close as T_g. Once again, as implied, the T_g of the asphalt binder used in this work might be around -20 °C.

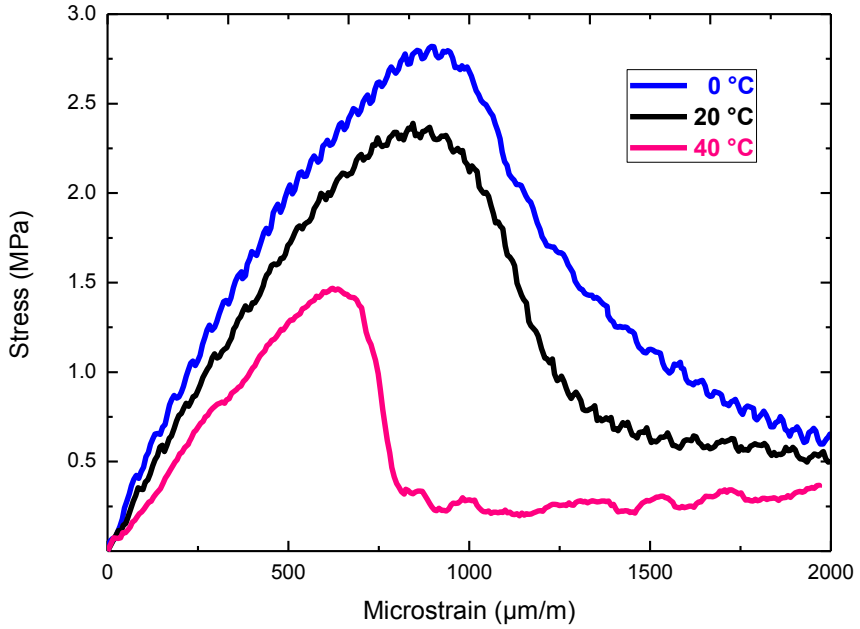

Fig 6.9 Stress-strain curves of CAM-I at intermediate temperatures

Table 6.3 Bending parameters of CAM-I at intermediate temperatures

Tem. (°C)	σ_b (MPa)	E_b (GPa)	ε_f (μm/m)	G_f (J/m^3)
0	2.75	4.64	889	1456.64
20	2.32	3.80	881	1223.04
40	1.47	2.77	679	562.83

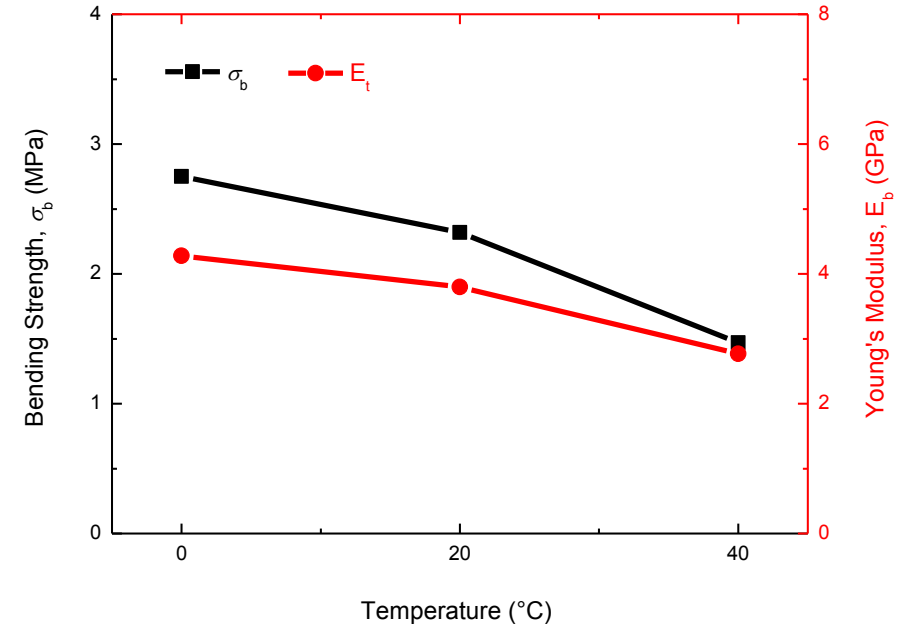

(a)

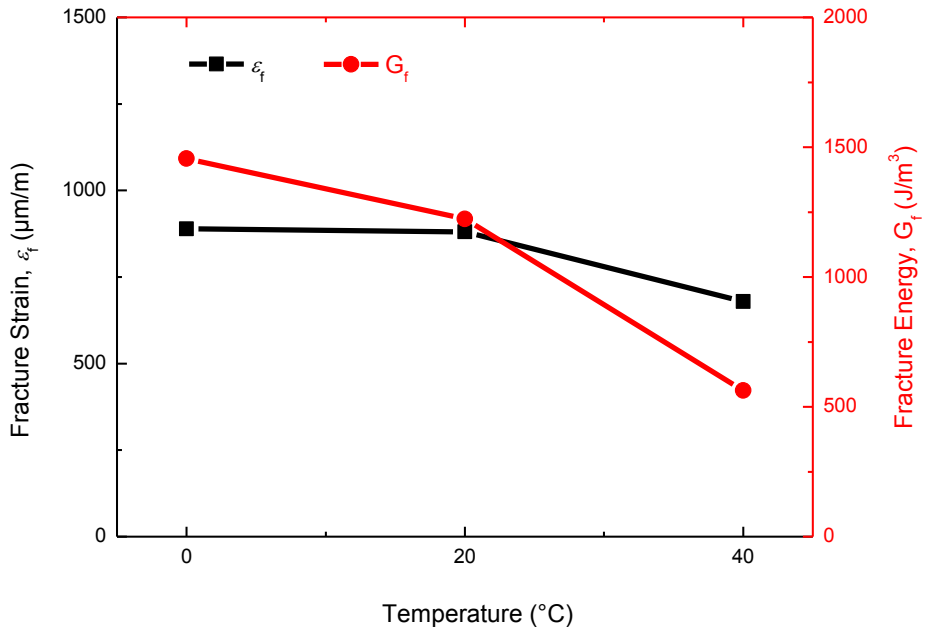

(b)

Fig 6.10 Bending properties of CAM-I at intermediate temperatures (a) strength and modulus; (b) failure strain and failure energy

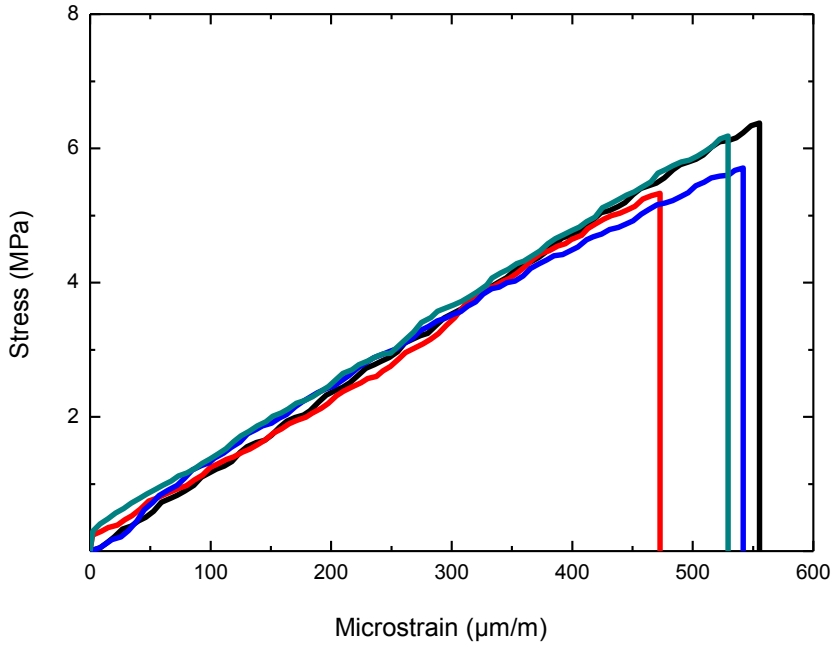

(a)

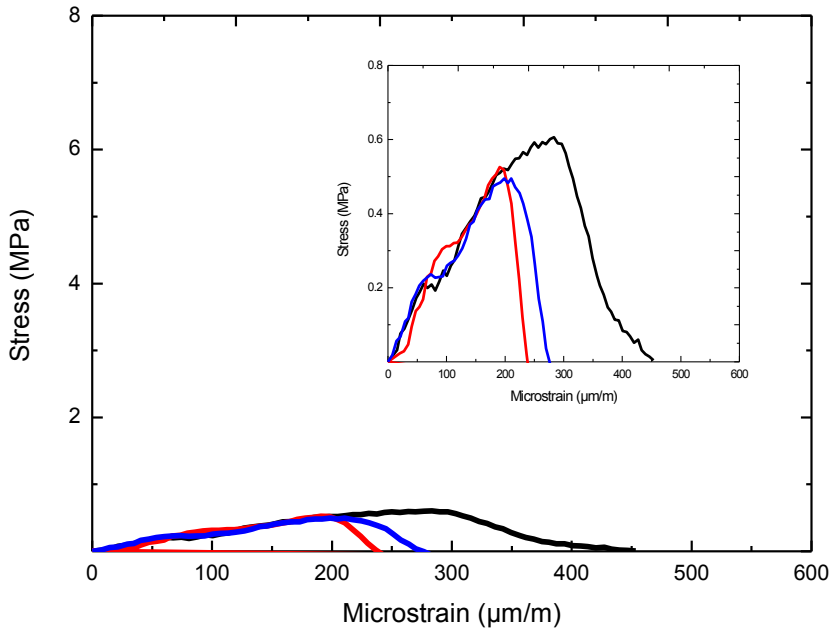

(b)

Fig 6.11 Stress-strain curves of CAM-I at (a) -20 °C and (b) 60 °C

6.3.4.2 Influence of intermediate temperature on 4PB fatigue

Controlled-strain 4PB tests of CAM-I were conducted under the temperature of 0 °C and 40 °C, to obtain ε-N curves at low and high temperatures (0 °C and 40 °C) in comparison to room temperature. Because the fracture strain was improved at 0 °C, three higher tensile strain levels, 400 μm/m, 450 μm/m and 500 μm/m, were designed for fatigue of CAM-I; in contrast, three lower tensile strain levels, 200 μm/m, 300 μm/m and 400 μm/m, were designed for fatigue tests at 40 °C.

ε-N curves of CAM-I were plotted in **Fig 6.12** under the temperature of 0 °C 20 °C and 40 °C. From the positions of the curves, it was more than evident that low temperature was beneficial to fatigue life whereas higher temperature was detrimental to the fatigue life, refuting a contradicting viewpoint in literature on temperature effect of CAM-I (Wang and Liu, 2008), as well discussed in **Section 2.5.2** of **Chapter 2**. Three basic material constants of CAM-I, k_1, k_2 and strain amplitude to 1 million cycles, ε_6, were calculated and listed in **Table 6.3**. The values of k_1 and k_2, within intermediate temperatures, decreased as the test temperature fell to 0 °C. But the ε_6 value at 0 °C was almost the same compared with that at room temperature. And at 40 °C, this value started to be decreased to some extent. This variation of the ε_6 value with temperature, interestingly, was found to be similar to that of one of bending parameters, the fracture strain. A further comparison was made between those two strain parameters versus temperature in **Fig 6.13**. It was very clearly indicated that those two strain parameters of CAM-I, ε_6 and ε_f, followed the similar trend with temperature, and most possibly suggested that there might exist an intrinsic relationship between them. It was also implied that the strain parameter for fatigue, ε_6, might be only dependent on the fracture strain, ε_f, rather than bending strength or modulus. Of course, this interesting finding demanded more data to support it, and more research work was needed in the future.

Table 6.4 Main coefficients from *ε*-N curves under different intermediate temperatures

Tem.	k_1	k_2	R^2	ε_6
0 °C	2.23×10^{18}	5.44	68.97 %	187 μm/m
20 °C	1.96×10^{23}	7.60	95.43 %	188 μm/m
40 °C	2.57×10^{41}	15.93	97.23 %	167 μm/m

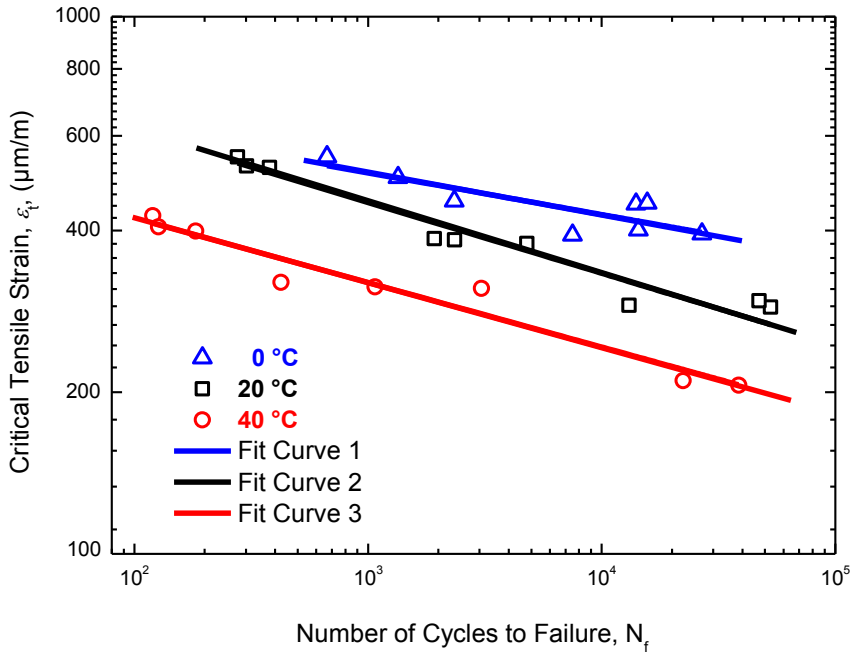

Fig 6.12 *ε*-N curves of CAM-I under different temperatures

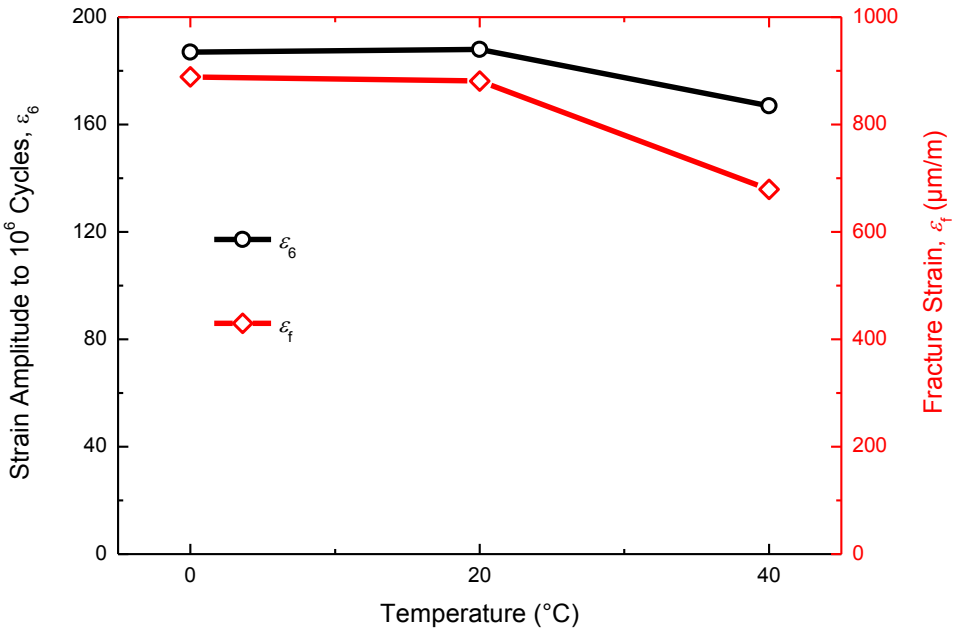

Fig 6.13 Comparison between two strain parameters under intermediate temperatures of 0 °C, 20 °C and 40 °C

6.3.5 Summary

In the first section, controlled-strain 4PB fatigue tests of CAM-I were firstly performed, with the aim to understand the fatigue cracking of the CAM layer in CRTS I. Conclusions could be drawn as follows.

1. Using similar test method, the analysis method of test results and main controlling variables to asphalt mixtures, controlled-strain 4PB fatigue tests of CAM-I were found to be rational and reliable.
2. It was better to use the real tensile strain value applied on CAM-I when 4PB fatigue testing was stable and a modified ER-based fatigue failure criterion to define failure.
3. The strain amplitude corresponding to 1 million loading cycles to failure of CAM-I, ε_6, was calculated to be 188 μm/m, and this value was comparable to those of asphalt mixtures (150 ~ 200 μm/m) used in European countries with the same test methods (4PB).
4. Influence of temperature on bending strength, modulus, fracture strain and fracture energy of CAM-I was significant and therefore choosing appropriate temperature range for fatigue of CAM-I was essential, and its temperature spectrum as tested by the DMA method in **Chapter 5** provided a good reference.
5. The low temperature was beneficial to the fatigue life of CAM-I whereas higher temperature was detrimental to its fatigue life.
6. It was interesting to find and imply that the ε_6 value of CAM-I might be only dependent on fracture strain, amongst static bending parameters tested under standard conditions.

6.4 Controlled-stress 4PB Fatigue of CAM-II

Fatigue properties and behaviour of CAM-II was tested in controlled-stress 4PB tests in the laboratory. Likewise, a trial fatigue test was conducted on a CAM-II beam firstly. With the same test method but a different mode of loading for CAM-I, fatigue tests of CAM-II were conducted under different normalised stress levels and the classical S-N curve could be obtained. The influence of stress ratio, *R*, including the reversal effect, and influence of temperature on fatigue of CAM-II would be studied.

6.4.1 Fatigue failure

In the trial fatigue test of CAM-II, a maximum tensile stress, σ_a = 4 MPa, with the consideration of its ultimate bending strength (5.66 MPa) from static bending tests in **Chapter 4**, was designed and the *R* value was set to be 0.1 as in the common case of fatigue testing on plain concretes. Obviously, such 4PB fatigue test was conducted in a typically tension-tension mode.

The first 10 loading cycles of the trial fatigue test on CAM-II were plotted in **Fig 6. 14**. It seemed that the maximum force, S_{max}, and the minimum force, S_{min}, as designed, could be not achieved immediately, but after a few, even hundreds of, loading cycles of fatigue loading. That was why, as can be seen from **Fig 6.14**, both amplitudes of force and deflection increased gradually with the running time at the beginning of fatigue. By using the **MATLAB 7.8.0**, a large number of repetitive calculations were conducted in a programming to convert all forces and deflections into tensile stresses and tensile strains, respectively, and then stress amplitude, σ_a, and strain amplitude, ε_a, could be obtained. **Fig 6.15** showed the evolution of stress amplitude and strain amplitude with loading cycles during fatigue testing of CAM-II. It was clearly demonstrated that, after about 350 loading cycles, both stress amplitude and strain amplitude reached a steady value almost at the same time. Despite this, it was unnecessary to revise the raw fatigue test data as in the data analysis of fatigue on CAM-I, because it would complicate the fatigue data processing. After this gradual change, they could be maintained at a relatively stable value throughout most of the running

time. In fatigue testing of concrete like materials, by the way, it was the maximum tensile stress, σ_{max}, that was more concerned. Its value, as discussed in **Section 3.6.4.2** of **Chapter 3**, could be calculated based on **Equation (6-8)** and **Equation (6-9)** below. In a similar way**,** the maximum tensile strain, ε_{max}, could be calculated as well. More than evident, the relationship between σ_{max} and σ_a, or ε_{max} and ε_a, was linear.

$$\sigma_{max} - \sigma_{min} = \Delta\sigma = 2\sigma_a \tag{6-8}$$

$$\sigma_a = \frac{1-R}{2}\sigma_{max} \tag{6-9}$$

$$\varepsilon_a = \frac{1-R}{2}\varepsilon_{max} \tag{6-10}$$

Close to failure, however, the values of stress amplitude and strain amplitude suddenly fell to zero after experiencing a very short period of decreasing as shown in **Fig 6.15**. This point could be defined as complete failure, as in the classical fatigue failure criterion for cement-based materials like concretes. And this type of failure was usually referred to as catastrophically, which would pose a great danger to structures. In additional to the classical fatigue failure criterion used in the controlled-stress mode, there are some other fatigue failure criteria for concrete materials, such as some based on strain (Tepfers, 1979, Saito, 1983, Cornelissen, 1984, Do et al., 1993), or strain rate (Sparks and Menzies, 1973, Do et al., 1993). But compared to the classical one, they were more complex to apply. Unlike asphalt mixtures, in fact, there are not so many fatigue failure criteria available for controlled-stress fatigue tests of cement-based materials. Therefore, the modified ER-based fatigue failure criterion used for CAM-I was tried on CAM-II. **Fig 6.16** or **Table 6.5** gave the number of cycles to failure based on this criterion. It was interesting to find this number equivalent to that from the classical one, which indicated that this fatigue failure criterion is independent of mode of loading. Whatsoever, the classical fatigue failure criterion was thought to be more convenient to use because no calculation was involved. Real maximum tensile stress was also listed in this table as well, 3.98 MPa, slightly less than the designed one, 4 MPa.

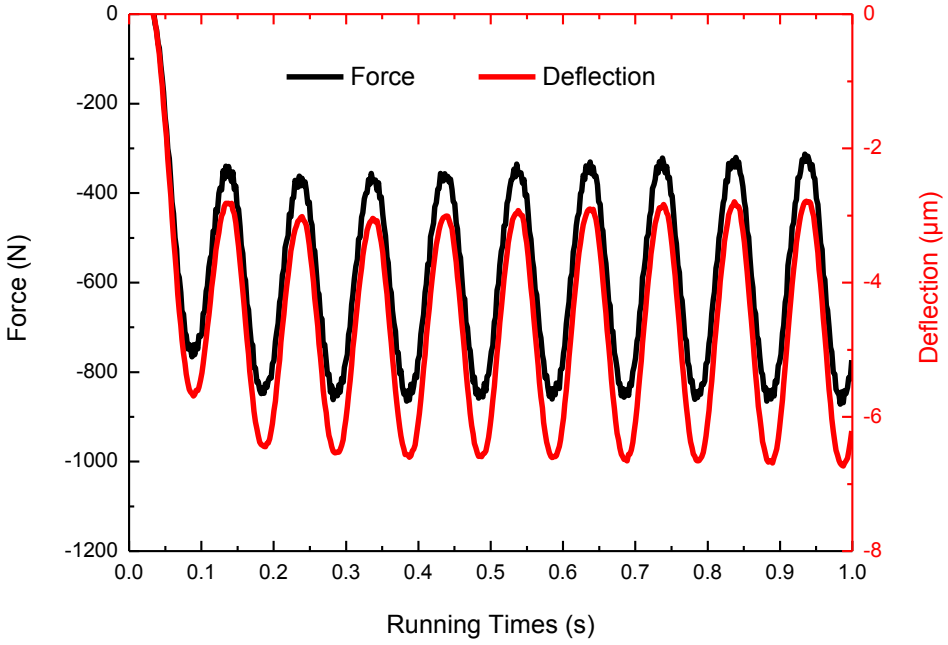

Fig 6.14 The first 10 cycles of a trial fatigue test of CAM-II

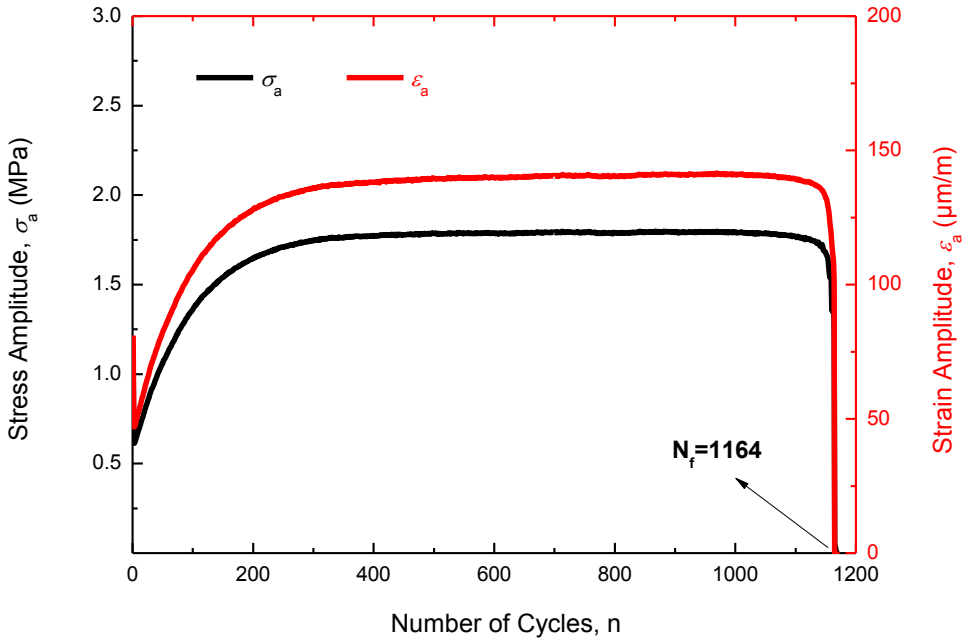

Fig 6.15 Evolution of stress amplitude and strain amplitude with loading cycles during fatigue testing of CAM-II

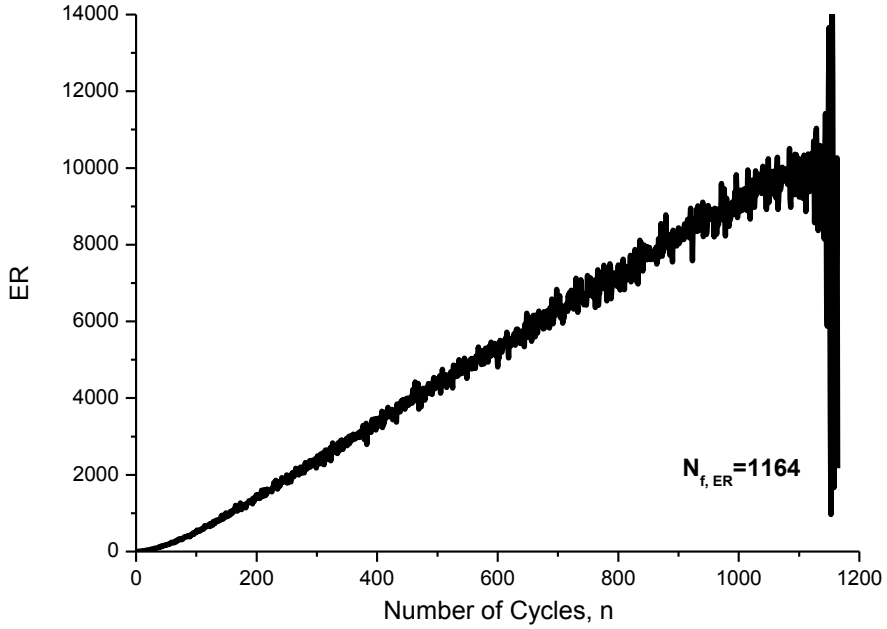

Fig 6.16 Number of cycles to failure using the modified ER-based fatigue failure criterion used for CAM-I, $N_{f, ER}$

Table 6.5 Results from the trial fatigue test

Maximum Stress, σ_{max}	***R***	**Number of Cycles to Failure**	
3.98 MPa (σ_a = 1.79MPa)	0.1	N_f = 1164	$N_{f, ER}$ = 1164

6.4.2 S-N curve

A typical S-N curve of cement-based materials, as discussed in **Section 2.5.4.3** of **Chapter 2**, was plotted in a semi-logarithmic mode. Like concrete materials, normalised stress level, S, used for CAM-II would be defined as the ratio of the maximum bending stress applied, σ_{max}, to the ultimate bending strength, σ_{max}, as shown in **Equation (6-11)**. From the preceding section, we knew that the maximum bending stress could be unstable at the beginning of fatigue loading but reached a steady value after a number of loading cycles. This steady value would be used as σ_{max}. The number of cycles to failure, N_f, could be defined using the classical fatigue failure criteria. In this way, the S-N curve of CAM-II could be obtained.

$$S = \frac{\sigma_{\max}}{\sigma_b} \tag{6-11}$$

Fig 6.17 showed the typical *S*-N curve of CAM-II at room temperature. The number of cycles to failure, obviously, decreased with the increase of the normalised stress level, *S*. But when *S* was higher than 0.8, the scatteredness of the fatigue test data was relatively higher. In future fatigue tests, by the way, it was suggested that a normalised stress level less than 0.8 should be used to get more reliable data. Although a small number of beam specimens (≥3) were used for each stress level in this work, a fairly good linear relationship could be obtained. To understand its fatigue strength or limit, the normalised stress level extrapolated at one million loading cycles to failure ($N_f = 10^6$), S_6, which was consistent with the method to get the ε_6 value of CAM-I in the preceding **Section 6.3.3**, could be calculated as in **Equation (6-12)** and then fatigue strength, σ_6, could be obtained by using **Equation (6-13)**. Their values were listed in **Table 6.6**, together with the two fitting coefficients to the fatigue test data, α and β.

The S_6 value for CAM-II, as tested at 20 °C in this thesis, was 0.396 and the fatigue strength was 2.24 MPa.

$$S_6 = \alpha - 6\beta \tag{6-12}$$

$$\sigma_6 = (\alpha - 6\beta)\sigma_b \tag{6-13}$$

To know what this S_6 value represents for fatigue of CAM-II, we calculated the same S_6 values according to three classical refined S-N curves or fatigue models of plain concretes based on literature (Aas-Jakobsen, 1970, Hsu, 1981, Zhang et al., 1996) and compared them with the S_6 value of CAM-II as shown in **Table 6.7**. It was interesting to find that the S_6 value of CAM-II was much lower than those of plain concretes. This fact indicated that, with the inclusion of asphalt binder, the fatigue strength of CAM-II was greatly reduced. It is also noted that, for plain concretes, the S_6 value from the refined S-N curves by Hsu (1981) was the lowest, about 0.5, which implied that using such a fatigue model to describe fatigue properties of plain concretes possibly produced conservative results in the end.

Table 6.6 Main coefficients from the *S*-N curve of CAM-II (*R* = 0.1)

Tem.	α	β	R^2	S_6	σ_6
20 °C	1.119	0.121	91.35 %	0. 396	2.24 MPa

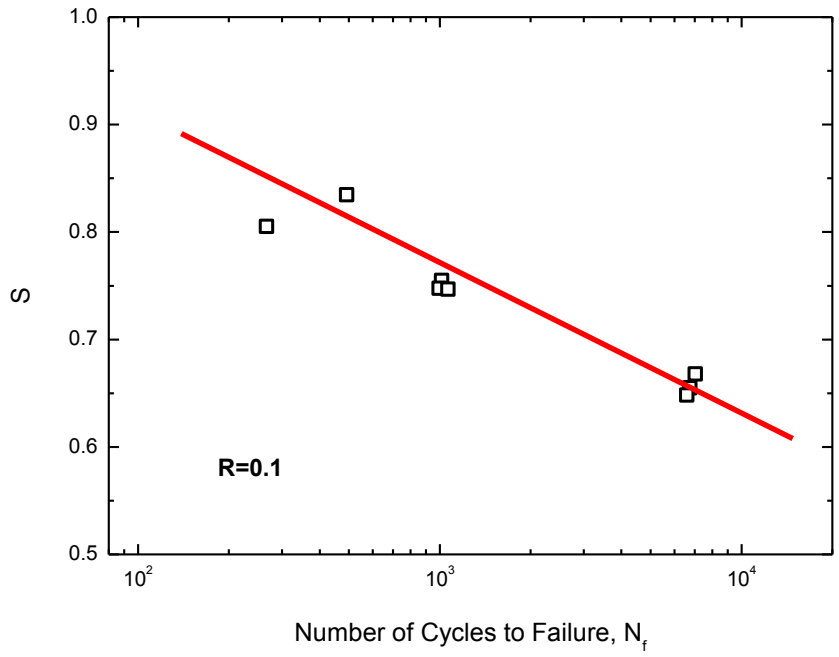

Fig 6.17 The *S*-N curve of CAM-II at room temperature (*R* = 0.1)

Table 6.7 Comparison of S6 values for CAM-II and plain concretes

Material	**S_6**	**Reference**
CAM-II	0.396	In this thesis
Plain concretes	0.630	**Equation (2-16)** (Tepfers and Kutti, 1979)
	0.627	**Equation (2-16)** (Oh, 1986)
	0.495	**Equation (2-18)** (Hsu, 1981)
	0.674	**Equation (2-19)** (Zhang et al., 1996)

6.4.3 Influence of *R*

For flexural fatigue, as well discussed in **Section 2.5.4.4** and **Section 2.5.4.5** of **Chapter 2**, stress ratio, *R*, has a definite influence on fatigue properties of plain concretes. When $R \geq 0$, the number of cycles to failure, or fatigue life, will increase as *R* increases; if a reversal stress is considered ($R < 0$), it will reduce the fatigue life, but not such significant as in the case of $R \geq 0$.

To understand the influence of *R* on the fatigue properties of CAM-II, two different *R* values were considered. One is 0.2 ($R \geq 0$), which was usually used in fatigue tests of plain concretes (Hop, 1968, Tepfers, 1979, Tepfers and Kutti, 1979, Shi et al., 1993, Zhang et al., 1996, Zhang and Wu, 1997). The other one is -1 chosen from $R < 0$, where a completely reversal stress would be applied on CAM-II. Then the two S-N curves with $R = 0.2$ and $R = -1$ were tested at room temperature, as shown in **Fig 6.18**. For comparison, *S*-N curves with three different *R* values, -1, 0.1 and 0.2, were plotted in one diagram (**Fig 6.19**) and main coefficients fitted from the *S*-N curves, especially fatigue strength, were listed in **Table 6.8**. In the case of $R = 0.2$, the fatigue life of CAM-II was slightly improved, if compared to that from routine 4PB fatigue tests of CAM-II ($R = 0.1$). But the fatigue strength was maintained at almost the same level, even slightly lower. Different from plain concretes, however, the fatigue life of CAM-II was significantly reduced due to the reversal stress ($R = -1$), which could be clearly demonstrated in **Fig.6.19** and in terms of the S_6 value (**Table 6.8**). And the slope of the S-N curve (the β value) with $R = 0.2$ or $R = -1$ was larger than that with $R = 0.1$. Different from plain concretes, obviously, the reversal stress had a significant impact on the fatigue life of CAM-II, which could not be ignored.

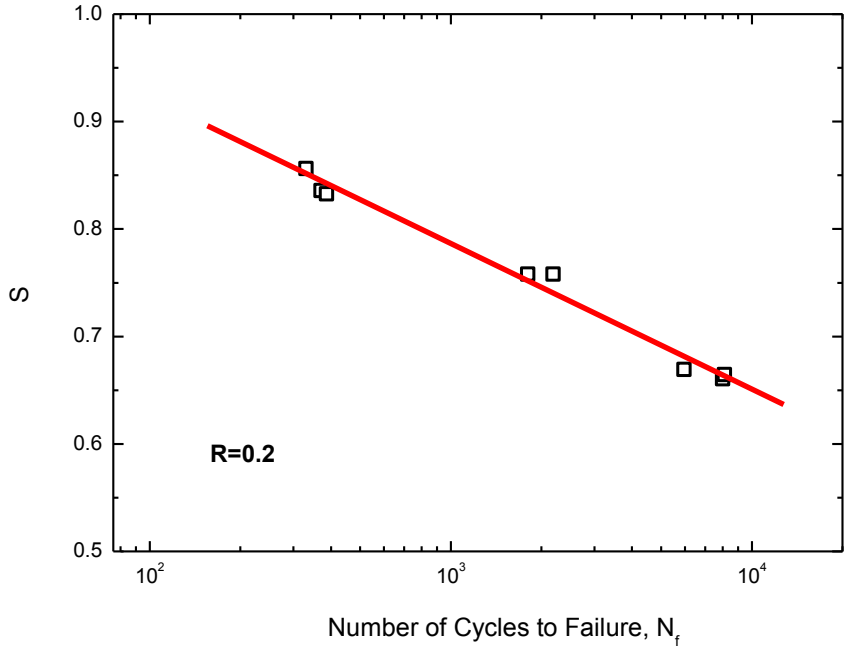

(a)

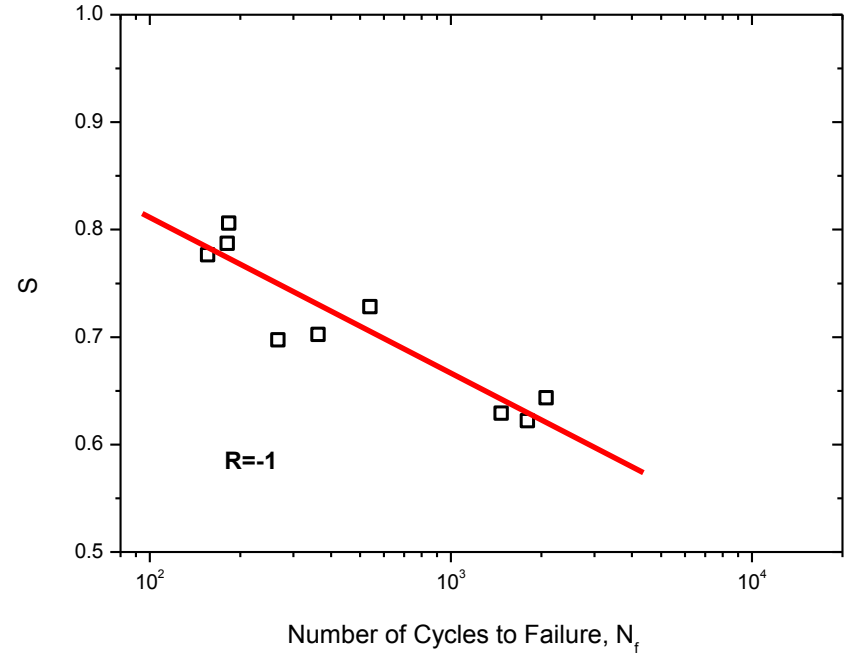

(b)

Fig 6.18 The *S*-N curves of CAM-II at room temperature with (a) *R* = 0.2 and (b) *R* = -1

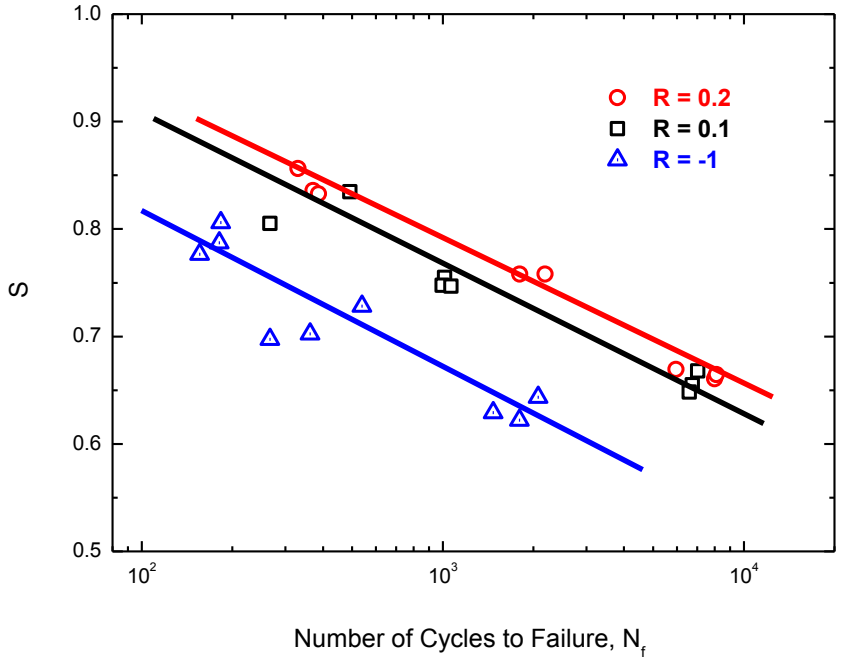

Fig 6.19 Influence of *R* on *S*-N curves

Table 6.8 Main coefficients from the *S*-N curves of CAM-II with different *R* values

Tem.	*R*	*α*	*β*	R^2	S_6	σ_6
20 °C	0.2	1.189	0.134	98.25 %	0.382	2.16 MPa
20 °C	0.1	1.119	0.121	91.35 %	0.396	2.24 MPa
20 °C	-1	1.090	0.141	81.36 %	0.242	1.37 MPa

6.4.4 Influence of temperature

Static 4PB tests of CAM-II were performed firstly under a wide temperature range from -20 °C to 60 °C, to obtain basic bending parameters at different temperatures. On the basis of these parameters, flexural fatigue properties of CAM-II under different temperatures were measured using controlled-stress 4PB fatigue tests, to understand the temperature effect on its fatigue.

6.4.4.1 Bending properties at different temperatures

Fig 6.20 showed the stress-strain curves of CAM-II under low, normal and high temperatures. Under low temperatures, the bending strength and modulus of CAM-II were enhanced and the failure mode remained brittle. In comparison, under high temperatures, its strength was greatly lowered but its modulus seemed unchangeable, and CAM-II started to fail from typically brittle to ductile mode.

Four bending parameters under the temperature of -20 °C, 0 °C, 20 °C, 40 °C and 60 °C obtained from static 4PB tests of CAM-II were plotted in **Fig 6.21** and summarised in **Table 6.9**. As temperature increased, bending strength and modulus of CAM-II were reduced. The decreasing trend for strength and modulus with temperature, however, was different but more than evident not linear as reported (Qiu et al., 2013b). An S-shaped decreasing trend of bending strength was observed, but under higher temperatures (40 °C and 60 °C), bending modulus remained almost the same value with that at room temperature. Obviously, the influence of test temperature on bending strength and modulus of CAM-II was more significant than on its compressive strength and modulus, as compared from **Fig 2.19** in the review chapter. Regarding fracture strain and fracture energy which was used to characterise the deformability and fracture capacity of CAMs as defined in **Chapter 4**, those two mechanical parameters would increase with the decrease of temperature, until peak values appeared at 0 °C.

To sum up, unlike plain concretes as discussed in **Section 2.5.4.6** of **Chapter 2**, the influence of temperature on static bending properties of CAM-II was significant because of the incorporation of asphalt binder.

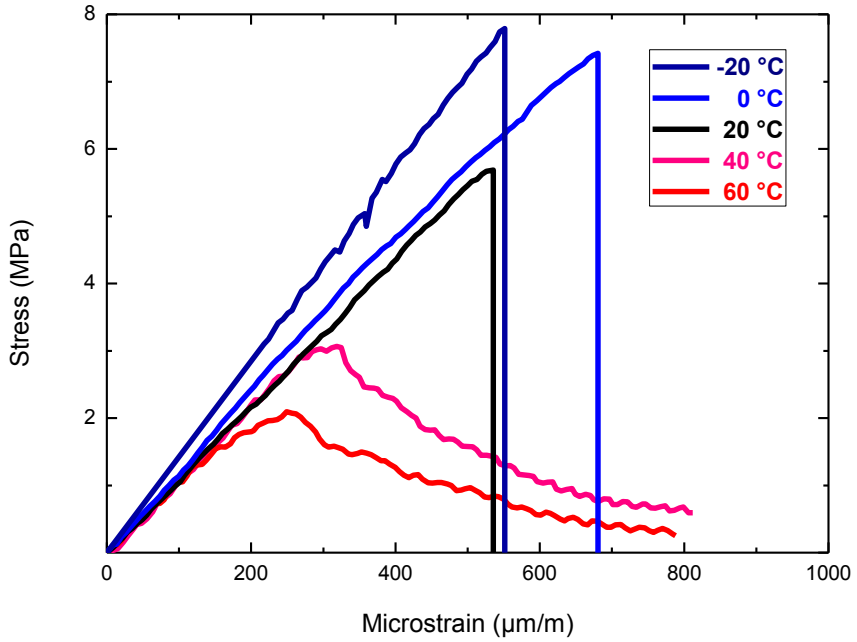

Fig 6.20 Stress-strain curves of CAM-II under different temperatures

Table 6.9 Bending parameters of CAM-II at different temperatures

Tem. (°C)	σ_b (MPa)	E_b (GPa)	ε_f (μm/m)	G_f (J/m^3)
-20	7.63	15.41	503	2192.50
0	7.29	12.60	616	2370.22
20	5.66	10.59	539	1489.36
40	3.06	10.17	308	518.57
60	2.13	10.09	269	338.14

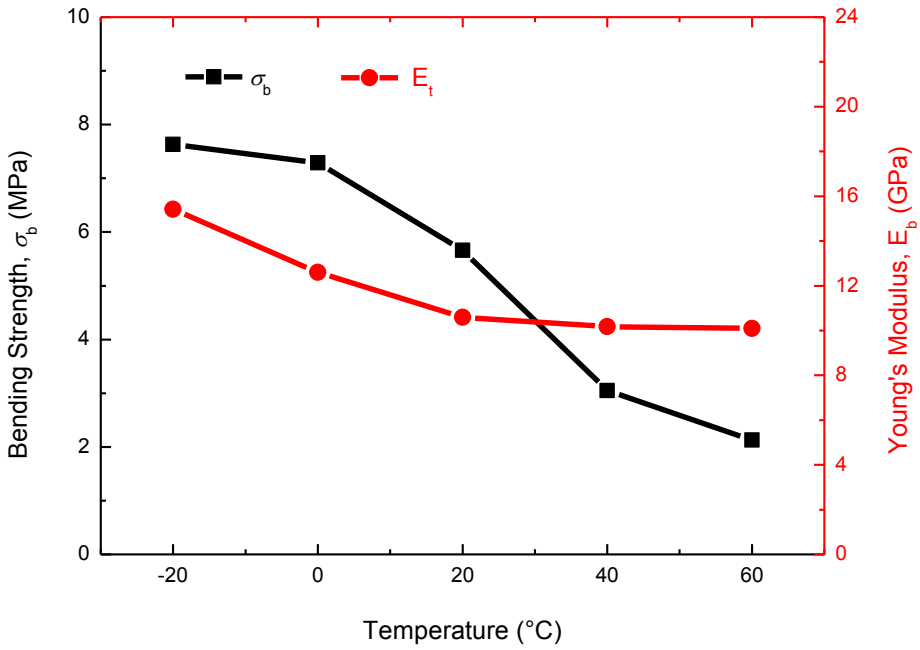

(a)

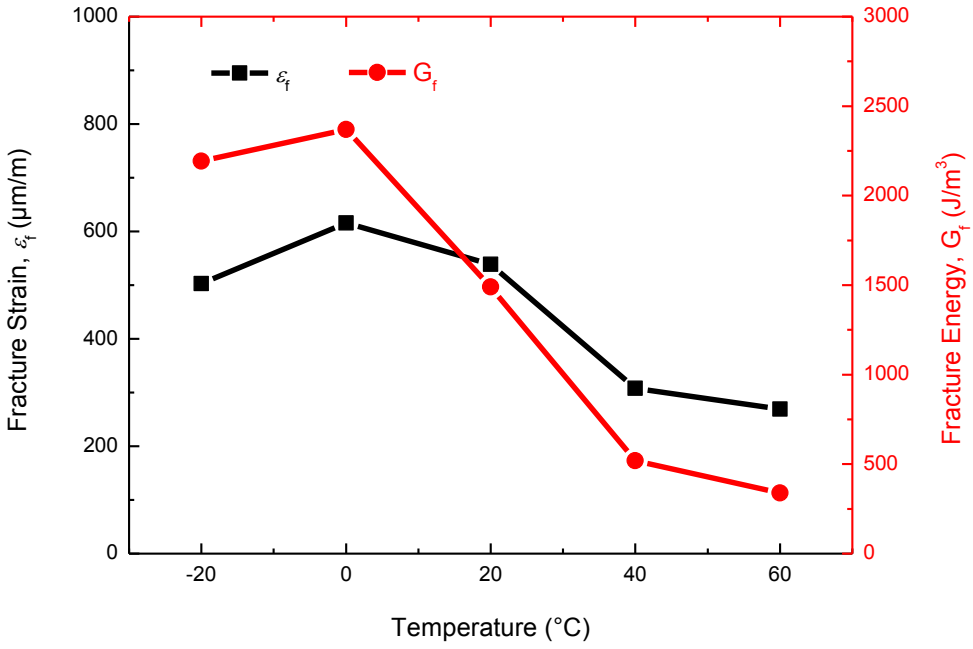

(b)

Fig 6.21 Bending properties of CAM-II under different temperatures (a) strength and modulus; (b) failure strain and failure energy

6.4.4.2 Influence of temperature on 4PB fatigue

For plain concretes, as discussed in **Section 2.5.4.6** in the review chapter, the influence of temperature on fatigue is insignificant and negligible under normal service temperatures, implying that plain concretes share the same S-N curve within that normal temperature range. That is partly because the compressive strength changes slightly with test temperature. However, as just reported in the preceding section, the test temperature had a significant impact on the bending strength of CAM-II (**Fig 6.20 (a)**). From -20 °C to 60 °C, the bending strength was lowered from 7.63 MPa to 2.13 MPa, which was a huge change. And it seemed that, furthermore, CAM-II turned from a brittle material to a ductile one under high temperatures (40 °C and 60 °C), whereas under low temperatures of 0 °C and -20 °C, it remained brittle. Therefore, it was better to study the temperature effect of CAM-II on fatigue separately, under high temperatures or under low temperatures.

Under high temperatures, during fatigue testing of CAM-II, it was found that some test processes were unstable and abnormal phenomena happened for high stress levels designed. **Fig 6.22** showed the abnormality under the temperature of 40 °C and 60 °C. When the designed stress level was 0.8, the real stress level applied on CAM-II rose to a value much lower than the designed one and the beam specimen failed all of a sudden. The abnormality described indicated that, probably because the viscoelastic effect of CAM-II was more pronounced under high temperatures, the coupling effect of creep and fatigue manifested in the fatigue process with the rise of temperature and stress level, and greatly accelerated the failure, and that the fatigue tests in the tension-tension mode were questionable at high temperatures. Except for those abnormal points, the remaining fatigue data were plotted in the S-N curves under high temperatures (**Fig 6.23**) and main coefficients could be obtained in **Table 6.10**. Obviously, as the temperature increased, the fatigue life of CAM-II was generally reduced, although the scatteredness of fatigue test data at 60 °C was so huge (R^2 = 21.76%). This indicated that, when service temperature was higher than the softening point of the asphalt binder ($T_{R\&B}$ = 48 °C), it was much detrimental to the fatigue life of CAM-II.

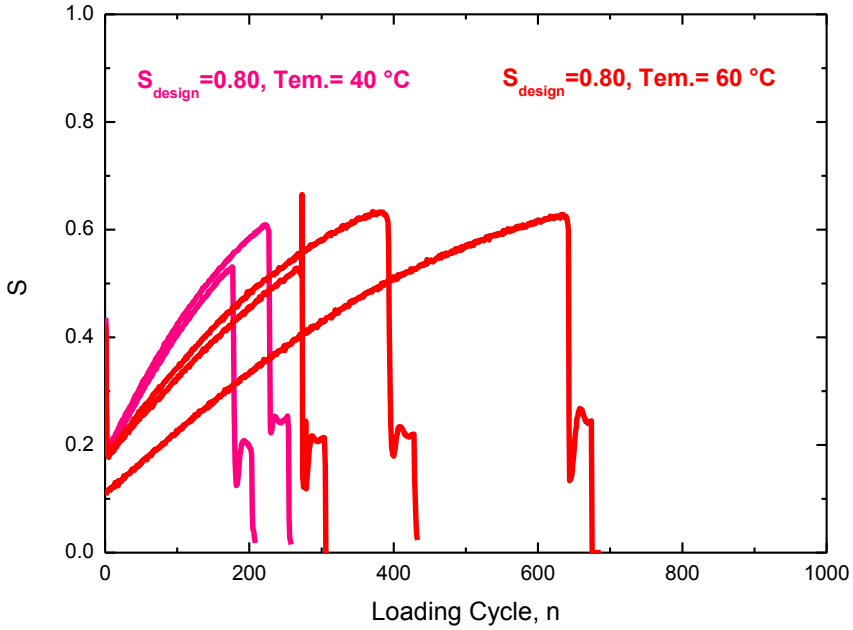

Fig 6.22 The abnormality during fatigue testing under high temperatures

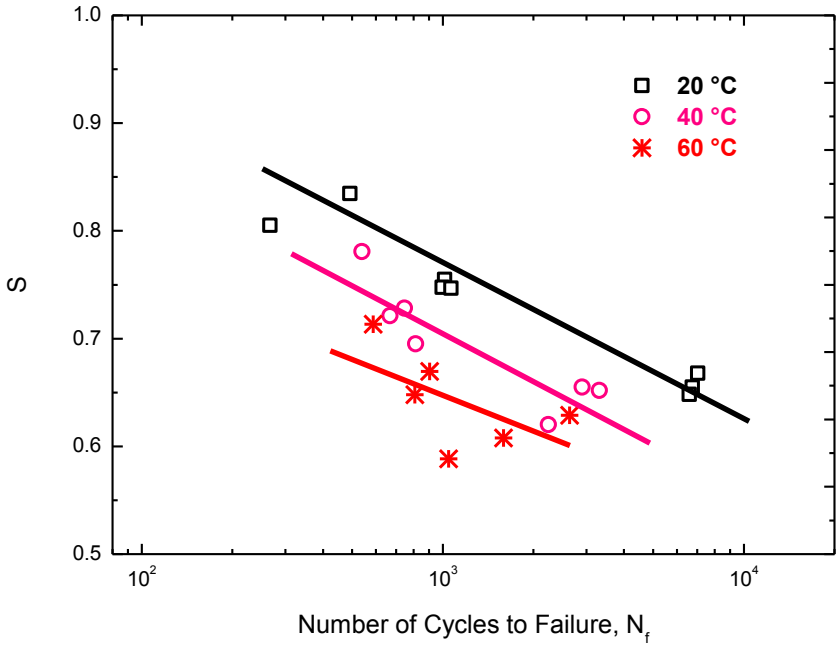

Fig 6.23 The *S*-N curves of CAM-II under high temperatures

Table 6.10 Main coefficients from the *S*-N curves of CAM-II at the high temperature of 40 °C or 60 °C

Tem.	*R*	*α*	*β*	R^2	S_6	σ_6
60 °C	0.1	1.003	0.118	21.76 %	0.269	0.57 MPa
40 °C	0.1	1.145	0.146	72.22 %	0.293	0.90 MPa
20 °C	0.1	1.189	0.134	98.25 %	0.382	2.16 MPa

Under low temperatures, on the other hand, the *S*-N curves of CAM-II were shown in **Fig 6.24**. It was found that, compared with the fatigue life at room temperature, the fatigue life of CAM-II at 0 °C was slightly reduced. When test temperature fell to -20 °C around T_g of the asphalt binder, however, the fatigue life was enhanced significantly, which could be shown via the S_6 values listed in **Table 6.11**. Further, it was interesting to find that the S_6 value of CAM-II at -20 °C was comparable to that of plain concretes (Zhang et al., 1996). This fact showed that CAM-II was more like cement-based materials including plain concretes when temperature decreased to a value around T_g of the asphalt binder. Another fact was that, clearly, the fatigue strength of CAM-II at 0 °C was almost equivalent to that at room temperature. To further demonstrate this relationship, the S-N curves could be revised into the S_{max}-N curves, where S_{max} was calculated based on **Equation (6-14)**. From the S_{max}-N curves of CAM-II at the temperature of 0 °C and 20 °C (**Fig 6.25**), the two curves most possibly intersected at one million (10^6) loading cycles as schematically shown. From the S_{max}-N curves, it was obvious that the fatigue life at 0 °C of CAM-II was longer than that at room temperature, if the same stress, rather than normalised stress level, was applied.

$$S_{\max} = \sigma_{\max} = S\sigma_b \tag{6-14}$$

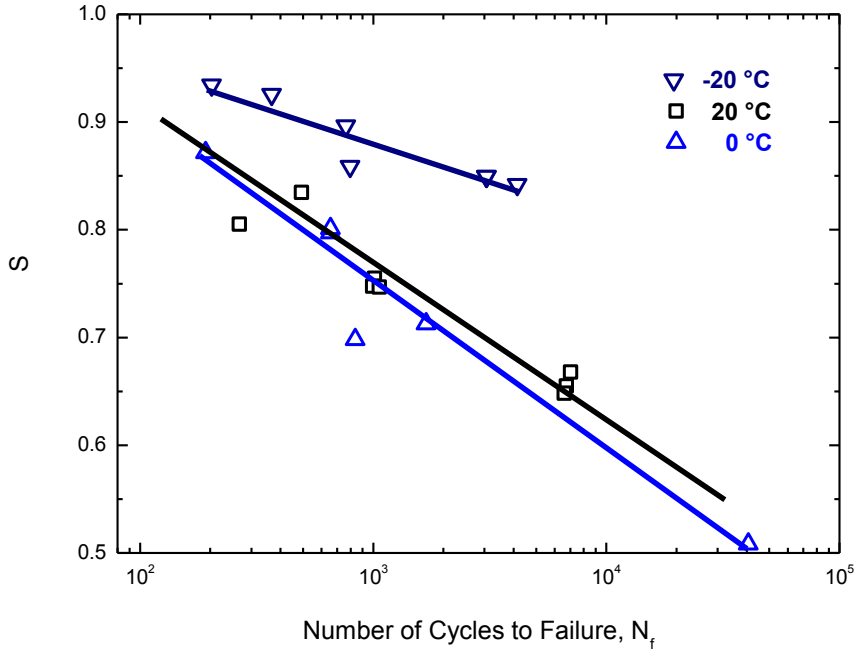

Fig 6.24 The *S*-N curves of CAM-II under low temperatures

Table 6.11 Main coefficients from the *S*-N curves of CAM-II at the low temperature of 0 °C or -20 °C

Tem.	*R*	*α*	*β*	R^2	S_6	σ_6
20 °C	0.1	1.189	0.134	98.25 %	0.382	2.16 MPa
0 °C	0.1	1.211	0.154	92.05 %	0.287	2.09 MPa
-20 °C	0.1	1.097	0.0718	84.89 %	0.667	4.86 MPa

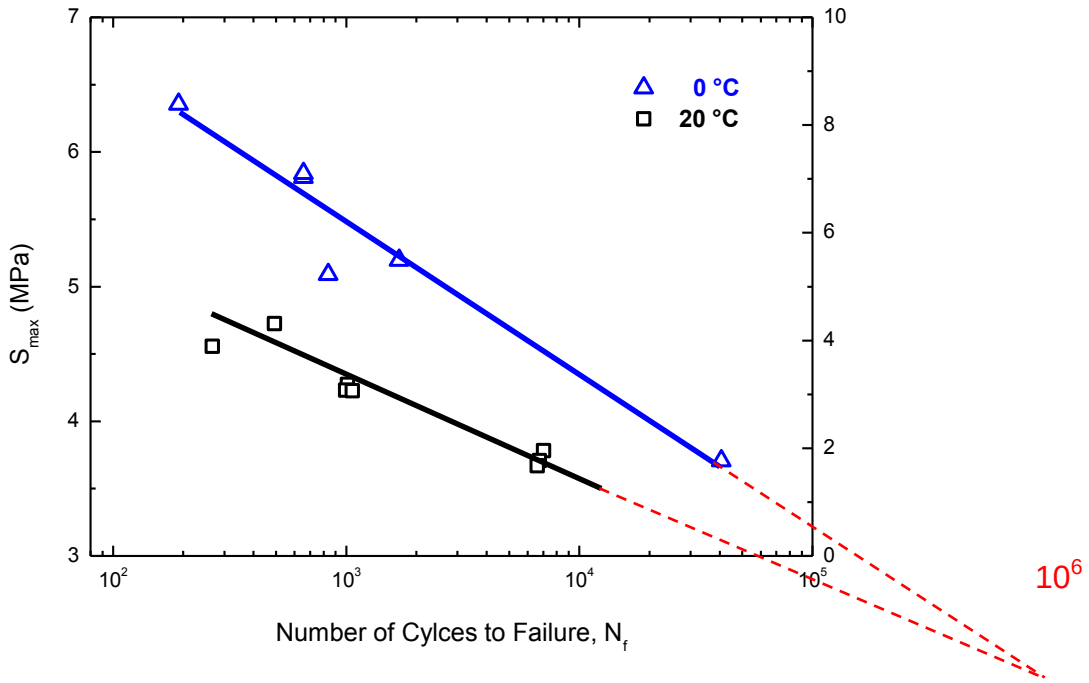

Fig 6.25 The S_{max}-N curve of CAM-II at 0 °C compared with that at 20 °C

6.4.5 Summary

This section dealt with the flexural fatigue of CAM-II through controlled-stress 4PB fatigue tests, and the influences of stress ratio, *R*, or test temperature were studied and discussed. Main conclusions could be made as follows.

1. Using the similar test method and analysis method of test results to plain concretes, controlled-strain 4PB fatigue tests of CAM-II were found to be reliable at room temperature.
2. The modified ER-based fatigue failure criterion used for CAM-I was found to be independent of mode of loading, although not used in CAM-II.
3. It was better to use the real maximum tensile stress applied on CAM-II beams when fully stable 4PB fatigue testing was achieved and the classical fatigue failure criterion used in the controlled-stress mode to define failure.
4. The normalised stress level corresponding to 1 million loading cycles to failure of CAM-II, S_6, was calculated to be 0.396, much lower than those from classical refined S-N curves for plain concretes in literature, indicating that the inclusion of asphalt binder into CAM-II reduced the fatigue strength.
5. Different from plain concretes, the reversal stress had a significant impact on the fatigue life of CAM-II, which could not be ignored.
6. Unlike plain concretes, the influence of temperature on static bending properties of CAM-II was significant because of the incorporation of asphalt binder.
7. Higher temperature would greatly reduce the fatigue life of CAM-II, and this temperature should not be higher than $T_{R\&B}$ of the asphalt binder used in CAM-II.
8. Much longer fatigue life of CAM-II was observed if the same stress, instead of normalised stress level, was applied under low temperatures, and CAM-II was more like plain concretes when the temperature fell to around T_g of the asphalt binder.

6.5 A discussion on fatigue test schemes

Different fatigue test schemes, including fatigue test method, mode of loading, analysis method of test results and main controlling variables, were critically reviewed for asphalt mixtures or cement-based materials like plain concrete, respectively, in **Section 2.5.3** and **Section 2.5.4** of **Chapter 2**.

It was recognised that choosing an appropriate fatigue test method in the laboratory for a material was primarily dependent on the type of the material and the state of loads or deformation in a specific component or structure where the material was applied. On the one hand, different test method should be chosen for different types of materials. But if the material property changed with temperature, for one type of materials, it was inappropriate to use the same test method but necessary to convert to another one under that temperature. That is why controlled-strain fatigue tests of asphalt mixtures were conducted just under intermediate temperatures, not under extremely high or low ones. On the other hand, different test methods would be used for the same material if it was used in different applications. For plain concretes used in pavements, for instance, the 4PB test method might be commonly used, but for concretes used in buildings or dams, it was better to use the conventional compression test method. As to the mode of loading, it mainly depended on the material to be tested, but also needed to consider the state of loads or deformation in the structure. Both two modes of loading were used in fatigue of asphalt mixtures, for instance, because loads or deformation in asphalt pavements changed with the thickness of the layer (Pell, 1973). For cement-based materials including plain concretes, on the contrary, only the controlled-stress mode was used most possibly because of their specific material properties. Of course, in some test methods like IDT, only the controlled-stress mode could be used because of the characteristics of the test method itself. On the basis of fatigue test method and mode of loading as just discussed, the analysis method of test results and main test variables to be considered, accordingly, would be adjusted during fatigue testing as required.

Harbouring such basic knowledge and the research question in this work, the author of this thesis tried to use the 4PB test method but with different modes of loading into fatigue tests of CAM-I and CAM-II, in order to define the fatigue properties of different CAMs in the laboratory. The similar analysis method of test results and main test variables following those of asphalt mixtures and cement-based materials, respectively, since CAM-I and CAM-II were close to those two extreme materials. Results indicated that the fatigue test scheme of asphalt mixtures was perfectly used in CAM-I, except for a different but better fatigue failure criterion used. The fatigue strain parameter, ε_6, was slightly higher than those of asphalt mixtures, an indication of a longer fatigue life. And the influence of temperature was clear and definite. However, on the contrary, the fatigue test scheme of cement-based materials might not an ideal one for CAM-II, especially when the influence of R or temperature was separately considered. Due to the incorporation of asphalt binder, the reversal stress greatly reduced the fatigue life of CAM-II, which was different from cement-based materials. At higher temperatures, CAM-II turned from a brittle or quasi-brittle material at room temperature into a ductile one, making the reliability of this fatigue test scheme lowered and resulting in the instability of the fatigue testing and test results.

After such a discussion, a simple but significant conclusion could be reached here that, in terms of the fatigue behaviour, the CAM-I can be considered as a cement-modified asphalt mortar, one of asphalt mixtures, whilst the CAM-II as an asphalt-modified cement mortar but different from cement-based materials.

6.6 Chapter summary

In the most important chapter, flexural fatigue properties of CAM-I and CAM-II were measured in the laboratory using the same test method, 4PB, but under different mode of loading, either controlled-strain or controlled-stress. Similar analysis methods of test results and main controlling variables to asphalt mixtures and plain concrete were used for CAM-I and CAM-II, respectively. Reliable fatigue test results could be obtained as a consequence and some significant conclusions could be summarised as follows.

1. The fatigue test scheme of asphalt mixtures was perfectly used in CAM-I and the strain amplitude corresponding to 1 million loading cycles to failure, ε_6, was comparable to those of asphalt mixtures.
2. The low temperature was beneficial to the fatigue life of CAM-I whereas higher temperature was detrimental to its fatigue life.
3. It was interesting to find and imply that the ε_6 value of CAM-I might be only dependent on fracture strain, amongst static bending parameters tested under standard conditions.
4. The fatigue test scheme of cement-based materials might not an ideal one for CAM-II, especially when the influence of *R* or temperature was separately considered.
5. Different from plain concretes, the reversal stress had a significant impact on the fatigue life of CAM-II, which could not be ignored.
6. Unlike plain concretes, the influence of temperature on static bending properties and 4PB fatigue of CAM-II was significant because of the incorporation of asphalt binder.
7. T_g and $T_{R\&B}$ obtained from **Chapter 5** not only defined the intermediate temperature range for fatigue tests of CAM-I, but also the boundaries of service temperatures for CAM-I and CAM-II under traffic loads.
8. CAM-I was one of asphalt mixtures and although CAM-II was close to cement-based materials including plain concretes, it is a totally different one from cement-based materials.

CHAPTER 7 CONCLUSIONS AND RECOMMENDATIONS

The final chapter will summarise the conclusions firstly based on the results and discussion in **Chapter 4**, **5**, and **6** of the two typical CAMs, namely, CAM-I and CAM-II, used in CRTS I and CRTS II of China's HSR network, respectively, and then give some recommendations for further research work in the future.

7.1 Conclusions within this research

The overall aim of the research work in this thesis was to study the bending fatigue properties of the two typical CAMs, namely, CAM-I and CAM-II, where the influence of temperature was considered as an important factor. After a comprehensive literature review in **Chapter 2**, it was proposed to use different test protocols or schemes, the controlled-strain 4PB fatigue tests for CAM-I whilst the controlled-stress 4PB fatigue tests for CAM-II, because they are two totally different materials in terms of mechanical properties.

To achieve the overall aim and verify the hypothesis, a mini-4PB apparatus was developed, firstly to test the static bending properties of the two CAMs at room temperature, in order to obtain basic bending parameters as a reference for fatigue tests, and most importantly to test their 4PB fatigue properties, in order to verify the research hypothesis throughout this thesis. Moreover, to consider the temperature effects, the DAM tests were proposed to use for the two CAMs, in order to determine the most suitable test temperature range which would be used in fatigue tests. Through studying static, dynamic mechanical properties and above all bending fatigue properties of those two CAMs, namely, CAM-I and CAM-II, main conclusions could be summarised as follows.

1. It has been proved to be appropriate to use the newly-developed 4PB test method to characterise the static bending properties of those two CAMs in the laboratory, and more reliable results could be obtained, especially for measuring the modulus of elasticity, compared to the

compression test method; whatever the test method is used, CAM-I and CAM-II are found to be totally distinct in static mechanical properties at room temperature, which is the basis for the research hypothesis throughout this thesis; and the bending parameters obtained provided a good reference for fatigue tests.

2. Via the DMA method, the temperature spectra of dynamical modulus and loss factors of CAMs or CABs can be obtained, to characterise their temperature susceptibility and viscoelasticity, respectively, and a balance should be considered among them in the future design of new CAMs; the two characteristic temperatures of the asphalt binder, T_g implied to be around -20 °C and $T_{R\&B}$ measured to be 48 °C, could be determined from the temperature spectra of CAM-I, and those two not only define the viscoelastic zone for CAM-I, but also the most suitable temperature range to be used for fatigue tests of both CAM-I and CAM-II.

3. It has been verified that it is reasonable to use different fatigue test schemes for CAM-I and CAM-II, respectively, to characterise their 4PB fatigue properties; results indicated that in terms of the fatigue behaviour, CAM-I can be considered as a cement-modified asphalt mortar, one of asphalt mixtures, whilst CAM-II an asphalt-modified cement mortar.
4. The fatigue test scheme of asphalt mixtures was perfectly used in CAM-I and the strain amplitude corresponding to 1 million loading cycles to failure, ε_6 = 188 μm/m, was comparable to those of asphalt mixtures (150 ~ 200 μm/m); low temperature was beneficial to fatigue life of CAM-I whereas high temperature was detrimental to its fatigue life.
5. On the other hand, the fatigue test scheme of cement-based materials might not an ideal one for CAM-II, especially when the influence of the reversal stress, *R*, or the test temperature was separately considered; different from plain concretes, the reversal stress or the temperature has a significant impact on its 4PB fatigue.

7.2 Recommendations for future work

In the future research work, the first challenge is how to use those static and dynamic mechanical properties of two typical CAMs for their formulation design and quality evaluation, and furthermore to incorporate these test results from the laboratory into analysis, design and structural analysis of the two typical slab tracks with the CAM layer, i.e. CRTS I and CRTS II.

Regarding 4PB fatigue properties of CAM-I and CAM-II in this thesis where two different fatigue test schemes were for the first time used, some improvements or recommendations are needed.

1. Those two fatigue test schemes for CAM-I and CAM-II used in the laboratory were generally based on the phenomenological approach, and if necessary in the future, the mechanistic approach using fracture mechanics or damage mechanics would be applied to understand the mechanisms of fatigue, especially when it was found that the fatigue test scheme of cement-based materials might not an ideal one for CAM-II.
2. The influence of loading frequency or rest period in connection with healing on fatigue was ignored in this thesis, but in the future research work, these factors should be included.
3. Another form of fatigue, thermal fatigue, was mentioned to be possibly the mechanism of fatigue cracking as well, which was manifested itself under very high or low temperatures, and this type of fatigue would be the next topic of fatigue of CAMs in the future work.

REFERENCES

A, R., YAN, P. & WANG, Q. 2009. Research on the influencing factor of high strength cement asphalt mortar *Journal of Building Materials* 12**,** 519-522 (In Chinese).

AAS-JAKOBSEN, K. 1970. *Fatigue of concrete beams and columns,* Trondheim, Department of Concrete Structures, Norwegian Institute of Technology.

ABOJARADEH, M. 2013. Development of Fatigue Failure Criterion for Hot-Mix Asphalt Based on Dissipated Energy and Stiffness Ratio. *Jordan Journal of Civil Engineering,* 7**,** 54-69.

ADHIKARI, S., SHEN, S. & YOU, Z. 2009. Evaluation of fatigue models of hot-mix asphalt through laboratory testing. *Transportation Research Record: Journal of the Transportation Research Board,* 2127**,** 36-42.

ADHIKARI, S. & YOU, Z. 2010. Fatigue evaluation of asphalt pavement using beam fatigue apparatus. *The Technology Interface Journal,* 10.

AFRIDI, M., OHAMA, Y., IQBAL, M. Z. & DEMURA, K. 1995. Water retention and adhesion of powdered and aqueous polymer-modified mortars. *Cement and Concrete Composites,* 17**,** 113-118.

AGGARWAL, L., THAPLIYAL, P. & KARADE, S. 2007. Properties of polymer-modified mortars using epoxy and acrylic emulsions. *Construction and Building Materials,* 21**,** 379-383.

AI 1989. *The asphalt handbook* Lexington, US, Asphalt Institute.

AL-KHATEEB, G. & SHENOY, A. 2004. A distinctive fatigue failure criterion. *Journal of the Association of Asphalt Paving Technologists,* 73**,** 585-622.

AL-KHATEEB, G. & SHENOY, A. 2011. A Simple Quantitative Method for Identification of Failure due to Fatigue Damage. *International Journal of Damage Mechanics,* 20**,** 3-21.

ALIGIZAKI, K. K. 2005. *Pore structure of cement-based materials: testing, interpretation and requirements*, CRC Press.

ALLICHE, A. & FRANCOIS, D. 1986. Fatigue behavior of hardened cement paste. *Cement and Concrete Research,* 16**,** 199-206.

AMOS, P., BULLOCK, D. & SONDHI, J. 2010. High-speed rail: the fast track to economic development. Beijing, P. R. China: The World Bank.

ANDO, K., SUNAGA, M., AOKI, H. & HAGA, O. 2001. Development of slab tracks for Hokuriku Shinkansen line. *Quarterly Report of RTRI,* 42**,** 35-41.

ANTRIM, J. D. 1965. A study of the mechanism of fatigue in cement paste and plain concrete. Indiana, US: Purdue University.

ANTRIM, J. D. C. & MCLAUGHLIN, J. F. Fatigue study of air-entrained concrete. ACI Journal Proceedings, 1959. ACI.

ARDUIN, J.-P. 1994. Develoment and economic evalutioan of high speed in France. *Japan Railway & Transport Review***,** 26-31.

ARDUIN, J.-P. & NI, J. 2005. French TGV network development. *Japan Railway & Transport Review***,** 22-28.

ARTAMENDI, I. & KHALID, H. 2005. Characterization of fatigue damage for paving asphaltic materials. *Fatigue & fracture of engineering materials & structures,* 28**,** 1113-1118.

ASHTEYAT, A. M. & RAMADAN, K. Z. 2009. Utilization of white cement bypass dust as filler in asphalt concrete mixtures. *Canadian Journal of Civil Engineering,* 36**,** 191-195.

BARKSDALE, R. D. & MILLER, J. H. 1977. Development of equipment and techniques for evaluating fatigue and rutting characteristics of asphalt concrete mixes. Georgia Institute of Technology.

BASTIN, R. 2006. Development of German non-ballasted track forms. *Proceedings of the ICE, Transport,* 159**,** 25-39.

BEARDS, C. 1996. *Structural vibration: analysis and damping*, Butterworth-Heinemann.

BENNETT, E. & MUIR, S. S. J. 1967. Some fatigue tests of high-strength concrete in axial compression. *Magazine of concrete research,* 19**,** 113-117.

BENSTED, J. & BARNES, P. 2002. Structure and Performance of Cements. Second Edition ed. London: Spon Press.

BHASIN, A., CASTELO BRANCO, V. T., MASAD, E. & LITTLE, D. N. 2009. Quantitative comparison of energy methods to characterize fatigue in asphalt materials. *Journal of Materials in Civil Engineering,* 21**,** 83-92.

BHATTACHARJEE, S., SWAMY, A. & DANIEL, J. 2009. Application of elastic-viscoelastic correspondence principle to determine fatigue endurance limit of hot-mix asphalt. *Transportation Research Record: Journal of the Transportation Research Board***,** 12-18.

BIAN, X.-C., CHAO, C., JIN, W.-F. & CHEN, Y.-M. 2011. A 2.5 D finite element approach for predicting ground vibrations generated by vertical track irregularities. *Journal of Zhejiang University SCIENCE A,* 12**,** 885-894.

BOUDABBOUS, M., MILLIEN, A., PETIT, C. & NEJI, J. 2013a. Energy approach for the fatigue of thermoviscoelastic materials: application to asphalt materials in pavement surface layers. *International Journal of Fatigue,* 47**,** 308-318.

BOUDABBOUS, M., MILLIEN, A., PETIT, C. & NEJI, J. 2013b. Shear test to evaluate the fatigue of asphalt materials. *Road Materials and Pavement Design,* 14**,** 86-104.

BRITPAVE. *Why build slab track?* [Online]. Available: http://www.britpave.org.uk/RailWhyBuild.ink [Accessed 2nd November 2012].

BROUWERS, H. 2004. The work of Powers and Brownyard revisited: Part 1. *Cement and Concrete Research,* 34**,** 1697-1716.

BROUWERS, H. 2005. The work of Powers and Brownyard revisited: Part 2. *Cement and Concrete Research,* 35**,** 1922-1936.

BROUWERS, H. The work of Powers and Brownyard revisited: Part 3. Proceedings of 12th International Cogress on the Chemistry of Cement, 2007 Montreal, Canada.

BROUWERS, H. 2012. Paste models for hydrating calcium sulfates, using the approach by Powers and Brownyard. *Construction and Building Materials,* 36**,** 1044-1047.

BROWN, S. Practical test procedures for mechanical properties of bituminous materials. Proceedings of the Institution of Civil Engineers: Transport, 1995.

BROWN, S., BRUNTON, J. & STOCK, A. 1985. The analytical design of bituminous pavements. *Proceedings of Institution of Civil Engineers, Part 2,* 79**,** 1-31.

BROWN, S. & NEEDHAM, D. A study of cement modified bitumen emulsion mixtures. Proceeding of the Annual Meeting of Association of Asphalt Paving Technologies, 2000a Reno, Navada, US. 92-121.

BROWN, S. F. Achievements and challenges in asphalt pavement engineering. Proc. of 8th Int. Conf. on Asphalt Pavements, Seattle, 1997.

BROWN, S. F. & NEEDHAM, D. 2000b. A Study of Cement Modified Bitumen Emulsion Mixtures. *the 2000 Annual Meeting of the Association of Asphalt Paving Technologists.* St. Paul.

BUN, P., ESPION, B., LEUNG, C. & WAN, K. 2011. Fatigue behavior of high performance concrete in compression. *Advances in Construction Materials through Science and Technology,* 79.

BUREAU, L., ALLICHE, A., PILVIN, P. & PASCAL, S. 2001. Mechanical characterization of a styrene–butadiene modified mortar. *Materials Science and Engineering: A,* 308**,** 233-240.

C. L. MONISMITH, J. A. EPPS, D. A. KASIANCHUK & BMCLEAN, D. 1970. Asphalt Mixture Behavior In Repeated Flexure. Berkeley, US: Institute of Transportation and Traffic Engineering, University of California.

CAMPOS, J. & RUS, G. D. 2009. Some stylized facts about high-speed rail: a review of HSR experiences around the world. *Transport Policy,* 16**,** 19-28.

CARPENTER, S. & SHEN, S. 2006. Dissipated energy approach to study hot-mix asphalt healing in fatigue. *Transportation Research Record: Journal of the Transportation Research Board***,** 178-185.

CARPENTER, S. H., GHUZLAN, K. A. & SHEN, S. 2003. Fatigue endurance limit for highway and airport pavements. *Transportation Research Record: Journal of the Transportation Research Board,* 1832**,** 131-138.

CEB-FIP 1993. CEB-FIP Model code 1990–design code. London, UK: CEB, Thomas Telford.

CHEUNG, C. & CEBON, D. 1997a. Deformation mechanisms of pure bitumen. *Journal of Materials in Civil Engineering,* 9**,** 117-129.

CHEUNG, C. & CEBON, D. 1997b. Experimental study of pure bitumens in tension, compression, and shear. *Journal of Rheology (1978-present),* 41**,** 45-74.

CLOUGH, R. & PENZIEN, J. 2003. *Dynamics of structures (3rd Edition),* Berkeley, US, Computers & Structures, Inc.

COCURULLO, A., AIREY, G., COLLOP, A. & SANGIORGI, C. 2008. Indirect tensile versus two-point bending fatigue testing. *Proceedings of the ICE-Transport,* 161**,** 207-220.

CORNELISSEN, H. 1984. Fatigue failure of concrete in tension. *Henron,* 29**,** 1-68.

CORNELISSEN, H. & REINHARDT, H. 1984. Uniaxial tensile fatigue failure of concrete under constant-amplitude and programme loading. *Magazine of concrete Research,* 36**,** 216-226.

DAHLBERG, T. 2003. Railway track settlements-a literature review. *Report for the EU project SUPERTRACK.* Linköping, Sweden: Division of Solid Mechanics, IKP. Linköping University.

DAHLBERG, T. 2006. Track Issues. *Handbook of railway vehicle dynamics***,** 143.

DARROCH, T., MOLERA, L. A., BELUZSÁR, J., BILEK, V., FERRARI, M., FREUDENSTEIN, S., GIANNAKOS, K., KIEFER, B., LUCHERONI, E., MALMQUIST, U., MATTSON, S., MCQUEEN, J., PETIT, C., SALO, E. & WORMAN, C. 2006. Precast Concrete Railway Track Systems. *fib Bulletin.* Lausanne, Switzland: Fédération Internationale Du Béton (fib).

DEACON, J. A., COPLANTZ, J. S., TAYEBALI, A. A. & MONISMITH, C. L. 1994. Temperature considerations in asphalt-aggregate mixture analysis and design. *Transportation Research Record***,** 97-112.

DEACON, J. A., TAYEBALI, A. A., ROWE, G. M. & MONISMITH, C. L. 1995. Validation of SHRP A-003A flexural beam fatigue test. *Engineering properties of asphalt mixtures and the relationship to their performance,* 1265**,** 21.

DELATTE, N. 2008. *Concrete Pavement Design, Construction, and Performance,* New York, NY 10016, USA, Taylor & Francis.

DEPT. OF SCI & TECH, M. O. R. 2008a. Tentative specifications for cement-emulsified asphalt mortars used in CRTS I ballastless slab tracks of passenger-dedicated lines. Beijing, P. R. China: China Railway Press.

DEPT. OF SCI & TECH, M. O. R. 2008b. Tentative specifications for cement-emulsified asphalt mortars used in CRTS II ballastless slab tracks of passenger-dedicated lines. Beijing, P. R. China: China Railway Press.

DFT 2009. Britain's Transport Infrastructure: High Speed Two. *In:* DFT (ed.). London: Crown.

DI BENEDETTO, H., DE LA ROCHE, C., BAAJ, H., PRONK, A. & LUNDSTRÖM, R. 2004. Fatigue of bituminous mixtures. *Materials and Structures,* 37**,** 202-216.

DO, M.-T., CHAALLAL, O. & AÏTCIN, P.-C. 1993. Fatigue behavior of high-performance concrete. *Journal of Materials in civil Engineering,* 5**,** 96-111.

DONDI, G., PETTINARI, M., SANGIORGI, C. & ZOOROB, S. E. 2013. Traditional and Dissipated Energy approaches to compare the 2PB and 4PB flexural methodologies on a Warm Mix Asphalt. *Construction and Building Materials,* 47**,** 833-839.

DYDUCH, K., SZERSZEŃ, M. & DESTREBECQ, J.-F. 1994. Experimental investigation of the fatigue strength of plain concrete under high compressive loading. *Materials and Structures,* 27**,** 505-509.

EBELING, K. 2005. High-speed railways in Germany. *Japan Railway & Transport Review***,** 36-45.

EISENMANN, J., LEYKAUF, G. & MATTNER, L. 1994. Recent developments in German railway track design. *Proceedings of the Institue of Civil Engineers-Transport,* 105**,** 91-96.

EL-BASYOUNY, M. & JEONG, M. 2009. Effective temperature for analysis of permanent deformation and fatigue distress on asphalt mixtures. *Transportation Research Record: Journal of the Transportation Research Board***,** 155-163.

EPPS, J. A. & MONISMITH, C. L. 1972. Fatigue of asphalt concrete mixtures-summary of existing information. *Fatigue of compacted bituminous aggregate mixtures, ASTM STP,* 508**,** 19-45.

ESVELD, C. 1997. Low maintenance ballastless track structure. *Rail Engineering International,* 26.

ESVELD, C. 1999. Recent developments in slab track application. *Rail Tech Europe.*

ESVELD, C. 2001. *Modern railway track,* The Netherlands, MRT-Productions.

ESVELD, C. Developments in high-speed track design. International Association for Bridge and Structural Engineering, 2003a. 37-45.

ESVELD, C. 2003b. Recent development in slab track. *European Railway Review.*

ESVELD, C. & MARKINE, V. 2006. Assessment of high-speed slab track design. *European Railway Review.*

FANG, M. & CERDAS, S. F. 2015. Theoretical analysis on ground vibration attenuation using sub-track asphalt layer in high-speed rails. *Journal of Modern Transportation,* 23**,** 214-219.

FANG, M., QIU, Y., ROSE, J. G., WEST, R. C. & AI, C. 2011. Comparative analysis on dynamic behavior of two HMA railway substructures. *Journal of Modern Transportation,* 19**,** 26-34.

FELDMAN, R. & SEREDA, P. 1970. A new model for hydrated Portland cement and its practical implications. *Engineering Journal,* 53**,** 53-59.

FERRY, J. D. 1980. *Viscoelastic properties of polymers*, John Wiley & Sons.

FIB 2006. Precast concrete railway track systems. Lausanne, Switzerland.

FREUDENSTEIN, S., LIU, J. & REN, J. 2010. The development of high-speed railways in China and its impact on the Chinese economy. *European Railway Review.*

FU, D., HUANG, J. & ZHENG, X. 2002. Construction technology of CA mortar for ballastless slab track over bridges. *Railway Construction Technology***,** 28-31 (In Chinese).

FU, Q., XIE, Y.-J., LONG, G.-C., MENG, F. & SONG, H. 2015. Temperature sensitivity and model of stress relaxation properties of cement and asphalt mortar. *Construction and Building Materials,* 84**,** 1-11.

FU, Q., XIE, Y., ZHENG, K., CAI, F. & ZHOU, X. 2013. Age Effect of Mechanical Propertyof Cement and Emulsified-asphalt Mortar. *Journal of BEIJING University of Technology,* 39**,** 1607-1611 (in Chinese).

FUMEY, M., CRAIL, S., HOFMANN, C., KLÖSTERS, F., MIßLER, M., SCHILDER, R., TRÉVIN, J., GODART, P., SIMOVIC, T. & FILA, R. 2002. Feasibility study<< ballastless track>>. Paris, France: UIC Infrastructure Commission Civil Engineering Support Group.

FURTAK, K. 1984. Ein verfahren zur berechnung der betonfestigkeit unter schwellenden belastungen. *Cement and Concrete Research,* 14**,** 855-865.

FWA, T. F. 2006. *The Handbook of Highway Engineering,* Boca Raton, New York, CRC Press, Taylor & Francis Group

GALLOWAY, J. & RAITHBY, K. 1973. Effects of rate loading on flexural strength and fatigue performance of concrete.

GAO, L. & HSU, C.-T. T. 1998. Fatigue of concrete under uniaxial compression cyclic loading. *ACI Materials Journal,* 95.

GHUZLAN, K. & CARPENTER, S. 2000. Energy-derived, damage-based failure criterion for fatigue testing. *Transportation Research Record: Journal of the Transportation Research Board***,** 141-149.

GHUZLAN, K. A. & CARPENTER, S. H. 2006. Fatigue damage analysis in asphalt concrete mixtures using the dissipated energy approach. *Canadian Journal of Civil Engineering,* 33**,** 890-901.

GRAY, W. H., MCLAUGHLIN, J. F. & ANTRIM, J. D. Fatigue properties of lightweight aggregate concrete. ACI Journal Proceedings, 1961. ACI.

HANNA, A. N. 1981. Technical and economic feasibility study of at-grade concrete slab track for urban rail transit systems. Urban Mass Transportation Administration (UMTA).

HARTMAN, A., GILCHRIST, M. & NOLAN, D. 2001. Wheeltracking fatigue simulation of bituminous mixtures. *Road Materials and Pavement Design,* 2**,** 141-160.

HE, D., XIANG, J. & QINGYUANZENG 2007. A new method for dynamics modeling of ballastless track *Journal of Central South University (Science and Technology)* 38**,** 1206-1211 (in Chinese).

HEWLETT, P. 2004. *Lea's Chemistry of Cement and Concrete,* London, Elsevier Science &Technology Books.

HILSDORF, H. K. & KESLER, C. E. Fatigue strength of concrete under varying flexural stresses. ACI Journal Proceedings, 1966. ACI.

HODGKINSON, A. & VISSER, A. The role of fillers and cementitious binders when recycling with foamed bitumen or bitumen emulsion. 8th Conference on Asphalt Pavements for Southern Africa (CAPSA'04), 2004.

HOLMEN, J. O. 1982. Fatigue of concrete by constant and variable amplitude loading. *ACI Special Publication,* 75.

HOP, T. 1968. Fatigue of high strength concrete. *Building Science,* 3**,** 65-80.

HSU, T.-W. & TSENG, K.-H. 1996. Effect of rest periods on fatigue response of asphalt concrete mixtures. *Journal of transportation engineering,* 122**,** 316-322.

HSU, T. T. Fatigue of plain concrete. Journal Proceedings, 1981. 292-305.

HU, A. & WU, Y. An Analysis on the Dynamic Response of a Poroelastic Half Space under the Ballast-Less Slab Track with a High-Speed Load. E-Product E-Service and E-Entertainment (ICEEE), 2010 International Conference on, 2010. IEEE, 1-4.

HU, H., SHAO, P. & LI, H. 2011. Experimental study on the low temperature property and fatigue property of cement-emulsified asphalt mortar used in severe cold region. *China Railway Science,* 32**,** 1-6 (In Chinese).

HU, S., WANG, T. & WANG, F. 2008. Effects of expansive agents on deformation property of CA Mortar. *Journal of Southwest Jiaotong University,* 43**,** 341-345 (In Chinese).

HU, S., WANG, T., WANG, F. & LIU, Z. 2009. Adsorption behaviour between cement and asphalt emulsion in cement-asphalt mortar. *Advances in Cement Research,* 21**,** 11-14.

HU, S., XU, X. & DING, Q. 2003. Experiment on emulsified asphalt modified cement mortar in dry condition. *Journal of Wuhan University of Technology,* 25**,** 1-3 (In Chinese).

HU, S., ZHANG, Y. & WANG, F. 2012. Effect of temperature and pressure on the degradation of cement asphalt mortar exposed to water. *Construction and Building Materials,* 34**,** 570-574.

HU, S. G. & WANG, F. Z. State-of-the-art report on cement asphalt mortar. Proceedings of the 6th Asian Symposium on Polymers in Concrete, 2009. 530-538.

HUANG, Y. H. 2004. *Pavement analysis and design (2nd Edition),* New Jersey, USA, Pearson Education, Inc.

HUANG, Z., ZENG, X., GAO, Z., WANG, X. & WANG, F. 2013. Research on the main factors influencing the strength of high elastic modulus CAM. *Journal of WUHAN UNIVERSITY OF TECHNOLOGY (Transportation Science & Engineering),* 37**,** 11-14 (in Chinese).

ISSA, R., ZAMAN, M., MILLER, G. & SENKOWSKI, L. 2001. Characteristics of cold processed asphalt millings and cement-emulsion mix. *Transportation Research Record: Journal of the Transportation Research Board***,** 1-6.

IWNICKI, S. 2009. Future trends in railway engineering. *Proceedings of the Institution of Mechanical Engineers, Part C: Journal of Mechanical Engineering Science,* 223**,** 2743-2750.

JALILI, M. & NIAZI, Y. 2009. Effect of Portland cement and lime additives on properties of cold in-place recycled mixtures with asphalt emulsion. *Construction and Building Materials,* 23**,** 1338-1343.

JAMES, A. D., NEEDHAM, D. & BROWN, S. F. The benefits of using Ordinary Portland Cement in solvent free dense graded bituminous emulsion mixtures. The International Symposium on Asphalt Technology, 1996 Washington.

JANG, S. Y., LEE, H. S., KIM, Y. B., KIM, E., LEE, I. W. & KANG, Y. S. Development of prefabricated concrete slab track systems and trial installation on revenue line. 8th World Congress on Railway Research, 2008 Seoul, Republic of Kokean.

JANIC, M. 2003. High-speed rail and air passenger transport: a comparison of the operational environmental performance. *Proc. Instn Mech. Engrs, Part F: J. Rail and Rapid Transit,* 217**,** 259-269.

JENNINGS, H. M. & TENNIS, P. D. 1994. Model for the developing microstructure in Portland cement pastes. *Journal of the American Ceramic Society,* 77**,** 3161-3172.

JIN, S. & CHEN, X. 2004. Technical characteristics of the construction of Qin-Shen Passenger Special line and the inspiration for high-speed railway. *Engineering Sciences,* 2**,** 26-34.

JIN, S., CHEN, X. & YANG, J. 2006. Key technologies of CA mortar for slab track. *China Railway Science,* 27**,** 20-25 (In Chinese).

JOHN, P. L., LOTT, J. L. & KESLER, C. E. 1968. Fatigue of concrete *In:* RIGGINS, A. C. (ed.). Illinois, US: University of Illinois at Urbana-Champaign (UIUC).

JRTT. *Railway construction technologies* [Online]. Available: http://www.jrtt.go.jp/11English/pdf/p_rw_010.pdf [Accessed 21st July 2015].

KARDON, J. B. 1997. POLYMER-MODIFIED CONCRETE: REVIEW. *Journal of MATERIALS IN CIVIL ENGINEERING,* 9**,** 85-92.

KHALID, H. 2000a. A comparison between bending and diametral fatigue tests for bituminous materials. *Materials and Structures,* 33**,** 457-465.

KHALID, H. 2000b. Evaluation of asphalt fatigue properties in the laboratory. *Proceedings of the Institution of Civil Engineers-Transport,* 141**,** 171-178.

KIANI, M., PARRY, T. & CENEY, H. 2008. Environmental life-cycle assessment of railway track beds. *Proceedings of the ICE-Engineering Sustainability,* 161**,** 135-142.

KIM, C.-H. 2005. Transportation revolution: the Korean high-speed railway. *Japan Railway & Transport Review***,** 8-13.

KIM, Y.-R., LITTLE, D. & LYTTON, R. 2003. Fatigue and healing characterization of asphalt mixtures. *Journal of Materials in Civil Engineering,* 15**,** 75-83.

KIM, Y., KHOSLA, N. & KIM, N. 1991. Effect of temperature and mixture variables on fatigue life predicted by diametral fatigue testing. *Transportation Research Record***,** 128-137.

KIM, Y. R., LEE, Y. C. & LEE, H. J. 1995. Correspondence Principle for Characterization of Asphalt Concrete. *Journal of Materials in Civil Engineering,* 7**,** 59-68.

KINGHAM, R. I. 1973. Failure criteria developed from AASHO road test data. *Proceeding of the Third International Conference on the Structural Design of Asphalt Pavements to prevent fatigue cracking.* Highway Research Board.

KLAIBER, F. W. & LEE, D.-Y. 1982. The effects of air content, water-cement ratio, and aggregate type on the flexural fatigue strength of plain concrete. *ACI Special Publication,* 75.

KONG, X. & LI, Q. 2009. Properties and microstructure of polymer modified mortar based on different acrylate latexes. *Journal of the Chinese Ceramic Society,* 37**,** 107-14.

KONG, X. & LIU, Y. Dynamic mechanical properties of cement asphalt binders at early age. International Conference on Building Material, 2009 Weimar.

KONG, X., LIU, Y. & YAN, P. 2010a. Effect of loading rate on mechanical properties of cement asphalt mortars. *Journal of Building Materials,* 13**,** 187-192 (In Chinese).

KONG, X., LIU, Y. & YAN, P. 2010b. Temperature sensitivity of mechanical properties of cement asphalt mortars. *Journal of The Chinese Ceramic Society,* 38**,** 553-557 (In Chinese).

KONG, X., LIU, Y., ZHANG, Y., ZHANG, Z., YAN, P. & BAI, Y. 2014. Influences of temperature on mechanical properties of cement asphalt mortars. *Materials and Structures,* 47**,** 285-292.

KORIATH, H., HAMPRECHT, A., HUESMANN, H. & ABLINGER, P. 2003. Objektivierung der Systementscheidung Schotteroberbau versus Feste Fahrbahn bei der DB AG. *ETR. Eisenbahntechnische Rundschau,* 52**,** 113-122.

KRISHNAN, J. M. & RAJAGOPAL, K. 2003. Review of the uses and modeling of bitumen from ancient to modern times. *Applied Mechanics Reviews,* 56**,** 149-214.

LACOTE, F. 2001. 50 years of progress in railway technology. *Japan Railway & Transport Review***,** 25-31.

LEE, D., ENUSTUN, B. & KIM, S. 1991. Asphalt Cement Characterization by Thermomechanical Analysis. *Materials Characterization by Thermomechanical Analysis.* ASTM International.

LEE, H.-J., DANIEL, J. S. & KIM, Y. R. 2000. Continuum damage mechanics-based fatigue model of asphalt concrete. *Journal of Materials in Civil Engineering,* 12**,** 105-112.

LEE, H. J. & KIM, Y. R. 1997. Viscoelastic continuum damage model of asphalt concrete with healing. *Journal of Materials in Civil Engineering,* 124**,** 1224-1232.

LEE, K. C. 2007. Launch of Korean high-speed railway and efforts to innovate future Korean railway. *Japan Railway & Transport Review***,** 30-35.

LEI, X. & WANG, J. 2014. Dynamic analysis of the train and slab track coupling system with finite elements in a moving frame of reference. *Journal of Vibration and Control,* 20**,** 1301-1307.

LEI, X. & ZHANG, B. 2011. Analysis of Dynamic Behavior for Slab Track of High-Speed Railway Based on Vehicle and Track Elements. *JOURNAL OF TRANSPORTATION ENGINEERING,* 137**,** 227-240.

LEINSON, D., MATHIEU, J. M., GILLEN, D. & KANAFANI, A. 1997. The full cost of high-speed rail: an engineering approach. *The Annal of Regional Science,* 31**,** 189-215.

LESUEUR, D. 2009. The colloidal structure of bitumen: Consequences on the rheology and on the mechanisms of bitumen modification. *Advances in colloid and interface science,* 145**,** 42-82.

LETHERSICH, W. 1942. The mechanical behaviour of bitumen. *Journal of the Society of Chemical Industry,* 61**,** 101-108.

LI, G., HUANG, W. & DENG, X. 1998a. On cement-asphalt emulsion pavement composite. *Journal of The Chinese Ceramic Society,* 26**,** 445-450 (In Chinese).

LI, G., ZHAO, Y., PANG, S.-S. & HUANG, W. 1998b. Experimental study of cement-asphalt emulsion composite. *Cement and Concrete Research,* 28**,** 635-641.

LI, G. Q., ZHAO, Y., PANG, S. S., WEI, L. Y. & DENG, X. J. Laboratory studies on cement-asphalt emulsion composite. Seventh International Conference on Low-Volume Roads 1999. 210-214.

LI, N., PRONK, A., MOLENAAR, A., VAN DE VEN, M. & WU, S. 2013. Comparison of Uniaxial and Four-Point Bending Fatigue Tests for Asphalt

Mixtures. *Transportation Research Record: Journal of the Transportation Research Board***,** 44-53.

LI, S., XIE, Y., ZHENG, X. & LIU, J. 2011. Research on factors influencing shrinkage of CRTS II cment and emulsified apshalt mortar. *Railway Engineering***,** 126-128 (In Chinese).

LI, Y., XIE, B., BAO, J. & ZHOU, X. 2010a. Status and Prospects of the Slab Track CA Mortar *The World of Building Materials,* 31**,** 46-49 (In Chinese).

LI, Y., XIE, B., HU, S. & WANG, F. 2010b. The influences of figure load types on the residual strength of of CRTS II CA mortar. *CHINA CIVIL ENGINEERING JOURNAL,* 43**,** 358-362 (In Chinese).

LI, Z. & LIANG, N. 2001. Experiment on Emulsified Asphalt Modified Cement Mortar. *Highway***,** 117-119 (In Chinese).

LIANG, J., REN, X. & LI, J. 2016. A competitive mechanism driven damage-plasticity model for fatigue behavior of concrete. *International Journal of Damage Mechanics,* 25**,** 377-399.

LIAO, M.-C., CHEN, J.-S. & TSOU, K.-W. 2011. Fatigue characteristics of bitumen-filler mastics and asphalt mixtures. *Journal of Materials in Civil Engineering,* 24**,** 916-923.

LICHTBERGER, B. 2005. *Track compendium,* Hamburg, Germany, Eurailpress, Tetzlaff-Hestra GmbH & CO. KG.

LIU, X., ZHAO, P., YANG, R. & WANG, P. 2010. *Theory and method for ballastless track design in passenger dedicated lines,* Chengdu, Sichuan Province. China, Southwest Jiaotong University Press.

LIU, Y. 2009. *Investigation on mechanical properties of cement asphalt mortars.* MSc Research, Tsinghua University.

LIU, Y., KONG, X. & YAN, P. 2011a. Investigation on dynamic mechanical behaviors of cement asphalt binders. *Engineering Mechanics,* 28**,** 53-58 (In Chinese).

LIU, Y., KONG, X., ZHANG, Y. & YAN, P. 2011b. Effect of curing temperature on strength development of cement-asphalt mortars. *Journal of Building Materials,* 15**,** 211-217 (In Chinese).

LIU, Y., KONG, X., ZHANG, Y. & YAN, P. 2013. Static and dynamic mechanical properties of cement-asphalt composites. *Journal of Materials in Civil Engineering,* 25**,** 1489-1497.

LIU, Y., KONG, X., ZOU, Y. & YAN, P. 2009. Static and dynamic mechanical properties of cement asphalt mortars. *Journal of Railway Engineering,* 6**,** 1-7 (In Chinese).

LOEBER, L., MULLER, G., MOREL, J. & SUTTON, O. 1998. Bitumen in colloid science: a chemical, structural and rheological approach. *Fuel,* 77**,** 1443-1450.

LUNDSTRÖM, R. & ISACSSON, U. 2004. Linear viscoelastic and fatigue characteristics of styrene-butadiene-styrene modified asphalt mixtures. *Journal of materials in civil engineering,* 16**,** 629-638.

LUO, X., LUO, R. & L. LYTTON, R. 2012a. Characterization of Fatigue Damage in Asphalt Mixtures Using Pseudostrain Energy. *Journal of Materials in Civil Engineering,* 25**,** 208-218.

LUO, X., LUO, R. & LYTTON, R. L. 2012b. Characterization of asphalt mixtures using controlled-strain repeated direct tension test. *Journal of Materials in Civil Engineering,* 25**,** 194-207.

MAGGIORE, C. 2014. *A comparison of different test and analysis methods for asphalt fatigue.* PhD, University of Nottingham.

MATTHEWS, J. M., MONISMITH, C. L. & CRAUS, J. 1993. Investigation of laboratory fatigue testing procedures for asphalt aggregate mixtures. *Journal of Transportation Engineering,* 119**,** 634-654.

MAXBÖGL. *FFB – Slab Track System Bögl* [Online]. Available: http://max-boegl.de/fileadmin/content/download-

center/produktbroschueren/EN/Produktbroschueren_EN_FFB_Feste_Fahrbahn_Boegl.pdf [Accessed 7th February 2012].

MAXBÖGL. *Slab Track China* [Online]. Available: http://max-boegl.de/fileadmin/content/download-center/projektbroschueren/EN//C_EN_Feste_Fahrbahn_China.pdf [Accessed 27th November 2013].

MCNEELEY, D. J. & LASH, S. D. 1963. Tensile Strength of Concrete. *Journal Proceedings,* 60.

MENARD, K. P. 2008. *Dynamic mechanical analysis: a practical introduction*, CRC press.

MICHAS, G. 2012. *Slab track systems for high-speed railways.* MSc, Royoal Institute of Technology.

MINDESS, S., YOUNG, J. F. & DARWIN, D. 2003. *Concrete,* Upper Saddle River, NJ, Prentice Hall.

MONTEPARA, A. & GUILIANI, F. The role of cement in the recycling of asphalt pavement cold-stabilized with bituminous emulsions. Second International Symposium on Maintenance and Rehabilitation of Pavements and Technological Control, 2001.

MORLAT, R., GODARD, P., BOMAL, Y. & ORANGE, G. 1999. Dynamic mechanical thermoanalysis of latexes in cement paste. *Cement and concrete research,* 29**,** 847-853.

MÖRSCHER, J. Slab track roadbeds in Germany-implementation and experience. Proceedings of The 1999 AREMA Annual Conferences Track & Structures, 1999 Chicago, US.

MU, B., SUBRAMANIAM, K. V. & SHAH, S. 2004. Failure mechanism of concrete under fatigue compressive load. *Journal of Materials in Civil Engineering,* 16**,** 566-572.

MURDOCK, J. W. 1965. A critical review of research on fatigue of plain concrete. *In:* BERG, R. (ed.). Illinois, USA: University of Illinois.

MURDOCK, J. W. & KESLER, C. E. Effect of range of stress on fatigue strength of plain concrete beams. ACI Journal Proceedings, 1958. ACI.

NASH, C. A. 1991. The case for high speed rail. *Investigaciones Economicas(Seguanda epoca),* XV**,** 337-354.

NEJAD, F. M., AFLAKI, E. & MOHAMMADI, M. 2010. Fatigue behavior of SMA and HMA mixtures. *Construction and Building Materials,* 24**,** 1158-1165.

NEVILLE, A. M. 1995. *Properties of concrete*, Pearson Education.

NEVILLE, A. M. 1999. *Properties of concrete,* Essex, Pearson Education Limited.

NORDBY, G. M. Fatigue of concrete-a review of research. Journal Proceedings, 1958. 191-219.

OH, B. H. 1986. Fatigue analysis of plain concrete in flexure. *Journal of Structural Engineering,* 112**,** 273-288.

OH, B. H. 1991. Fatigue life distributions of concrete for various stress levels. *ACI Materials Journal,* 88.

OHAMA, Y. 1997. Recent progress in concrete-polymer composites. *Advn Cem Bas Mat,* 5**,** 31-40.

OKADA, H. 1994. Features and economic and social effects of the Shinkansen. *Japan Railway & Transport Review***,** 9-16.

OKADA, H. 2007. High-speed railways in China. *Japan Railway & Transport Review***,** 22-29.

ORUC, S., CELIK, F. & AKPINAR, M. V. 2007. Effect of cement on emulsified asphalt mixtures. *Journal of Materials Engineering and Performance,* 16**,** 578-583.

ORUC, S., CELIK, F. & AKSOY, A. 2006a. Performance of cement modified dense graded cold-mix asphalt and establishing mathematical model. *Indian Journal of Engineering and Materials Sciences,* 13**,** 512-519.

ORUC, S., CELIK, F. & AKSOY, A. 2006b. Performance of cement modified dense graded cold mix asphalt and establishing mathematical model. *Indian Journal of Engineering & Materials Sciences,* 13**,** 512-519.

OZSAHIN, T. S. & ORUC, S. 2008. Neural network model for resilient modulus of emulsified asphalt mixtures. *Construction and Building Materials,* 22**,** 1436–1445.

PANG, X., DARBE, R., RAVI, K. & MEYER, C. 2012. Low-Cycle Fatigue of Oil Well Cements in Compression. *ACI Materials Journal,* 109.

PASCAL, S., ALLICHE, A. & PILVIN, P. 2004. Mechanical behaviour of polymer modified mortars. *Materials Science and Engineering: A,* 380**,** 1-8.

PASKOVA, T. & MEYER, C. 1994. Optimum number of specimens for low-cycle fatigue tests of concrete. *Journal of Structural Engineering,* 120**,** 2242-7.

PCAT. *Precast advanced track: next generation slab track technology* [Online]. Available: http://www.precastadvancedtrack.com/what-is-pcat/ [Accessed 19th July 2015].

PELL, P. Pavement materials: key-note address. Proceedings of 6th international conference of structural design of asphalt pavements, 1987. University of Michigan Ann Arbor, 36-70.

PELL, P., MCCARTHY, P. & GARDNER, R. 1961. Fatigue of bitumen and bituminous mixes. *International Journal of Mechanical Sciences,* 3**,** 247-267.

PELL, P. S. 1973. Characterization of fatigue behavior. *Highway Research Board Special Report***,** 49-63.

PETERMAN, D. R., FRITTELLI, J. & MALLETT, W. J. 2009. High speed rail (HSR) in the United States Congressional Research Service.

PETKOVIC, G., LENSCHOW, R., STEMLAND, H. & ROSSELAND, S. 1990. Fatigue of high-strength concrete. *ACI Special Publication,* 121.

PETTINARI, M., SANGIORGI, C., PETRETTO, F. & PICARIELLO, F. Comparison between 2PB and 4PB Methodologies Based on the Dissipated Energy Approach. 7th RILEM International Conference on Cracking in Pavements, 2012. Springer, 31-39.

PICHLER, D. & FENSKE, J. Ballastless track systesms: experiences gained in Austria and Germany. AREMA 2013, 2013.

PINDADO, M. Á., AGUADO, A. & JOSA, A. 1999. Fatigue behavior of polymer-modified porous concretes. *Cement and concrete research,* 29**,** 1077-1083.

POEL, V. & DER, C. 1954. A general system describing the visco‐elastic properties of bitumens and its relation to routine test data. *Journal of applied chemistry,* 4**,** 221-236.

PORR. *Slab Track Austria System OBB-PORR: elastically supproted slab* [Online]. Available: http://www.porr-group.com/fileadmin/content/03_Leistungen/03_Infrastruktur/04_Bahnbau/Prospekt_OEBB-Porr_FF-System_en.pdf [Accessed 22th March 2013].

PORTER, B. W. & KENNEDY, T. W. 1975. Comparison of fatique test methods for asphalt materials. University of Texas at Austin.

POULIOT, N., MARCHAND, J. & PIGEON, M. 2003. Hydration mechanisms, microstructure, and mechanical properties of mortars prepared with mixed binder cement slurry-asphalt emulsion. *Journal of Materials in Civil Engineering,* 15**,** 54-59.

POVEDA, E., RENA, C. Y., LANCHA, J. C. & RUIZ, G. 2015. A numerical study on the fatigue life design of concrete slabs for railway tracks. *Engineering Structures,* 100**,** 455-467.

POWERS, T. C. & BROWNYARD, T. L. Studies of the physical properties of hardened Portland cement paste. ACI Journal Proceedings, 1946. ACI.

PRONK, A. & HOPMAN, P. 1991. Energy dissipation: the leading factor of fatigue.

PROWELL, B. D. & BROWN, E. R. Methods for determining the endurance limit using beam fatigue tests. Proceedings, 2006. Citeseer.

QIU, K., CHEN, H., SUN, W., SUN, L., HONG, J. & ZHAO, G. 2013a. Determination of mechanical properties of cement asphalt mortar via UPV method. *Journal of Materials in Civil Engineering*.

QIU, K., CHEN, H., YE, H., HONG, J., SUN, W. & JIANG, J. 2013b. Thermo-mechanical coupling effect on fatigue behavior of cement asphalt mortar. *International Journal of Fatigue,* 51**,** 116-120.

QUANTE, F. & OGILVIE, N. 2001. Innovative track systems-criteria for their selection. *Innovations for RailwayTrack.*

RADJY, F. & HANSEN, T. C. 1973. Fracture of hardened cement paste and concrete. *Cement and Concrete Research,* 3**,** 343-361.

RAITHBY, K. 1979. Flexural fatigue behaviour of plain concrete. *Fatigue & Fracture of Engineering Materials & Structures,* 2**,** 269-278.

RAITHBY, K. & GALLOWAY, J. 1974. Effects of moisture condition age, and rate of loading on fatigue of plain concrete. *ACI Special Publication,* 41.

RAJU, N. Comparative Study of the Fatigue Behavior of Concrete, Mortar, and Paste in Uniaxial Compression. ACI Journal Proceedings, 1970. ACI.

RAMACHANDRAN, V. S., FELDMAN, R. & BEAUDOIN, J. 1981. *Concrete science*, Heyden London.

RAO-TANGELLA, S. C. S., CRAUS, J., DEACON, J. A. & MONISMITH, C. L. 1990. Summary report on fatigue response of asphalt mixtures. Institute of Transportation Studies, University of California, Berkeley, California.

READ, J. & WHITEOAK, D. 2003. *The shell bitumen handbook*, Thomas Telford.

REDJEL, B. 1995. Etude expérimentale de la fatigue du béton en flexion 3 points. *Cement and concrete research,* 25**,** 1655-1666.

REINHARDT, H. W., CORNELISSEN, H. A. & HORDIJK, D. A. 1986. Tensile tests and failure analysis of concrete. *Journal of Structural Engineering,* 112**,** 2462-2477.

REN, J., XIANG, R. & LECHNER, B. An innovative slab track test-line in China. 8th International Conference (BCR2A'09) Bearing Capacity of Roads, Railways and Airfields., 2009. CRC Press.

REN, J., XIANG, R. & LIU, X. 2010. Force characteristics of longitudinally coupled slab track turnout on bridges under temperature action. *Transportation Research Record: Journal of the Transportation Research Board***,** 85-90.

ROESLER, J. R., HILLER, J. E. & LITTLETON, P. C. Large-scale airfield concrete slab fatigue tests. Eighth International Conference on Concrete Pavements, 2005.

ROSE, J. G. & BRYSON, L. S. Hot mix asphalt railway trackbeds: trackbed materials, performance evaluations, and significant implications. 2009 International Conference on Perpetual Pavements, Ohio Research Institute for Trans. and Envirn., Columbus, OH, 2009.

ROSTÁSY, F. S., SCHNEIDER, U. & WIEDEMANN, G. 1979. Behaviour of mortar and concrete at extremely low temperatures. *Cement and Concrete Research,* 9**,** 365-376.

ROUND, D. J. 1993. Section 14 Nonballased Tracks, Track Technology Course. British Rail Research, UK.

ROWE, G. 1993. Performance of asphalt mixtures in the trapezoidal fatigue test. *Asphalt Paving Technology,* 62**,** 344-344.

ROWE, G. M. 1996. *Application of the dissipated energy concept to fatigue cracking in asphalt pavements.* PhD, The University of Nottingham.

ROWE, G. M. & BOULDIN, M. G. Improved techniques to evaluate the fatigue resistance of asphaltic mixtures. 2nd Eurasphalt & Eurobitume Congress Barcelona, 2000.

RUIZ, G., MEDEIROS, A. & ZHANG, X. 2011. Loading frequency effect on the compressive fatigue behaviour of plain concrete and fiber reinforced concrete. *Anales de Mecánica de la Fractura,* 28.

RUTHERFORD, T., WANG, Z., SHU, X., HUANG, B. & CLARKE, D. 2014. Laboratory investigation into mechanical properties of cement emulsified asphalt mortar. *Construction and Building Materials,* 65**,** 76-83.

SAAL, R. N. & PELL, P. S. 1960. Fatigue of bituminous road mixes. *Colloid & Polymer Science,* 171**,** 61-71.

SABOURI, M. & KIM, Y. 2014. Development of a failure criterion for asphalt mixtures under different modes of fatigue loading. *Transportation Research Record: Journal of the Transportation Research Board***,** 117-125.

SAEMANN, J. & WASHA, G. Variation of mortar and concrete properties with temperature. Journal Proceedings, 1957. 385-395.

SAIJA, L. M. 1995. Waterproofing of portland cement mortars with a specially designed polyacrylic latex. *Cement and Concrete Research,* 25**,** 503-509.

SAITO, M. Direct tensile fatigue of concrete by the use of friction grips. ACI Journal Proceedings, 1983. ACI.

SALOMON, D. R. 2006. Overview of Asphalt Emulsions. *In:* BOARD, T. R. (ed.) *Asphalt Emulsion Technology.* Washingtong.

SCHAPERY, R. 1990. A theory of mechanical behavior of elastic media with growing damage and other changes in structure. *Journal of the Mechanics and Physics of Solids,* 38**,** 215-253.

SCHAPERY, R. A. 1984. Correspondence principles and a generalized J integral for large deformation and fracture analysis of viscoelastic media. *International Journal of Fracture,* 25**,** 195-223.

SCHIJVE, J. 2003. Fatigue of structures and materials in the 20th century and the state of the art. *International Journal of Fatigue,* 25**,** 679-702.

SCHIJVE, J. 2009. *Fatigue of structures and materials (2nd edition)*, Springer.

SCHILDER, R. & DIEDERICH, D. 2007. Installation uality of slab track- a decisive factor for maintenance. *RTR Special-Maintenance and Renewal***,** 76-78.

SCHÖLL, L. M. Slab track system BÖGL: past, present and future. 6th World Congress on High Speed Rail, 2008 Amsterdam, Netherlands.

SCHÜTZ, W. 1996. A history of fatigue. *Engineering Fracture Mechanics,* 54**,** 263-300.

SHATNAWI, S. 1997. Fatigue performance of asphalt concrete mixes using a new repetitive direct tension test. *Internal Caltrans report*.

SHAW, M. T. & MACKNIGHT, W. J. 2005. *Introduction to polymer viscoelasticity,* New Jersey, John Wiley & Sons.

SHEN, J. 2001. *Road performance of bitumen and bituminous mixtures* Beijing, People' Transportation Press.

SHEN, S., AIREY, G. D., CARPENTER, S. H. & HUANG, H. 2006. A dissipated energy approach to fatigue evaluation. *Road materials and pavement design,* 7**,** 47-69.

SHEN, S. & CARPENTER, S. 2005. Application of the dissipated energy concept in fatigue endurance limit testing. *Transportation Research Record: Journal of the Transportation Research Board***,** 165-173.

SHEN, S. & CARPENTER, S. An energy approach for airport pavement low damage fatigue Beha-viour. FAA Worldwide Airport Technology Transfer Conference, Atlantic City, New Jersey, USA, 2007a.

SHEN, S. & CARPENTER, S. H. 2007b. Dissipated energy concepts for HMA performance: fatigue and healing. Illinois, US: Department of Civil and Environmental Engineering, University of Illinois at Urbana-Champaign (UIUC).

SHEN, S. & LU, X. 2010. Energy based laboratory fatigue failure criteria for asphalt materials. *Journal of Testing and Evaluation,* 39**,** 1-8.

SHI, X., FWA, T. & TAN, S. 1993. Flexural fatigue strength of plain concrete. *ACI Materials Journal,* 90.

SHRP 1994. Fatigue Response of Asphalt-Aggregate Mixes. Washington, DC, US: Institute of Transportation Studies, University of California, Berkeley,US.

SMITH, K. D., ROESLER, J. R. & HOUGHTON, J. 2002. Review of fatigue models for concrete airfield pavement design. *American Concrete Pavement Association, Skokie, Illinois*.

SMITH, R. A. 2001. Railway technology-the last 50 years and future prospects. *Japan Railway & Transport Review***,** 16-24.

SOLTANI, A. & ANDERSON, D. A. 2005. New test protocol to measure fatigue damage in asphalt mixtures. *Road materials and pavement design,* 6**,** 485-514.

SONG, H., DO, J. & SOH, Y. 2006. Feasibility study of asphalt-modified mortars using asphalt emulsion. *Construction and Building Materials,* 20**,** 332-337.

SOUSA, J. B., PAIS, J. C., PEREIRA, P., WAY, G. & PARTL, M. Mode of loading on flexural fatigue laboratory properties of conventional and asphalt rubber mixes: a model validation. The Sixth International RILEM Symposium on Performance Testing and Evaluation of Bituminous Materials, 2003. RILEM Publications SARL, 364-371.

SPARKS, P. 1982. The influence of rate of loading and material variability on the fatigue characteristics of concrete. *ACI Special Publication,* 75.

SPARKS, P. R. & MENZIES, J. 1973. The effect of rate of loading upon the static and fatigue strengths of plain concrete in compression. *Magazine of Concrete Research,* 25**,** 73-80.

STRAWHECKER, K. & MANIAS, E. 2000. Structure and properties of poly (vinyl alcohol)/Na+ montmorillonite nanocomposites. *Chemistry of Materials,* 12**,** 2943-2949.

STRUBLE, L. J., STUTZMAN, P. E. & FULLER, E. R. 1989. Microstructural aspects of the fracture of hardened cement paste. *Journal of the American Ceramic Society,* 72**,** 2295-2299.

SUN, L., CHEN, L. & ZELELEW, H. H. 2013. Stress and Deflection Parametric Study of High-Speed Railway CRTS-II Ballastless Track Slab on Elevated Bridge Foundations. *Journal of Transportation Engineering,* 139**,** 1224-1234.

SUSMEL, L. 2014. A unifying methodology to design un-notched plain and short-fibre/particle reinforced concretes against fatigue. *International Journal of Fatigue,* 61**,** 226-243.

TAILOR, H. F. W. 1997. *Cement chemistry,* London, Thomas Telford Publishing.

TAKAGI, R. 2005. High-speed railways: the last 10 years. *Japan Railway & Transport Review***,** 4-7.

TAKAI, H. 40 years experiences of the slab track on Japanese high speed lines. 1st International Conferences organized by Euskal Trenbide Sarea, 2007.

TAKATSU, T. 2007. The history and future of high speed railways in Japan. *Japan Railway & Transport Review***,** 6-21.

TAKGI, K. 2011. Develoment of high-speed railways in China. *Japan Railway & Transport Review***,** 36-41.

TAN, Y., OUYANG, J., WANG, J., LI, Y. & CHEN, H. 2011. Factors influencing strength of cement asphalt mortar and strength mechanism. *Journal of Harbin Institute of Technology,* 43**,** 80-83 (In Chinese).

TAN, Y., OUYANG, J., WANG, J., ZHANG, R. & LI, Y. 2012. Research on factors influencing mechanical properties of high strength cement asphalt

mortar and mechanical mechanism. *Journal of the China Railway Society,* 34**,** 122-125 (in Chinese).

TAPSOBA, N., SAUZÉAT, C. & BENEDETTO, H. D. 2012. Analysis of fatigue test for bituminous mixtures. *Journal of Materials in Civil Engineering,* 25**,** 701-710.

TAPSOBA, N., SAUZÉAT, C., DI BENEDETTO, H., BAAJ, H. & ECH, M. 2015. Three‐dimensional analysis of fatigue tests on bituminous mixtures. *Fatigue & Fracture of Engineering Materials & Structures,* 38**,** 730-741.

TAREFDER, R. A. & BATEMAN, D. 2013. Comparison of Fatigue Failure Criterion in Flexural Fatigue Test. *International Journal of Fatigue,* 55**,** 213-219.

TAYABJI, S. & BILOW, D. 2001. Concrete slab track state of the practice. *Transportation Research Record: Journal of the Transportation Research Board***,** 87-96.

TEPFERS, R. Tensile fatigue strength of plain concrete. ACI Journal Proceedings, 1979. ACI.

TEPFERS, R. 1982. Fatigue of Plain Concrete Subjected to Stress Reversals. *ACI Special Publication,* 75.

TEPFERS, R. & KUTTI, T. Fatigue strength of plain, ordinary, and lightweight concrete. ACI Journal Proceedings, 1979. ACI.

THOMPSON, M. R. & CARPENTER, S. H. 2006. Considering hot mix asphalt fatigue endurance limit in full-depth mechanistic-empirical pavement design. *Urbana,* 51**,** 61801-2350.

TIAN, H. & YU, J. 2010. Effect of Waterborne Epoxy on Performances of Cement Asphalt Mortar. *Journal of Wuhan University of Technology,* 32**,** 201-205.

TITUS-GLOVER, L., MALLELA, J., DARTER, M., VOIGT, G. & WAALKES, S. 2005. Enhanced portland cement concrete fatigue model for streetpave.

Transportation Research Record: Journal of the Transportation Research Board, 29-37.

TSAI, B.-W. 2001. *High temperature and fatigue damage process of aggregate-asphalt mxies.* PhD, University of California, Berkeley.

UIC. *General definition of high speed* [Online]. Available: www.uic.org/spip.php?article871 [Accessed 20th July 2014].

VICKERMAN, R. 1997. High-speed rail in Europe: experience and issues for future development. *The Annal of Regional Science,* 31**,** 21-38.

VUCHIC, V. R. & CASELLO, J. M. 2002. An evaluation of maglev technology and its comparison with high speed rail. *Transportation Quarterly,* 56**,** 33-50.

WAN, Y., LIU, J. & HONG, J. 2014. Calculation of elastic modulus of high strength cement asphalt mortar via multi-level binary mixture rule. *JOURNAL OF THE CHINESE CERAMIC SOCIETY,* 42**,** 198-202 (In Chinese).

WANG, F. & LIU, Y. 2012. The compatibility and preparation of the key components for cement and asphalt mortar in high-speed railway. *In:* PERPINYA, X. (ed.) *Reliability and safety in railway.* InTech.

WANG, F. & LIU, Z. 2008. Research on the fatigue behavior of CA mortar used in ballastless slab track of high speed railway. *Journal of Wuhan University of Technology,* 30**,** 79-83 (In Chinese).

WANG, F., LIU, Z. & HU, S. 2008a. Influence of loading rate on compressive strength of CA mortar *Journal of BEIJING University of Technology,* 34**,** 1059-1064 (In Chinese).

WANG, F., LIU, Z. & HU, S. 2010a. Early age volume change of cement asphalt mortar in the presence of aluminum powder. *Materials and Structures,* 43**,** 493-498.

WANG, F., LIU, Z., HU, S., GAO, T. & ZOU, J. 2008b. Influence of setting process of cement system in the presence of asphalt emulsion on the properties of CA Mortar. *Journal of Building Materials,* 11**,** 162-166 (In Chinese).

WANG, F., LIU, Z., WANG, T. & H, S. 2010b. Temperature Stability of Compressive Strength of Cement Asphalt Mortar. *ACI MATERIALS JOURNAL*, 27-30.

WANG, F., LIU, Z., WANG, T. & HU, S. 2008c. A novel method to evaluate the setting process of cement and asphalt emulsion in CA mortar. *Materials and Structures,* 41, 643-647.

WANG, F., WANG, T., HU, S., LIU, Z., GAO, T. & CHEN, L. 2008d. Rheological behavior of cement asphalt mortar. *Engineering Journal of Wuhan University,* 41, 69-72 (In Chinese).

WANG, J., CHEN, Y., FAN, X. & LI, J. 2015. Effects of strain rate and confining pressure on compressive behavior of cement asphalt mortar. *Materials & Design,* 65, 772-779.

WANG, J., JIN, F., MO, H. & WANG, F. 2009a. Spatiotemporal evolution of China's railway network in the 20th century: An accessibility approach. *Transportation Research Part A: Policy and Practice,* 43, 765-778.

WANG, Q., A, R. & YAN, P. 2008e. Influence of m(S) /m(C) and sand gradation on compressive strength and fluidity of CA mortar. *Journal of Railway Science and Engineering,* 15, 1-5 (In Chinese).

WANG, Q. & HAN, Q. 2002. *Design and construction of slab tracks,* Chengdu, Sichuan, P. R. China, Southwest Jiaotong University Press.

WANG, Q. & YAN, P. 2009. Application of CA mortar in ballastless track. *Ready mix concrete,* 12, 32-33 (In Chinese).

WANG, Q., YAN, P., A, R., YANG, J. & KONG, X. 2011a. Strength Mechanism of Cement-Asphalt Mortar. *Journal of Materials in Civil Engineering,* 23, 1353-1359.

WANG, Q., YAN, P., YANG, J. & KONG, X. 2011b. Strength Mechanism of Cement-Asphalt Mortar. *Journal of Materials in Civil Engineering*.

WANG, R., WANG, P.-M. & LI, X.-G. 2005a. Physical and mechanical properties of styrene–butadiene rubber emulsion modified cement mortars. *Cement and Concrete Research,* 35**,** 900-906.

WANG, T. 2008. *Research and application of CA mortar in ballastless slab track of high speed railway.* Ph.D, Wuhan University of Technology.

WANG, T., HU, S., WANG, F., LIU, Z., GAO, T. & CHEN, L. 2008f. Research on main influencing factors on strength of CA Mortars. *Railway Engineering***,** 109-111 (In Chinese).

WANG, T., HU, S., WANG, F., LIU, Z., GAO, T. & ZOU, J. 2007. Mechanism study on the effects of mixing sequence of asphalt emulsion on strength development of CA mortar. *Railway Construction Technology***,** 1-3 (In Chinese).

WANG, X. 2004. Experimental investigation on performances of emulsified asphalt-cement composite cementitious material. *Municipal Engineering Technology,* 22**,** 394-396 (In Chinese).

WANG, X., SHA, A., HU, L. & YUAN, W. 2005b. Research on Mechanics Performance of Cement Emulsified Asphalt Concrete. *Journal of Highway and Transportation Research and Development,* 22**,** 57-60.

WANG, Y., ZUO, J., ZHOU, S. & WU, Z. 2013. Research on factors influencing flowability of CRTS II cement and emulsified asphalt mortar. *Railway Engineering***,** 112-114 (In Chinese).

WANG, Z. & LI, S. 2009. Microstructure characters of cement emulsified asphalt mortar (CAM). *Journal of Wuhan University of Technology,* 31**,** 32-35 (In Chinese).

WANG, Z. & SHA, A. 2009. Microstructure characters of cement emulsified asphalt composite mastics. *Journal of Chang'an University (Natural Science Edition),* 29**,** 11-14 (In Chinese).

WANG, Z. & SHA, A. 2010. Micro hardness of interface between cement asphalt emulsion mastics and aggregates. *Materials and Structures,* 43**,** 453-461.

WANG, Z., SHA, A., XIAO, J. & DU, S. 2009b. Improvement mechanism of ordinary Portland cement on microstructure of emulsified asphalt. *Journal of Wuhan University of Technology,* 31**,** 16-19 (In Chinese).

WANG, Z. J. & WANG, R. 2011. Influences and mechanisms of ordinary portland cement on properties of asphalt emulsion composites. *Materials Science and Engineering Applications, Pts 1-3,* 160-162**,** 235-240.

WEN, H. 2001. *Fatigue Performance Evaluation of WesTrack Asphalt Mixtures Based on Viscoelastic Analysis of Indirect Tensile Test.* PhD, North Carolina State University.

WEN, H. 2003. Investigation of effects of testing methods on characterization of asphalt concrete. *Journal of testing and evaluation,* 31**,** 507-513.

WEN, H., BHUSAL, S. & SUN, R. 2013. Innovative Approach to Characterizing Damage Evolution in Asphalt Concrete during Fatigue Tests. *Journal of Materials in Civil Engineering,* 26**,** 04014024.

WIKI. *High-speed rail* [Online]. Available: http://en.wikipedia.org/wiki/high-speed_rail [Accessed 20th July 2014].

WIKI. *High-speed rail in China* [Online]. Available: http://en.wikipedia.org/wiki/high-speed_rail_in_China [Accessed 20th July 2014].

WITTMANN, F. 1977. The fundamentals of a model for the description of concrete characteristics. *Schriftenreihe Deutscher Ausschuss fur Stahlbeton***,** 43-101.

XIAN, S., SHEN, Y. & LI, L. 2006. Experimental research on mechanical property of emulsion asphalt modified cement sand pulp. *Shanxi Architecture,* 32**,** 150-151 (In Chinese).

XIANG, J., HE, D. & ZENG, Q. 2009. Effect of cement asphalt mortar disease on dynamic performance of slab track. *Journal of Central South University (Science and Technology),* 40**,** 791-796.

XIAO, F. 2006. *Development of fatigue predictive models of rubberized asphalt concrete (RAC) containing reclained asphalt pavement (RAP) mixtures.* PhD, Clemson University

XIE, Y.-J., FU, Q., LONG, G.-C., ZHENG, K.-R. & SONG, H. 2014. Creep properties of cement and asphalt mortar. *Construction and Building Materials,* 70**,** 9-16.

XIE, Y., ZENG, X., DENG, D., HUANG, W., TAO, M., GAO, H. & LIN, J. 2011. Mixing kinetics of China Railway Track System (CRTS) I type ballastless slab tracks cement and emulsifiled (CA) mortar. *Journal of Building Materials,* 14**,** 191-195 (In Chinese).

XIE, Y., ZENG, X., DENG, D., LIU, B. & ZHENG, K. 2010. Mechanical characteristics of China Railway Track System (CRTS) I type slab tracks CA mortar under different strain rates. *Journal of Building Materials,* 13**,** 483-486 (In Chinese).

XU, J., CHEN, Z., WANG, K. & YANG, Y. 2009. Research and application of CA mortar in ballastless slab track of high speed railway. *Journal of East China Jiaotong University,* 26**,** 58-62 (In Chinese).

YAN, L., ZHANG, H., PENG, F. & WANG, S. 2007. Study on workability of emulsion asphalt modified highly fluidized mortar *Technology Consulting Herald***,** 238-241 (In Chinese).

YANG, J., YAN, P., KONG, X. & LI, X. 2010. Study on the hardening mechanism of cement asphalt binder. *Science China: Technology Sciences,* 53**,** 1406-1412.

YANG, T., LUO, W., XU, P., WEI, Y. & GANG, Q. G. 2004. *Theory and application of viscoelasticity,* Beijing, China, Science Press.

YAO, Y. & SUN, H. 2012. Performance and microanalysis of cement asphalt mortar with admixture of coal fly ash. *Journal of Materials Science Research,* 1**,** p193.

YEN, S. & LEE, Y. 2007. Parameter identification and analysis of a slab track system using 3D ABAQUS program. *Journal of transportation engineering*.

YIN, X., FU, Q., DONG, C., ZHAO, C., YANG, J. & GAO, Y. 2013. Influence of drying and wetting cycles on the mechanical properties of CA mortar. *Journal of Yangtze River Scientific Research Institute,* 30**,** 91-96 (In Chinese).

YUN, K.-K., KIM, D.-H. & KIM, K. W. Fatigue Behavior of Pavement Concrete by Split Tension Fatigue Test. Transportation Research Board 82nd Annual Meeting, 2003 Washington, D. C. , US.

ZENG, X., XIE, Y. & DENG, D. 2013. A study of the mixing of cement and emulsified asphalt mortar. *Magazine of Concrete Research,* 65**,** 1255-1264.

ZENG, X., XIE, Y., DENG, D., GUO, H., JIA, S. & LU, Y. 2011. Electrical conductivity characteristics and applications of fresh CA mortar. *Journal of Building Materials,* 14**,** 52-57 (In Chinese).

ZENG, Z.-P., YU, Z.-W., ZHAO, Y.-G., XU, W.-T., CHEN, L.-K. & LOU, P. 2014. Numerical simulation of vertical random vibration of train-slab track-bridge interaction system by PEM. *Shock and Vibration,* 2014.

ZENG, Z., ZHENG, X., WENG, Z., WANG, Y. & LIU, J. 2009. Construction technologise of cement aspaht emulsion mortar used in CRTS II ballastless slab track. *Railway Engineering***,** 97-100 (In Chinese).

ZHAI, W., HAN, W., CAI, C. & WANG, Q. 1999. Dynamic properties of high-speed railway slab tracks. *Journal of The China Railway Society,* 21**,** 65-69 (In Chinese).

ZHAI, W., HE, Z. & SONG, X. 2010. Prediction of high-speed train induced ground vibration based on train-track-ground system model. *Earthquake Engineering and Engineering Vibration,* 9**,** 545-554.

ZHAI, W., WANG, K. & CAI, C. 2009. Fundamentals of vehicle–track coupled dynamics. *Vehicle System Dynamics,* 47**,** 1349-1376.

ZHANG, B., PHILLIPS, D. & WU, K. 1996. Effects of loading frequency and stress reversal on fatigue life of plain concrete. *Magazine of concrete research,* 48**,** 361-375.

ZHANG, B. & WU, K. 1997. Residual fatigue strength and stiffness of ordinary concrete under bending. *Cement and concrete research,* 27**,** 115-126.

ZHANG, J., SABOURI, M., GUDDATI, M. N. & KIM, Y. R. 2013. Development of a failure criterion for asphalt mixtures under fatigue loading. *Road Materials and Pavement Design,* 14**,** 1-15.

ZHANG, J., ZHAO, Y., ZHANG, Y.-H., JIN, X.-S., ZHONG, W.-X., WILLIAMS, F. & KENNEDY, D. 2012a. Nonstationary random vibration of a coupled vehicle-slab track system using a parallel algorithm based on the pseudo excitation method. *Proceedings of the Institution of Mechanical Engineers, Part F: Journal of Rail and Rapid Transit***,** 0954409712458403.

ZHANG, L., FENG, Z. & WANG, W. 2011a. A study of vibration mixing cement mortar and emulsified asphalt. *Journal of Guangxi University: Nat Sci Ed,* 36**,** 751-757 (In Chinese).

ZHANG, N., ZHOU, S., XIA, H. & SUN, L. 2014. Evaluation of vehicle-track-bridge interacted system for the continuous CRTS-II non-ballast track slab. *Science China Technological Sciences,* 57**,** 1895-1901.

ZHANG, S. 2006. *A practical coursebook on MATLAB,* Beijing, China Machine Press.

ZHANG, W. & ZENG, J. 2013. A review of vehicle system dynamics in the development of high-speed trains in China. *International Journal of Dynamics and Control,* 1**,** 1-17.

ZHANG, Y., KONG, X., CAO, E., LIU, Y. & HUANG, W. 2010. Influence of temperature on flowability and hydration rate of fresh cement asphalt binder. *Journal of the Chinese Ceramic Society,* 38**,** 156-161 (In Chinese).

ZHANG, Y., KONG, X., HOU, S., LIU, Y. & HAN, S. 2012b. Study on the rheological properties of fresh cement asphalt paste. *Construction and Building Materials,* 27**,** 534-544.

ZHANG, Y., KONG, X., ZHANG, J., MA, X., CAO, E., LIU, Y. & HUANG, W. 2011b. Influence of asphalt emulsion on flowability and microstructure of fresh cement asphalt binder. *Journal of Building Materials,* 14**,** 569-675 (In Chinese).

ZHAO, D. 2003a. *Study of CA mortar mixture ratio and construction technology for slab track on Qin-Shen passenger railway.* Master, Southwest Jiaotong University.

ZHAO, D., WANG, T., LIU, X. & WU, L. 2008. Configuration and performance of CA mortar for ballastless slab track. *Journal of Tianjin University,* 41**,** 793-799 (In Chinese).

ZHAO, P. 2003b. *Analysis of slab track's dynamic performance and study of parameter.* Master, Southwest Jiaotong University.

ZHAO, P. The Dynamic Characteristics and Parameter Study of Slab Track. Third International Conference on Transportation Engineering (ICTE), 2011.

ZHENG, S. & KAHN, M. E. 2013. China's bullet trains facilitate market integration and mitigate the cost of megacity growth. *Proceedings of the National Academy of Sciences,* 110**,** E1248–E1253.

ZHOU, S., WANG, Z. & WANG, X. 2006. Mechanism s of strength formation of emulsified asphalt cement pavement concrete. *Concrete***,** 15-17 (In Chinese).

ZHU, J., LIU, W., XU, Q. & ZHANG, H. 2008. Performance of cement-emulsified asphlat mortar based on dynamic modulus tests. *Journal of Highway and Transportation Research and Development,* 25**,** 39-43 (In Chinese).

ZHU, Y. Design and Innovation of Ballastless Track System on Chengdu-Dujiangyan Express Railway. Proceedings of the 1st International Workshop on High-Speed and Intercity Railways, 2012. Springer, 279-287.

ZOETEMAN, A. & ESVELD, C. Evaluating track structures: life cycle cost analysis as a structured approach. World Congress on Railway Research, 1999 Tokyo, Japan.

ZUO, J., JIANG, Q. & FU, D. 2005. Research on CA mortars used as cushion layer in slab track *Railway Engineering***,** 96-98 (In Chinese).

APPENDIX I OPERATION PROCEDURES OF THE MINI-4PB APPARATUS ON THE MTS

To test the bending properties and 4PB fatigue of CAM-I and CAM-II by the newly developed apparatus on the MTS machine, operation procedures should be strictly followed in the following sequence of a-f.

a. Turn on and set up the MTS;

For the MTS 810, there include a loading frame (**Fig 3.12(a)**), a controller with a computer (**Fig 3.12(b)**), a hydraulic power machine and a cooling facility. To start with, the controller is firstly turn on and then the computer. Log into the computer, find '**Station Manager**' and open its interface. Secondly, start the cooling system before turning on and resetting the hydraulic power machine. Get back to the interface, click '**HPU**' and '**HSM**' buttons in turn and choose the **MPT** interface. Open the dialog box '**Manual Control'**, and choose displacement control mode. From this moment, the main loading frame can be controlled at a relatively slow displacement rate.

Remember to check and set up the limit of force or displacement first in bending tests, to protect the facility. Before any fatigue test at a fixed frequency, on the other hand, tuning is needed using a **PIDF** dialog box until the MTS machine can perform dynamic loadings in a stable and reliable way.

b. Install the 4PB apparatus;

To connect the 4PB apparatus onto the MTS loading frame, two steel connectors and connecting bars are needed. Firstly use one connector to be clamped into the top gridding head and connect the 4PB apparatus to this connector. In the second place, install the other connector to the 4PB facility and adjust the bottom gridding head up to its position. Finally, examine the effectiveness in movements of the 4PB apparatus by controlling the bottom gridding head up and down, and after this, adjust it to a proper position, making

sure the four screws on the 4PB apparatus in a horizontal line, as shown in **Fig 3.15(a)**, which is a necessary procedure.

c. Place the CAM specimen in position;

The first important step in this procedure is to change the control mode, in the dialog box '**Manual Control'**, from displacement to force. The next is to set up the force value to zero and place the CAM beam into the 4PB apparatus. In the last step, tighten the four screws slowly by hand and each two in one group. The basic sequence is to start from the two outside screws and end up with the two inside ones. Wait for a few minutes until the values are stable on the interface, change force control mode back to displacement in the dialog box.

d. Fixate the LVDT and the supporting bridge

A supporting bridge, designed for positioning the LVDT, is placed on the top surface of the CAM specimen, and fixated in position using two rubber bands. Then Insert the LVDT through a hole in the bridge and adjust it to a proper position by moving it slowly, making sure the tip of the LVDT in contact with the top surface and its reading close to zero.

e. Operate the MTS for loading tests;

Remember to check whether the readings of all offsets are zero before a loading test, be static mechanical or fatigue, is performed. If not, click '**Offsets**'. After a double check, click a green button in the interface and the MTS machine starts to work. In the process of loading, it is necessary to keep an open eye on all diagrams demonstrated in the interface of the MTS controller.

f. Take out the failed specimen

Whatever mode of loading it is used in the test, it is important to check the '**Manual Control'** frequently, making sure displacement as the control mode, before you stop the loading test. After finishing the test, input zero displacement and the facility will be back to the original position. Loose the rubber bands and the screws, and take the failed specimen out.

APPENDIX II MATLAB PROGRAMMING FOR FATIGUE TEST DATA PROCESSING

To analysis the fatigue test data of different CAMs, a MFile was programmed using MATLAB. The main goal was to calculate the stress amplitude, the strain amplitude, and the lag angle in every circle during fatigue. In this way, the dissipated energy at the loading circle of n, E(n), can be obtained.

The details of the MATLAB Mfile were shown as follows.

File name: Fatigue_Calculation.m

```
clear all; close all; clc;

%% Open Files

rfile_name = 'specimen.dat';

wfile_name = 'specimen_pure_data.dat';

file_name = 'result.dat';

fidr = fopen(rfile_name,'r');

fidw = fopen(wfile_name,'w');

fid = fopen(file_name,'w');

%% Skip Lines
```

```
line = fgetl(fidr);
while(~feof(fidr))
    line = fgetl(fidr);
    if(isempty(line))
        line = fgetl(fidr);
        line = fgetl(fidr);
        line = fgetl(fidr);
        line = fgetl(fidr);
    end
    fprintf(fidw,'%s\n',line);
end

%% Load Data
data = load(wfile_name);
data = data(1:end,:);

%% Parameter Configuration
L = length(data(:,1));
M = 50;
N = floor(L/M);
f = 10;
```

```
%% Data Fitting

X = zeros(N,3);

Y = zeros(N,3);


for n = 1 : N

    t = data(50*n-49:50*n,1);

    d = data(50*n-49:50*n,2);

    F = data(50*n-49:50*n,3);


    if n == 1

        md = (max(d) + min(d)) / 2;

        mF = (max(F) + min(F)) / 2;


        Ad = (max(d) - min(d)) / 2;

        AF = (max(F) - min(F)) / 2;


        Psid = (md - d(1)) / Ad;

        PsiF = (mF - F(1)) / AF;


        if Psid > 1
```

```
        Psid = 1;
    elseif Psid < -1
        Psid = -1;
    end

    if PsiF > 1
        PsiF = 1;
    elseif PsiF < -1
        PsiF = -1;
    end

    Psid = 2*pi*f*t(1)-asin(Psid);
    PsiF = 2*pi*f*t(1)-asin(PsiF);

    X(n,:) = [md,Ad,Psid];
    Y(n,:) = [mF,AF,PsiF];
else
    X(n,:) = X(n-1,:);
    Y(n,:) = Y(n-1,:);
end
```

```
    X(n,:) = lsqcurvefit(@(X,xdata) X(1) - X(2)*sin(2*pi*f*t - X(3)),X(n,:),t,d);
    Y(n,:) = lsqcurvefit(@(Y,xdata) Y(1) - Y(2)*sin(2*pi*f*t - Y(3)),Y(n,:),t,F);
end

 %% Fatigue Calculation
a = 40;
b = 30;
h = 40;
L = 120;

et = 2*12*X(:,2)*h/(3*L^2-4*a^2);
St = L*Y(:,2)/(b*h^2);
E = St./et;
psi = abs(X(:,3) - Y(:,3));
w = pi*St.*et.*sin(psi)*1e6;
Wf = nan(N,1);

Wf(1) = w(1);
for n = 2 : N
    Wf(n) = Wf(n-1) + w(n);
end
```

```
%% Save Data as "result"

for n = 1 : N

    fprintf(fid,'%d\t%.6f\t%.6f\t%.6f\t%.6f\n',n,E(n),psi(n),w(n),Wf(n));

end


fclose all;


%% Classical Failure Criterion for CAM-I £¨Nf50£© if necessary

delta = abs(E - E(2)/2);

[value,Nf] = min(delta);

display(Nf);


load (file_name);
```